Etiologies and Clinical Consequences of Enlarged Perivascular Spaces

By

Corey William Bown

Dissertation
Submitted to the Faculty of the
Graduate School of Vanderbilt University
in partial fulfillment of the requirements
for the degree of

DOCTOR OF PHILOSOPHY

in

Neuroscience

December 17, 2022

Nashville, Tennessee

Approved:

Timothy J. Hohman, Ph.D.

Angela L. Jefferson, Ph.D.

Bennett A. Landman, Ph.D.

Matthew S. Schrag, M.D., Ph.D.

Roxana O. Carare, M.D., Ph.D.

DEDICATION

To my parents, who provide me with strength and raised me to believe I can do anything.

ACKNOWLEDGEMENTS

I would like to thank the Vanderbilt Memory and Aging Project participants and their loved ones who made this work possible. I would also like to thank the Vanderbilt QCB Program, the Vanderbilt Memory and Alzheimer's Center, and my funding (F31-AG066358). I would like to thank my committee for providing me with the mentorship, knowledge, and tools to succeed, especially Drs. Timothy Hohman and Angela Jefferson. I would like to thank my fiancé Laura for providing me with so much support and taking my mind off science occasionally. Finally, I would like to thank my family, who are always there for me and helped me to keep working towards this accomplishment, especially when times were tough.

TABLE OF CONTENTS

LIST OF TABLES

LIST OF FIGURES

Figure Page

CHAPTER 1

INTRODUCTION

Portions of this chapter are published under the titles “Apolipoprotein E Genotype Modifies the Association Between Cardiac Output and Cognition in Older Adults” in *Journal of the American Heart Association*, 2019; “Lower Cardiac Output Relates to Longitudinal Cognitive Decline in Aging Adults” in *Frontiers in Psychology*, 2020; “Elevated Aortic Pulse Wave Velocity Relates to Longitudinal Gray and White Matter Changes” in *Arteriosclerosis, Thrombosis, and Vascular Biology*, 2021; and “Physiology and Clinical Relevance of Enlarged Perivascular Spaces in the Aging Brain” in *Neurology*, 2022.

Cardiac Function and Brain Health

The arterial system begins with a pump (the heart), continues as a series of tubes descending in diameter and consisting of varying mechanical properties, and ends with microscopic capillaries. The brain is a high-flow organ, receiving 12% of cardiac output despite accounting for only 2% of overall body weight,[1] which illustrates the importance of healthy blood flow delivery to the brain parenchyma. Unfortunately, though, the system connecting oxygenated blood to brain cells can become damaged at every step along the way, and this damage can have detrimental effects on brain health.

Starting with the heart, preserved cardiac function is essential to cerebral blood flow delivery and hemodynamic regulation. Evidence suggests subtle reductions in

cardiac output relate to increased risk of dementia, including clinical Alzheimer's disease (AD), in community-based aging adults.[2] Altered cardiac hemodynamics have been associated with cerebral blood flow (CBF) disturbances,[3] smaller brain volumes,[4] and poorer cognitive performances.[4,5] In a previous study among community-dwelling older adults free of clinical dementia, stroke, and heart failure, we (Bown et al., 2020) found lower cardiac output at study entry related to faster decline in language, information processing speed, visuospatial skill, and episodic memory abilities over a mean 3.5-year follow-up period.[6]

Chronic lower blood flow delivery to the brain could create a gradual metabolic energy crisis for neurons[7] and oxidative stress[8] that concurrently promotes increased tau phosphorylation,[9] mitochondrial dysfunction,[10] and astrocyte dysregulation.[11] These changes are known to drive neurodegeneration, but lower blood flow could affect the brain through other pathways by inducing blood-brain barrier dysregulation[12] or neuroinflammation,[13] both of which might contribute to clinical symptoms and subsequent dementia.

Tests of language, information processing speed, visuospatial skills, and episodic memory were all implicated in main effect models relating baseline cardiac output to longitudinal cognitive trajectory.[6] Language abilities generally localize to the temporal lobes[14] but the Boston Naming Test, a word-retrieval task implicated in this study, requires the convergence of semantic memory,[15] lexical selection[15] and visual-perceptual processing[16] and can be indicative of a global phenomenon. Still, there may be specific brain regions that are more susceptible to hemodynamic fluctuations than others. For example, regions that are likely to have higher metabolic energy demand[17,18]

or are located in territories that are difficult to perfuse are more vulnerable.[19] A large portion of energy expenditure in the brain occurs at synapses[20] and regions with high neuronal density could be more vulnerable to oligemia or hypoperfusion. The temporal lobes mediate memory and language functions, have higher synaptic density in older adults with normal cognition,[21] and have a less extensive network of collateral blood vessels in humans,[22] which may increase vulnerability to alterations in cerebral blood flow delivery. Additionally, basal ganglia nuclei, which mediate information processing speed,[23] are some of the most susceptible brain regions to ischemic damage in the context of hypoperfusion[18] due to being located in the internal watershed region of the brain.[24]

The apolipoprotein E ε4 allele (*APOE*-ε4) is a genetic susceptibility risk factor for AD. Possession of one ε4 allele increases risk of clinical AD 3-fold and both alleles increase risk 12-fold.[25] Meanwhile, possession of the ε2 allele is considered protective against AD. *APOE*-ε4 is purportedly a moderator of cerebrovascular damage that precedes neuronal dysfunction[26,27] and contributes to blood brain barrier (BBB) degradation.[28] Additionally, among older adults, *APOE*-ε4 carriers have lower cross-sectional cerebral blood flow (CBF)[29] and greater CBF decline over time than non-carriers.[30] We (Bown et al., 2019) also found lower cardiac output was associated with worse cognitive performance at baseline among *APOE*-ε4 carriers but not non-carriers. The pattern of results implicated language, information processing speed, and executive function,[31] which overlap somewhat with associations between cardiac output and longitudinal cognition.

Our work suggests *APOE*-ε4 carriers are particularly vulnerable to worse cognitive performance in the context of subclinical reductions in cardiac output. As a robust genetic susceptibility risk factor for AD[32,33] and molecular moderator of vascular damage,[32] the *APOE*-ε4 allele may promote a stronger association between cardiac output and cognitive aging through multiple pathways, such as disruption in autoregulation,[26,34,35] blood-brain barrier (BBB) dysfunction,[26] neuroinflammation,[36,37] and oxidative stress.[38–41] The brain has complex autoregulatory mechanisms, including vasodilation,[34,42] to protect it from damaging fluctuations and reductions in blood flow delivery. These mechanisms may be compromised in *APOE*-ε4 carriers.[26] Transgenic *APOE*-ε4 mouse models suggest *APOE*-ε4 relates to more extensive BBB breakdown due to upregulation of metalloproteinase 9.[26] Vasodilation factors function at the neurovascular unit,[34,35] so damage to the BBB, a core component of the neurovascular unit, may result in a weakened dilatory response and reduced regional CBF.[26] Additionally, among humanized *APOE* targeted-replacement mice, the *APOE*-ε4 allele is associated with elevated brain levels of proinflammatory cytokine tumor necrosis factor alpha (TNF-α),[36] which is upregulated in heart failure[37] and could be modestly upregulated with subclinical cardiac dysfunction. TNF-α correlates with brain natriuretic peptide (BNP) in patients with chronic heart failure[43] and growing evidence suggests an association exists between BNP and cognitive impairment, separate from atherogenic or AD risk factors.[44] Though speculative, taken together, *APOE*-ε4 status may relate to worse cognition in the presence of chronic subclinical cardiac dysfunction by degrading capillary basement membrane and BBB tight-junction proteins through

metalloproteinase 9 upregulation.[45,46] Additional burden is likely promoted due to TNF-α-associated inflammation.

Information processing speed and executive functions are thought to be mediated by frontal-subcortical networks,[47,48] which rely heavily on basal ganglia nuclei[23] and are supplied by particularly vulnerable, small perforating arteries.[49,50] It is plausible in the setting of subtle reductions in cardiac output, these structures accumulate burden and subclinical damage throughout midlife with late-life cognitive consequences. This explanation is supported by extensive evidence linking hemodynamic fluctuations and ischemic damage to slowed information processing speed[51,52] and executive dysfunction.[51–53] Contrary to expectation, we found no association between cardiac output and episodic memory in models comparing *APOE*-ε4 carrier status groups, but we did find cardiac output related to language performance, which localizes, in part, to temporal lobe structures. Temporal lobe structures may be more vulnerable to reduced cardiac output and corresponding reductions in CBF as we recently reported[3] and as mentioned above, presumably due to high synaptic density[21] or poor collateral circulation,[22] as exists in the hippocampus.[3,54] However, the absence of episodic memory results here suggests mechanisms involved in the modifying effect of *APOE*-ε4 may be more complex in temporal lobe regions.

Collectively, results suggest subtle reductions in cardiac output predispose aging adults to global cognitive changes, especially in language, information processing speed, visuospatial skill, and episodic memory longitudinally, as well as in language, information processing, and executive function domains for *APOE*-ε4 carriers, all prior to the onset of dementia. Given the common co-occurrence of cerebral small vessel

disease and AD pathology,[55] clinical dementia may manifest because of a combination of AD-related neurodegeneration and coexisting tissue vulnerability secondary to chronic, subtle hemodynamic fluctuations. This latter injury may affect regions or networks mediating language, information processing, visuospatial skills, episodic memory, and executive function.

Systemic Vascular Health and Brain Health

Moving up the system, we next focus on the aorta. Age-related vessel wall thickening and elastin loss result in aortic stiffening which may impair autoregulatory mechanisms[56] and precede the development of hypertension.[57,58] A healthy aorta is elastic and helps diffuse pressure waves leaving the heart,[59] but this elasticity declines over one's life course. As the aorta stiffens, distal cerebral microvasculature receives damaging pressure waves, eventually resulting in vessel wall damage. Aortic stiffening can even result in downstream cognitive consequences[60,61] and has been shown to increase the risk of developing dementia.[62]

In the presence of high pulse pressures, cerebral microvasculature may lose its integrity[63] and result in reduced brain perfusion and nutrient delivery. Reductions in perfusion drive atrophy-inducing excitotoxicity[64–66] and reduced nutrient transport to the parenchyma[67,68] results in ischemia and oligemia[69] which drive white matter hyperintensity (WMH) formation.[70,71] Cross-sectionally in middle-aged cohorts, increased brachial-ankle PWV is associated with greater global WMH[72] while increased aortic PWV is inversely correlated with lower global grey matter volume.[73] We (Bown et al., 2021) have found higher baseline aortic pulse wave velocity (PWV) to be associated

with more rapid decline in grey matter volume over a mean 4.2-year follow-up period in the hippocampus and occipital lobe. Neither *APOE*-ε4 nor cognitive diagnosis modified associations. Higher baseline aortic PWV, a measure of the degree of aortic stiffness was also associated with greater increase in white matter hyperintensity (WMH) volumes in the temporal lobe over the follow-up period.[74] While associations were not modified by diagnosis, the *baseline aortic PWV x APOE-ε4* interaction term was related to longitudinal WMH volume in the temporal lobe. Associations between higher baseline aortic PWV and greater increase in WMH volume appear to be driven by *APOE*-ε4 non-carriers. Our results suggest that central arterial stiffening predicts greater decrease in grey matter volume in the hippocampus. These observations are particularly interesting considering the regions affected by aortic stiffening overlap with regions that accumulate AD pathology early in the disease process.[6]

Reduced cerebral blood flow due to higher PWV is likely the result of microvascular remodeling and higher vascular resistance.[75] Chronic reductions in cerebral blood flow may lead to unmet cerebral metabolic demands which disrupt cerebral homeostasis and result in cell dysfunction, death, and subsequent atrophy due to excitotoxicity.[76,77] Interestingly, the hippocampus and temporal lobes are regions with particularly high energy consumption. The hippocampus is one of the most densely populated brain regions in terms of synapses,[78,79] and the medial temporal lobes are involved in the highly active default mode network.[80] The metabolic demand of these regions may make them particularly vulnerable to excitotoxicity. Potential mechanisms can be viewed in **Figure 1.1**.[74] However, it is plausible that other damaging cascades,

such as oxidative stress or blood-brain barrier breakdown, play a role in the longitudinal atrophy observed here.

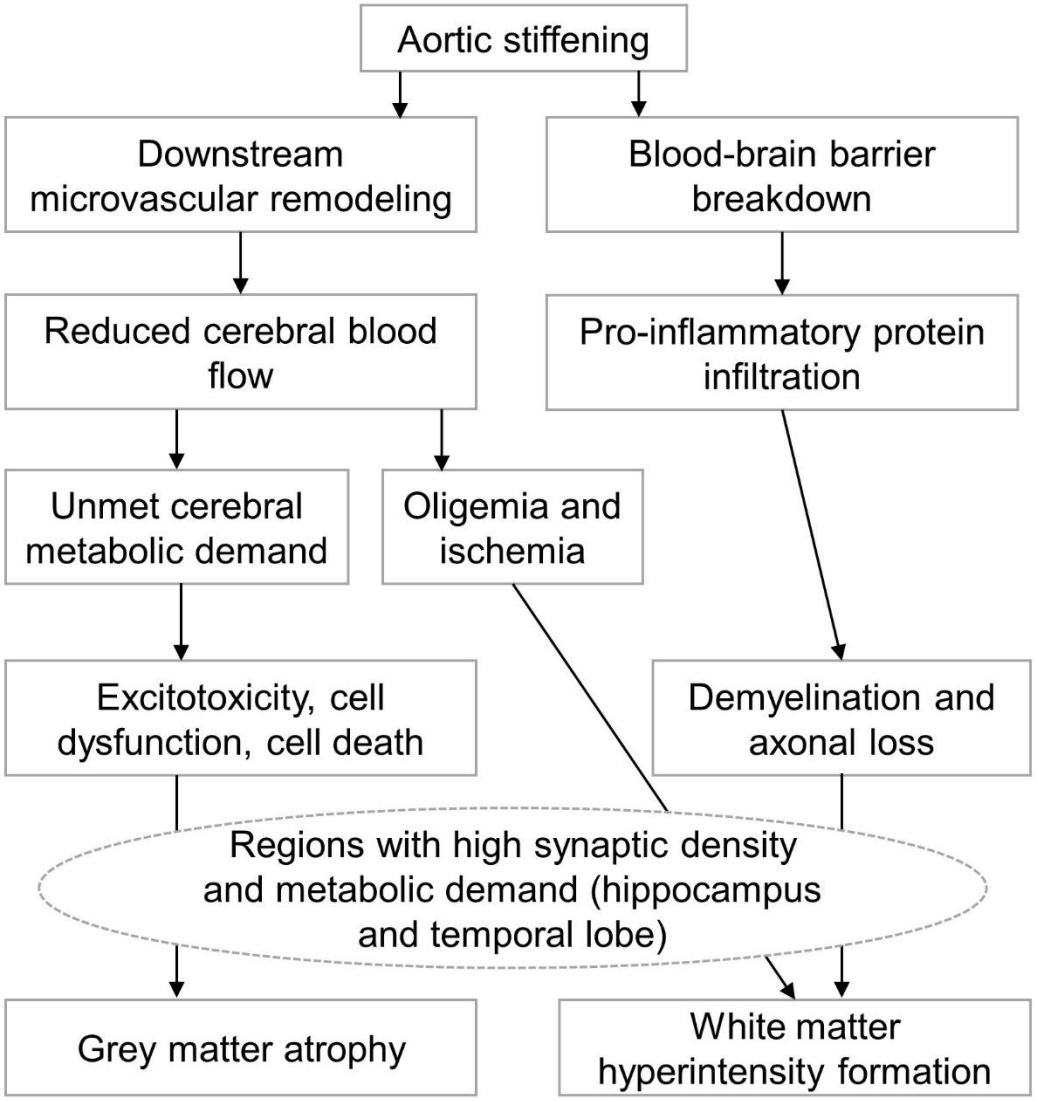

Figure 1.1. Aortic stiffening to structural brain changes flowchart. Flowchart representing potential pathways by which aortic stiffening could lead to grey matter atrophy and white matter hyperintensity formation. Adapted from Bown et al., 2021 *Arteriosclerosis, Thrombosis, and Vascular Biology*, graphical abstract.

Central arterial stiffening also contributes to greater increase in WMH volume in the temporal lobe. One explanation aligned with the aforementioned discussion is that arterial stiffness is linked to reduced cerebral blood flow,[75] resulting in oligemia and

possibly ischemia. Ischemia is a well-established driver of WMH formation in animal models,[81] and *in vivo* ischemia is related to WMHs in humans.[82] Alternatively, blood-brain barrier breakdown, a purported consequence of increased pulsatility,[83] results in pro-inflammatory protein infiltration into the parenchyma[84–87] creating a toxic environment that can result in demyelination[88] and axonal loss.[84,89]

As noted above, the temporal[90] lobe is metabolically demanding. Brain regions with increased neuronal activity could be preferentially susceptible to white matter damage in the context of arterial stiffening since damaged vessels would impede adequate nutrient delivery. Focusing on how age-related systemic cardiovascular changes influence neurodegeneration is an essential aspect of understanding the multifactorial contributors to adverse cognitive aging and dementia risk. Our work shows aortic stiffness is associated with longitudinal grey matter and white matter damage, particularly in the temporal lobes.

Neck Vessels

Further up the arterial tree comes the neck vessels, primarily the carotid and vertebral arteries. Less work has been done into the effects of neck vessel health on brain health. In one study, low carotid flow velocities were associated with higher cerebral small vessel disease burden.[91] Another study found, in a cohort of patients with MCI, that carotid artery stiffening may drive reduced cerebral blood flow and increased cerebral vascular reactivity.[92] To complete the heart to brain connection, more studies must focus on how neck vessel health can contribute to worse brain health. Still, early

studies suggest that carotid artery health does indeed play a role in downstream brain health.

Small Vessel Disease

Now we move even further up the system, focusing on the small arteries and arterioles that perfuse the brain. Cerebral small vessel disease (SVD) is a vascular disease associated with lower cerebral blood flow[93] and impaired cerebral hemodynamic autoregulation,[94] leading to numerous pathologies and clinical symptoms.[95] Vascular pathology in the form of moderate to severe atherosclerosis, arteriosclerosis, or cerebral amyloid angiopathy (CAA), exists in up to 87% of autopsy confirmed cases of AD[96] and can significantly contribute to cognitive decline. SVD is caused by arteriosclerosis and cerebral amyloid angiopathy and can result in pathology that can be seen on brain magnetic resonance imaging (MRI).

The four most common pathologies attributed to SVD visible on MRI are WMHs, enlarged perivascular spaces (ePVS), cerebral microbleeds (CMBs), and lacunes. WMHs are an ambiguous imaging feature that are viewed using fluid-attenuated inversion recovery (FLAIR) images and often represent ischemic damage. ePVS are fluid filled spaces surrounding blood vessels that have become enlarged and can be viewed on T_1-weighted, T_2-weighted, and FLAIR images. CMBs are between 1 and 10 mm in diameter and are viewed using susceptibility weighted imaging. Lacunes are focal ischemic lesions that are between 2 and 20 mm in diameter and viewed on T_1 and FLAIR.

SVD leads to cerebral tissue damage and can even drive atrophy. With tissue damage and loss, cognitive decline follows. Prior work from our group has shown that increased WMH were associated with worse baseline language, information processing, visuospatial abilities, and executive function performances.[97] ePVS were related to worse baseline information processing and executive function performances.[97] CMBs were associated with worse executive function performance and lacunes were associated with worse information processing, visuospatial abilities, and executive function performances.[97] When assessing combined models, results suggested that WMHs, ePVS, and CMBs affect cognition through unique vascular pathways. Interestingly, ePVS had the largest contribution to variance for multiple cognitive domains when assessing combined models, highlighting the importance of further studying ePVS.[97]

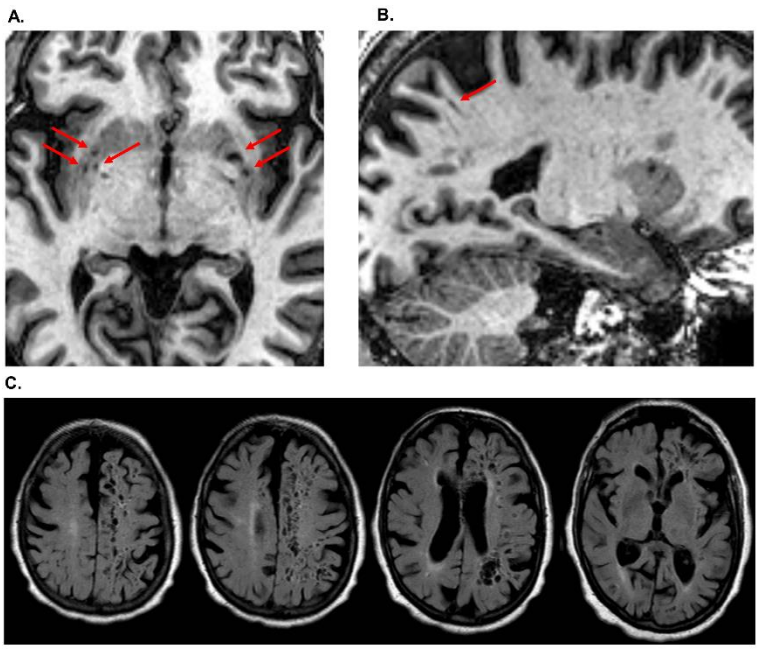

Figure 1.2. ePVS Appearance on Brain MRI. **(A)** An axial slice depicting ePVS in the basal ganglia. **(B)** A sagittal slice of the same participant depicting ePVS in white matter. Note that the ePVS in the basal ganglia appear larger in diameter than the ePVS in the white matter. Such morphological differences are typical and may be because cortical arteries have one layer of pia mater while perforating arteries of the basal ganglia have two. **(C)** While less common, ePVS can grow much larger than 3 mm and in some rare cases may present throughout large regions of the brain.

Perivascular Spaces

For my dissertation we chose to investigate potential causes and consequences of ePVS, the most understudied pathology of the four hallmark SVD imaging features. ePVS are

fluid filled compartments that surround cerebral blood vessels and aid in fluid transport to and from the brain. According to the Standards for ReportIng Vascular changes on nEuroimaging (STRIVE), ePVS follow vessels coursing through the basal ganglia or white matter. ePVS are isointense with cerebrospinal fluid (CSF), appear round when imaged perpendicular to penetrating vessels and linear when parallel to a vessel. The cross-sectional diameter of an ePVS is normally less than 3 mm (although in pathological states they can be much larger) and at higher resolutions a vessel may be seen inside the ePVS.[98] Healthy perivascular spaces (PVS) house a range of immune cells contributing to immune surveillance and potentially neuroinflammation.[99] Increasing evidence demonstrates the important role PVS play in transporting molecular debris from the brain into CSF[100] where debris is carried to and filtered by cervical lymph nodes located in the neck. ePVS (see **Figure 1.2 A-C**),[101] visible on brain MRI and possibly indicative of impaired PVS, therefore have potential implications in neurological diseases where abnormal proteins accumulate, such as AD.[102]

ePVS were long thought to be benign imaging features when visible on *in vivo* neuroimaging or a manifestation of cerebral atrophy. Neuropathologically, they were often considered artifacts of fixation methods, although they can certainly be seen in unfixed, neuropathological specimens. See **Figure 1.3**.[101] ePVS range in size from microscopic to so-called “tumefactive ePVS,” a poorly

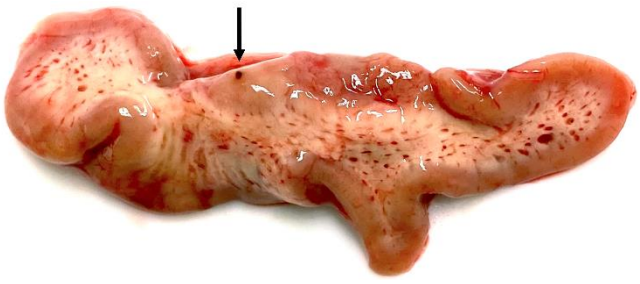

Figure 1.3. Unfixed brain tissue from a patient with CAA. The tissue sample displays clear and widespread ePVS throughout the white matter along with a cortical microhemorrhage (black arrow).

understood condition in which ePVS are enlarged to more than 1.5 cm in diameter.[103] See **Figure 1.2 C**.

Table 1.1 PVS Definitions

Term	Definition
Abluminal	Occurring on the outer surface of a vessel
Glia Limitans	A thin barrier of astrocyte end-feet that surrounds the central nervous system and cerebral blood vessels
Pia Mater	The thin, innermost layer of the meninges which are membranes surrounding the central nervous system
Basal Lamina	A form of extracellular matrix that acts as connective tissue and is often termed the basement membrane
Intramural Peri-arterial Drainage	A drainage system that flows through the smooth muscle cell basement membrane network of capillary, arteriole, and artery walls and clears metabolic waste from the brain
Glymphatics	A system in the brain that uses perivascular spaces encapsulated by astrocyte end-feet to clear proteins and metabolic waste from the central nervous system, facilitated by CSF flowing along the periarterial space, into the parenchyma, and out along the perivenous space
Cisterna Magna	A large, subarachnoid cistern or opening that lies between the cerebellum and medulla and is filled with CSF
Subarachnoid Space	A space between the arachnoid membrane and pia mater that encapsulates the central nervous system and acts as a channel for CSF, arteries, and veins.
Para-arterial	Occurring outside the artery or arteriole but inside the glia limitans
Interstitial Fluid	Extracellular fluid between vessels and cells that contains nutrients expelled by capillaries and waste expelled by cells
Lenticulostriate Arteries	A group of small arteries that branch off the anterior Circle of Willis, perforate and perfuse the basal ganglia

Perivascular Space Anatomy

Anatomically, PVS are found abluminal to the endothelium of cerebral blood vessels but within the glia limitans of vessels.[104] See **Figure 1.4**[101] for illustration and **Table 1.1** for definitions.[105] ePVS visible on MRI typically run parallel to penetrating cerebral arterioles which run perpendicular to the brain surface. PVS are considered fluid-filled compartments that lie between endothelial cells and astrocytes. A layer of pia mater constrains PVS at the arteriole level and is replaced by astrocytic end-feet at the capillary level, acting as an additional layer of the blood-brain barrier. From there, PVS are thought to continue through capillaries into venules and out of the brain through veins. What surrounds PVS differs depending on the location within the vascular tree (i.e., a layer of pia mater along the arterioles and a fragmented pia mater along venules, whereas capillaries only have astrocyte end-feet as the perivascular boundary). A general model of PVS anatomy is displayed in **Figure 1.5**.[101] In the glial cell-mediated lymphatic (or glymphatic) model of PVS clearance (Pathway 1), PVS are described as compartments between the smooth muscle cell (SMC) and pia layers of arterioles and between the endothelium and pia layers of venules where the pia layer acts as the outer PVS wall. These spaces are constrained by two layers of leptomeninges that perforate through the basal lamina of the vessel

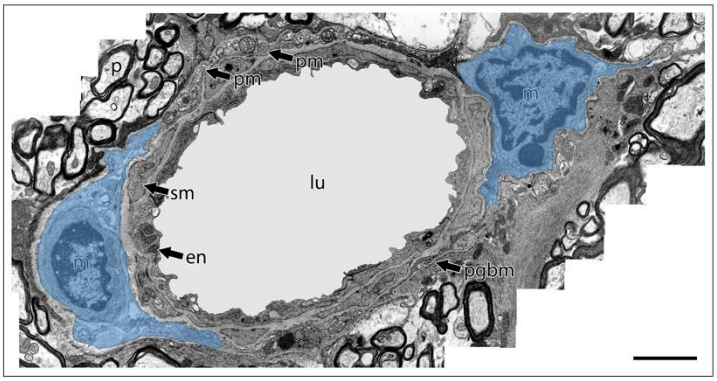

Figure 1.4. PVS appearance on electron microscopy. Pictured is an example electron microscopy image of a healthy blood vessel lumen (lu) with normal appearing perivascular spaces (highlighted in blue) which also contain macrophages (m). The pial-glial basement membrane (pgbm) is extended away from the vessel only in the presence of macrophages. Also pictured are normal smooth muscle cells (sm), pia mater (pm), and endothelium (en). Image courtesy of Roxana Carare, MD, PhD.

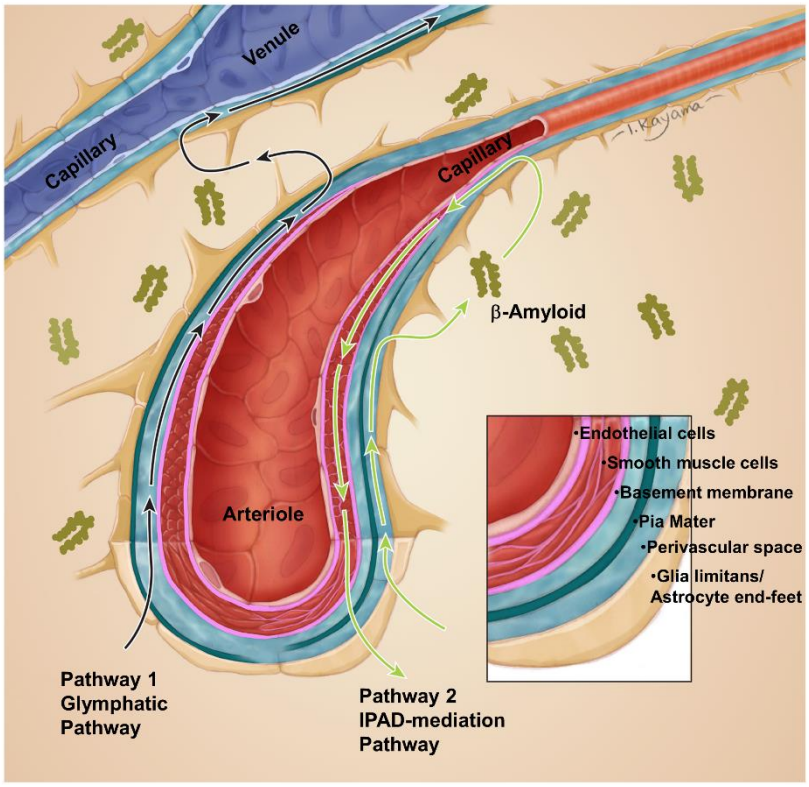

Figure 1.5. Two theoretical models for PVS anatomy and physiology. Pathway 1 is the glymphatic clearance pathway. Pathway 2 is the intramural peri-arterial drainage pathway. In pathway 2, the perivascular space is occupied by the fused basement membranes of pia mater and glia limitans.

wall.[106] Pathway 2 in **Figure 1.5**[101] illustrates the anatomy described in the Intramural Peri-arterial Drainage (IPAD) pathway model of PVS clearance proposed by Carare et al,[104] who has detailed the microanatomy of PVS. At the arteriolar level, several alternating layers of basement membrane and smooth muscle wrap around the endothelium in a braided, twisting fashion.[100] The IPAD pathway courses through the basement membrane network interspersed between layers of SMCs.[104] The strength of the smooth muscle contractions appears to drive IPAD.[107] Abluminal to the SMCs is an additional basement membrane, adjacent to the pia mater and the pial-glial basement membrane.[104] The order of layers from vessel lumen to parenchyma includes the endothelium, basement membrane, multiple layers of SMCs interspersed by basement membrane, basement membrane, an additional concentric layer of basement membrane, pia mater, basement membrane/PVS, and glia limitans. See **Figure 1.5**. Using tracers injected into the

cisterna magna of rodents, it was demonstrated that the tracers enter the cerebral parenchyma along the pial-glial basement membrane.[104] At the capillary level, interstitial spaces are in continuity with PVS.[104] The essential difference in PVS anatomy in humans across brain regions is that cortical arterioles (originating from the pial surface and leptomeningeal vessels) acquire one layer of pia mater while perforating arterioles of deep subcortical structures and white matter possess two such layers.[108] Such anatomical differences could account for the predominant location of ePVS in areas other than cortex. Anatomical differences could also be a reason for the morphological differences that are often seen on brain MRI between ePVS in the basal ganglia and ePVS in white matter where ePVS in the basal ganglia tend to be larger in diameter (except in rare cases of massively enlarged PVS). See **Figure 1.2 A-B**. Perivascular compartments exist in the cortex along which CSF and solutes enter and exit the brain, but these compartments are thought to be smaller than PVS. Cerebral blood vessels and their BBB are extraordinarily complex and a more thorough understanding of their microstructure and molecular function is needed to increase our understanding of the role PVS play in human brain health and disease.

Perivascular Space Fluid Dynamics

The anatomical descriptions outlined above correspond to two separate models of PVS physiology. The first pathway, visible in **Figure 1.5**, known as the glymphatic model, proposes that CSF enters the brain along para-arterial spaces (highlighted by the black arrows), mixes with interstitial fluid (ISF) in the parenchyma (including metabolic waste products), and exits the brain along para-venous spaces that surround

venules and veins. The PVS in glymphatic drainage are proposed to lie outside SMCs but inside the glia-limitans (astrocytic end-feet) in arterioles and outside the endothelium but inside the glia-limitans of venules.[109] The second pathway in **Figure 1.5**, known as the IPAD model, proposes that CSF from the subarachnoid space infiltrates the brain along the pial-glial basement membrane on the external parts of artery and arteriole walls (highlighted by the green arrows).[100,104] CSF then enters the brain parenchyma at the arteriole level, mixes with ISF and cellular debris, and exits the brain parenchyma along SMC basement membranes of arterioles and arteries.[104] Key similarities and differences between the glymphatic pathway and the IPAD pathway are highlighted in **Table 1.2**.

Table 1.2. Pathway Feature Comparison

Pathway 1: Glymphatic Pathway	Pathway 2: IPAD Pathway
CSF flows into the brain along the PVS of arteries and arterioles, spurred on by vascular smooth muscle cell contractions.	CSF flows into the brain along the PVS of arteries and arterioles, between the pia mater and glia limitans, spurred on by vascular smooth muscle cell contractions.
CSF enters the parenchyma, possibly through aquaporin-4 channels at the arteriole/capillary level	CSF enters the parenchyma, possibly through aquaporin-4 channels at the arteriole/capillary level
CSF mixes with ISF and metabolic waste in the parenchyma	CSF mixes with ISF and metabolic waste in the parenchyma
The CSF/ISF mixture diffuses throughout the parenchyma and crosses into the PVS at the capillary level, possibly through aquaporin-4 channels	The CSF/ISF mixture diffuses throughout the parenchyma and crosses into the PVS at the capillary level, possibly through aquaporin-4 channels
The mixture flows out of the brain along PVS of the venules and veins	The mixture flows out of the brain through the basement membrane network that

	interweaves with smooth muscle cells along arterioles and arteries

CSF can likely freely diffuse into PVS but is driven by a pressure gradient created with CSF production in the ventricles and spurred on by arterial pulsations.[110] At the arteriole or capillary level, CSF is transported across the glia limitans into the parenchyma and Aquaporin-4, a water permeable protein, may play a role in facilitating this fluid transport, although this is still unclear. Once in the parenchyma, CSF mixes with ISF and other waste products and diffuses throughout the parenchyma to reach the BBB at the capillary level. The fluid mixture then crosses into the basement membrane at the capillary level and travels up the IPAD pathway in the arteriole wall, counter-intuitively against the direction of blood flow, or up the para-venous drainage pathway aligned with the direction of blood flow. The mixture of CSF, ISF, and waste then traverses the subarachnoid space to lymphatic vessels to be filtered in cervical lymph nodes.

The fluid dynamics that allow for perivascular drainage against the direction of blood flow is a debated topic but work by Richardson et al. suggests that SMCs produce a contractile wave that travels in the opposite direction of blood flow and forces fluid through the IPAD basement membrane in arterioles, similar to peristalsis.[111] A recent study by van Veluw et al. shows *in vivo* evidence of para-arteriole clearance of nanoparticles in the opposite direction of blood flow[112] (although the data require replication). Additionally, β-amyloid accumulates in the abluminal basement membrane of vascular SMCs in human CAA samples,[113] suggesting an impairment of IPAD.

In addition to the IPAD pathway, evidence suggests PVS around venules and veins play a role in transporting ISF out of the brain. In a mouse model, Nedergaard et al.,[109] showed that tracer injected into the cisterna magna travels into the brain through arterial PVS and appears in venule walls within one hour. Additionally, when tracer is injected directly into the striatum of the brain, it appears in the same PVS compartments of venules.[109] Collectively, these findings provide evidence for para-venous drainage pathways. By contrast, Carare et al.,[104] argue that the primary efflux route for ISF is through IPAD pathways which do not exist in the walls of venules as SMCs and their basement membrane networks are largely nonexistent in venules. Given 30 minutes to flow throughout the system, β-amyloid is primarily deposited in a ring-like structure around SMCs in the IPAD pathways and is almost nonexistent in PVS surrounding venules.[104] This is reminiscent of the ring-shaped pattern of deposition of β-amyloid in the tunica media of cerebral arterioles and leptomeningeal arteries in CAA and suggests a failure of IPAD may contribute to CAA. ePVS visible on MRI are much more likely spaces surrounding arteries or arterioles versus venules or veins for two reasons. First, ePVS that occur in the basal ganglia often track well with penetrating lenticulostriate arteries and second, ePVS in the centrum semiovale are often correlated with CAA-related imaging findings and CAA pathology,[114] conditions primarily affecting arteries and arterioles. Additional evidence of MRI-visible ePVS corresponding to arteries and arterioles was published by Jochems et al. as they showed low spatial overlap between ePVS and venules visible on 3T brain MRI.[115] However, further research is needed to investigate whether ISF efflux can occur along both para-arterial and para-venous pathways simultaneously.

Enlarged Perivascular Spaces

When PVS are visible *in vivo* on MRI they are considered ePVS. ePVS are most common in the centrum semiovale and basal ganglia[116] and, to a lesser extent, in the midbrain and hippocampus. ePVS were long thought to be benign imaging features when visible on *in vivo* neuroimaging or a manifestation of cerebral atrophy. Neuropathologically, they were often considered artifacts of fixation methods, although they can certainly be seen in unfixed, neuropathological specimens. See **Figure 1.3**.[101] ePVS were first described as “etat criblé” in 1842 by Charles Louis Maxime Durand-Fardel to characterize the diffuse ePVS seen in the basal ganglia of some brains. PVS later came to be known as Virchow-Robin spaces when they were characterized in the mid-1800’s by Rudolf Virchow and Charles Philippe Robin.

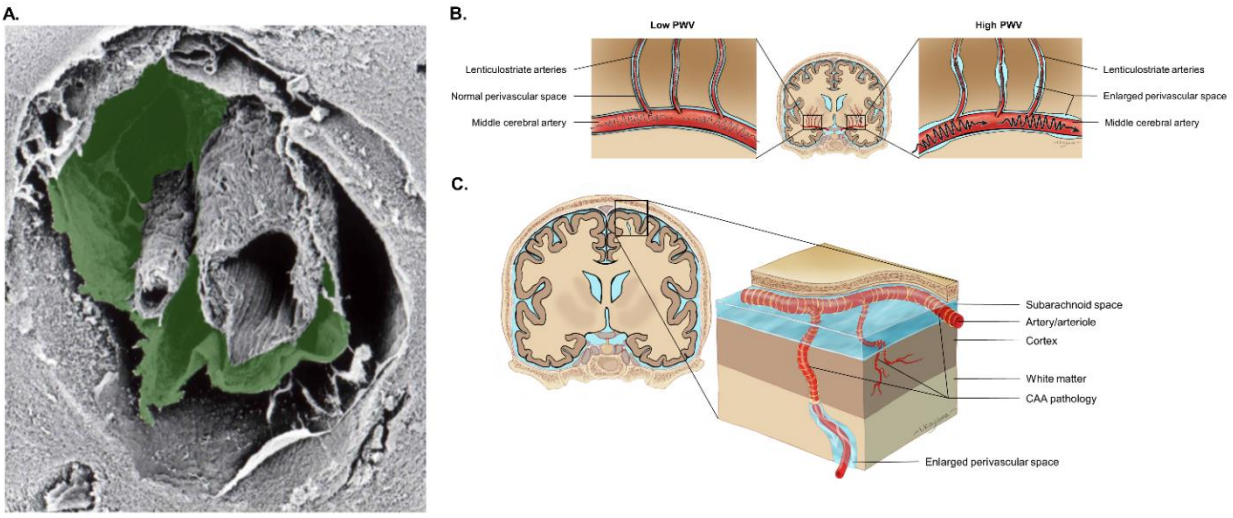

Figure 1.6. ePVS appearance on scanning electron micrograph and theoretical models for PVS enlargement. **(A)** Pictured is scanning electron micrograph of an enlarged perivascular space (the outer layer of pia mater is green) surrounding an artery in the basal ganglia. The enlarged perivascular space appears between two layers of leptomeninges. Image courtesy of Roy Weller, MD, PhD (Weller et al., *Acta Neuropathologica*, 2018). **(B)** Increased aortic pulse wave velocity results in higher pulse waves travelling to perforating arteries of the basal ganglia, resulting in vessel wall damage and enlarged PVS. The tissue boxes illustrate the basal ganglia, where the walls of arteries are subject to pulsatile damage, leaving wider spaces that fill with interstitial fluid and possibly CSF (in blue). **(C)** Increased vascular amyloid accumulation upstream could create a blockage, resulting in enlarged PVS in

Enlarged Perivascular Space Etiology and Pathophysiology

PVS function normally as microscopic routes for fluid and metabolic transport but they can become enlarged and pathologic. See **Figure 1.6 A**.[101,117] While several possibilities exist, two major mechanisms likely contribute to ePVS: arterial stiffening and protein aggregation. These proposed mechanisms are still largely hypotheses that require more concrete evidence, but research to date offers clues as to how these mechanisms play a role in ePVS development. First, arterial stiffening likely contributes to ePVS that develop in the basal ganglia.[118] Arterial stiffening is an early marker of arterial aging that predicts subsequent increase in blood pressure, incident hypertension, and pulsatility.[119] PWV is a measure of arterial stiffness associated with ePVS burden in the basal ganglia.[118] This association may be because higher pulse

waves lead to vessel wall damage and remodeling[120] that result in larger ePVS around cerebral arteries and arterioles. See **Figure 1.6 B**[101] for illustration. The perforating arteries feeding the basal ganglia may be particularly vulnerable to damage from higher pulsatility.[119] Another potential consequence of arterial stiffening is reduced vasomotion. With the vessel wall thickening and elastin loss that occurs with arterial stiffening, the SMC contractile phenotype may become impaired and at late stages may be lost entirely. SMCs may play a key role in the efflux of metabolic waste from the parenchyma, so their impairment may result in a failure to eliminate waste, creating build-up that further drives PVS enlargement.

Second, abnormal protein aggregation, such as β-amyloid, can clog up the system upstream within the cortical arteries and block the drainage of ISF in the deep underlying white matter (See **Figure 1.6 C**). There is strong evidence that CAA severity is associated with the number and extent of ePVS.[121] The relationship has also been seen between β-amyloid measured on positron emission tomography (PET) and ePVS in the centrum semiovale,[122] and ePVS in the centrum semiovale are increasingly recognized as a marker of CAA.[114] In perhaps some of the most compelling evidence, one study showed ePVS associations with β-amyloid load in the cortex and CAA severity in human pathology samples[123] while another study related juxtacortical ePVS on brain MRI to CAA severity in overlying cortical areas stained positively for β-amyloid.[124] In the latter study, representative samples were taken from each participant for each level of ePVS severity score for further histopathological evaluation. More severe ePVS burden was significantly associated with more severe CAA pathology (cumulative odds ratio=3.3).[124] The perivascular compartment may be more susceptible

to enlargement in white matter due to lower cellular density compared to grey matter, while the compact nature of the grey matter does not allow ePVS to occur.

While the two pathways outlined above are potential pathological drivers of ePVS, the possibility also exists that ePVS seen *in vivo* on MRI may not reflect any PVS pathology but instead may be due to atrophy of surrounding tissue. That is, when tissue degenerates, spaces between blood vessels and brain tissue could enlarge and become visible on MRI as ePVS. However, it is important to note that areas in which ePVS primarily develop (i.e., basal ganglia, centrum semiovale) do not overlap with brain regions most susceptible to atrophy. Albeit less often, ePVS develop in regions that often atrophy with aging and disease, such as the white matter of the temporal pole, but ePVS in these regions can more likely be attributed to double-layered leptomeninges that allow edema fluid to collect between the two layers. Thus, the plausibility is low that ePVS seen on MRI are due to brain atrophy. Still, other mechanisms driving PVS enlargement may be at play, such as inflammation or oxidative stress due to perivascular macrophage activation or microglia activation.

Enlarged Perivascular Space Risk Factors

Several demographic, genetic, and vascular health factors are associated with increased ePVS. First, the largest risk factor for ePVS is advancing age, and many older adults have one or more ePVS on *in vivo* neuroimaging. Age correlates with ePVS burden in both the basal ganglia and centrum semiovale,[125] but associations tend to be strongest in the basal ganglia. Limited evidence suggests regional vulnerabilities to ePVS by sex whereby females are susceptible to hippocampal ePVS burden and males

are susceptible to white matter ePVS burden.[126] PVS play an important role in metabolic waste clearance particularly during sleep.[127] Recently, Del Brutto et al. showed that poor sleep efficiency was associated with basal ganglia ePVS in a population study of older adults.[128] Opel et al. provided further evidence of associations between worse sleep and greater ePVS burden, particularly among participants with a history of traumatic brain injury.[129] Therefore, poor sleep quality may be an additional risk factor for ePVS.

Some data suggests ePVS are heritable, but specifics have yet to be elucidated.[130] *APOE*-ε4 might be one genetic risk factor for ePVS formation but findings to date are mixed. In one study of older adults, *APOE*-ε4 carrier status was associated with greater ePVS in the basal ganglia.[131] However, a study of 520 patients referred for memory evaluations found no association between *APOE*-ε4 and ePVS.[132] Interestingly, when genetic risk variants for WMH volume (a purported marker of SVD) were combined into a polygenetic risk score, genetic risk for WMH volume was associated with basal ganglia ePVS.[130] Additional research is warranted to understand possible genetic links to ePVS development and progression.

Among vascular health factors, hypertension is the most prominent risk factor for ePVS, particularly in the basal ganglia. Hypertension is often synonymous with arterial stiffening since arterial stiffening leads to higher blood pressure, pulsatility, and increased tissue damage. Higher systolic blood pressure is associated with ePVS in the basal ganglia but not the centrum semiovale.[133] Since ePVS are a marker of SVD, other vascular risk factors such as diabetes, smoking, and hypercholesterolemia, might

presumably play a role in ePVS development. However, few studies have examined how these risk factors are associated with ePVS.

While age and hypertension are two well supported risk factors for ePVS, additional risk factors likely exist. As studies emerge utilizing more robust ePVS quantification methods, it is probable that additional risk factors will be discovered and delineated.

Rationale and Aims

AD and related dementias are an increasing public health issue. Cerebral SVD is the most common pathology to co-occur with AD, contributing to over 80% of all autopsy-confirmed dementia cases. ePVS are a common form of SVD in aging adults, seen on MRI as small cylindrical spaces. PVS reflect extensions of the subarachnoid space surrounding blood vessels perfusing the brain.[103]

The etiology of ePVS remains poorly understood despite emerging evidence suggesting ePVS have clinical relevance.[97,134,135] Recent data shows increased basal ganglia ePVS burden is associated with hypertension,[136] a marker of age-related vascular damage. However, arterial stiffness is an earlier marker of arterial aging that predicts subsequent blood pressure increase[137] and incident hypertension.[57,58] Arterial stiffness drives elevated blood pressure and pulsatility,[119] and failure to dampen rising pulsatility results in uncontrolled hypertension.[138,139] Aortic PWV is a well-established imaging marker of arterial stiffening that may better reflect the underlying etiology of ePVS. Arterial stiffening drives the transmission of damaging pressure waves to the microvasculature and adjacent tissue, which results in ePVS morphologic changes. The

perforating arteries of the basal ganglia are particularly susceptible to increased pulsatility[119] due to their proximal location to the Circle of Willis.[140] Therefore, increased pulsatility may be an essential etiology of ePVS burden in the basal ganglia. This project tested whether arterial stiffening, assessed using the gold standard measurement of PWV on cardiac MRI, contributed to longitudinal ePVS burden in the basal ganglia. Other predictors such as age, hypertension medication usage, inflammatory markers, sleep quality, and AD-related CSF biomarkers were also tested.

Historically, ePVS have been regarded as benign,[116] but increasing evidence, including our work,[97] suggests ePVS have important clinical relevance.[134,135] The basal ganglia, a region particularly vulnerable to ePVS in aging, facilitates information processing and executive function through reciprocal frontal-subcortical networks.[48] Our recent cross-sectional work found basal ganglia ePVS burden (quantified using a 5-point ordinal rating system) compromises these abilities in aging adults.[97] This research project applied a sophisticated deep learning algorithm to quantify total ePVS volume. Given the clinical relevance of ePVS cross-sectionally,[97,135] it is critical to understand how these spaces relate to cognitive trajectory. I applied the algorithm to examine the impact of ePVS volume and count on longitudinal cognitive trajectory.

APOE-ε4 is the strongest genetic susceptibility risk factor for sporadic AD and a moderator of vascular damage. Previous work from my mentor suggests arterial stiffness as measured by PWV interacts with *APOE*-ε4 on brain health outcomes such that higher PWV is associated with worse cognition[141] and lower cerebral blood flow delivery in ε4 carriers.[75] It is plausible that *APOE*-ε4 and arterial stiffness act synergistically to damage the basal ganglia vasculature, resulting in greater regional

ePVS. Given ePVS burden is increased in clinical AD,[102] it is essential to understand whether *APOE*-ε4 affects the etiology or clinical impact of ePVS.

The overarching objective of this project was to determine if ePVS in the basal ganglia are (a) the result of increased pulsatility and (b) associated with worse longitudinal information processing and executive function trajectory. Secondarily, I assessed if associations were exacerbated by the presence of the *APOE*-ε4 allele. This research leveraged the Vanderbilt Memory and Aging Project, a longitudinal study of older adults undergoing serial evaluations over a 7-year period, including cardiac MRI, multi-modal brain MRI, and neuropsychological assessment. Utilizing exceptional resources and an automated ePVS quantification method designed for T_1-weighted and T_2-weighted fluid attenuated inversion recovery brain MRI sequences, I investigated the following aims:

Aim 1: Determine if arterial stiffness is an etiology of ePVS and if APOE-ε4 moderates this association. I hypothesized that baseline aortic PWV would be associated with a longitudinal increase in ePVS volume and count in the basal ganglia. Secondarily, I tested whether baseline PWV interacted with *APOE*-ε4 status on longitudinal ePVS change hypothesizing that greater PWV would be associated with increased ePVS volume among ε4 carriers.

Aim 2: Characterize the longitudinal clinical consequences of ePVS and determine if *APOE*-ε4 moderates these outcomes. I hypothesized that baseline ePVS volume in the basal ganglia would be associated with worse information processing and executive function trajectory over the 7-year follow-up. Secondarily, I tested whether baseline ePVS volume in the basal ganglia interacted with *APOE*-ε4

status on longitudinal cognition hypothesizing that greater ePVS burden would be related to worse cognitive trajectory among ε4 carriers. I also tested if age, hypertension medication usage, inflammation, sleep quality, and AD pathology were predictive of longitudinal increase in ePVS burden.

This work provides us with critical information about the etiology, clinical consequences, and relevance of ePVS, especially in the presence of *APOE*-ε4, which may lead to future therapeutic targets for reducing the clinical impact of these spaces.

CHAPTER 2

ENLARGED PERIVASCULAR SPACE QUANTIFICATION

Introduction

Enlarged perivascular spaces (ePVS) can be pervasive in affected brain regions and difficult to track through brain magnetic resonance imaging (MRI) slices, making manual quantification difficult. To date, semi-quantitative methods (i.e., ordinal scale ratings) have been the most widespread method for assessing ePVS severity. One of the most commonly used systems is the Patankar et al.,[142] scale which rates ePVS separately in the basal ganglia and centrum semiovale. Another similar quantification method is by Hansen et al.,[143] which was adapted from Doubal et al.[116] Using this method, scores are assessed separately for the centrum semiovale and the basal ganglia. For both regions, the slice and side with the most ePVS is manually identified and scored. These ordinal rating systems are an efficient option for manually coding large datasets, but they minimize individual variation between participants, introduce ceiling effects, and restrict longitudinal ePVS assessment. In practice, the Patankar and Hansen manual systems are efficient for capturing ePVS variability if comprehensive automated or semi-automated methods are unavailable.

Fortunately, newer methods are emerging that allow for automated and improved semi-automated quantification of ePVS, making continuous measurements, rather than just ordinal counts, possible. As one example, Boespflug et al., established an

automated method that performs a voxel-wise comparison between multiple image sequences to identify voxels that resemble ePVS.[144] By incorporating multiple sequences, including T_1-weighted, T_2-weighted, fluid attenuated inversion recovery, and proton density, a more robust decision can be made about ePVS coding. Voxel intensities are used to identify potential ePVS and then the morphology of identified voxel clusters is used to decide if the cluster is an ePVS.[144] The Boespflug et al. method offers an excellent opportunity for quantifying ePVS total volume and count throughout entire brain regions. While this method requires access to multiple MRI sequences, it offers a more comprehensive picture of ePVS burden throughout the brain. Another promising method segments ePVS using 3-dimensional filtering.[145] An ordered logit model and prior ordinal visual ratings of ePVS burden inform how many ePVS likely exist within a given brain. Frangi filtering (suited for identifying vessel-like structures) parameters and thresholds are applied to T_1-weighted images to identify ePVS. Ordinal visual ratings, such as the Hansen or Patankar scores, are then cross-referenced in the model to optimize the filtering parameters using the likelihood of the image having a given ePVS quantity. In summary, introducing and refining automated, quantitative, and reproducible measures of ePVS burden will lead to a better understanding of the etiology and clinical consequences of ePVS. Semi-automated assessment of ePVS burden will also allow for a more comprehensive view of a patient's clinical picture.

While semi-automated ePVS assessment methods can be helpful tools for clinicians, more fully automated methods that only require one or two MRI sequences and minimal manual coding are being developed. Our group and others[146] are applying deep learning methods to segment ePVS and acquire volume and count measures

throughout the entire brain. Such methods require a minimum of 50 manually coded images as a training and testing dataset, but once a model is successfully trained and tested, ePVS volume and count measures can be generated in a matter of minutes. Deep learning for ePVS quantification may be the easiest and most efficient way for clinicians to comprehensively assess ePVS burden throughout the brain.

Leveraging machine learning approaches in segmentation and analysis of radiological images is becoming increasingly popular as datasets increase in size and more powerful computational resources become more accessible.[147] Patch-based deep learning U-nets have proven exceptionally accurate in image segmentation[148] and are utilized here to segment ePVS, a form of cerebral small vessel disease.

ePVS have been notoriously difficult to quantify due to their small size (often just a few millimeters in length and diameter), diffuse distribution, and often vast prevalence throughout the brain. Semi-quantitative approaches have been most commonly used, and these methods typically involve selecting one image slice, counting ePVS in particular regions, and then applying an ordinal scale.[116,142,143] Semi-quantitative methods suffer from ceiling effects, place equal weighting on ePVS of different sizes, and lack the ability to adequately assess ePVS longitudinal change, so opting for a robust continuous measure would be advantageous. Semi- and fully-automated approaches using multiple MR imaging sequences, filtering methods, and regression models have also been utilized; however, these methods do not segment entire brain regions,[149] they rely on interpolation,[145] and they perform poorly in brain regions with high image intensity variability, such as the basal ganglia.[144] To better understand potential etiologies of ePVS[150] and downstream clinical consequences,[97,151,152] the

creation and validation of a reliable and less time-consuming continuous measure of ePVS is needed.

We hypothesized that a deep learning U-net trained on quality data would accurately segment ePVS in T_1-weighted brain MR images. We additionally hypothesized that an automated method for quantifying ePVS volume and count would offer a more robust and accurate method for determining overall ePVS burden compared to predominantly used ordinal scores, while minimizing manual effort needed to quantify ePVS burden and allowing for quantification of ePVS longitudinal change.

Methods

Study Cohort

The Vanderbilt Memory and Aging Project is a longitudinal study assessing connections between brain aging and vascular health in older adults.[74] The current study utilized the Vanderbilt Memory and Aging Project Legacy Cohort. Inclusion in the original study required participants to be ≥60 years of age, have intact visual and auditory functions, speak English, and have a consistent study partner. Eligible participants underwent an interview (including a daily activities questionnaire and Clinical Dementia Rating),[153] a neuropsychological evaluation to assess cognitive health, and medical history review. Exclusion criteria from the original study included: a cognitive diagnosis other than normal cognition, early mild cognitive impairment, or mild cognitive impairment; previous neurological disease (e.g., stroke, epilepsy); clinical heart failure; MRI contraindication; major psychiatric illness (e.g., schizophrenia); head injury with a loss of consciousness for >5 minutes; and a systemic or terminal illness

affecting future participation in the study. This study leverages data collected at enrollment (September 2012-November 2014), as well as at 18-month, 3-year, 5-year, and 7-year follow-up visits, including a clinical interview, fasting blood draw, physical examination, medication review, neuropsychological assessment, echocardiogram, cardiac magnetic resonance (CMR) imaging, and brain MRI. Participants with missing cardiac MRI, brain MRI, covariate, or neuropsychological data were excluded listwise from specific models employing those variables.

Standard Protocol Approvals, Registrations, and Participant Consents

The protocol was approved by the Vanderbilt University Medical Center Institutional Review Board. Written informed consent was obtained prior to data collection. Due to participant consent restrictions in data sharing, a subset of data is available for purposes of reproducing results or replicating procedures. Data, analytic methods, and study materials can be obtained by contacting the corresponding author.

Brain MRI

Participants (n=327) were scanned at the Vanderbilt University Institute of Imaging Science on a 3T Philips Achieva system with an 8-channel SENSE receiver head coil. T_1-weighted MPRAGE (1x1x1mm^3) and T_2-weighted fluid-attenuated inversion recovery (FLAIR, .45x.45x4 mm^3) images were taken.

ePVS Quantification Method

Image Pre-Processing

T_1-weighted and FLAIR images were co-registered. T_1-weighted images were segmented into regions of interest using Multi-Atlas Segmentation.[154] FSL FAST was used for bias-field correction of T_1 images.[155] Multi-Atlas Segmentation regions of interest were combined to create T_1 basal ganglia and white matter masks. Then, a histogram-based normalization technique known as Nyúl Normalization was applied to T_1 images.[156]

Manual Quantification

Manual ePVS voxelwise segmentations of the entire basal ganglia and white matter were performed on 50 T_1-weighted images (CWB) with final edits applied by a

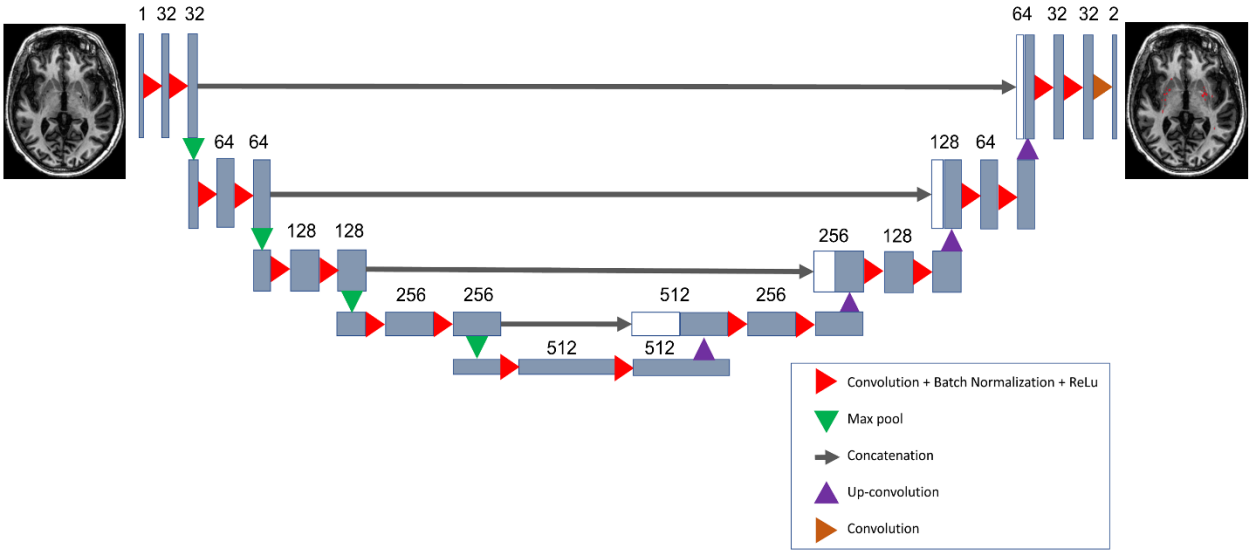

Figure 2.1. Architecture for deep learning U-net model. Displayed is the architecture for the deep learning model that was trained to autonomously segment ePVS using a T_1-weighted brain MR image. The architecture consists of multiple convolutional neural network steps along with a series of max-pooling and up-convolution steps (numbers above steps represent the number of 2D or 3D kernels). Each max-pooling and up-convolution pair also consists of a concatenation step to help maintain spatial specificity. The activation for all convolution layers is ReLU except for the final convolution which uses a sigmoid activation. The final convolution step outputs a binary map indicating ePVS versus no ePVS for every single voxel. ePVS, enlarged perivascular space.

board-certified neuroradiologist (LTD). FLAIR images were consulted to ensure lacunes and white matter hyperintensities (WMHs) were not mistaken for ePVS. If the lesion had a signal on the T_1 scan nearing cerebrospinal fluid (CSF) and appeared hypointense on FLAIR with a rim of hyperintensity, it was identified as a lacune, not an ePVS. Segmentation primarily occurred using axial slices, but coronal slices were consulted as needed to assess the morphology of a potential ePVS.

Model Architecture and Training

We implemented a U-Net architecture, previously described by Remedios et al.,[148] with a series of four down convolution blocks and four up convolution blocks, along with concatenation steps at each level to help the model retain maximum spatial resolution (see **Figure 2.1**). Training was performed on 2D patches for the basal ganglia and 3D patches for white matter derived from 40 of the original 50 manually segmented images. Patch dimensions were chosen based off model performance on the test set. The remaining 10 images were used for testing the model. The learning rate was set at $1x10^{-4}$ with the Adam optimizer[157] and Dice coefficient was used as the loss function. Convergence was achieved once the model completed 10 epochs without improving by more than $1x10^{-4}$ on the validation set. The final output was the probability for whether each voxel represents ePVS [0,1]. The output threshold was set at 0.5. Due to differences in tissue intensity between basal ganglia structures and white matter, basal ganglia and white matter were split into separate images using masks, and two separate models were created. For the basal ganglia model, 64 x 64 voxel patches, representing a portion of an axial slice, were used with a batch size of 100 and one channel (T_1 voxel intensity). For the white matter model, 32 x 32 x 32 patches were

used with a batch size of 100 and two channels (T_1 and WMH mask derived from the FLAIR image).

Automated Segmentation

The two models created with the training data (i.e., the basal ganglia and white matter models) were used to segment remaining baseline MR images (n=277 for basal ganglia and n=162 for white matter). Probability thresholding maps of ePVS were generated and final edits were performed. Voxel dimensions were 1 mm^3, so the total segmented ePVS voxels gives the volume in mm^3. To obtain the total ePVS count for an entire brain region, we used a MATLAB (MathWorks, Natick, MA) script to identify clusters of ePVS voxels using a 26-connectivity parameter, and the resulting clusters were then counted.

Basal Ganglia ePVS Ordinal Rating

Ordinal basal ganglia ratings using both Hansen et al., 2015[143] and Patankar et al., 2005[142] were applied to all baseline T_1 images. ePVS that persisted through two or more slices were counted as a single ePVS. The Hansen method involved selecting a basal ganglia axial slice with the most apparent ePVS and then counting the number of ePVS on that slice. The Hansen score was coded as follows: 0=no ePVS present, 1=1-10 ePVS, 2=11-20 ePVS, 3=21-30 ePVS, and 4=>30 ePVS. The Patankar score considers regional variations in ePVS and involves selecting the basal ganglia axial slice with the most apparent ePVS and counting ePVS in particular regions. The Patankar score is coded as follows: 0= ePVS only present in the substantia innominate and fewer than 5 on either side, 1= ePVS only in the substantia innominate and more than 5 ePVS on either side, 2= fewer than 5 ePVS in the lentiform nucleus on either

side, 3= 5-10 ePVS in the lentiform nucleus or fewer than 5 in the caudate nucleus on either side, 4= more than 10 in the lentiform nucleus and fewer than 5 in the caudate nucleus on either side, and 5= more than 10 in the lentiform nucleus and more than 5 in the caudate nucleus on either side.

Neuropsychological Assessment

Participants underwent a comprehensive neuropsychological protocol at each time point, including Boston Naming Test,[158] Animal Naming,[159] WAIS-IV Coding,[160] DKEFS Number Sequencing,[161] DKEFS Tower Test,[161] DKEFS Color-Word Inhibition,[161] DKEFS Number-Letter Switching,[161] Letter Fluency (FAS),[162] Hooper Visual Organization Test,[163] Biber Figure Learning Test,[164] and California Verbal Learning Test-II.[165] Measures were chosen to minimize floor or ceiling effects and were not utilized for participant selection, screening, or diagnosis. Z-scores were initiated for episodic memory and executive function performances to minimize multiple comparisons. Bifactor latent variable models which fit the data well (i.e., root mean square error of approximation: 0.03 for executive function and 0.09 for memory) were created by leveraging item-level data from DKEFS Tower Test, DKEFS Color-Word Inhibition, DKEFS Number-Letter Switching, and Letter Fluency for the executive function composite as well as the Biber Figure Learning Test and California Verbal Learning Test-II for the episodic memory composite.[5]

Analytical Plan

Covariates

Systolic blood pressure was calculated as the mean of two measurements. Diabetes mellitus was defined as fasting blood glucose ≥126 mg/dL, hemoglobin A1C≥6.5%, or oral hypoglycemic medication or insulin use. Left ventricular hypertrophy wad determined using echocardiogram (left ventricle mass index >95 g/m^2 in women, >115 g/m^2 in men). Anti-hypertensive medication utilization was documented using medication review. Prevalent cardiovascular disease (CVD) from self-report with supporting medical record evidence included angina, coronary heart disease, or myocardial infarction (heart failure was a parent study exclusion). Self-reported atrial fibrillation was validated by one or more of the following sources: echocardiogram, CMR, documented prior atrial fibrillation ablation/procedure, or relevant medication usage. Current cigarette smoking (within one year prior to baseline) was identified by self-report. Framingham Stroke Risk Profile (FSRP) score was determined by calculating points by sex for age, systolic blood pressure accounting for anti-hypertensive medication usage, diabetes mellitus, current cigarette smoking, CVD, atrial fibrillation, and left ventricular hypertrophy. Apolipoprotein E (*APOE*) genotyping was performed using DNA extracted from whole blood samples, and *APOE*-ε4 carrier status was defined as positive (ε2/ε4, ε3/ε4, ε4/ε4) or negative (ε2/ε2, ε2/ε3, ε3/ε3).

Deep Learning Model Performance

Dice coefficient,[166,167] Pearson correlation coefficient,[168] and mean symmetric surface distance[169,170] were used as metrics for comparing ground-truth ePVS segmentations to predicted segmentations. These statistical tools help determine how

well the automated model is performing at predicting ePVS pathology. Dice coefficient (**Equation 1**) is calculated using the following equation,

$$DSC = \frac{2|X \cap Y|}{|X| + |Y|} \quad [1]$$

which takes twice the number of coded ePVS voxels from both the ground-truth and predicted sets and divides by the sum of the number of coded ePVS voxels in each set. Volume correlations between ground-truth and predicted segmentations were assessed using a Pearson correlation coefficient. Mean symmetric surface distance calculations were performed by finding the average distance between ground-truth and predicted sets of coded ePVS voxels. Each ePVS voxel from the manual ground-truth segmentation was matched to an ePVS voxel from the model predicted segmentation, minimizing the distance between voxels, and then the average of all distances is calculated. Two separate values were derived by first comparing the ground-truth image to the predicted image and then comparing the predicted image to the ground-truth image. Comparisons are run both ways because a given ground-truth voxel may be closest to a given predicted voxel but that given predicted voxel may be closest to a separate ground-truth voxel and therefore the distance metric would vary depending on the direction of comparison. The average of those two values was calculated to achieve the final mean symmetric surface distance value for a set of ePVS codings.

ePVS Segmentation Reliability

Reliability statistics were performed on samples of 5-10 images to determine how consistent two independent raters can be when segmenting ePVS as well as how consistent a single rater can be when segmenting ePVS in the same image at two different timepoints. Inter-rater Dice similarity coefficient, volume correlation, and mean

symmetric surface distance were calculated between two trained raters (CWB and L. Taylor Davis, MD) who performed fully manual ePVS segmentation on 5 basal ganglia images and 10 white matter images. Intra-rater Dice similarity coefficient, volume correlation, and mean symmetric surface distance were calculated between two separate coding sessions for a trained rater (CWB) who performed fully manual ePVS segmentation in the basal ganglia. To assess the reliability of edits performed on ePVS maps output from the deep learning U-net model, inter-rater Dice similarity coefficient, volume correlation, and mean symmetric surface distance were calculated between two trained raters (CWB and L. Taylor Davis, MD) who performed edits to 5 basal ganglia ePVS maps.

Maximizing Model Quality with Given ePVS Predictor Variables

To determine the ePVS predictor or combination of predictors with the most predictive utility, ePVS volume and count (derived using the automated method described above) were combined with and compared to previously established ePVS ordinal scores (Patankar et al., 2005;[124] Hansen et al., 2015)[143] on outcomes of longitudinal cognition. Each of the four ePVS predictors (i.e., ePVS volume, ePVS count, Patankar et al., 2005 ordinal score, Hansen et al., 2015 ordinal score) were used individually or in combination with one another to create 15 unique predictor combinations. Mixed-effects regression models were used to assess associations between each of the 15 predictors and seven cognitive outcomes (with one predictor and outcome combination per model). Models were adjusted for baseline age, sex, race/ethnicity, education, baseline FSRP (excluding points for age), baseline cognitive status, *APOE*-ε4 carrier status, and baseline intracranial volume. Covariates were

selected a priori based on known associations with brain health and cognition, previously described in greater detail.[6] Next, Akaike information criterion (AIC)[171] and Bayesian information criterion (BIC)[172] values were utilized to determine the most advantageous combination of ePVS volume, ePVS count, Patankar et al., 2005 ordinal score and Hansen et al., 2015 ordinal score for predicting longitudinal cognitive trajectory. AIC was calculated as (**Equation 2**):

$$AIC = -2(\text{log-likelihood}) + 2K \quad [2]$$

where K is the number of model parameters and log-likelihood is a measure of model fit. BIC was calculated as (**Equation 3**):

$$BIC = -2(\text{log-likelihood}) + \log(N)*K \quad [3]$$

where N is the number of observations. Comparisons were made between the 15 predictors for a single cognitive outcome at a time.

Selecting ePVS Predictor Variable to Maximize Predictive Utility

Lastly, we wanted to determine which ePVS variable would be the most useful in future analyses aimed at determining the clinical consequences of ePVS. Pseudo-conditional R^2 values were calculated using the r.squaredGLMM function from the MuMIn (version 1.40.4) package in R for each model to determine which ePVS predictor accounted for the most variance in the longitudinal cognitive outcomes. All analyses were conducted using R 3.5.2 (www.r-project.org).

Assessing ePVS Volume Variability in Participants with the Same Ordinal Score

To evaluate the level of variability that can be missed when using an ordinal measure versus a continuous measure, we assessed the range of ePVS volumes that existed within a subset of participants with the same Hansen et al., 2015 ordinal score.

Results

Participant Characteristics

Participants included 327 adults (73±7 years, 59% male, 87% non-Hispanic White). See **Table 2.1**. Forty images were used for training the U-Net, 10 images were used for testing, and the remaining 277 images were segmented using the U-Net model. Basal ganglia ePVS volumes ranged 43-1177 mm^3 (237±172), and white matter ePVS volumes ranged 5-3869 mm^3 (442±426). Mean follow-up time for the longitudinal cognitive assessments was 5.2±1.7 years.

Table 2.1. Baseline Participant Characteristics

	Total n=327	NC n=169	eMCI n=27	MCI n=131	Test Statistic
Demographic and Health Characteristics					
Age, years	73±7	72±7	73±6	73±8	p=0.67
Sex, % male	59	58	74	56	p=0.23
Race, % non-Hispanic White	87	87	85	86	p=0.96
Education, years	16±3	16±3	16±3	15±3	**p<0.001**
APOE-ε4, % carrier	35	30	22	44	**p=0.01**
Montreal Cognitive Assessment	25.3±3.3	27.0±2.2	25.4±2.4	23.1±3.4	**p<0.001**
Intracranial Volume, mm^3	1506±150	1502±152	1541±123	1504±154	p=0.39
Framingham Stroke Risk Profile, total	12.5±4.2	12.0±4.3	13.6±3.4	12.9±4.3	p=0.05
Systolic blood pressure	143±18	140±17	150±18	145±19	**p=0.005**
Antihypertensive medication use, %	54	53	56	56	p=0.91
Diabetes, %	18	16	22	21	p=0.51
Cigarette smoking, % current	2	2	4	3	p=0.70
Prevalent CVD, %	5	6	4	3	p=0.49
Atrial fibrillation, %	7	6	11	7	p=0.60
Left ventricular hypertrophy, %	4	3	4	6	p=0.41
Ordinal Neuroimaging Variables					
ePVS Hansen Basal Ganglia Score, %					p=0.42
1	56	60	44	53	
2	38	36	52	38	
3	5	4	4	6	
4	2	1	0	3	
ePVS Patankar Basal Ganglia Score, %					p=0.36
1	0	0	0	0	
2	8	7	7	9	
3	44	48	33	41	
4	21	20	37	19	
5	27	25	22	31	
Automated Neuroimaging Variables					
ePVS Volume Basal Ganglia, mm^3	237±173	213±140	236±133	267±211	p=0.70
ePVS Volume White Matter, mm^3	442±426	387±322	779±895	442±367	p=0.13
ePVS Count Basal Ganglia, total	60±36	56±34	63±30	65±40	p=0.09
ePVS Count White Matter, total	147±102	133±81	218±184	150±99	p=0.16

Neuropsychological Baseline Outcomes					
Boston Naming Test	26.7±3.2	27.9±2.0	26.6±2.4	25.3±3.9	**p<0.001**
Animal Naming, total	18.9±5.4	20.9±4.8	19.4±3.4	16.2±5.2	**p<0.001**
WAIS-IV Coding	53±13	57±12	53±11	46±12	**p<0.001**
DKEFS Number Sequencing, seconds	43±21	36±13	42±13	52±26	**p<0.001**
Executive Function Composite	0.009±0.89	0.44±0.61	0.17±0.42	-0.58±0.94	**p<0.001**
Hooper Visual Organization Test	24.4±3.1	25.3±2.5	24.7±2.2	23.2±3.6	**p<0.001**
Episodic Memory Composite	-0.02±0.96	0.56±0.72	-0.06±0.76	-0.75±0.75	**p<0.001**
Neuropsychological Annual Change Outcomes					
Boston Naming Test	-0.23±0.90	-0.005±0.42	-0.16±0.68	-0.57±1.3	**p<0.001**
Animal Naming, total	-0.51±1.20	-0.23±0.97	-0.97±1.7	-0.82±1.3	**p<0.001**
WAIS-IV Coding	-1.35±2.87	-0.65±1.5	-0.41±2.7	-2.59±3.9	**p<0.001**
DKEFS Number Sequencing, seconds	3.12±9.86	1.24±3.3	1.55±2.9	6.25±15	**p<0.001**
Executive Function Composite	-0.09±0.20	-0.04±0.10	-0.07±0.15	-0.16±0.29	**p=0.004**
Hooper Visual Organization Test	-0.21±0.91	-0.05±0.41	-0.14±0.30	-0.46±1.4	**p=0.02**
Episodic Memory Composite	-0.05±0.17	0.0004±0.14	-0.14±0.25	-0.09±0.17	**p<0.001**
CSF Biomarker Baseline Outcomes					
$A\beta_{40}$	6151±1635	6268±1740	6494±1868	5894±1390	p=0.60
$A\beta_{42}$	549±265	600±255	695±368	437±206	**p<0.001**
Tau	426±227	373±175	429±125	502±288	**p=0.01**
P-tau	61±26	56±22	63±30	65±40	p=0.09
sTREM2	3675±1818	3551±1869	4053±2002	3754±1704	p=0.48
MMP2	70029±16563	68210±17444	77135±15057	70744±15310	p=0.12
MMP3	313±166	293±161	422±230	311±144	p=0.11
MMP9	121±87	119±82	121±66	125±99	p=0.81
Blood Biomarker Baseline Outcomes					
TNF-α	6.2±2.9	6.1±3.1	5.9±2.3	6.5±2.7	p=0.39
IL-6	3.8±4.3	3.9±5.0	2.9±1.6	3.9±3.5	p=0.37

Note. Values denoted as mean±SD or frequency. *APOE*-ε4 indicates apolipoprotein E ε4 allele. CVD, cardiovascular disease. DKEFS, Delis-Kaplan Executive Function System. eMCI, early mild cognitive impairment (ambiguous at risk). Aβ, amyloid beta. ePVS, enlarged perivascular space. IL-6, interleukin 6. MCI, mild cognitive impairment. MMP, matrix metalloproteinase. NC, normal cognition. P-tau, phosphorylated tau. sTREM2, soluble triggering receptor expressed on myeloid cells 2. TNF-α, tumor necrosis factor alpha. WAIS, Wechsler Adult Intelligence Scale. *****A modified Framingham Stroke Risk Profile Score was included in statistical models, which excluded points assigned to age (total=6.6±3.1).

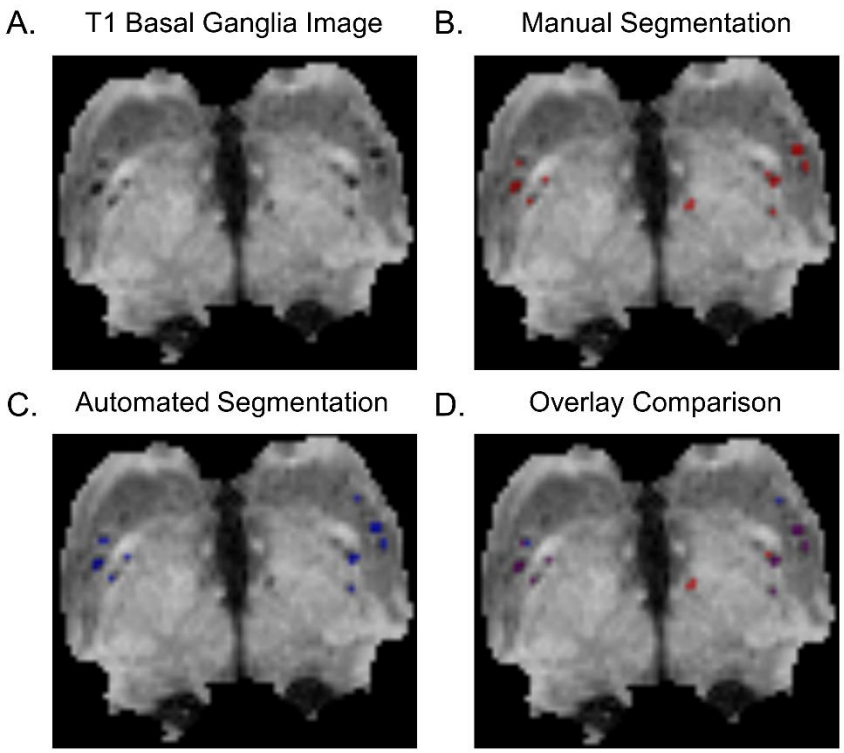

Figure 2.2. ePVS appearance in T_1-weighted axial slices of the basal ganglia and U-net model performance. Displayed is an axial slice of the basal ganglia with numerous visible ePVS (yellow arrows). Images consist of **(A)** the original T_1 image, **(B)** the manual segmentation performed by a trained rater (red), **(C)** the segmentation created by the deep learning model (blue), and **(D)** the overlap between manual and automated segmentation (purple). ePVS, enlarged perivascular space.

Qualitative Evaluation

Most voxels that were of similar intensity to CSF (i.e., hypointense), indicating a likely ePVS, were correctly labelled as such (see **Figures 2.2 and 2.3**). Occasionally, the algorithm missed calling extremely low intensity (i.e., equal to or darker than CSF) voxels that are likely ePVS (see **Figure 2.3 B**). However, most errors made by the algorithm occurred among voxels with intensities between CSF and grey matter voxel intensities (see **Figure 2.3 C**). That is, voxels with similar intensity to the cutoff intensity for what was and was not an ePVS were difficult for the algorithm to label correctly. These algorithmic errors arose from the fact that voxels around the ePVS cutoff intensity level were also difficult for the manual raters to label correctly.

The algorithm performed well when ePVS were larger than 1 mm in diameter, when ePVS were isointense with CSF, and when ePVS occurred in common anatomical regions, such as the caudate, putamen, and white matter, away from border zones (see **Figure 2.3**). Manual segmentation of ePVS throughout the entire brain took 25 to 60 minutes depending on the severity of disease. Edits to model outputs took 5 to 12 minutes (measured across a sample of

5 images). The amount of time saved utilizing the automated segmentation is anywhere from 20 to 50 minutes per image.

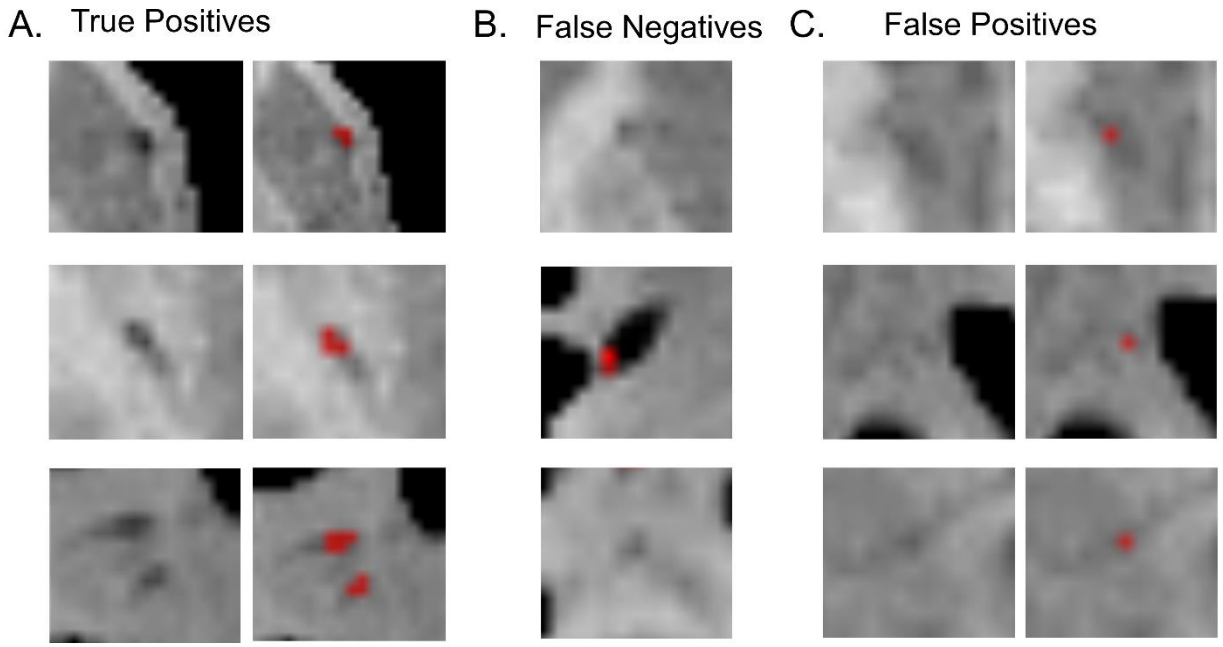

Figure 2.3. U-net model performance in the basal ganglia and white matter. Displayed are patches from axial basal ganglia and white matter slices that represent **(A)** true positive model segmentations, **(B)** false positive model segmentations, and **(C)** false negative model segmentations. Voxels highlighted in red indicate voxels that were segmented with the automated ePVS deep learning model. ePVS voxels that are accurately segmented have intensities approaching the intensity of constrained cerebrospinal fluid. The model tends to struggle with voxel intensities similar to dark grey matter. Such voxels are where false positives and false negatives typically occur. False negatives occasionally occur in larger ePVS that have extremely dark intensities (as displayed in column c, panel 2), likely because the model does not receive many of these larger ePVS to train on and may confuse such ePVS as normal cerebrospinal fluid. False negatives for larger ePVS are much easier to spot and correct, highlighting the need for post-segmentation review. ePVS, enlarged perivascular space.

Quantitative Evaluation of Model Performance

Dice similarity coefficient, volume correlations, and mean symmetric surface distance were used as the primary metrics for evaluating the accuracy of model-based segmentations. The mean dice similarity coefficient achieved by the basal ganglia U-net model on 8 holdout images was 0.76 with a Pearson volume correlation of 0.95 (p=0.002; see **Figure 2.4 A**). The mean symmetric surface distance for the basal

ganglia was 1.16 mm. The mean dice similarity coefficient achieved by the white matter model on 10 holdout images was 0.75 with a Pearson volume correlation of 0.97 (p<0.001; see **Figure 2.4 B**). The mean symmetric surface distance for the white matter was 1.24 mm.

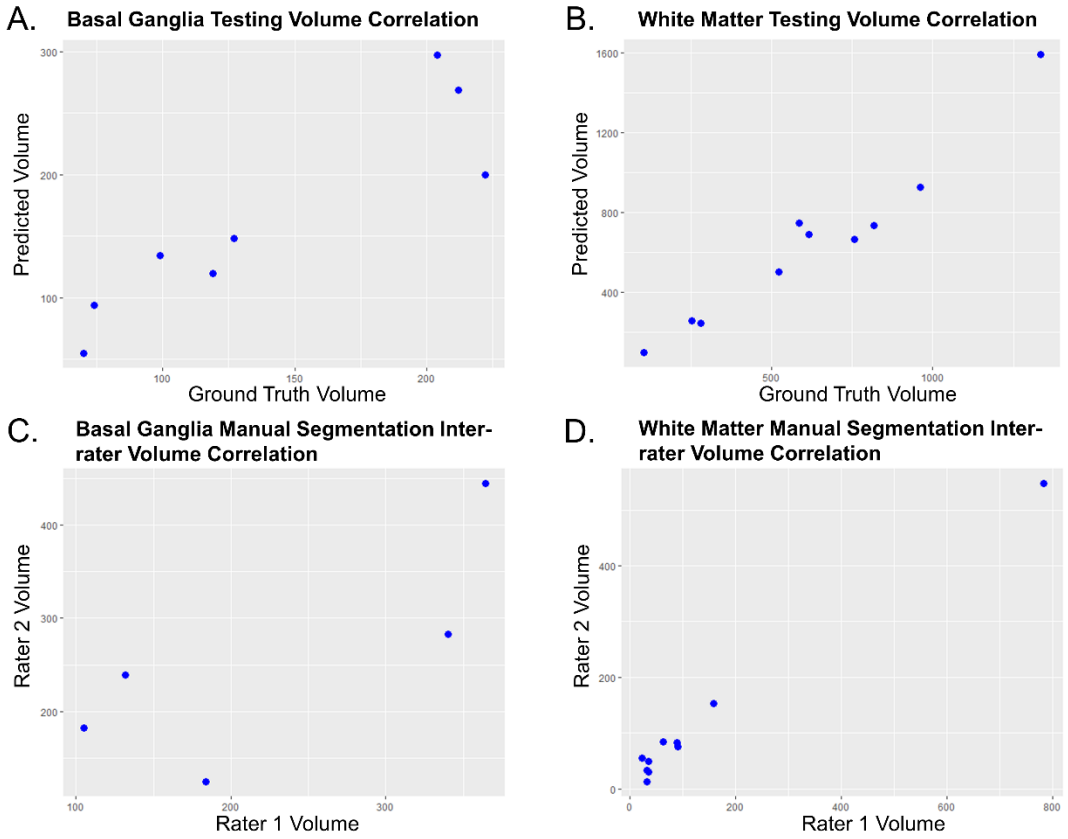

Figure 2.4. Volume correlations between ePVS segmentations. Displayed are plots that represent volume correlations between two sets of ePVS volume segmentations. Plots include, **(A)** basal ganglia volumes between ground truth image segmentations and predicted image segmentations performed by the model (n=8, r=0.95, p=0.002), **(B)** white matter volumes between ground truth image segmentations and predicted image segmentations performed by the model (n=10, r=0.97, p<0.001), **(C)** basal ganglia inter-rater volumes between two independent trained raters (n=5, r=0.77, p=0.12), and **(D)** white matter inter-rater volumes between two independent trained raters (n=10, r=0.99, p<0.001). ePVS, enlarged perivascular space.

Evaluation of ePVS Segmentation Reliability

Inter-rater reliability Dice similarity coefficient[166,167] for the basal ganglia, performed on 5 images, was 0.56 when the starting slice was pre-selected for both raters and 0.50 when the starting slice was not pre-selected. Inter-rater volume correlation in the basal ganglia was 0.77 and inter-rater mean symmetric surface distance in the basal ganglia was 1.36 mm. Inter-rater reliability Dice coefficient for the white matter, performed on a subset of 10 images, was 0.57 for full manual segmentation when averaged and 0.62 when summed across the 10 images. Inter-rater volume correlation in the white matter was 0.99 and inter-rater mean symmetric surface distance in the white matter was 3.89 mm. Intra-rater reliability Dice coefficient for full manual segmentation was 0.73 in the basal ganglia. Intra-rater volume correlation in the basal ganglia was 0.99 and intra-rater mean symmetric surface distance in the basal ganglia was 0.81 mm. When applying edits to model outputs instead of full manual segmentation, inter-rater Dice coefficient was 0.67, inter-rater volume correlation was 0.92, and inter-rater mean symmetric surface distance was 0.89 mm, all in the basal ganglia (starting from the same slice, dice coefficient was 0.56 when starting slice was not pre-selected).

Evaluation of Best Basal Ganglia ePVS Marker for Longitudinal Cognition Prediction

For all seven longitudinal cognitive outcomes assessed, models with one basal ganglia ePVS variable as the predictor achieved lower or similar AIC and BIC values (reflecting better models) compared to models with multiple ePVS predictors (see **Table 2.2**). For example, for the episodic memory composite, models with a single basal

ganglia ePVS variable acting as the predictor, namely basal ganglia ePVS Hansen et al., 2015, ePVS Volume, or ePVS count, had lower AIC and BIC values than all other predictor combinations. Additionally, for the executive function composite, the model with ePVS count as the single predictor had a lower AIC and BIC than all other single-variable and multi-variable predictors. Because models with one ePVS predictor performed as well or better than models with multiple ePVS predictors, we focused on models with one ePVS predictor for further analyses.

Table 2.2. Model Selection Based on Number of Predictors: Head-to-Head Regression Models for Longitudinal Episodic Memory

Predictor	AIC	BIC
ePVS Hansen	1796.8	1887.6
ePVS Volume	1798.8	1889.5
ePVS Count	1799.5	1890.2
ePVS Count, ePVS Hansen	1800.0	1900.8
ePVS Volume, ePVS Count	1800.3	1901.2
ePVS Volume, ePVS Hansen	1800.4	1901.2
ePVS Hansen, ePVS Patankar	1800.5	1901.4
ePVS Volume, ePVS Count, ePVS Hansen	1800.9	1911.9
ePVS Patankar	1801.2	1892.0
ePVS Volume, ePVS Patankar	1802.3	1903.2
ePVS Count, ePVS Patankar	1803.5	1904.3
ePVS Volume, ePVS Hansen, ePVS Patankar	1803.7	1914.6
ePVS Count, ePVS Hansen, ePVS Patankar	1803.9	1914.9
ePVS Volume, ePVS Count, ePVS Patankar	1804.3	1915.2
ePVS Volume, ePVS Count, ePVS Hansen, ePVS Patankar	1804.9	1925.9

Note. AIC = -2(log-likelihood) + 2K. BIC = -2(log-likelihood) + log(N)*K. Where K represents the number of parameters and N represents the sample size. Smaller AIC and BIC values represent a superior model. ePVS, enlarged perivascular space.

Assessing ePVS Variable Predictive Utility

All four ePVS predictors assessed (i.e., basal ganglia ePVS volume, ePVS count, ePVS Hansen et al., 2015, ePVS Patankar et al., 2005) achieved similar pseudo-

conditional R^2 values on all seven longitudinal cognitive outcomes (see **Table 2.3** and **Figure 2.5**). For longitudinal episodic memory composite, pseudo-conditional R^2 values ranged from 0.893-0.894 for all four basal ganglia ePVS predictors. Pseudo-conditional R^2 values for all four ePVS predictors ranged from 0.829-0.831 for longitudinal executive function composite. Basal ganglia ePVS volume had the highest pseudo-conditional R^2 value on 3 of 7 outcomes; it tied for the highest on 1 of 7 outcomes; and for 2 of 7 outcomes, it was only 0.001 less in value than the highest pseudo-conditional R^2 value.

Table 2.3. Model Selection for a Single Predictor: Head-to-Head Regression Models for Longitudinal Episodic Memory

Predictor	Pseudo-conditional R^2
ePVS Volume	0.894
ePVS Count	0.893
ePVS Hansen	0.893
ePVS Patankar	0.893

Note. Higher pseudo-conditional R^2 values represent a more predictive model. ePVS, enlarged perivascular space.

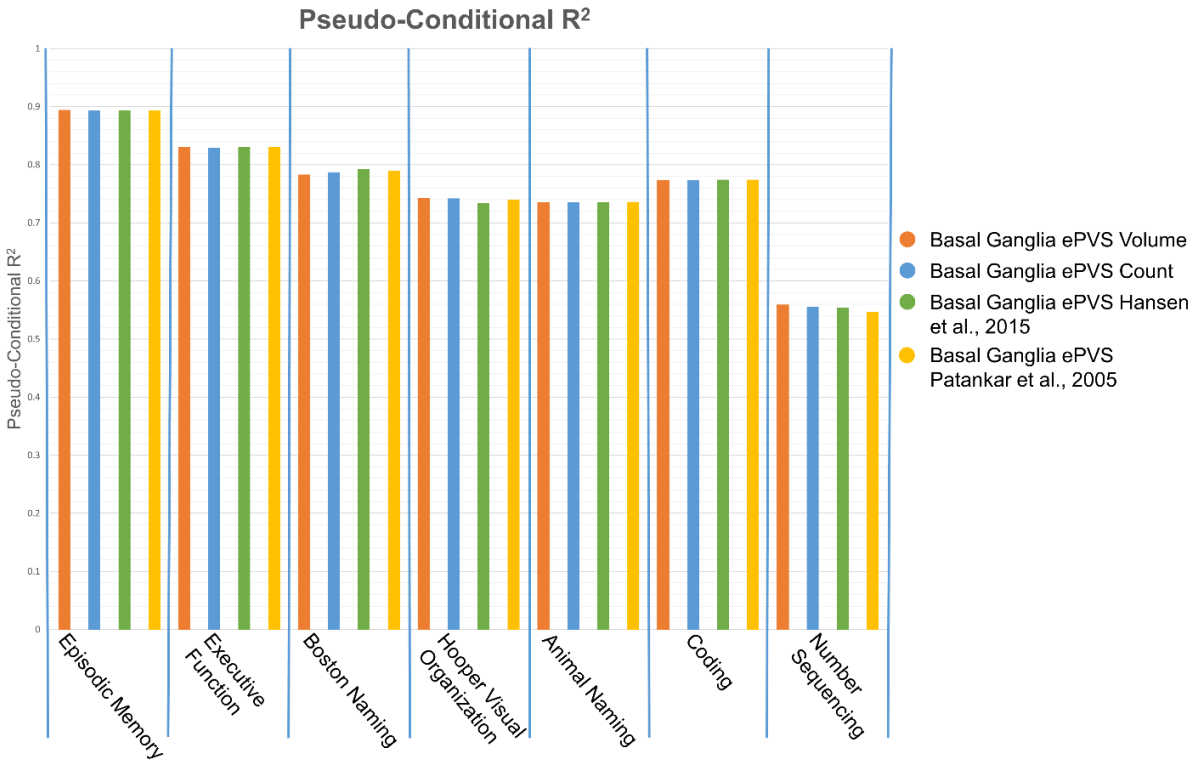

Figure 2.5. Pseudo-conditional R^2 values for ePVS predictors of longitudinal cognition. Pseudo-conditional R^2 values are displayed on the y-axis and are used to indicate the predictive utility of each ePVS predictors (ePVS Volume, ePVS Count, ePVS Hansen Score, and ePVS Patankar Score) for each longitudinal cognitive outcome. Pseudo-conditional R^2 values are largely similar for each outcome and are highest for longitudinal episodic memory performance. ePVS, enlarged perivascular space.

ePVS Volume Variability in Participants with the Same Ordinal Score

Fourteen participants with an ePVS basal ganglia Hansen et al., 2015 ordinal score of 2 were evaluated to identify the range of volumes present in participants with the same ordinal score (see **Table 2.4**). Average ePVS volume among this subset of participants was 8.57 mm^3 per 1000 mm^3 of tissue with a standard deviation of 1.87 mm^3 per 1000 mm^3 of tissue. More importantly, the range of volumes for these participants was 6.0-11.6 mm^3 per 1000 mm^3 of tissue. Some participants in this subset (which all had the same ePVS Hansen et al., 2015 ordinal score) had almost twice the ePVS volume in the basal ganglia compared to other participants.

Table 2.4. Variation in Basal Ganglia ePVS Volume Among Participants with Equivalent Hansen et al., 2015 Basal Ganglia ePVS Score

Participant	Basal Ganglia ePVS Volume mm3 /1000 mm3 of tissue	Hansen et al., 2015 Basal Ganglia ePVS Score
1	11.5	2
2	7.7	2
3	8.9	2
4	11	2
5	7	2
6	9.6	2
7	8.9	2
8	8.4	2
9	6.5	2
10	8.3	2
11	6	2
12	8.6	2
13	11.6	2
14	6	2
Average:	8.57	
SD:	1.87	
Range:	6.0-11.6	

Note. A large range of basal ganglia ePVS volume values exist among a subset of participants with the same Hansen basal ganglia ePVS score. ePVS, enlarged perivascular space.

Discussion

In the present study, we show that a deep learning U-net model reliably segments ePVS in both the basal ganglia and white matter. The Dice similarity coefficient for the hold-out set showed good agreement in the basal ganglia (0.76) and white matter (0.75) with high volume correlations as well (0.95 and 0.97, respectively). When comparing the hold-out ground-truth segmentations to predicted segmentations, the mean symmetric surface distances indicated that the error in the predicted ePVS segmentation was approximately one voxel (1.16 mm for the basal ganglia and 1.24 mm for the white matter). For all seven longitudinal cognitive outcomes assessed, models with a single basal ganglia ePVS variable predictor achieved lower or similar AIC and BIC values compared to models with a multiple basal ganglia ePVS variable

predictor (see **Table 2.2**). All four basal ganglia ePVS predictors assessed (ePVS volume, ePVS count, Hansen et al., 2015 ordinal score, Patankar et al., 2005 ordinal score) achieved similar pseudo-conditional R^2 values on all seven longitudinal cognitive outcomes. Basal ganglia ePVS volume most consistently had the highest pseudo-conditional R^2 value.

Overall, the segmentation algorithm does a good job of labelling ePVS. ePVS are similar in intensity to CSF, but, because of partial volume effects, they may appear brighter. Thus, due to the small size of ePVS and similarity in intensity to CSF, segmentation can be challenging. While reviewing each model output for potential edits is recommended, the amount of time saved by using an automated segmentation method is massive. The automated method will typically save the rater about 30 minutes per image compared to fully manual segmentation. Additionally, thorough edits are not always required and quality control of ePVS volumetric maps can be done in less than 5 minutes.

The basal ganglia model trained on 2-dimensional image patches, while the white matter model trained on 3-dimensional image patches. Despite the pronounced anatomical differences between the basal ganglia and white matter, both models performed similarly. The Dice similarity coefficients achieved by these models are limited by human inconsistencies that existed in the training data. The existence of inconsistencies is expected given that the intra-rater reliability was a Dice similarity coefficient of 0.73 for the basal ganglia. Given these statistics, it is not surprising that the models perform to a similar level.

Inter-rater reliability assessed using Dice similarity coefficient proved that

challenges exist in precisely and consistently labeling ePVS. ePVS are typically just a few voxels in size and due to partial volume effects possess similar intensity to surrounding tissue. Combined with the fact that ePVS are prevalent in large regions of the brain, accurate spatial alignment in ePVS codings from one rater to another is difficult to achieve. Another challenge, when segmenting ePVS in the basal ganglia, is deciding which slice to start from when moving ventral-to-dorsal through axial image slices. The ventral basal ganglia often presents with large ePVS and pronounced inaccuracies between two raters may occur if starting from different slices.

When dealing with small structures such as ePVS that only occupy a few voxels on brain MRI, Dice similarity coefficient may not be an adequate metric and certainly does not describe the full picture of model and reliability performance. Thus, we also assessed volume correlation. Volume correlations between ground-truth and predicted segmentations were >0.95 and ranged from 0.77-0.99 when assessing reliability statistics. Strong correlation coefficients here are encouraging since one of our variables of interest is ePVS volume. Volume correlation may be a better metric in this case than Dice similarity coefficient since spatial precision is of lower importance than accurately estimating total regional ePVS volumes. The volume correlations presented here suggest that our regional volume values are highly accurate. Another metric of importance is mean symmetric surface distance. Mean symmetric surface distance matches coded ePVS voxels from two images and finds the average distance between each matched pair. Mean symmetric surface distance penalizes based on the magnitude of inconsistencies in spatial locations whereas Dice similarity coefficient makes a binary call as to whether matched pairs line up. Therefore, scenarios where

predicted ePVS voxels are misaligned by a few millimeters are more suited for evaluation via mean symmetric surface distance. Thus, mean symmetric surface distance values between ground-truth and predicted images of 1.16 mm in the basal ganglia and 1.24 mm in the white matter are particularly good and indicate that the average matched pair is only misaligned by less than two voxels. Mean symmetric surface distance values for reliability statistics are also good at <3.89 mm.

When comparing models with a single ePVS variable as the predictor (volume, count, Hansen et al., 2015, Patankar et al., 2005) to models with multiple ePVS variables as the predictor on outcomes of longitudinal cognition, models with a single ePVS variable as the predictor consistently achieved superior or equivalent AIC and BIC values to models with multiple ePVS variables as the predictor. When assessing ePVS predictive utility for outcomes of longitudinal cognition we found all four predictors achieved similar pseudo-conditional R^2 values for all seven cognitive outcomes. However, the ePVS volume predictor was consistently the most or nearly the most predictive on six out of seven cognitive measures. The automated measures derived here perform as well as, if not better than, previously used ordinal measures. Measures that can be derived quickly and efficiently using an automated method should be prioritized. Further, if one wishes to assess longitudinal change of a variable, that variable should be continuous. The ePVS volume differences that can exist among participants with the same ePVS ordinal score are large and highlight the information loss taking place when collapsing ePVS burden into a small range of ordinal scores. We therefore feel that the method presented in this manuscript allows for the derivation of a superior measure of ePVS burden.

The value of this work lies in establishing an automated method for obtaining a reliable and comprehensive continuous measure of ePVS burden, thereby avoiding the drastic time consumption that comes with full manual segmentation of ePVS throughout the entire brain or even existing semi-quantitative ordinal measures. Due to the time-consuming nature of manual ePVS segmentation, previous quantification methods have consisted of counting ePVS on a single image slice and designating an ordinal score to each image based off the single slice count.[116,142,143] Our method not only saves time, but it also creates robust continuous total volume and total count measures for entire brain regions. ePVS are additionally difficult to segment and errors frequently occur between raters and even within raters, raising questions around the reliability of manual ePVS measurements between participants. Having a consistent automated model will minimize human error that can occur during segmentation. Our method is also highly applicable because it utilizes 3T T_1-weighted imaging, which is one of the most common sequences captured in brain MRI studies. The present paper also takes a comprehensive approach to identifying an ePVS variable (ePVS volume) with the most predictive utility for longitudinal clinical outcomes. An additional strength is in the amount of longitudinal cognitive data used (5.2±1.7 years) and the breadth of cognitive domains assessed.

Some disadvantages exist for the automated ePVS method described here. While using a deep learning model to segment ePVS saves time, creating good training data is a time-consuming process. In addition, model outputs are never perfect, and we recommend reviewing each output image for potential edits, which adds more time to the overall pipeline. Lastly, volumetric segmentation of ePVS comes with

inconsistencies that arise because of human error in training data and model output edits, as evidenced by the previously discussed inter-rater and intra-rater statistics.

In conclusion, we have described and detailed an automated method for quantifying ePVS volumes and counts throughout entire brain regions with a deep learning U-net. ePVS are typically small but are pervasive throughout the basal ganglia and white matter, making them difficult to quantify with a continuous measure. We have shown that using a deep learning U-net is an effective way for obtaining reliable and comprehensive continuous measures of ePVS in large datasets. We have also shown that ePVS volume may be the superior measure for using ePVS burden to predict cognitive decline. Having a comprehensive continuous measure of ePVS burden will allow for more impactful studies into the etiologies and clinical consequences of ePVS moving forward.

CHAPTER 3

POTENTIAL DRIVERS OF ENLARGED PERIVASCULAR SPACES

Introduction

The study of what drives enlarged perivascular space (ePVS) formation is still in its infancy. Older age is a known risk factor for ePVS, and ePVS appear to be directly related to hypertension[133] and cerebral amyloid angiopathy (CAA).[121] However, preliminary evidence suggests inflammation[173] and sleep quality[127–129] may also play a role in perivascular space enlargement.

Older age is one of the largest risk factors for ePVS. Most older adults have at least a few ePVS and multiple datasets show that age correlates with ePVS burden. We hypothesize that increased age will be associated with increased ePVS burden at baseline and longitudinal increase in ePVS burden in the Vanderbilt Memory and Aging Project cohort.

Significant associations exist between ePVS, both in the basal ganglia and white matter, and the presence of vascular dementia.[174] In a study conducted by Ding et al., large ePVS (>3mm) at baseline were found to greatly increase the chances of an individual developing vascular cognitive impairment over the mean follow-up time of 5.2 years.[134] Considering ePVS are a marker of small vessel disease (SVD) and SVD pathology constitutes a form of vascular dementia, it is not surprising that ePVS and vascular health are closely related.

One potential mechanism underlying ePVS formation is hypertensive arteriopathy,[150] a condition that affects small perforating vessels of the basal ganglia characterized by vessel wall disorganization, arteriosclerosis, and cell death.[175] Systemic vascular disease may also play a role in ePVS formation. While hypertension has been related to ePVS in the basal ganglia,[133] studies addressing systemic drivers are sparse. Arterial stiffening is a precursor to hypertension, so a reliable arterial stiffness marker may provide a subtle and earlier marker of vascular damage.[57,137] More specifically, amplified pressure waves that accompany arterial stiffening may damage vascular walls in downstream small vessels, particularly in high-flow organs like the brain, which could concurrently drive enlargement in surrounding PVS. We aim to test the hypothesis that increased arterial stiffness as measured by aortic pulse wave velocity (PWV), along with hypertension medication usage, may both be associated with worse ePVS burden. We additionally predict that due to the damaging effects apolipoprotein E ε4 (*APOE*-ε4) can have on blood vessels, associations between PWV and ePVS, as well as hypertension medication usage and ePVS, will be stronger among *APOE*-ε4 carriers at baseline. We do not expect PWV or hypertension medication usage to interact with cognitive diagnosis on ePVS burden at baseline. Associations between PWV or hypertension and ePVS burden likely happen upstream of any observed cognitive effects. Therefore, we do anticipate high PWV and hypertension could predict longitudinal increase in ePVS burden among participants who already have mild cognitive impairment (MCI) at baseline.

CAA, another disease state closely related to ePVS, is characterized by extensive β-amyloid build-up in the walls of cerebral arterioles resulting in lytic smooth

muscle death, extracellular matrix remodeling,[176] structural degradation[177] and eventually hemorrhage. Failed clearance pathways contribute to the vascular accumulation of β-amyloid and result in impeded flow of interstitial fluid (ISF) exiting the brain, leading us to hypothesize that there is increased interstitial pressure which results in PVS dilation upstream of the blockage (See **Figure 1.5 C**). There is strong evidence that CAA severity is associated with the number and extent of ePVS.[121] In perhaps some of the most compelling evidence, one study showed ePVS associations with β-amyloid load in the cortex and CAA severity in human pathology samples[123] while another study related juxtacortical ePVS on brain MRI to CAA severity in overlying cortical areas stained positively for β-amyloid.[178] In the latter study, representative samples were taken from each participant for each level of ePVS severity score for further histopathological evaluation. More severe ePVS burden was significantly associated with more severe CAA pathology (cumulative odds ratio=3.3).[178]

The species of β-amyloid most commonly found in the vessel wall is $A\beta_{40}$.[179] Other AD associated proteins can also be found in the vessel wall such as $A\beta_{42}$, total tau (t-tau), and phosphorylated tau (p-tau).[180] The brain attempts to clear toxic proteins, partially through the perivascular space, but we hypothesize that these proteins accumulate in the perivascular space and cause an enlargement of the space. We predict that decreased cerebrospinal fluid (CSF) levels of $A\beta_{40}$ will be associated with longitudinal increase in basal ganglia ePVS burden.

Other preliminary evidence points to inflammation as being intimately involved in ePVS formation. Both vascular damage[181] and toxic protein accumulation[182] can elicit inflammatory cascades that may drive perivascular space enlargement. Previous

studies have shown an association between circulating inflammatory markers and ePVS.[183] Soluble triggering receptor expressed on myeloid cells 2 (sTREM2) is a marker of microglia related inflammatory response[184–186] and a study found a positive association between CSF sTREM2 levels and ePVS in the white matter.[173] It was also found that CSF sTREM2 mediated the association between CSF p-tau levels and ePVS burden.[173] Neuroinflammation can also induce matrix metalloproteinase (MMP) activation,[187–191] which can lead to breakdown of the glia limitans,[192,193] one of the main barriers between the perivascular space and the parenchyma. We hypothesize that circulating inflammatory markers tumor necrosis factor alpha (TNF-a) and interleukin-6 (IL-6), as well as the microglia activation marker sTREM2 and extracellular matrix degradation marker family of MMPs will be associated with greater ePVS burden at baseline and longitudinal increase over time.

Metabolic waste clearance through the PVS occurs primarily during sleep.[127] Del Brutto et al. showed that, among older adults, poor sleep efficiency was associated with worse basal ganglia ePVS burden[128] and Opel et al. provided further evidence of associations between worse sleep and greater ePVS burden.[129] Therefore, poor sleep quality may be an additional risk factor for ePVS. We hypothesize that poor sleep quality, measured using the Pittsburgh Sleep Quality Index (PSQI), will be associated with greater ePVS burden at baseline and longitudinal increase in ePVS burden.

Some data suggests ePVS are heritable, but specifics have yet to be elucidated.[130] *APOE*-ε4 might be one genetic risk factor for ePVS formation but findings to date are mixed. In one study of older adults, *APOE*-ε4 carrier status was associated with greater ePVS in the basal ganglia.[131] ePVS may tend to be worse among

participants with MCI,[152] and ePVS volume in the white matter was greater among participants with a clinical diagnosis of AD compared to those participants with normal cognition.[194] Some evidence points to regional vulnerabilities of ePVS by sex but findings to date are ambiguous.[126] We hypothesize that associations with ePVS burden will be stronger among *APOE*-ε4 positive participants at baseline and participants with MCI longitudinally.

Methods

For details about study cohort, hypertensive medication usage, brain MRI, ePVS quantification, and covariates, please refer to the Methods in Chapter 2 (pages 33-42).

ePVS Harmonization

During evaluation of longitudinal ePVS measures, we discovered that different scanner, software, and head coil types can affect the appearance of ePVS on brain MRI. Baseline imaging data was captured with a uniform software and hardware configuration, but longitudinal data was not. Two software/hardware updates resulted in drastic group-wise changes to longitudinal ePVS burden trajectory. Through a thorough qualitative evaluation of the ePVS imaging data we identified two dates in which software/hardware changes occurred that significantly impacted the appearance of ePVS on T_1-weighted images and therefor affected ePVS volume and count outputs. We utilized a harmonization technique known as ComBat that batches data based off the software and hardware configuration, and then uses Bayesian inference to bring the batches into better alignment with one another.[195] ComBat has been shown to

successfully remove inter-site variability among imaging data while maintaining biological variability.[196] Here, we have applied the technique to remove variability that was introduced into the data due to scanner software and hardware changes. The technique simply requires inputting a data matrix where rows are features and columns are participants, as well as the scanner software/hardware variable. To evaluate the efficacy of the harmonization method we created pre-harmonization plots and post-harmonization plots that were stratified by batches and displayed the volume change in ePVS from timepoint to timepoint. There were large discrepancies in average ePVS volume change between different batches in pre-harmonization plots but in post-harmonization plots these discrepancies were largely corrected.

Aortic PWV

Aortic PWV measures were acquired using CMR as previously described,[75] using a 1.5T Siemens Avanto system (Siemens Medical Solutions USA, Inc., Malvern, PA) with a phased-array torso receiver coil at Vanderbilt University Medical Center. Two blinded raters (James G. Terry and Sangeeta Nair) overseen by a board-certified radiologist (John Jeffrey Carr, MD) quantified velocity-encoded flow data of the aorta. The centerline length (cm) of the ascending to descending aorta was measured and flow transit time was calculated as the difference in time (milliseconds) between the half-max of the leading edge of the ascending and descending aortic flow curves. Aortic PWV (m/s) was calculated as the centerline length (m) divided by the transit time (seconds). Inter-reader reliability for the PWV measurement had a coefficient of

variation =6.6% as determined by independent review of 34 scans by 2 readers (James G. Terry and Sangeeta Nair).

Cerebrospinal Fluid Acquisition

At baseline, a subset of the study cohort underwent a fasting lumbar puncture (n=153). CSF was acquired via polypropylene syringes using a Sprotte 25-gauge spinal needle in an intervertebral lumbar space. Samples were immediately mixed and centrifuged, and supernatants were aliquoted in 0.5 mL polypropylene tubes and stored at -80 °C. Samples were analyzed in batch using commercially available enyzme-linked immunosorbent assays (Fujirebio, Ghent, Belgium) to determine the levels of $A\beta_{42}$ (INNOTEST β-AMYLOID$_{(1-42)}$), $A\beta_{40}$ (INNOTEST β-AMYLOID$_{(1-40)}$), t-tau (INNOTEST hTAU), and p-tau (INNOTEST PHOSPHO-TAU$_{(181P)}$). Samples were analyzed using an in house enzyme-linked immunosorbent assay to determine the levels of sTREM2.[197] Samples were analyzed using Milliplex MAP Human MMP magnetic bead panels (EMD Millipore Corp., Billerica, MA, USA) to quantify MMP2, MMP3, and MMP9.[198] Board-certified laboratory technicians processed data blinded to clinical information, as previously described.[199]

Blood Biomarkers

Participant plasma samples were collected with a morning fasting venous blood draw. Plasma was separated from whole blood by centrifugation at 2000 g and 4 °C for 15 minutes and stored in ten 0.5 mL aliquots. Plasma samples were analyzed in batch using the Milliplex Map Kit (EMD Millipore Corporation, Billerica, MA, Cat. No.

HCCBP1MAG-58K) to measure IL-6 and TNF-α according to manufacturer instructions. Seven working standards were generated by serial dilution (1:3) of the reconstituted standard provided in the kit. Two quality control samples were included in each plate run. Assay plate was read on Luminex 200 with XPONENT software. Milliplex Analyst 5.0 was used for data analysis. The mean intra-assay coefficients of variation were 5.9% for IL-6 and 6.6% for TNF-α.

Sleep Quality

Participants completed a self-report sleep questionnaire known as the PSQI. The PSQI assesses sleep quality over the previous month using 19 self-rated questions covering seven components of sleep health (i.e., sleep quality, sleep duration, sleep disturbances, sleep latency, habitual sleep efficiency, use of sleeping medications, and daytime dysfunction).[200] Each component is scored from 0 = not during the past month to 3 = three or more times a week, then summed for a total ranging from 0-21. Higher scores denote poorer sleep health.

Analytical Plan

ePVS volume and count measures were log-transformed due to their logarithmic distribution. ePVS volumes were divided by total basal ganglia tissue volume to standardize the volume measurement and account for different sized heads.
Linear regression models related predictors of interest to log-standardized ePVS volume and log-ePVS count. Predictors of interest included age, PWV, hypertension medication usage, TNF-α, IL-6, CSF sTREM2, CSF MMP2, CSF MMP3, CSF MMP9,

PSQI score, CSF $A\beta_{40}$, CSF $A\beta_{42}$, CSF t-tau, and CSF p-tau. Models adjusted for age, sex, race/ethnicity, education, Framingham Stroke Risk Profile (excluding points for age), diagnosis, *APOE*-ε4 carrier status, and intracranial volume. To test hypotheses related to *APOE*-ε4 carrier status, models were repeated with a *predictor x APOE-ε4 carrier status* interaction term with follow-up models stratified by carrier status (carrier and non-carrier). Models were also repeated with a *predictor x cognitive diagnosis* interaction term with follow-up models stratified by cognitive diagnosis (normal cognition and MCI). Lastly, models were repeated with a *predictor x sex* interaction term with follow-up models stratified by sex (female and male). Mixed-effects regression models related predictors of interest at study entry to longitudinal standardized ePVS volume and ePVS count. Predictors of interest were the same as those used in linear regression models. Fixed effects included baseline age, sex, race/ethnicity, education, diagnosis, Framingham Stroke Risk Profile (excluding points for age), *APOE*-ε4 carrier status, intracranial volume, and the predictor, as well as time (defined as years since the first brain MRI) and an interaction term for predictor x time, which is the term of interest. Random effects included the intercept and time by each individual participant. Models were repeated testing a *predictor x APOE-ε4 status x time* interaction term, a *predictor x cognitive diagnosis x time* interaction term, and a *predictor x sex x time* interaction term, followed by stratification by *APOE*-ε4 carrier status (carrier and non-carrier), by cognitive diagnosis (normal cognition and MCI), and by sex (female and male). Lower order interaction terms were included in all models when applicable. Sensitivity analyses were performed on all models (a) excluding participants with prevalent CVD and atrial fibrillation and (b) excluding outliers above 4 standard

deviations. Significance was set *a* priori at $p<0.05$. Benjamini-Hochberg false discovery rate-corrected p-values were provided in data tables. P-values were grouped based off the type of predictor of interest where similar predictors were grouped together (age: 1 predictor, aortic stiffening: 1 predictor, hypertension: 2 predictors, inflammation and miscellaneous CSF variables: 7 predictors, sleep: 4 predictors, AD biomarkers: 4 predictors). All analyses were conducted using R 3.5.2 (www.r-project.org).

Results

Participant Characteristics

Participants included 327 adults (73±7 years, 59% male, 87% non-Hispanic white), including 169 cognitively unimpaired, 27 with early MCI, and 131 with MCI. PWV ranged 3.5 to 25.5 m/s. 178 participants were on at least one anti-hypertensive medication at baseline. TNF-α levels ranged from 1.43 to 33.47 pg/ml. IL-6 levels ranged from 0.23 to 63.21 pg/ml. CSF sTREM2 levels ranged from 660 to 10084 pg/ml. CSF MMP2 levels ranged from 37484 to 117861 pg/ml. CSF MMP3 levels ranged from 83.61 to 884.1 pg/ml. CSF MMP9 levels ranged from 5.93 to 506.5 pg/ml. Pittsburgh Sleep Quality Index scores ranged from 0 to 16. CSF $A\beta_{40}$ levels ranged from 2283 to 10919 pg/ml. CSF $A\beta_{42}$ levels ranged from 156 to 1471 pg/ml. CSF t-tau levels ranged from 77 to 1542 pg/ml. CSF p-tau levels ranged from 13 to 157 pg/ml. Standardized basal ganglia ePVS volumes ranged 0.0005 to 0.01 while ePVS counts ranged 11 to 268. Standardized basal ganglia ePVS volume and ePVS count are highly correlated ($r=0.80$, $p<0.001$). The cohort was followed for 5.1±1.9 years. See **Table 2.1** in Chapter 2 for more details.

Age and Baseline ePVS Burden Outcomes

Increased age was associated with increased basal ganglia log-ePVS count (β=0.02, p<0.001) and increased basal ganglia log-standardized ePVS volume (β=7.96x10^{-5}, p<0.001) at baseline. Results were the same when excluding outliers as well as when excluding participants with CVD and atrial fibrillation. See **Table 3.1** and **Figure 3.1** for details.

The *age x APOE-ε4 status* interaction term was unrelated to basal ganglia log-ePVS count and log-standardized ePVS volume (p>0.09). In stratified models, age was associated with increased basal ganglia log-ePVS count (β=0.03, p<0.001) and log-standardized ePVS volume (β=9.32x10^{-5}, p<0.001) among *APOE*-ε4 non-carriers at baseline. Results among *APOE*-ε4 carriers were null (p>0.18). Results were the same when excluding outliers as well as when excluding participants with CVD and atrial fibrillation. See **Table 3.1** for details.

The *age x cognitive diagnosis* interaction term was unrelated to basal ganglia ePVS burden (p>0.59). In stratified models, increased baseline age was associated with increased baseline basal ganglia log-ePVS count and log-standardized ePVS volume among participants with normal cognition and participants with MCI (p<0.005). See **Table 3.1** for details.

The *age x sex* interaction term was unrelated to basal ganglia ePVS burden (p>0.84). In stratified models, increased age was associated with increased basal ganglia log-ePVS count and log-standardized ePVS volume among male and female participants (p<0.001) at baseline. See **Table 3.1** for details.

Table 3.1. Cross-sectional Age Associations with Basal Ganglia ePVS Burden

	β	95% CI	*p-value*	*FDR p-value*
Basal Ganglia ePVS Burden				
ePVS Volume	$7.96x10^{-5}$	$5.06x10^{-5}$, $1.09x10^{-4}$	**<0.001**	**<0.001**
ePVS Count	0.02	0.02, 0.04	**<0.001**	**<0.001**
***APOE*-ε4 Status Interaction Basal Ganglia ePVS Burden**				
ePVS Volume	$-5.19x10^{-5}$	$-1.16x10^{-4}$, $1.22x10^{-5}$	0.11	0.11
ePVS Count	-0.01	-0.03, 0.002	0.09	0.11
***APOE*-ε4 Carriers Basal Ganglia ePVS Burden**				
ePVS Volume	$4.17x10^{-5}$	$-1.99x10^{5}$, $1.03x10^{-4}$	0.18	0.18
ePVS Count	0.01	-0.004, 0.03	0.13	0.18
***APOE*-ε4 Non-carriers Basal Ganglia ePVS Burden**				
ePVS Volume	$9.32x10^{-5}$	$6.01x10^{-5}$, $1.26x10^{4}$	**<0.001**	**<0.001**
ePVS Count	0.03	0.02, 0.04	**<0.001**	**<0.001**
Diagnosis Interaction Basal Ganglia ePVS Burden				
ePVS Volume	$-1.70x10^{-6}$	$-6.00x10^{-5}$, $5.66x10^{-5}$	0.95	0.95
ePVS Count	-0.004	-0.02, 0.01	0.60	0.90
Normal Cognition Basal Ganglia ePVS Burden				
ePVS Volume	$8.68x10^{-5}$	$5.39x10^{5}$, $1.20x10^{-4}$	**<0.001**	**<0.001**
ePVS Count	0.03	0.02, 0.04	**<0.001**	**<0.001**
MCI Basal Ganglia ePVS Burden				
ePVS Volume	$8.12x10^{5}$	$2.60x10^{-5}$, $1.36x10^{-4}$	**0.004**	**0.004**
ePVS Count	0.02	0.01, 0.04	**<0.001**	**0.001**
Sex Interaction Basal Ganglia ePVS Burden				
ePVS Volume	$2.58x10^{-7}$	$-5.64x10^{-5}$, $5.69x10^{-5}$	0.99	0.99
ePVS Count	-0.001	-0.02, 0.01	0.85	0.99
Male Basal Ganglia ePVS Burden				
ePVS Volume	$8.06x10^{-5}$	$3.98x10^{-5}$, $1.21x10^{-4}$	**<0.001**	**<0.001**
ePVS Count	0.03	0.02, 0.04	**<0.001**	**<0.001**
Female Basal Ganglia ePVS Burden				
ePVS Volume	$8.13x10^{-5}$	$3.72x10^{-5}$, $1.25x10^{-4}$	**<0.001**	**<0.001**
ePVS Count	0.02	0.01, 0.03	**<0.001**	**<0.001**

Note. ePVS volume represents a log-transformed standardized measure of ePVS volume (values were divided by total basal ganglia tissue volume and then log-transformed). ePVS count represents a log-transformed measure of ePVS count. Analyses performed on n=326 participants. Models were adjusted for age, sex, race/ethnicity, education, *APOE*-ε4 status, cognitive diagnosis, and Framingham Stroke Risk Profile (excluding points assigned for age). *APOE*-ε4, apolipoprotein E ε4. CI, confidence interval. ePVS, enlarged perivascular space. The parameter estimates (β) for the interaction models are for the *age x APOE-ε4 carrier status* interaction term or the *age x cognitive diagnosis* interaction term or the *age x sex* interaction term and are interpreted as the difference in slopes between carriers and non-carriers or normal cognition and MCI or male and female. The parameter estimates (β) for the stratified models represent the changes in ePVS burden associated with one unit change in age. Bold p-values meet the *a priori* significance threshold. FDR, false discovery rate.

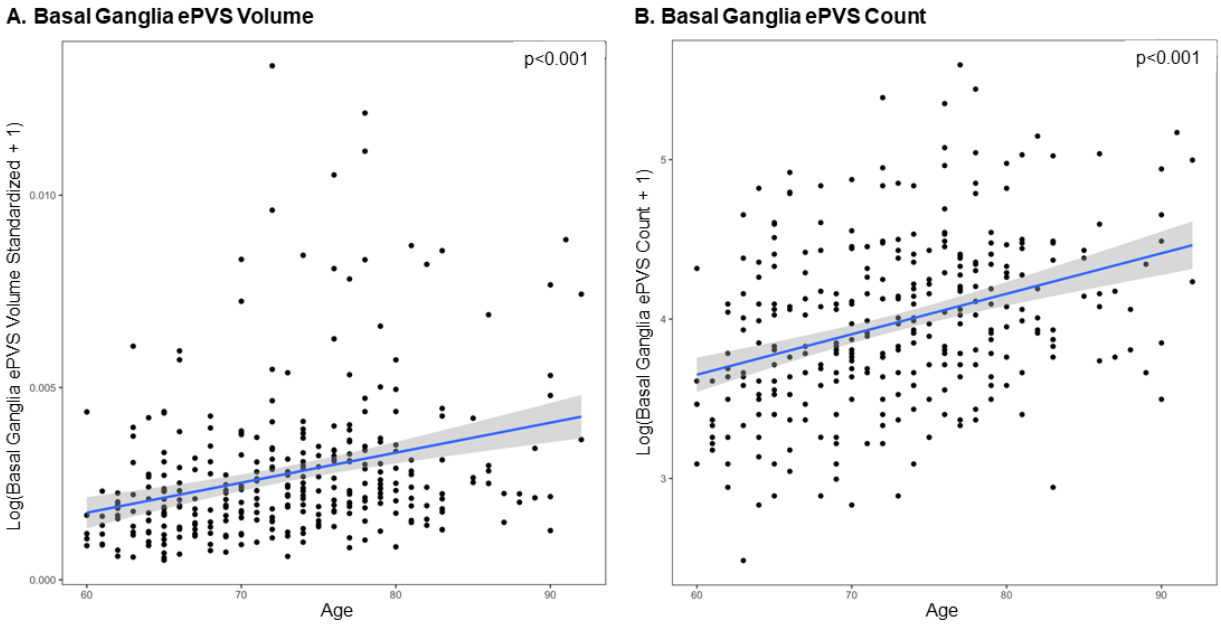

Figure 3.1. Cross-sectional age associations with basal ganglia ePVS burden. **(A)** baseline basal ganglia ePVS volume and **(B)** baseline basal ganglia ePVS count. The ePVS volume variable is standardized by dividing by basal ganglia tissue volume and is then log-transformed. The ePVS count variable is log-transformed. Plot includes outliers.

PWV and Baseline ePVS Burden Outcomes

Increased aortic PWV was associated with increased basal ganglia log-ePVS count (β=0.02, p=0.03) and log-standardized ePVS volume ($\beta=7x10^{-5}$, p=0.04) at baseline. When excluding outliers or participants with CVD and atrial fibrillation, the association between PWV and log-ePVS count remained (p<0.05), but the association with ePVS volume was attenuated (p-values>0.17). See **Table 3.2** and **Figure 3.2** for details.

The *aortic PWV x APOE-ε4 status* interaction term was unrelated to basal ganglia log-ePVS count and log-standardized ePVS volume (p>0.05). In stratified models, aortic PWV was associated with increased log-ePVS count (β=0.05, p=0.005) and log-standardized ePVS volume (β=0.0002, p=0.002) among *APOE*-ε4 carriers at

baseline. When excluding outliers, the association between aortic PWV and log-standardized ePVS volume was attenuated (p=0.60) but the association with ePVS count remained (p=0.005). When excluding participants with CVD and atrial fibrillation, both associations were attenuated (p-values>0.28). See **Table 3.2** for details.

The *aortic PWV x cognitive diagnosis* interaction term was unrelated to basal ganglia log-ePVS count and log-standardized ePVS volume (p>0.72) at baseline. Stratified models in cognitively unimpaired participants and participants with MCI were both null (p>0.07). See **Table 3.2** for details.

The *aortic PWV x sex* interaction term was unrelated to basal ganglia log-ePVS count and log-standardized ePVS volume (p>0.05). In stratified models, aortic PWV was associated with basal ganglia log-ePVS count (β=0.04, p=0.007) and log-standardized ePVS volume (β=0.0001, p=0.01) among male participants at baseline. Results were attenuated when excluding outliers (p>0.05) and when excluding participants with CVD and atrial fibrillation (p>0.14). Among female participants, results were null. See **Table 3.2** for details.

Table 3.2. Cross-sectional Aortic PWV Associations with Basal Ganglia ePVS Burden

	β	95% CI	*p-value*	*FDR p-value*
Basal Ganglia ePVS Burden				
ePVS Volume	7.01×10^{-5}	1.87×10^{-6}, 1.38×10^{-4}	**0.04**	0.07
ePVS Count	0.02	0.002, 0.04	**0.03**	0.07
***APOE*-ε4 Status Interaction Basal Ganglia ePVS Burden**				
ePVS Volume	0.0001	-4.18×10^{-6}, 0.0003	0.06	0.17
ePVS Count	0.03	-0.01, 0.07	0.14	0.21
***APOE*-ε4 Carriers Basal Ganglia ePVS Burden**				
ePVS Volume	0.0002	8.24×10^{-5}, 0.0003	**0.002**	**0.006**
ePVS Count	0.05	0.02, 0.09	**0.005**	**0.008**
***APOE*-ε4 Non-carriers Basal Ganglia ePVS Burden**				
ePVS Volume	2.00×10^{-5}	-6.03×10^{-5}, 0.0001	0.62	0.74
ePVS Count	0.01	-0.01, 0.03	0.30	0.74

Diagnosis Interaction Basal Ganglia ePVS Burden				
ePVS Volume	-2.39×10^{-5}	-1.57×10^{-4}, 1.09×10^{-4}	0.72	0.95
ePVS Count	0.001	-0.03, 0.04	0.95	0.95
Normal Cognition Basal Ganglia ePVS Burden				
ePVS Volume	7.81×10^{-5}	-5.59×10^{-6}, 1.62×10^{-4}	0.07	0.20
ePVS Count	0.02	-0.008, 0.04	0.19	0.28
MCI Basal Ganglia ePVS Burden				
ePVS Volume	6.72×10^{-5}	-5.82×10^{-5}, 1.93×10^{-4}	0.29	0.44
ePVS Count	0.03	-0.005, 0.06	0.10	0.30
Sex Interaction Basal Ganglia ePVS Burden				
ePVS Volume	-1.22×10^{-4}	-2.50×10^{-4}, 5.07×10^{-6}	0.06	0.09
ePVS Count	-0.03	-0.07, 1.29×10^{-4}	0.05	0.09
Male Basal Ganglia ePVS Burden				
ePVS Volume	1.27×10^{-4}	2.96×10^{-5}, 2.24×10^{-4}	**0.01**	**0.02**
ePVS Count	0.04	0.01, 0.06	**0.007**	**0.02**
Female Basal Ganglia ePVS Burden				
ePVS Volume	5.69×10^{-6}	-9.28×10^{-5}, 1.04×10^{-4}	0.91	0.91
ePVS Count	0.003	-0.02, 0.03	0.79	0.91

Note. ePVS volume represents a log-transformed standardized measure of ePVS volume (values were divided by total basal ganglia tissue volume and then log-transformed). ePVS count represents a log-transformed measure of ePVS count. Analyses performed on n=301 participants. Models were adjusted for age, sex, race/ethnicity, education, *APOE*-ε4 status, cognitive diagnosis, and Framingham Stroke Risk Profile (excluding points assigned for age). *APOE*-ε4, apolipoprotein E ε4. CI, confidence interval. ePVS, enlarged perivascular space. The parameter estimates (β) for the interaction models are for the *PWV x APOE-ε4 carrier status* interaction term or the *PWV x cognitive diagnosis* interaction term or the *PWV x sex* interaction term and are interpreted as the difference in slopes between carriers and non-carriers or normal cognition and MCI or male and female. The parameter estimates (β) for the stratified models represent the changes in ePVS burden associated with one unit change in PWV. Bold p-values meet the *a priori* significance threshold. FDR, false discovery rate.

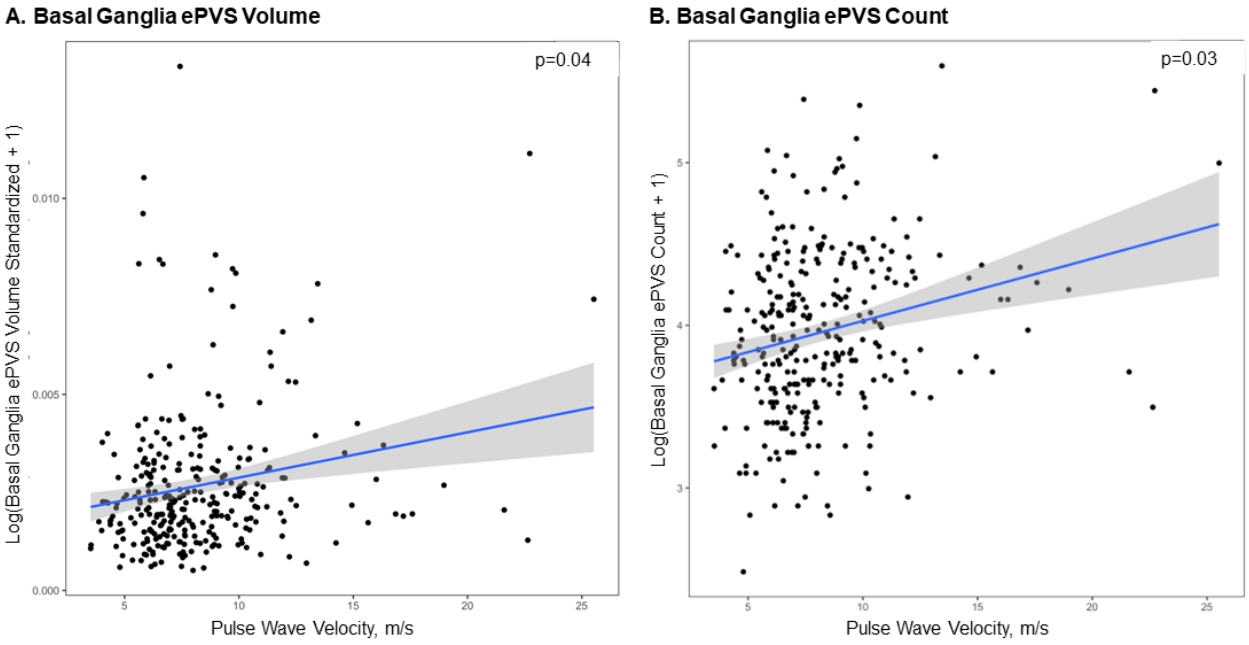

Figure 3.2. Cross-sectional aortic PWV associations with basal ganglia ePVS burden. **(A)** baseline basal ganglia ePVS volume and **(B)** baseline basal ganglia ePVS count. The basal ganglia ePVS volume variable is standardized by dividing by basal ganglia tissue volume and is then log-transformed. The basal ganglia ePVS count variable is log-transformed. Plot includes outliers. When outliers are excluded, the association with ePVS volume is attenuated (p=0.16) but the association with ePVS count remains (p=0.03).

Hypertension Medication Usage and Baseline ePVS Burden Outcomes

Hypertension medication usage was associated with increased basal ganglia log-ePVS count (β=0.14, p=0.01) and basal ganglia log-standardized ePVS volume (β=0.0004, p=0.04) at baseline. When excluding outliers, the association between hypertension and ePVS volume was attenuated (p=0.10) but the association with ePVS count remained (p=0.01). When excluding participants with CVD and atrial fibrillation results remained the same. See **Table 3.3** and **Figure 3.3** for details.

The *hypertension medication usage x APOE-ε4 status* interaction term was unrelated to baseline basal ganglia ePVS burden (p>0.07). In stratified models, hypertension was associated with increased baseline basal ganglia log-ePVS count

(β=0.32, p=0.001) and log-standardized ePVS volume (β=0.001, p=0.009) among *APOE*-ε4 carriers. Among non-carriers, associations between hypertension and basal ganglia ePVS burden were null (p>0.52). Results were the same when excluding outliers as well as when excluding participants with CVD and atrial fibrillation. See **Table 3.3** for details.

The *hypertension medication usage x cognitive diagnosis* interaction term was unrelated to baseline basal ganglia ePVS burden (p>0.82). Stratified models were largely null. See **Table 3.3** for details.

The *hypertension medication usage x sex* interaction term was unrelated to baseline basal ganglia ePVS burden (p>0.58). Stratified models were null. See **Table 3.3** for details.

Table 3.3. Cross-sectional Hypertension Medication Usage Associations with Basal Ganglia ePVS Burden

	β	95% CI	*p-value*	*FDR p-value*
Basal Ganglia ePVS Burden				
ePVS Volume	$4.40x10^{-4}$	$2.52x10^{-5}$, $8.56x10^{-4}$	**0.04**	0.08
ePVS Count	0.14	0.03, 0.25	**0.01**	0.08
***APOE*-ε4 Status Interaction Basal Ganglia ePVS Burden**				
ePVS Volume	$7.36x10^{-4}$	$-1.08x10^{-4}$, 0.002	0.09	0.17
ePVS Count	0.20	-0.02, 0.42	0.08	0.17
***APOE*-ε4 Carriers Basal Ganglia ePVS Burden**				
ePVS Volume	0.001	$2.64x10^{-5}$, 0.002	**0.009**	**0.02**
ePVS Count	0.32	0.13, 0.50	**0.001**	**0.007**
***APOE*-ε4 Non-carriers Basal Ganglia ePVS Burden**				
ePVS Volume	$9.72x10^{-5}$	$-4.10x10^{-4}$, $6.05x10^{4}$	0.71	0.97
ePVS Count	0.04	-0.09, 0.18	0.53	0.97
Diagnosis Interaction Basal Ganglia ePVS Burden				
ePVS Volume	$9.50x10^{-5}$	$-7.65x10^{-4}$, $9.55x10^{-4}$	0.83	0.95
ePVS Count	-0.008	-0.23, 0.22	0.94	0.95
Normal Cognition Basal Ganglia ePVS Burden				
ePVS Volume	$4.36x10^{-4}$	$-2.99x10^{-5}$, $9.02x10^{-4}$	0.07	0.17
ePVS Count	0.15	0.01, 0.29	**0.03**	0.17
MCI Basal Ganglia ePVS Burden				
ePVS Volume	$4.62x10^{-4}$	$-3.92x10^{-4}$, 0.001	0.29	0.58

ePVS Count	0.12	-0.08, 0.32	0.23	0.58
Sex Interaction Basal Ganglia ePVS Burden				
ePVS Volume	$2.31x10^{-4}$	$-6.12x10^{-4}$, 0.001	0.59	0.69
ePVS Count	0.04	-0.18, 0.27	0.69	0.69
Male Basal Ganglia ePVS Burden				
ePVS Volume	$3.70x10^{-4}$	$-1.36x10^{4}$, $8.76x10^{-4}$	0.15	0.30
ePVS Count	0.12	-0.02, 0.26	0.10	0.30
Female Basal Ganglia ePVS Burden				
ePVS Volume	$4.38x10^{-4}$	$-3.35x10^{-4}$, 0.001	0.26	0.53
ePVS Count	0.13	-0.06, 0.31	0.17	0.53

Note. ePVS volume represents a log-transformed standardized measure of ePVS volume (values were divided by total basal ganglia tissue volume and then log-transformed). ePVS count represents a log-transformed measure of ePVS count. Analyses performed on n=326 participants. Models were adjusted for age, sex, race/ethnicity, education, *APOE*-ε4 status, cognitive diagnosis, and Framingham Stroke Risk Profile (excluding points assigned for age). *APOE*-ε4, apolipoprotein E ε4. CI, confidence interval. ePVS, enlarged perivascular space. The parameter estimates (β) for the interaction models are for the *hypertension medication usage x APOE-ε4 carrier status* interaction term or the *hypertension medication usage x cognitive diagnosis* interaction term or the *hypertension medication usage x sex* interaction term and are interpreted as the difference in slopes between carriers and non-carriers or normal cognition and MCI or male and female. The parameter estimates (β) for the stratified models represent the changes in ePVS burden associated with one unit change in hypertension medication usage. Bold p-values meet the *a priori* significance threshold. FDR, false discovery rate.

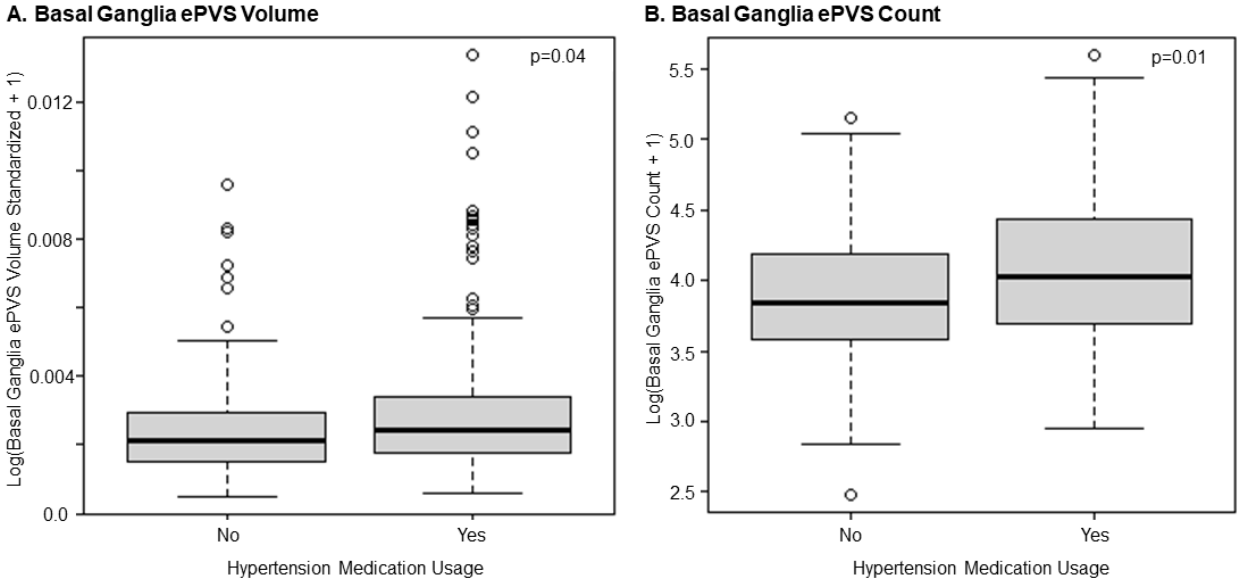

Figure 3.3. Cross-sectional hypertension medication usage associations with basal ganglia ePVS burden. **(A)** baseline ePVS volume and **(B)** baseline ePVS count. The ePVS volume variable is standardized by dividing by basal ganglia tissue volume and is then log-transformed. The ePVS count variable is log-transformed.

Inflammation and Baseline ePVS Burden Outcomes

Associations between TNF-α, IL-6, CSF sTREM2, CSF MMP2, CSF MMP3, CSF MMP9 and baseline basal ganglia ePVS burden were all null (p>0.08). See **Tables 3.4** to **3.9** for details.

The *CSF sTREM2 x APOE-ε4 status* interaction term was associated with baseline basal ganglia log-ePVS count (β=-0.0001, p=0.003) and log-standardized ePVS volume (β=-4.67x10^{-7}, p=0.02). Associations remained significant when excluding outliers as well as when excluding participants with CVD and atrial fibrillation. In stratified models, CSF sTREM2 was not associated with ePVS burden among *APOE*-ε4 carriers (p>0.05). Among *APOE*-ε4 non-carriers, higher CSF sTREM2 levels were associated with greater baseline basal ganglia log-ePVS count (β=5.77x10^{-5}, p=0.05) and log-standardized ePVS volume (β=2.77x10^{-7}, p=0.02). When excluding outliers, the association between CSF sTREM2 and ePVS volume among *APOE*-ε4 non-carriers was attenuated (p=0.12) but the association with ePVS count remained (p=0.05). When excluding participants with CVD and atrial fibrillation results were the same. See **Tables 3.4** to **3.9** and **Figure 3.4** for details.

The *CSF MMP3 x APOE-ε4 status* interaction term was associated with baseline basal ganglia log-standardized ePVS volume (β=-6.11x10^{-6}, p=0.02) but not ePVS count (p=0.23). The association remained significant when excluding outliers as well as when excluding participants with CVD and atrial fibrillation. In stratified models, CSF MMP3 levels were not associated with baseline basal ganglia ePVS burden among *APOE*-ε4 carriers (p>0.07). Among *APOE*-ε4 non-carriers, greater CSF MMP3 levels were associated with greater baseline basal ganglia log-standardized ePVS volume

(β=2.60x10^{-6}, p=0.03) but not log-ePVS count (p=0.16). The association was attenuated when excluding outliers (p=0.18) but not when excluding participants with CVD and atrial fibrillation (p=0.01). See **Tables 3.4** to **3.9** for details.

Associations between the *TNF-α x APOE-ε4 status*, *IL-6 x APOE-ε4 status*, *CSF MMP2 x APOE-ε4 status*, and *CSF MMP9 x APOE-ε4 status* interaction terms and baseline basal ganglia ePVS burden were all null (p>0.18). All stratified models were also null (p>0.22). See **Tables 3.4** to **3.9** for details.

Associations between *TNF-α x cognitive diagnosis*, *IL-6 x cognitive diagnosis*, *CSF sTREM2 x cognitive diagnosis*, *CSF MMP2 x cognitive diagnosis*, *CSF MMP3 x cognitive diagnosis*, and *CSF MMP9 x cognitive diagnosis* interaction terms and baseline basal ganglia ePVS burden were all null (p>0.05). In stratified models, greater TNF-α levels were associated with greater baseline basal ganglia log-ePVS count (β=0.02, p=0.05) among normal participants. The association was attenuated when excluding participants with CVD and atrial fibrillation (p=0.27) but remained when excluding outliers (p=0.02). All other stratified models were null (p>0.12). See **Tables 3.4** to **3.9** for details.

The *IL-6 x sex* interaction term was associated with baseline basal ganglia log-standardized ePVS volume (β=0.0001, p=0.05) but not log-ePVS count (p=0.94). The association between *IL-6 x sex* and ePVS volume was attenuated when excluding outliers (p=0.65) but remained when excluding participants with CVD and atrial fibrillation (p=0.04). In stratified models, IL-6 levels were not related to ePVS burden among male participants (p>0.34). Among female participants, greater IL-6 levels were associated with greater baseline basal ganglia log-standardized ePVS volume

(β=0.0001, p=0.05) but not log-ePVS count (p=0.80). The significant association among female participants was attenuated when excluding outliers as well as when excluding participants with CVD and atrial fibrillation (p>0.07). See **Tables 3.4** to **3.9** for details.

Associations between *TNF-α x sex*, *CSF sTREM2 x sex*, *CSF MMP2 x sex*, *CSF MMP3 x sex*, and *CSF MMP9 x sex* interaction terms and baseline basal ganglia ePVS burden were all null (p>0.12). In stratified models, greater CSF MMP3 levels were associated with greater baseline basal ganglia log-standardized ePVS volume among female participants (β=4.81x10^{-6}, p=0.01). All other baseline inflammation models stratified by sex were null (p>0.18). See **Tables 3.4** to **3.9** for details.

Table 3.4. Cross-sectional TNF-α Associations with Basal Ganglia ePVS Burden

	β	95% CI	*p-value*	*FDR p-value*
Basal Ganglia ePVS Burden				
ePVS Volume	-1.18x10^{-5}	-8.18x10^{-5}, 5.83x10^{-5}	0.74	0.98
ePVS Count	0.010	-0.009, 0.03	0.31	0.65
***APOE*-ε4 Status Interaction Basal Ganglia ePVS Burden**				
ePVS Volume	9.57x10^{-5}	-5.93x10^{-5}, 2.51x10^{-4}	0.23	0.42
ePVS Count	0.007	-0.03, 0.05	0.75	0.78
***APOE*-ε4 Carriers Basal Ganglia ePVS Burden**				
ePVS Volume	8.52x10^{-5}	-6.41x10^{-5}, 2.34x10^{-4}	0.26	0.46
ePVS Count	0.02	-0.01, 0.06	0.23	0.46
***APOE*-ε4 Non-carriers Basal Ganglia ePVS Burden**				
ePVS Volume	-4.56x10^{-5}	-1.25x10^{-4}, 3.35x10^{-5}	0.26	0.50
ePVS Count	0.005	-0.02, 0.03	0.64	0.95
Diagnosis Interaction Basal Ganglia ePVS Burden				
ePVS Volume	-3.85x10^{-5}	-1.87x10^{-4}, 1.10x10^{-4}	0.61	0.72
ePVS Count	-0.04	-0.07, 0.003	0.07	0.72
Normal Cognition Basal Ganglia ePVS Burden				
ePVS Volume	-1.85x10^{-6}	-7.40x10^{-5}, 7.03x10^{-5}	0.95	0.97
ePVS Count	0.02	3.52x10^{-4}, 0.04	**0.05**	0.49
MCI Basal Ganglia ePVS Burden				
ePVS Volume	-3.72x10^{-5}	-1.90x10^{-4}, 1.16x10^{-4}	0.63	0.87
ePVS Count	-0.01	-0.05, 0.03	0.58	0.87
Sex Interaction Basal Ganglia ePVS Burden				
ePVS Volume	-1.23x10^{-4}	-2.78x10^{-4}, 3.24x10^{-5}	0.12	0.54
ePVS Count	-0.02	-0.06, 0.02	0.32	0.80
Male Basal Ganglia ePVS Burden				

ePVS Volume	$2.38x10^{-5}$	$-5.44x10^{-5}$, $1.02x10^{-4}$	0.55	0.92
ePVS Count	0.01	-0.007, 0.04	0.19	0.92
Female Basal Ganglia ePVS Burden				
ePVS Volume	$-8.04x10^{-5}$	$-2.28x10^{-4}$, $6.75x10^{-5}$	0.28	0.60
ePVS Count	-0.002	-0.04, 0.03	0.91	0.91

Note. ePVS volume represents a log-transformed standardized measure of ePVS volume (values were divided by total basal ganglia tissue volume and then log-transformed). ePVS count represents a log-transformed measure of ePVS count. Analyses performed on n=326 participants. Models were adjusted for age, sex, race/ethnicity, education, *APOE*-ε4 status, cognitive diagnosis, and Framingham Stroke Risk Profile (excluding points assigned for age). *APOE*-ε4, apolipoprotein E ε4. CI, confidence interval. ePVS, enlarged perivascular space. The parameter estimates (β) for the interaction models are for the *TNF-α x APOE-ε4 carrier status* interaction term or the *TNF-α x cognitive diagnosis* interaction term or the *TNF-α x sex* interaction term and are interpreted as the difference in slopes between carriers and non-carriers or normal cognition and MCI or male and female. The parameter estimates (β) for the stratified models represent the changes in ePVS burden associated with one unit change in TNF-α. Bold p-values meet the *a priori* significance threshold. FDR, false discovery rate.

Table 3.5. Cross-sectional IL-6 Associations with Basal Ganglia ePVS Burden

	β	95% CI	*p-value*	*FDR p-value*
Basal Ganglia ePVS Burden				
ePVS Volume	$6.13x10^{-6}$	$-4.10x10^{-5}$, $5.33x10^{-5}$	0.80	0.98
ePVS Count	0.002	-0.01, 0.01	0.75	0.98
***APOE*-ε4 Status Interaction Basal Ganglia ePVS Burden**				
ePVS Volume	$6.00x10^{-5}$	$-1.28x10^{-4}$, $2.48x10^{-4}$	0.53	0.62
ePVS Count	0.006	-0.04, 0.06	0.81	0.81
***APOE*-ε4 Carriers Basal Ganglia ePVS Burden**				
ePVS Volume	$6.79x10^{-5}$	$-1.35x10^{-4}$, $2.71x10^{-4}$	0.51	0.59
ePVS Count	0.009	-0.04, 0.06	0.72	0.75
***APOE*-ε4 Non-carriers Basal Ganglia ePVS Burden**				
ePVS Volume	$6.63x10^{-7}$	$-4.69x10^{-5}$, $4.82x10^{-5}$	0.98	0.98
ePVS Count	$6.83x10^{-4}$	-0.01, 0.01	0.92	0.98
Diagnosis Interaction Basal Ganglia ePVS Burden				
ePVS Volume	$6.57x10^{-5}$	$-4.29x10^{-5}$, $1.74x10^{-4}$	0.23	0.72
ePVS Count	0.008	-0.02, 0.04	0.58	0.72
Normal Cognition Basal Ganglia ePVS Burden				
ePVS Volume	$-1.40x10^{-5}$	$-5.84x10^{-5}$, $3.03x10^{-5}$	0.53	0.93
ePVS Count	-0.002	-0.01, 0.01	0.82	0.96
MCI Basal Ganglia ePVS Burden				
ePVS Volume	$6.28x10^{-5}$	$-5.60x10^{-5}$, $1.82x10^{-4}$	0.30	0.78
ePVS Count	0.01	-0.02, 0.04	0.47	0.87
Sex Interaction Basal Ganglia ePVS Burden				
ePVS Volume	$1.17x10^{-4}$	$1.86x10^{-6}$, $2.33x10^{-4}$	**0.05**	0.40
ePVS Count	0.001	-0.03, 0.03	0.94	0.94
Male Basal Ganglia ePVS Burden				
ePVS Volume	$-2.45x10^{-5}$	$-7.52x10^{-5}$, $2.61x10^{-5}$	0.34	0.92
ePVS Count	$3.31x10^{-4}$	-0.01, 0.01	0.96	0.99
Female Basal Ganglia ePVS Burden				
ePVS Volume	$1.13x10^{-4}$	$1.36x10^{-6}$, $2.25x10^{-3}$	**0.05**	0.30

ePVS Count	0.003	-0.02, 0.03	0.80	0.88

Note. ePVS volume represents a log-transformed standardized measure of ePVS volume (values were divided by total basal ganglia tissue volume and then log-transformed). ePVS count represents a log-transformed measure of ePVS count. Analyses performed on n=326 participants. Models were adjusted for age, sex, race/ethnicity, education, *APOE*-ε4 status, cognitive diagnosis, and Framingham Stroke Risk Profile (excluding points assigned for age). *APOE*-ε4, apolipoprotein E ε4. CI, confidence interval. ePVS, enlarged perivascular space. The parameter estimates (β) for the interaction models are for the *IL-6 x APOE-ε4 carrier status* interaction term or the *IL-6 x cognitive diagnosis* interaction term or the *IL-6 x sex* interaction term and are interpreted as the difference in slopes between carriers and non-carriers or normal cognition and MCI or male and female. The parameter estimates (β) for the stratified models represent the changes in ePVS burden associated with one unit change in IL-6. Bold p-values meet the *a priori* significance threshold. FDR, false discovery rate.

Table 3.6. Cross-sectional CSF sTREM2 Associations with Basal Ganglia ePVS Burden

	β	95% CI	*p-value*	*FDR p-value*
Basal Ganglia ePVS Burden				
ePVS Volume	1.61×10^{-7}	-2.36×10^{-8}, 3.46×10^{-7}	0.09	0.52
ePVS Count	2.81×10^{-5}	-1.93×10^{-5}, 7.56×10^{-5}	0.24	0.62
***APOE*-ε4 Status Interaction Basal Ganglia ePVS Burden**				
ePVS Volume	-4.67×10^{-7}	-8.45×10^{-7}, -8.87×10^{-8}	**0.02**	0.08
ePVS Count	-1.49×10^{-4}	-2.45×10^{-4}, -5.29×10^{-5}	**0.003**	**0.03**
***APOE*-ε4 Carriers Basal Ganglia ePVS Burden**				
ePVS Volume	-1.96×10^{-7}	-4.96×10^{-7}, 1.04×10^{-7}	0.19	0.46
ePVS Count	-7.85×10^{-5}	-1.60×10^{-4}, 2.83×10^{-6}	0.06	0.41
***APOE*-ε4 Non-carriers Basal Ganglia ePVS Burden**				
ePVS Volume	2.77×10^{-7}	3.98×10^{-8}, 5.15×10^{-7}	**0.02**	0.20
ePVS Count	5.77×10^{-5}	4.81×10^{-7}, 1.15×10^{-4}	**0.05**	0.25
Diagnosis Interaction Basal Ganglia ePVS Burden				
ePVS Volume	2.08×10^{-7}	-1.85×10^{-7}, 6.00×10^{-7}	0.30	0.72
ePVS Count	-2.99×10^{-5}	-1.31×10^{-4}, 7.14×10^{-5}	0.56	0.72
Normal Cognition Basal Ganglia ePVS Burden				
ePVS Volume	-1.48×10^{-8}	-2.16×10^{-7}, 1.86×10^{-7}	0.88	0.97
ePVS Count	1.02×10^{-5}	-4.72×10^{-5}, 6.76×10^{-5}	0.72	0.94
MCI Basal Ganglia ePVS Burden				
ePVS Volume	3.47×10^{-7}	-9.58×10^{-8}, 7.90×10^{-7}	0.12	0.78
ePVS Count	1.72×10^{-5}	-8.61×10^{-5}, 1.21×10^{-4}	0.74	0.87
Sex Interaction Basal Ganglia ePVS Burden				
ePVS Volume	-2.50×10^{-8}	-4.93×10^{-7}, 4.43×10^{-7}	0.92	0.94
ePVS Count	-1.01×10^{-5}	-1.30×10^{-4}, 1.10×10^{-4}	0.87	0.94
Male Basal Ganglia ePVS Burden				
ePVS Volume	1.14×10^{-7}	-9.08×10^{-8}, 3.19×10^{-7}	0.27	0.92
ePVS Count	2.94×10^{-5}	-2.52×10^{-5}, 8.39×10^{-5}	0.29	0.92
Female Basal Ganglia ePVS Burden				
ePVS Volume	2.31×10^{-7}	-2.42×10^{-7}, 7.03×10^{-7}	0.33	0.63
ePVS Count	3.98×10^{-5}	-7.97×10^{-5}, 1.59×10^{-4}	0.50	0.71

Note. ePVS volume represents a log-transformed standardized measure of ePVS volume (values were divided by total basal ganglia tissue volume and then log-transformed). ePVS count represents a

log-transformed measure of ePVS count. Analyses performed on n=153 participants. Models were adjusted for age, sex, race/ethnicity, education, *APOE*-ε4 status, cognitive diagnosis, and Framingham Stroke Risk Profile (excluding points assigned for age). *APOE*-ε4, apolipoprotein E ε4. CI, confidence interval. ePVS, enlarged perivascular space. The parameter estimates (β) for the interaction models are for the *sTREM2 x APOE-ε4 carrier status* interaction term or the *sTREM2 x cognitive diagnosis* interaction term or the *sTREM2 x sex* interaction term and are interpreted as the difference in slopes between carriers and non-carriers or normal cognition and MCI or male and female. The parameter estimates (β) for the stratified models represent the changes in ePVS burden associated with one unit change in sTREM2. Bold p-values meet the *a priori* significance threshold. FDR, false discovery rate.

Table 3.7. Cross-sectional CSF MMP2 Associations with Basal Ganglia ePVS Burden

	β	95% CI	*p-value*	*FDR p-value*
Basal Ganglia ePVS Burden				
ePVS Volume	-1.22×10^{-9}	-2.16×10^{-8}, 1.92×10^{-8}	0.91	0.98
ePVS Count	-1.97×10^{-7}	-5.44×10^{-6}, 5.04×10^{-6}	0.94	0.98
***APOE*-ε4 Status Interaction Basal Ganglia ePVS Burden**				
ePVS Volume	-2.43×10^{-8}	-6.60×10^{-8}, 1.74×10^{-8}	0.25	0.42
ePVS Count	-7.28×10^{-6}	-1.80×10^{-5}, 3.42×10^{-6}	0.18	0.42
***APOE*-ε4 Carriers Basal Ganglia ePVS Burden**				
ePVS Volume	-1.81×10^{-8}	-5.45×10^{-8}, 1.83×10^{-8}	0.32	0.46
ePVS Count	-5.86×10^{-6}	-1.59×10^{-5}, 4.19×10^{-6}	0.25	0.46
***APOE*-ε4 Non-carriers Basal Ganglia ePVS Burden**				
ePVS Volume	2.20×10^{-9}	-2.57×10^{-8}, 3.01×10^{-8}	0.88	0.98
ePVS Count	1.38×10^{-7}	-6.55×10^{-6}, 6.82×10^{-6}	0.97	0.98
Diagnosis Interaction Basal Ganglia ePVS Burden				
ePVS Volume	-2.35×10^{-8}	-6.70×10^{-8}, 2.00×10^{-8}	0.29	0.72
ePVS Count	-1.09×10^{-5}	-2.20×10^{-5}, 1.50×10^{-7}	0.05	0.72
Normal Cognition Basal Ganglia ePVS Burden				
ePVS Volume	-3.40×10^{-10}	-2.08×10^{-8}, 2.02×10^{-8}	0.97	0.97
ePVS Count	2.36×10^{-6}	-3.68×10^{-6}, 8.39×10^{-6}	0.44	0.93
MCI Basal Ganglia ePVS Burden				
ePVS Volume	-2.89×10^{-8}	-7.95×10^{-8}, 2.18×10^{-8}	0.26	0.78
ePVS Count	-7.77×10^{-6}	-1.92×10^{-5}, 3.70×10^{-6}	0.18	0.78
Sex Interaction Basal Ganglia ePVS Burden				
ePVS Volume	-5.67×10^{-9}	-5.07×10^{-8}, 3.94×10^{-8}	0.80	0.94
ePVS Count	-3.13×10^{-6}	-1.47×10^{-5}, 8.44×10^{-6}	0.59	0.94
Male Basal Ganglia ePVS Burden				
ePVS Volume	-2.51×10^{-9}	-2.60×10^{-8}, 2.10×10^{-8}	0.92	0.92
ePVS Count	1.03×10^{-6}	-5.29×10^{-6}, 7.35×10^{-6}	0.75	0.92
Female Basal Ganglia ePVS Burden				
ePVS Volume	-8.73×10^{-9}	-5.49×10^{-8}, 3.74×10^{-8}	0.70	0.82
ePVS Count	-2.99×10^{-6}	-1.46×10^{-5}, 8.60×10^{-6}	0.60	0.75

Note. ePVS volume represents a log-transformed standardized measure of ePVS volume (values were divided by total basal ganglia tissue volume and then log-transformed). ePVS count represents a log-transformed measure of ePVS count. Analyses performed on n=152 participants. Models were adjusted for age, sex, race/ethnicity, education, *APOE*-ε4 status, cognitive diagnosis, and Framingham Stroke Risk Profile (excluding points assigned for age). *APOE*-ε4, apolipoprotein E ε4.

CI, confidence interval. ePVS, enlarged perivascular space. The parameter estimates (β) for the interaction models are for the *MMP2 x APOE-ε4 carrier status* interaction term or the *MMP2 x cognitive diagnosis* interaction term or the *MMP2 x sex* interaction term and are interpreted as the difference in slopes between carriers and non-carriers or normal cognition and MCI or male and female. The parameter estimates (β) for the stratified models represent the changes in ePVS burden associated with one unit change in MMP2. Bold p-values meet the *a priori* significance threshold. FDR, false discovery rate.

Table 3.8. Cross-sectional CSF MMP3 Associations with Basal Ganglia ePVS Burden

	β	95% CI	*p-value*	*FDR p-value*
Basal Ganglia ePVS Burden				
ePVS Volume	$1.65x10^{-6}$	$-3.09x10^{-7}$, $3.61x10^{-6}$	0.10	0.52
ePVS Count	$3.45x10^{-4}$	$-1.59x10^{-4}$, $8.49x10^{-4}$	0.18	0.62
***APOE*-ε4 Status Interaction Basal Ganglia ePVS Burden**				
ePVS Volume	$-6.11x10^{-6}$	$-1.10x10^{-5}$, $-1.20x10^{-6}$	**0.02**	0.08
ePVS Count	$-7.82x10^{-4}$	-0.002, $5.05x10^{-4}$	0.23	0.42
***APOE*-ε4 Carriers Basal Ganglia ePVS Burden**				
ePVS Volume	$-4.00x10^{-6}$	$-8.46x10^{-6}$, $4.62x10^{-7}$	0.08	0.41
ePVS Count	$-5.95x10^{-4}$	-0.002, $6.78x10^{-4}$	0.35	0.46
***APOE*-ε4 Non-carriers Basal Ganglia ePVS Burden**				
ePVS Volume	$2.60x10^{-6}$	$2.79x10^{-7}$, $4.93x10^{-6}$	**0.03**	0.20
ePVS Count	$4.00x10^{-4}$	$-1.66x10^{-4}$, $9.66x10^{-4}$	0.16	0.39
Diagnosis Interaction Basal Ganglia ePVS Burden				
ePVS Volume	$1.16x10^{-6}$	$-3.09x10^{-7}$, $3.61x10^{-6}$	0.10	0.72
ePVS Count	$3.45x10^{-4}$	$-1.59x10^{-4}$, $8.49x10^{-4}$	0.18	0.72
Normal Cognition Basal Ganglia ePVS Burden				
ePVS Volume	$7.55x10^{-7}$	$-1.40x10^{-6}$, $2.91x10^{-6}$	0.49	0.93
ePVS Count	$4.63x10^{-4}$	$-1.71x10^{-4}$, 0.001	0.15	0.93
MCI Basal Ganglia ePVS Burden				
ePVS Volume	$1.80x10^{-6}$	$-3.19x10^{-6}$, $6.80x10^{-6}$	0.47	0.87
ePVS Count	$-9.43x10^{-5}$	-0.001, 0.001	0.87	0.87
Sex Interaction Basal Ganglia ePVS Burden				
ePVS Volume	$3.21x10^{-6}$	$-9.34x10^{-7}$, $7.35x10^{-6}$	0.13	0.54
ePVS Count	$-6.45x10^{-5}$	-0.001, 0.001	0.91	0.94
Male Basal Ganglia ePVS Burden				
ePVS Volume	$2.63x10^{-7}$	$-2.12x10^{-6}$, $2.65x10^{-6}$	0.83	0.92
ePVS Count	$3.60x10^{-4}$	$-2.77x10^{-4}$, $9.97x10^{-4}$	0.26	0.92
Female Basal Ganglia ePVS Burden				
ePVS Volume	$4.81x10^{-6}$	$1.13x10^{-6}$, $8.49x10^{-6}$	**0.01**	0.25
ePVS Count	$3.54x10^{-4}$	$-6.46x10^{-4}$, 0.001	0.48	0.71

Note. ePVS volume represents a log-transformed standardized measure of ePVS volume (values were divided by total basal ganglia tissue volume and then log-transformed). ePVS count represents a log-transformed measure of ePVS count. Analyses performed on n=151 participants. Models were adjusted for age, sex, race/ethnicity, education, *APOE*-ε4 status, cognitive diagnosis, and Framingham Stroke Risk Profile (excluding points assigned for age). *APOE*-ε4, apolipoprotein E ε4. CI, confidence interval. ePVS, enlarged perivascular space. The parameter estimates (β) for the interaction models are for the *MMP3 x APOE-ε4 carrier status* interaction term or the *MMP3 x cognitive diagnosis* interaction term or the *MMP3 x sex* interaction term and are interpreted as the

difference in slopes between carriers and non-carriers or normal cognition and MCI or male and female. The parameter estimates (β) for the stratified models represent the changes in ePVS burden associated with one unit change in MMP3. Bold p-values meet the *a priori* significance threshold. FDR, false discovery rate.

Table 3.9. Cross-sectional CSF MMP9 Associations with Basal Ganglia ePVS Burden

	β	95% CI	*p-value*	*FDR p-value*
Basal Ganglia ePVS Burden				
ePVS Volume	-1.49×10^{-6}	-5.18×10^{-6}, 2.19×10^{-6}	0.42	0.81
ePVS Count	-8.23×10^{-4}	-0.002, 1.20×10^{-4}	0.09	0.52
***APOE*-ε4 Status Interaction Basal Ganglia ePVS Burden**				
ePVS Volume	-2.50×10^{-6}	-1.01×10^{-5}, 5.06×10^{-6}	0.51	0.62
ePVS Count	-8.37×10^{-4}	-0.003, 0.001	0.39	0.52
***APOE*-ε4 Carriers Basal Ganglia ePVS Burden**				
ePVS Volume	-2.90×10^{-6}	-8.89×10^{-6}, 3.09×10^{-6}	0.33	0.46
ePVS Count	-8.87×10^{-4}	-0.002, 6.88×10^{-4}	0.26	0.46
***APOE*-ε4 Non-carriers Basal Ganglia ePVS Burden**				
ePVS Volume	-8.28×10^{-7}	-5.78×10^{-6}, 4.13×10^{-6}	0.74	0.95
ePVS Count	-5.55×10^{-4}	-0.002, 6.52×10^{-4}	0.36	0.64
Diagnosis Interaction Basal Ganglia ePVS Burden				
ePVS Volume	1.60×10^{-6}	-6.16×10^{-6}, 9.37×10^{-6}	0.68	0.74
ePVS Count	-3.83×10^{-4}	-0.002, 0.002	0.70	0.74
Normal Cognition Basal Ganglia ePVS Burden				
ePVS Volume	-1.93×10^{-6}	-5.79×10^{-6}, 1.93×10^{-6}	0.32	0.93
ePVS Count	-4.64×10^{-4}	-0.002, 7.56×10^{-4}	0.45	0.93
MCI Basal Ganglia ePVS Burden				
ePVS Volume	-7.65×10^{-7}	-8.23×10^{-6}, 6.70×10^{-6}	0.84	0.87
ePVS Count	-0.001	-0.003, 5.62×10^{-4}	0.19	0.78
Sex Interaction Basal Ganglia ePVS Burden				
ePVS Volume	-2.76×10^{-6}	-1.06×10^{-5}, 5.11×10^{-6}	0.49	0.93
ePVS Count	-9.63×10^{-4}	-0.003, 0.001	0.34	0.80
Male Basal Ganglia ePVS Burden				
ePVS Volume	-6.01×10^{-7}	-5.19×10^{-6}, 3.99×10^{-6}	0.80	0.92
ePVS Count	-5.12×10^{-4}	-0.002, 7.51×10^{-4}	0.42	0.92
Female Basal Ganglia ePVS Burden				
ePVS Volume	-2.45×10^{-6}	-9.54×10^{-6}, 4.64×10^{-6}	0.49	0.71
ePVS Count	-0.001	-0.003, 3.61×10^{-4}	0.12	0.42

Note. ePVS volume represents a log-transformed standardized measure of ePVS volume (values were divided by total basal ganglia tissue volume and then log-transformed). ePVS count represents a log-transformed measure of ePVS count. Analyses performed on n=142 participants. Models were adjusted for age, sex, race/ethnicity, education, *APOE*-ε4 status, cognitive diagnosis, and Framingham Stroke Risk Profile (excluding points assigned for age). *APOE*-ε4, apolipoprotein E ε4. CI, confidence interval. ePVS, enlarged perivascular space. The parameter estimates (β) for the interaction models are for the *MMP9 x APOE-ε4 carrier status* interaction term or the *MMP9 x cognitive diagnosis* interaction term or the *MMP9 x sex* interaction term and are interpreted as the difference in slopes between carriers and non-carriers or normal cognition and MCI or male and female. The parameter estimates (β) for the stratified models represent the changes in ePVS burden associated with one unit change in MMP9. Bold p-values meet the *a priori* significance threshold.

FDR, false discovery rate.

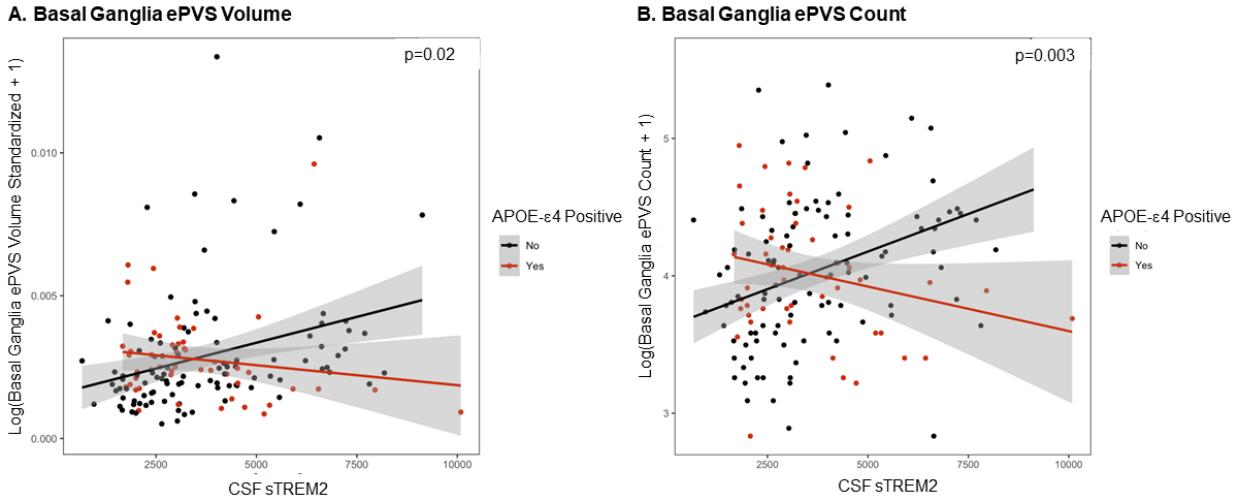

Figure 3.4. Cross-sectional *CSF sTREM2 x APOE-ε4 status* interactions on basal ganglia ePVS burden. **(A)** baseline ePVS volume and **(B)** baseline ePVS count. The ePVS volume variable is standardized by dividing by basal ganglia tissue volume and is then log-transformed. The ePVS count variable is log-transformed. In stratified models among *APOE*-ε4 non-carriers, CSF sTREM2 levels were associated with ePVS volume (p=0.02) and ePVS count (p=0.05).

Pittsburgh Sleep Quality Index and Baseline ePVS Burden Outcomes

PSQI score was unrelated to baseline basal ganglia ePVS burden (p>0.09). See **Table 3.10** for details.

Associations between the *PSQI score x APOE-ε4 status* interaction term and baseline basal ganglia ePVS burden were null (p>0.24). Stratified models were also null (p>0.06). See **Table 3.10** for details.

The *PSQI score x cognitive diagnosis* interaction term was associated with baseline basal ganglia log-ePVS count (β=0.06, p=0.003) and log-standardized ePVS volume (β=0.0002, p=0.02). In stratified models, PSQI score was unrelated to ePVS burden among participants with normal cognition (p>0.59). Among participants with MCI, worse sleep quality was associated with greater baseline basal ganglia log-ePVS

count (β=0.05, p=0.001) and log-standardized ePVS volume (β=0.0002, p=0.02). Results were the same when excluding outliers as well as when excluding participants with CVD and atrial fibrillation. See **Table 3.10** and **Figure 3.5** for details.

Associations between the *PSQI score x sex* interaction term and basal ganglia ePVS burden were null (p>0.11). In stratified models, among male participants, worse sleep quality was associated with greater baseline basal ganglia log-ePVS count (β=0.03, p=0.02) and log-standardized ePVS volume (β=$9.98x10^{-5}$, p=0.02). Results were the same when excluding outliers as well as when excluding participants with CVD and atrial fibrillation. Among female participants, models were null (p>0.63). See **Table 3.10** for details.

Table 3.10. Cross-sectional Pittsburgh Sleep Quality Index Score Associations with Basal Ganglia ePVS Burden

	β	95% CI	*p-value*	*FDR p-value*
Basal Ganglia ePVS Burden				
ePVS Volume	$5.86x10^{-5}$	$-1.08x10^{-5}$, $1.28x10^{-4}$	0.10	0.23
ePVS Count	0.01	-0.004, 0.03	0.13	0.27
***APOE*-ε4 Status Interaction Basal Ganglia ePVS Burden**				
ePVS Volume	$3.34x10^{-5}$	$-1.15x10^{-4}$, $1.82x10^{-4}$	0.66	0.72
ePVS Count	0.02	-0.02, 0.06	0.25	0.72
***APOE*-ε4 Carriers Basal Ganglia ePVS Burden**				
ePVS Volume	$9.13x10^{-5}$	$-4.15x10^{-5}$, $2.24x10^{-4}$	0.18	0.30
ePVS Count	0.03	-0.002, 0.07	0.07	0.27
***APOE*-ε4 Non-carriers Basal Ganglia ePVS Burden**				
ePVS Volume	$4.57x10^{-5}$	$-3.75x10^{-5}$, $1.29x10^{-4}$	0.28	0.67
ePVS Count	0.007	-0.02, 0.03	0.55	0.73
Diagnosis Interaction Basal Ganglia ePVS Burden				
ePVS Volume	$1.70x10^{-4}$	$2.60x10^{-5}$, $3.14x10^{-4}$	**0.02**	**0.04**
ePVS Count	0.06	0.02, 0.10	**0.003**	**0.03**
Normal Cognition Basal Ganglia ePVS Burden				
ePVS Volume	$-4.88x10^{-6}$	$-8.67x10^{-5}$, $7.69x10^{-5}$	0.91	0.92
ePVS Count	-0.007	-0.03, 0.02	0.60	0.92
MCI Basal Ganglia ePVS Burden				
ePVS Volume	$1.60x10^{-4}$	$2.21x10^{-5}$, $2.97x10^{-4}$	**0.02**	0.06
ePVS Count	0.05	0.02, 0.08	**0.001**	**0.006**
Sex Interaction Basal Ganglia ePVS Burden				

ePVS Volume	$-3.89x10^{-5}$	$-1.78x10^{-4}$, $1.01x10^{-4}$	0.58	0.60
ePVS Count	-0.03	-0.07, 0.007	0.11	0.50
Male Basal Ganglia ePVS Burden				
ePVS Volume	$9.98x10^{-5}$	$1.88x10^{-5}$, $1.81x10^{-4}$	**0.02**	0.07
ePVS Count	0.03	0.005, 0.05	**0.02**	0.07
Female Basal Ganglia ePVS Burden				
ePVS Volume	$2.89x10^{-5}$	$-1.01x10^{-4}$, $1.59x10^{-4}$	0.66	0.80
ePVS Count	-0.007	-0.04, 0.02	0.64	0.80

Note. ePVS volume represents a log-transformed standardized measure of ePVS volume (values were divided by total basal ganglia tissue volume and then log-transformed). ePVS count represents a log-transformed measure of ePVS count. Analyses performed on n=310 participants. Models were adjusted for age, sex, race/ethnicity, education, *APOE*-ε4 status, cognitive diagnosis, and Framingham Stroke Risk Profile (excluding points assigned for age). *APOE*-ε4, apolipoprotein E ε4. CI, confidence interval. ePVS, enlarged perivascular space. The parameter estimates (β) for the interaction models are for the *PSQI score x APOE-ε4 carrier status* interaction term or the *PSQI score x cognitive diagnosis* interaction term or the *PSQI score x sex* interaction term and are interpreted as the difference in slopes between carriers and non-carriers or normal cognition and MCI or male and female. The parameter estimates (β) for the stratified models represent the changes in ePVS burden associated with one unit change in sleep quality. Bold p-values meet the *a priori* significance threshold. FDR, false discovery rate.

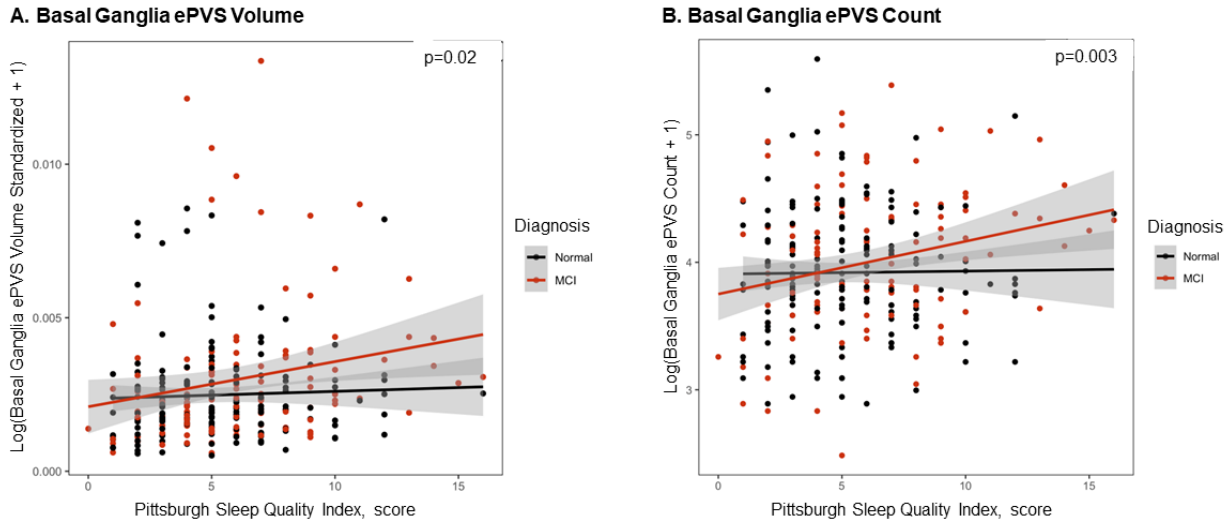

Figure 3.5. Cross-sectional *PSQI score x cognitive diagnosis* interactions on basal ganglia ePVS burden. **(A)** baseline ePVS volume and **(B)** baseline ePVS count. The ePVS volume variable is standardized by dividing by basal ganglia tissue volume and is then log-transformed. The ePVS count variable is log-transformed. In stratified models among participants with MCI, sleep quality was associated with ePVS volume (p=0.02) and ePVS count (p=0.003).

AD Biomarkers and Baseline ePVS Burden Outcomes

Associations between CSF $A\beta_{40}$, CSF $A\beta_{42}$, CSF t-tau, and CSF p-tau and

baseline basal ganglia ePVS burden were null (p>0.21). See **Tables 3.11** to **3.14** for details.

Associations between the *CSF $A\beta_{40}$ x APOE-ε4 status*, *CSF $A\beta_{42}$ x APOE-ε4 status*, *CSF t-tau x APOE-ε4 status*, and *CSF p-tau x APOE-ε4 status* interactions terms and baseline basal ganglia ePVS burden were null (p>0.07). All AD biomarker models stratified by *APOE*-ε4 status were null (p>0.17). See **Tables 3.11** to **3.14** for details.

The *CSF $A\beta_{42}$ x cognitive diagnosis* interaction term was associated with baseline basal ganglia log-ePVS count (β=0.0009, p=0.03) but not log-standardized ePVS volume (p=0.07). In stratified models, lower CSF $A\beta_{42}$ levels were associated with greater baseline basal ganglia log-standardized ePVS volume (β=-1.62x10^{-6}, p=0.03) but not log-ePVS count (p=0.16) among participants with normal cognition. In participants with MCI, models were null (p>0.24). Results were the same when excluding outliers as well as when excluding participants with CVD and atrial fibrillation. See **Table 3.11** for details.

Associations between the *CSF $A\beta_{40}$ x cognitive diagnosis*, *CSF t-tau x cognitive diagnosis*, and *CSF p-tau x cognitive diagnosis* interaction terms and baseline basal ganglia ePVS burden were null (p>0.14). Stratified results were null (p>0.43). See **Table 3.12** for details.

The *CSF t-tau x sex* interaction term was associated with baseline basal ganglia log-standardized ePVS volume (β=-3.07x10^{-6}, p=0.03) but not log-ePVS count (p=0.13). The interaction association was attenuated when excluding outliers (p=0.18) but remained when excluding participants with CVD and atrial fibrillation. In stratified models, greater CSF t-tau levels were associated with greater baseline basal ganglia

log-ePVS count (β=0.0006, p=0.04) but not log-standardized ePVS volume (p=0.08) among male participants. Among female participants, results were null (p>0.46). The stratified results were the same when excluding outliers as well as when excluding participants with CVD and atrial fibrillation. See **Table 3.13** for details.

The *CSF p-tau x sex* interaction term was associated with baseline basal ganglia log-standardized ePVS volume (β=-2.71x10^{-5}, p=0.03) but not log-ePVS count (p=0.18). The result was attenuated when excluding outliers (p=0.23) but remained when excluding participants with CVD and atrial fibrillation. Stratified models were null (p>0.08). See **Table 3.14** for details.

Associations between the *CSF Aβ_{40} x sex* and *CSF Aβ_{42} x sex* interaction terms and baseline basal ganglia ePVS burden were null (p>0.17). Stratified models were also null (p>0.13). See **Tables 3.11** and **3.12** for details.

Table 3.11. Cross-sectional CSF Aβ$_{42}$ Associations with Basal Ganglia ePVS Burden

	β	95% CI	*p-value*	*FDR p-value*
Basal Ganglia ePVS Burden				
ePVS Volume	-2.57x10^{-7}	-1.66x10^{-6}, 1.15x10^{-6}	0.72	0.90
ePVS Count	6.13x10^{-5}	-2.97x10^{-4}, 4.20x10^{-4}	0.74	0.90
***APOE*-ε4 Status Interaction Basal Ganglia ePVS Burden**				
ePVS Volume	-6.89x10^{-7}	-4.36x10^{-6}, 2.98x10^{-6}	0.71	0.78
ePVS Count	8.40x10^{-4}	-8.76x10^{-5}, 0.002	0.08	0.28
***APOE*-ε4 Carriers Basal Ganglia ePVS Burden**				
ePVS Volume	-1.65x10^{-6}	-5.11x10^{-6}, 1.81x10^{-6}	0.34	0.65
ePVS Count	6.51x10^{-4}	-2.97x10^{-4}, 0.002	0.17	0.62
***APOE*-ε4 Non-carriers Basal Ganglia ePVS Burden**				
ePVS Volume	-6.33x10^{-9}	-1.65x10^{-6}, 1.63x10^{-6}	0.99	0.99
ePVS Count	-2.88x10^{-5}	-4.21x10^{-4}, 3.63x10^{-4}	0.88	0.99
Diagnosis Interaction Basal Ganglia ePVS Burden				
ePVS Volume	2.94x10^{-6}	-2.25x10^{-7}, 6.09x10^{-6}	0.07	0.27
ePVS Count	9.03x10^{-4}	9.87x10^{-5}, 0.002	**0.03**	0.27
Normal Cognition Basal Ganglia ePVS Burden				
ePVS Volume	-1.62x10^{-6}	-3.09x10^{-6}, -1.58x10^{-7}	**0.03**	0.36
ePVS Count	-3.04x10^{-4}	-7.30x10^{-4}, 1.22x10^{-4}	0.16	0.64

MCI Basal Ganglia ePVS Burden				
ePVS Volume	$1.45x10^{-6}$	$-2.62x10^{-6}$, $5.52x10^{-6}$	0.48	0.73
ePVS Count	$5.43x10^{-4}$	$-3.75x10^{-4}$, 0.001	0.24	0.73
Sex Interaction Basal Ganglia ePVS Burden				
ePVS Volume	$2.02x10^{-6}$	$-8.95x10^{-7}$, $4.94x10^{-6}$	0.17	0.30
ePVS Count	$1.05x10^{-4}$	$-6.46x10^{-4}$, $8.55x10^{-4}$	0.78	0.91
Male Basal Ganglia ePVS Burden				
ePVS Volume	$-1.06x10^{-6}$	$-2.69x10^{-6}$, $5.57x10^{-7}$	0.20	0.36
ePVS Count	$-4.43x10^{-5}$	$-4.79x10^{-4}$, $3.90x10^{-4}$	0.84	0.92
Female Basal Ganglia ePVS Burden				
ePVS Volume	$2.51x10^{-6}$	$-7.90x10^{-7}$, $5.81x10^{-6}$	0.13	0.75
ePVS Count	$4.44x10^{-4}$	$-3.99x10^{-4}$, 0.001	0.29	0.75

Note. ePVS volume represents a log-transformed standardized measure of ePVS volume (values were divided by total basal ganglia tissue volume and then log-transformed). ePVS count represents a log-transformed measure of ePVS count. Analyses performed on n=153 participants. Models were adjusted for age, sex, race/ethnicity, education, *APOE*-ε4 status, cognitive diagnosis, and Framingham Stroke Risk Profile (excluding points assigned for age). *APOE*-ε4, apolipoprotein E ε4. CI, confidence interval. ePVS, enlarged perivascular space. The parameter estimates (β) for the interaction models are for the *$A\beta_{42}$ x APOE-ε4 carrier status* interaction term or the *$A\beta_{42}$ x cognitive diagnosis* interaction term or the *$A\beta_{42}$ x sex* interaction term and are interpreted as the difference in slopes between carriers and non-carriers or normal cognition and MCI or male and female. The parameter estimates (β) for the stratified models represent the changes in ePVS burden associated with one unit change in $A\beta_{42}$. Bold p-values meet the *a priori* significance threshold. FDR, false discovery rate.

Table 3.12. Cross-sectional CSF $A\beta_{40}$ Associations with Basal Ganglia ePVS Burden

	β	95% CI	*p-value*	*FDR p-value*
Basal Ganglia ePVS Burden				
ePVS Volume	$2.71x10^{-8}$	$-1.69x10^{-7}$, $2.23x10^{-7}$	0.79	0.90
ePVS Count	$2.26x10^{-5}$	$-2.74x10^{-5}$, $7.25x10^{-5}$	0.37	0.90
***APOE*-ε4 Status Interaction Basal Ganglia ePVS Burden**				
ePVS Volume	$-3.31x10^{-7}$	$-8.05x10^{-7}$, $1.43x10^{-7}$	0.17	0.29
ePVS Count	$-2.69x10^{-5}$	$-1.48x10^{-4}$, $9.45x10^{-5}$	0.66	0.78
***APOE*-ε4 Carriers Basal Ganglia ePVS Burden**				
ePVS Volume	$-2.39x10^{-7}$	$-6.14x10^{-7}$, $1.37x10^{-7}$	0.21	0.62
ePVS Count	$-1.29x10^{-5}$	$-1.19x10^{-4}$, $9.32x10^{-5}$	0.81	0.90
***APOE*-ε4 Non-carriers Basal Ganglia ePVS Burden**				
ePVS Volume	$9.18x10^{-8}$	$-1.53x10^{-7}$, $3.36x10^{-7}$	0.46	0.65
ePVS Count	$2.42x10^{-5}$	$-3.41x10^{-5}$, $8.26x10^{-5}$	0.41	0.65
Diagnosis Interaction Basal Ganglia ePVS Burden				
ePVS Volume	$2.09x10^{-7}$	$-2.57x10^{-7}$, $6.75x10^{-7}$	0.38	0.75
ePVS Count	$8.88x10^{-5}$	$-2.95x10^{-5}$, $2.07x10^{-4}$	0.14	0.42
Normal Cognition Basal Ganglia ePVS Burden				
ePVS Volume	$-7.53x10^{-8}$	$-2.76x10^{-7}$, $1.25x10^{-7}$	0.46	0.92
ePVS Count	$-1.55x10^{-5}$	$-7.29x10^{-5}$, $4.19x10^{-5}$	0.59	0.92
MCI Basal Ganglia ePVS Burden				
ePVS Volume	$1.46x10^{-7}$	$-3.89x10^{-7}$, $6.82x10^{-7}$	0.59	0.73
ePVS Count	$4.75x10^{-5}$	$-7.40x10^{-5}$, $1.69x10^{-4}$	0.44	0.73
Sex Interaction Basal Ganglia ePVS Burden				

ePVS Volume	-2.28×10^{-8}	-4.43×10^{-7}, 3.98×10^{-7}	0.91	0.91
ePVS Count	-1.05×10^{-5}	-1.18×10^{-4}, 9.66×10^{-5}	0.85	0.91
Male Basal Ganglia ePVS Burden				
ePVS Volume	1.14×10^{-9}	-2.38×10^{-7}, 2.40×10^{-7}	0.99	0.99
ePVS Count	1.83×10^{-5}	-4.50×10^{-5}, 8.17×10^{-5}	0.57	0.57
Female Basal Ganglia ePVS Burden				
ePVS Volume	9.05×10^{-8}	-2.91×10^{-7}, 4.72×10^{-7}	0.63	0.75
ePVS Count	2.77×10^{-5}	-6.80×10^{-5}, 1.23×10^{-4}	0.56	0.75

Note. ePVS volume represents a log-transformed standardized measure of ePVS volume (values were divided by total basal ganglia tissue volume and then log-transformed). ePVS count represents a log-transformed measure of ePVS count. Analyses performed on n=153 participants. Models were adjusted for age, sex, race/ethnicity, education, *APOE*-ε4 status, cognitive diagnosis, and Framingham Stroke Risk Profile (excluding points assigned for age). *APOE*-ε4, apolipoprotein E ε4. CI, confidence interval. ePVS, enlarged perivascular space. The parameter estimates (β) for the interaction models are for the *$A\beta_{40}$ x APOE-ε4 carrier status* interaction term or the *$A\beta_{40}$ x cognitive diagnosis* interaction term or the *$A\beta_{40}$ x sex* interaction term and are interpreted as the difference in slopes between carriers and non-carriers or normal cognition and MCI or male and female. The parameter estimates (β) for the stratified models represent the changes in ePVS burden associated with one unit change in $A\beta_{40}$. Bold p-values meet the *a priori* significance threshold. FDR, false discovery rate.

Table 3.13. Cross-sectional CSF T-Tau Associations with Basal Ganglia ePVS Burden

	β	95% CI	*p-value*	*FDR p-value*
Basal Ganglia ePVS Burden				
ePVS Volume	5.15×10^{-7}	-9.88×10^{-7}, 2.02×10^{-6}	0.50	0.90
ePVS Count	2.39×10^{-4}	-1.43×10^{-4}, 6.22×10^{-4}	0.22	0.90
***APOE*-ε4 Status Interaction Basal Ganglia ePVS Burden**				
ePVS Volume	-2.27×10^{-6}	-5.30×10^{-6}, 7.52×10^{-7}	0.14	0.28
ePVS Count	-4.14×10^{-4}	-0.001, 3.59×10^{-4}	0.29	0.39
***APOE*-ε4 Carriers Basal Ganglia ePVS Burden**				
ePVS Volume	-9.03×10^{-7}	-3.21×10^{-6}, 1.40×10^{-6}	0.43	0.65
ePVS Count	-4.53×10^{-5}	-6.89×10^{-4}, 5.98×10^{-4}	0.89	0.90
***APOE*-ε4 Non-carriers Basal Ganglia ePVS Burden**				
ePVS Volume	1.28×10^{-6}	-8.49×10^{-7}, 3.41×10^{-6}	0.24	0.63
ePVS Count	2.60×10^{-4}	-2.50×10^{-4}, 7.71×10^{-4}	0.31	0.63
Diagnosis Interaction Basal Ganglia ePVS Burden				
ePVS Volume	3.46×10^{-7}	-2.86×10^{-6}, 3.55×10^{-6}	0.83	0.83
ePVS Count	1.94×10^{-4}	-6.24×10^{-4}, 0.001	0.64	0.77
Normal Cognition Basal Ganglia ePVS Burden				
ePVS Volume	-2.06×10^{-7}	-2.33×10^{-6}, 1.92×10^{-6}	0.85	0.92
ePVS Count	4.36×10^{-5}	-5.64×10^{-4}, 6.51×10^{-4}	0.89	0.92
MCI Basal Ganglia ePVS Burden				
ePVS Volume	6.38×10^{-7}	-2.03×10^{-6}, 3.31×10^{-6}	0.63	0.73
ePVS Count	2.05×10^{-4}	-4.01×10^{-4}, 8.11×10^{-4}	0.50	0.73
Sex Interaction Basal Ganglia ePVS Burden				
ePVS Volume	-3.07×10^{-6}	-5.88×10^{-6}, -2.53×10^{-7}	**0.03**	0.20
ePVS Count	-5.58×10^{-4}	-0.001, 1.63×10^{-4}	0.13	0.30
Male Basal Ganglia ePVS Burden				
ePVS Volume	1.91×10^{-6}	-2.51×10^{-7}, 4.07×10^{-6}	0.08	0.26
ePVS Count	5.95×10^{-4}	2.40×10^{-5}, 0.001	**0.04**	0.26

Female Basal Ganglia ePVS Burden				
ePVS Volume	-8.12×10^{-7}	-3.04×10^{-6}, 1.42×10^{-6}	0.47	0.75
ePVS Count	-1.15×10^{-4}	-6.77×10^{-4}, 4.48×10^{-3}	0.68	0.75

Note. ePVS volume represents a log-transformed standardized measure of ePVS volume (values were divided by total basal ganglia tissue volume and then log-transformed). ePVS count represents a log-transformed measure of ePVS count. Analyses performed on n=153 participants. Models were adjusted for age, sex, race/ethnicity, education, *APOE*-ε4 status, cognitive diagnosis, and Framingham Stroke Risk Profile (excluding points assigned for age). *APOE*-ε4, apolipoprotein E ε4. CI, confidence interval. ePVS, enlarged perivascular space. The parameter estimates (β) for the interaction models are for the *t-tau x APOE-ε4 carrier status* interaction term or the *t-tau x cognitive diagnosis* interaction term or the *t-tau x sex* interaction term and are interpreted as the difference in slopes between carriers and non-carriers or normal cognition and MCI or male and female. The parameter estimates (β) for the stratified models represent the changes in ePVS burden associated with one unit change in t-tau. Bold p-values meet the *a priori* significance threshold. FDR, false discovery rate.

Table 3.14. Cross-sectional CSF P-Tau Associations with Basal Ganglia ePVS Burden

	β	95% CI	*p-value*	*FDR p-value*
Basal Ganglia ePVS Burden				
ePVS Volume	4.86×10^{-6}	-8.16×10^{-6}, 1.79×10^{-5}	0.46	0.90
ePVS Count	0.002	-0.002, 0.005	0.31	0.90
***APOE*-ε4 Status Interaction Basal Ganglia ePVS Burden**				
ePVS Volume	-2.30×10^{-5}	-4.99×10^{-5}, 3.93×10^{-6}	0.09	0.28
ePVS Count	-0.004	-0.01, 0.002	0.20	0.30
***APOE*-ε4 Carriers Basal Ganglia ePVS Burden**				
ePVS Volume	-8.94×10^{-6}	-2.95×10^{-5}, 1.16×10^{-5}	0.38	0.65
ePVS Count	-0.001	-0.007, 0.004	0.61	0.81
***APOE*-ε4 Non-carriers Basal Ganglia ePVS Burden**				
ePVS Volume	1.23×10^{-5}	-5.63×10^{-6}, 3.02×10^{-5}	0.18	0.63
ePVS Count	0.002	-0.002, 0.007	0.28	0.63
Diagnosis Interaction Basal Ganglia ePVS Burden				
ePVS Volume	5.93×10^{-6}	-2.10×10^{-5}, 3.29×10^{-5}	0.66	0.77
ePVS Count	0.003	-0.004, 0.009	0.46	0.77
Normal Cognition Basal Ganglia ePVS Burden				
ePVS Volume	-2.34×10^{-6}	-1.90×10^{-5}, 1.44×10^{-5}	0.78	0.92
ePVS Count	-2.29×10^{-4}	-0.005, 0.005	0.92	0.92
MCI Basal Ganglia ePVS Burden				
ePVS Volume	6.65×10^{-6}	-1.81×10^{-5}, 3.14×10^{-5}	0.59	0.73
ePVS Count	0.002	-0.004, 0.007	0.58	0.73
Sex Interaction Basal Ganglia ePVS Burden				
ePVS Volume	-2.71×10^{-5}	-5.18×10^{-5}, -2.33×10^{-6}	**0.03**	0.20
ePVS Count	-0.004	-0.01, 0.002	0.18	0.30
Male Basal Ganglia ePVS Burden				
ePVS Volume	1.55×10^{-5}	-1.94×10^{-6}, 3.30×10^{-5}	0.08	0.26
ePVS Count	0.004	-5.92×10^{-4}, 0.009	0.09	0.26
Female Basal Ganglia ePVS Burden				
ePVS Volume	-7.57×10^{-6}	-2.81×10^{-5}, 1.29×10^{-5}	0.46	0.75
ePVS Count	-0.001	-0.006, 0.004	0.69	0.75

Note. ePVS volume represents a log-transformed standardized measure of ePVS volume (values were divided by total basal ganglia tissue volume and then log-transformed). ePVS count represents a log-

transformed measure of ePVS count. Analyses performed on n=153 participants. Models were adjusted for age, sex, race/ethnicity, education, *APOE*-ε4 status, cognitive diagnosis, and Framingham Stroke Risk Profile (excluding points assigned for age). *APOE*-ε4, apolipoprotein E ε4. CI, confidence interval. ePVS, enlarged perivascular space. The parameter estimates (β) for the interaction models are for the *p-tau x APOE-ε4 carrier status* interaction term or the *p-tau x cognitive diagnosis* interaction term or the *p-tau x sex* interaction term and are interpreted as the difference in slopes between carriers and non-carriers or normal cognition and MCI or male and female. The parameter estimates (β) for the stratified models represent the changes in ePVS burden associated with one unit change in p-tau. Bold p-values meet the *a priori* significance threshold. FDR, false discovery rate.

Longitudinal ePVS Burden

The average annual change in ePVS volume was 5.70 mm^3 and the average annual change in ePVS count was 1.89. The average annual change in ePVS volume ranged from -49.30 mm^3 to 78.08 mm^3 and the average annual change in ePVS count ranged from -27.04 to 22.62.

Age and Longitudinal ePVS Burden Outcomes

Age was not associated with longitudinal change in basal ganglia ePVS burden (p>0.08). See **Table 3.15** for details.

The *age x APOE-ε4 status* interaction term was associated with longitudinal basal ganglia ePVS count (β=-0.26, p=0.001) and standardized ePVS volume (β=-$1.05x10^{-5}$, p<0.001). Results were the same when excluding outliers as well as when excluding participants with CVD and atrial fibrillation. In stratified models, among *APOE*-ε4 carriers, greater age was associated with longitudinal decrease in basal ganglia ePVS count (β=-0.14, p=0.03) and standardized ePVS volume (β=-$8.02x10^{-6}$, p=0.004). Among *APOE*-ε4 non-carriers, greater age was associated with longitudinal increase in basal ganglia ePVS count (β=0.13, p=0.003) but not standardized ePVS volume (p=0.08). Results were the same when excluding outliers. When excluding participants

with CVD and atrial fibrillation, associations among *APOE*-ε4 carriers were attenuated (p>0.09). See **Table 3.15** and **Figure 3.6** for details.

The *age x cognitive diagnosis* interaction term was unrelated to longitudinal basal ganglia ePVS burden (p>0.77). Stratified models were also null (p>0.13). See **Table 3.15** for details.

The *age x sex* interaction term was unrelated to longitudinal basal ganglia ePVS burden (p>0.50). Stratified models were also null (p>0.08). See **Table 3.15** for details.

Table 3.15. Age Associations with Longitudinal Basal Ganglia ePVS Burden

	β	95% CI	*p-value*	*FDR p-value*
Basal Ganglia ePVS Burden				
ePVS Volume	$1.63x10^{-7}$	$-2.59x10^{-6}$, $2.92x10^{-6}$	0.91	>0.99
ePVS Count	0.06	-0.009, 0.13	0.09	0.27
***APOE*-ε4 Status Interaction Basal Ganglia ePVS Burden**				
ePVS Volume	$-1.05x10^{-5}$	$-1.68x10^{-5}$, $-4.33x10^{-6}$	**<0.001**	**0.001**
ePVS Count	-0.26	-0.42, -0.10	**0.001**	**0.001**
***APOE*-ε4 Carriers Basal Ganglia ePVS Burden**				
ePVS Volume	$-8.02x10^{-6}$	$-1.34x10^{-5}$, $-2.60x10^{-6}$	**0.004**	**0.006**
ePVS Count	-0.14	-0.27, -0.01	**0.03**	**0.03**
***APOE*-ε4 Non-carriers Basal Ganglia ePVS Burden**				
ePVS Volume	$2.82x10^{-6}$	$-3.29x10^{-7}$, $5.97x10^{-6}$	0.08	0.10
ePVS Count	0.13	0.04, 0.21	**0.003**	**0.009**
Diagnosis Interaction Basal Ganglia ePVS Burden				
ePVS Volume	$8.24x10^{-7}$	$-4.94x10^{-6}$, $6.58x10^{-6}$	0.78	0.93
ePVS Count	-0.006	-0.16, 0.15	0.93	0.93
Normal Cognition Basal Ganglia ePVS Burden				
ePVS Volume	$-4.05x10^{-8}$	$-3.13x10^{-6}$, $3.05x10^{-6}$	0.98	0.98
ePVS Count	0.07	-0.02, 0.15	0.14	0.41
MCI Basal Ganglia ePVS Burden				
ePVS Volume	$6.59x10^{-7}$	$-4.56x10^{-6}$, $5.88x10^{-6}$	0.80	0.80
ePVS Count	0.05	-0.08, 0.18	0.43	0.80
Sex Interaction Basal Ganglia ePVS Burden				
ePVS Volume	$1.85x10^{-6}$	$-3.65x10^{-6}$, $7.35x10^{-6}$	0.51	0.56
ePVS Count	-0.04	-0.18, 0.10	0.56	0.56
Male Basal Ganglia ePVS Burden				
ePVS Volume	$-5.47x10^{-7}$	$-4.81x10^{-6}$, $3.72x10^{-6}$	0.80	0.80
ePVS Count	0.10	-0.01, 0.20	0.08	0.25
Female Basal Ganglia ePVS Burden				
ePVS Volume	$1.33x10^{-6}$	$-2.17x10^{-6}$, $4.82x10^{-6}$	0.46	0.46
ePVS Count	0.06	-0.04, 0.15	0.23	0.23

Note. ePVS volume represents a standardized measure of ePVS volume (values were divided by total basal ganglia tissue volume). Analyses performed on n=327 participants. Models were adjusted for age, sex, race/ethnicity, education, *APOE*-ε4 status, cognitive diagnosis, and Framingham Stroke Risk Profile (excluding points assigned for age). *APOE*-ε4, apolipoprotein E ε4. CI, confidence interval. ePVS, enlarged perivascular space. The parameter estimates (β) for the interaction models are for the *age x time x APOE-ε4 carrier status* interaction term or the *age x time x cognitive diagnosis* interaction term or the *age x time x sex* interaction term and are interpreted as the difference in longitudinal change slopes between carriers and non-carriers or normal cognition and MCI or male and female. The parameter estimates (β) for the stratified models represent the changes in longitudinal slopes for ePVS burden associated with one unit change in age. Bold p-values meet the *a priori* significance threshold. FDR, false discovery rate.

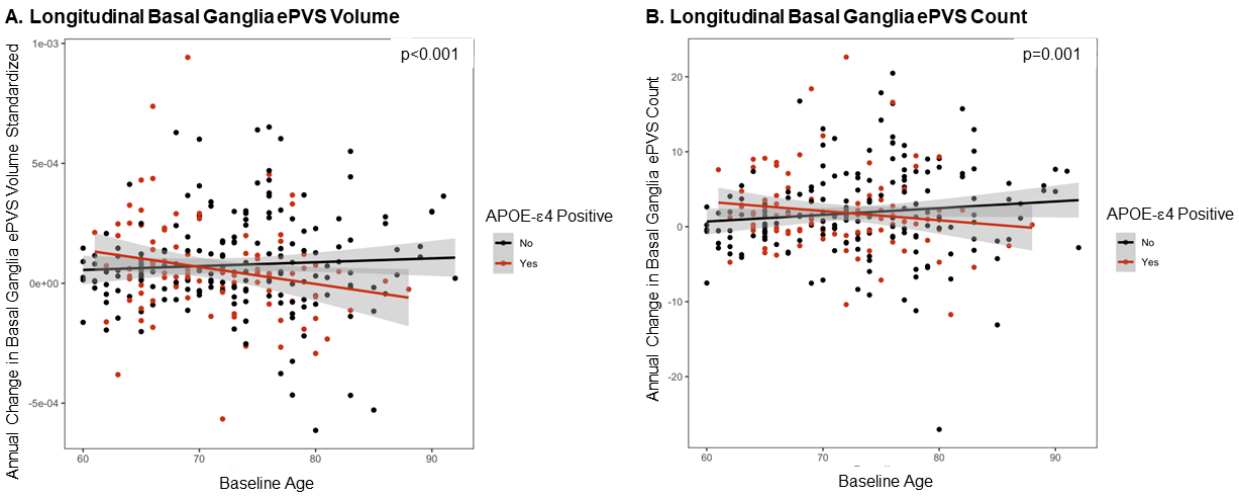

Figure 3.6. Baseline *Age x APOE-ε4 status* interactions on longitudinal basal ganglia ePVS burden. **(A)** longitudinal ePVS volume and **(B)** longitudinal ePVS count. The ePVS volume variable is standardized by dividing by basal ganglia tissue volume. In stratified models among *APOE*-ε4 carriers, age was associated with longitudinal ePVS volume (p=0.004) and ePVS count (p=0.03). Among *APOE*-ε4 non-carriers, baseline age was associated with longitudinal ePVS count (p=0.003).

PWV and Longitudinal ePVS Burden Outcomes

Aortic PWV was not associated with longitudinal basal ganglia ePVS burden (p>0.40). See **Table 3.16** for details.

The *aortic PWV x APOE-ε4 status* interaction term was unrelated to longitudinal basal ganglia ePVS burden (p>0.08). Stratified models were also null (p>0.13).

The *aortic PWV x cognitive diagnosis* interaction term was unrelated to longitudinal basal ganglia ePVS burden (p>0.33). Stratified models were also null

(p>0.31).

The *aortic PWV x sex* interaction term was unrelated to longitudinal basal ganglia ePVS burden (p>0.53). Stratified models were also null (p>0.73).

Table 3.16. Aortic PWV Associations with Longitudinal Basal Ganglia ePVS Burden

	β	95% CI	*p-value*	*FDR p-value*
Basal Ganglia ePVS Burden				
ePVS Volume	-1.09×10^{-6}	-7.86×10^{-6}, 5.69×10^{-6}	0.75	0.76
ePVS Count	-0.07	-0.25, 0.10	0.41	0.76
***APOE*-ε4 Status Interaction Basal Ganglia ePVS Burden**				
ePVS Volume	-1.55×10^{-5}	-3.29×10^{-5}, 1.95×10^{-6}	0.08	0.14
ePVS Count	-0.26	-0.71, 0.20	0.27	0.27
***APOE*-ε4 Carriers Basal Ganglia ePVS Burden**				
ePVS Volume	-1.24×10^{-5}	-2.89×10^{-5}, 4.07×10^{-6}	0.14	0.18
ePVS Count	-0.28	-0.65, 0.10	0.15	0.18
***APOE*-ε4 Non-carriers Basal Ganglia ePVS Burden**				
ePVS Volume	8.19×10^{-7}	-6.63×10^{-6}, 8.27×10^{-6}	0.83	0.90
ePVS Count	-0.05	-0.25, 0.16	0.67	0.90
Diagnosis Interaction Basal Ganglia ePVS Burden				
ePVS Volume	-6.81×10^{-6}	-2.06×10^{-5}, 6.96×10^{-6}	0.33	0.65
ePVS Count	-0.005	-0.38, 0.36	0.98	0.98
Normal Cognition Basal Ganglia ePVS Burden				
ePVS Volume	1.53×10^{-6}	-6.29×10^{-6}, 9.34×10^{-6}	0.70	0.85
ePVS Count	-0.08	-0.30, 0.14	0.46	0.85
MCI Basal Ganglia ePVS Burden				
ePVS Volume	-6.10×10^{-6}	-1.81×10^{-5}, 5.89×10^{-6}	0.32	0.35
ePVS Count	-0.14	-0.45, 0.16	0.35	0.35
Sex Interaction Basal Ganglia ePVS Burden				
ePVS Volume	4.41×10^{-6}	-9.41×10^{-6}, 1.82×10^{-5}	0.53	0.80
ePVS Count	-0.01	-0.37, 0.35	0.95	0.95
Male Basal Ganglia ePVS Burden				
ePVS Volume	-1.28×10^{-7}	-1.14×10^{-5}, 1.11×10^{-5}	0.98	0.98
ePVS Count	0.03	-0.26, 0.31	0.85	0.98
Female Basal Ganglia ePVS Burden				
ePVS Volume	1.02×10^{-6}	-7.19×10^{-6}, 9.24×10^{-6}	0.81	0.81
ePVS Count	-0.04	-0.26, 0.19	0.73	0.81

Note. ePVS volume represents a standardized measure of ePVS volume (values were divided by total basal ganglia tissue volume). Analyses performed on n=302 participants. Models were adjusted for age, sex, race/ethnicity, education, *APOE*-ε4 status, cognitive diagnosis, and Framingham Stroke Risk Profile (excluding points assigned for age). *APOE*-ε4, apolipoprotein E ε4. CI, confidence interval. ePVS, enlarged perivascular space. The parameter estimates (β) for the interaction models are for the *aortic PWV x time x APOE-ε4 carrier status* interaction term or the *aortic PWV x time x cognitive diagnosis* interaction term or the *aortic PWV x time x sex* interaction term and are interpreted as the difference in longitudinal change slopes between carriers and non-carriers or normal cognition and MCI

or male and female. The parameter estimates (β) for the stratified models represent the changes in longitudinal slopes for ePVS burden associated with one unit change in aortic PWV. Bold p-values meet the *a priori* significance threshold. FDR, false discovery rate.

Hypertension and Longitudinal ePVS Burden Outcomes

Hypertension medication usage was not associated with longitudinal basal ganglia ePVS burden (p>0.58). See **Table 3.17** for details.

The *hypertension medication usage x APOE-ε4 status* interaction term was unrelated to longitudinal basal ganglia ePVS burden (p>0.76). Stratified models were also null (p>0.50).

The *hypertension medication usage x cognitive diagnosis* interaction term was unrelated to longitudinal basal ganglia ePVS burden (p>0.05). Stratified models were also null (p>0.07).

The *hypertension medication usage x sex* interaction term was unrelated to longitudinal basal ganglia ePVS burden (p>0.70). Stratified models were also null (p>0.60).

Table 3.17. Hypertension Medication Usage Associations with Longitudinal Basal Ganglia ePVS Burden

	β	95% CI	*p-value*	*FDR p-value*
Basal Ganglia ePVS Burden				
ePVS Volume	7.61×10^{-6}	-3.09×10^{-5}, 4.61×10^{-5}	0.70	0.88
ePVS Count	0.28	-0.71, 1.26	0.59	0.88
***APOE*-ε4 Status Interaction Basal Ganglia ePVS Burden**				
ePVS Volume	1.21×10^{-5}	-6.85×10^{-5}, 9.28×10^{-5}	0.77	0.83
ePVS Count	-0.22	-2.30, 1.86	0.83	0.83
***APOE*-ε4 Carriers Basal Ganglia ePVS Burden**				
ePVS Volume	2.29×10^{-5}	-4.48×10^{-5}, 9.06×10^{-5}	0.51	0.83
ePVS Count	0.32	-1.24, 1.88	0.69	0.83
***APOE*-ε4 Non-carriers Basal Ganglia ePVS Burden**				
ePVS Volume	1.58×10^{-6}	-4.59×10^{-5}, 4.91×10^{-5}	0.95	0.99
ePVS Count	0.27	-1.03, 1.57	0.68	0.99
Diagnosis Interaction Basal Ganglia ePVS Burden				

ePVS Volume	$6.75x10^{-5}$	$-1.11x10^{-5}$, $1.46x10^{-4}$	0.09	0.13
ePVS Count	2.04	-0.04, 4.12	0.05	0.11
Normal Cognition Basal Ganglia ePVS Burden				
ePVS Volume	$-1.42x10^{-5}$	$-5.87x10^{-5}$, $3.03x10^{-5}$	0.53	0.54
ePVS Count	-0.39	-1.65, 0.86	0.54	0.54
MCI Basal Ganglia ePVS Burden				
ePVS Volume	$5.15x10^{-5}$	$-1.82x10^{-5}$, $1.21x10^{-4}$	0.15	0.22
ePVS Count	1.53	-0.18, 3.25	0.08	0.16
Sex Interaction Basal Ganglia ePVS Burden				
ePVS Volume	$-1.53x10^{-5}$	$-9.37x10^{-5}$, $6.32x10^{-5}$	0.70	0.84
ePVS Count	-0.05	-2.06, 1.97	0.96	0.96
Male Basal Ganglia ePVS Burden				
ePVS Volume	$1.31x10^{-5}$	$-3.90x10^{-5}$, $6.53x10^{-5}$	0.62	0.82
ePVS Count	0.30	-1.04, 1.63	0.66	0.82
Female Basal Ganglia ePVS Burden				
ePVS Volume	$1.87x10^{-6}$	$-5.48x10^{-5}$, $5.85x10^{-5}$	0.95	0.97
ePVS Count	0.40	-1.11, 1.92	0.60	0.90

Note. ePVS volume represents a standardized measure of ePVS volume (values were divided by total basal ganglia tissue volume). Analyses performed on n=327 participants. Models were adjusted for age, sex, race/ethnicity, education, *APOE*-ε4 status, cognitive diagnosis, and Framingham Stroke Risk Profile (excluding points assigned for age). *APOE*-ε4, apolipoprotein E ε4. CI, confidence interval. ePVS, enlarged perivascular space. The parameter estimates (β) for the interaction models are for the *hypertension medication usage x time x APOE-ε4 carrier status* interaction term or the *hypertension medication usage x time x cognitive diagnosis* interaction term or the *hypertension medication usage x time x sex* interaction term and are interpreted as the difference in longitudinal change slopes between carriers and non-carriers or normal cognition and MCI or male and female. The parameter estimates (β) for the stratified models represent the changes in longitudinal slopes for ePVS burden associated with one unit change in hypertension medication usage. Bold p-values meet the *a priori* significance threshold. FDR, false discovery rate.

Inflammation and Longitudinal ePVS Burden Outcomes

Greater CSF sTREM2 levels were associated with longitudinal increase in basal ganglia ePVS count (β=0.0006, p=0.001) and standardized ePVS volume ($\beta=1.83x10^{-8}$, p=0.01). Results were the same when excluding outliers as well as when excluding participants with CVD and atrial fibrillation. See **Table 3.18** and **Figure 3.7** for details.

Greater CSF MMP2 levels were associated with longitudinal increase in basal ganglia ePVS count ($\beta=6.13x10^{-5}$, p=0.007) and standardized ePVS volume ($\beta=1.77x10^{-9}$, p=0.03). Results were the same when excluding outliers. When excluding participants with CVD and atrial fibrillation, the association with ePVS count remained

(p=0.03) but the association with ePVS volume was attenuated (p=0.06). See **Table 3.19** and **Figure 3.7** for details.

Greater CSF MMP3 levels were associated with longitudinal increase in basal ganglia ePVS count (β=0.006, p=0.004) and standardized ePVS volume (β=1.81x10^{-7}, p=0.03). Results were the same when excluding outliers as well as when excluding participants with CVD and atrial fibrillation. See **Table 3.20** and **Figure 3.7** for details.

Associations relating TNF-α, IL-6, and CSF MMP9 to longitudinal basal ganglia ePVS burden were all null (p>0.61). See **Tables 3.21** to **3.23** for details.

The *CSF MMP2 x APOE-ε4 status* interaction term was associated with longitudinal basal ganglia ePVS count (β=-9.43x10^{-5}, p=0.04) but not standardized ePVS volume (p=0.47). In stratified models, among *APOE*-ε4 carriers, CSF MMP2 levels were unrelated to longitudinal basal ganglia ePVS burden (p>0.58). Among *APOE*-ε4 non-carriers, greater CSF MMP2 levels were associated with longitudinal increase in basal ganglia ePVS count (β=9.81x10^{-5}, p<0.001) and standardized ePVS volume (β=2.29x10^{-9}, p=0.03). Results were the same when excluding outliers as well as when excluding participants with CVD and atrial fibrillation. See **Table 3.19** for details.

Associations between the *TNF-α x APOE-ε4 status*, *IL-6 x APOE-ε4 status*, *CSF sTREM2 x APOE-ε4 status*, *CSF MMP3 x APOE-ε4 status*, and *CSF MMP9 x APOE-ε4 status* interaction terms and longitudinal basal ganglia ePVS burden were null (p>0.12). In stratified models, greater CSF sTREM2 levels were associated with longitudinal increase in basal ganglia ePVS count (β=0.0009, p<0.001) and standardized ePVS volume (β=2.54x10^{-8}, p=0.004) among *APOE*-ε4 non-carriers. Results for CSF sTREM2

models stratified by *APOE*-ε4 carrier status were unchanged when excluding outliers as well as when excluding participants with CVD and atrial fibrillation. Greater CSF MMP3 levels were associated with longitudinal increase in basal ganglia ePVS count (β=0.006, p=0.03) but not standardized ePVS volume (p=0.15), among *APOE*-ε4 non-carriers. The association between MMP3 and ePVS count among *APOE*-ε4 non-carriers remained significant when excluding outliers as well as when excluding participants with CVD and atrial fibrillation. All other TNF-α, IL-6, CSF sTREM2, CSF MMP3, and CSF MMP9 models stratified by *APOE*-ε4 carrier status were null (p>0.13). See **Tables 3.18** and **3.20** to **3.23** for details.

The *CSF sTREM2 x cognitive diagnosis* interaction term was associated with longitudinal basal ganglia standardized ePVS volume ($\beta=3.97\times10^{-8}$, p=0.02) but not ePVS count (p=0.56). The association remained significant when excluding outliers as well as when excluding participants with CVD and atrial fibrillation. In stratified models, among participants with normal cognition, greater CSF sTREM2 levels were associated with longitudinal increase in basal ganglia ePVS count (β=0.0005, p=0.05) but not standardized ePVS volume (p=0.75). The association was attenuated when excluding outliers (p=0.11) but remained when excluding participants with CVD and atrial fibrillation (p=0.04). Among participants with MCI, greater CSF sTREM2 levels were associated with longitudinal increase in basal ganglia ePVS count (β=0.0008, p=0.03) and standardized ePVS volume ($\beta=4.42\times10^{-8}$, p=0.003). When excluding participants with CVD and atrial fibrillation, results were unchanged. When excluding outliers, the association with ePVS count among MCI participants was attenuated (p=0.08) but the association with ePVS volume remained. See **Table 3.18** for details.

The *CSF MMP3 x cognitive diagnosis* interaction term was associated with longitudinal basal ganglia ePVS count (β=-0.01, p=0.04) but not standardized ePVS volume (p=0.46). The association was attenuated when excluding outliers (p=0.17) but remained when excluding participants with CVD and atrial fibrillation. In stratified models, among participants with normal cognition, greater CSF MMP3 levels were associated with longitudinal increase in basal ganglia ePVS count (β=0.008, p=0.002) but not standardized ePVS volume (p=0.08). Results were the same when excluding outliers as well as when excluding participants with CVD and atrial fibrillation. Among participants with MCI, results were null (p>0.52). See **Table 3.20** for details.

Associations between the *TNF-α x cognitive diagnosis*, *IL-6 x cognitive diagnosis*, *CSF MMP2 x cognitive diagnosis*, and *CSF MMP9 x cognitive diagnosis* interaction terms were unrelated to longitudinal basal ganglia ePVS burden (p>0.10). In stratified models, greater CSF MMP2 levels were associated with longitudinal increase in basal ganglia ePVS count among normal cognition participants (b=5.90x10^{-5}, p=0.04). The association was attenuated when excluding outliers (p=0.07) and when excluding participants with CVD and atrial fibrillation (p=0.10). All other TNF-α, IL-6, CSF MMP2, and CSF MMP9 models stratified by cognitive diagnosis were null (p>0.07). See **Tables 3.19** and **3.21** to **3.23** for details.

Associations between the *TNF-α x sex*, *IL-6 x sex*, *CSF sTREM2 x sex*, *CSF MMP2 x sex*, *CSF MMP3 x sex*, and *CSF MMP9 x sex* interaction terms were unrelated to longitudinal basal ganglia ePVS burden (p>0.06). In stratified models, greater CSF sTREM2 levels were associated with longitudinal increase in basal ganglia ePVS count (β=0.0006, p=0.007) and standardized ePVS volume (β=2.27x10^{-8}, p=0.007) among

male participants. Results were the same when excluding outliers as well as when excluding participants with CVD and atrial fibrillation. Among male participants, greater CSF MMP3 levels were associated with longitudinal increase in basal ganglia ePVS count (b=0.007, p=0.009) and standardized ePVS volume (b=$2.32x10^{-7}$, p=0.02). Results were the same when excluding outliers as well as when excluding participants with CVD and atrial fibrillation. All other TNF-a, IL-6, CSF sTREM2, CSF MMP2, CSF MMP3, and CSF MMP9 models stratified by sex were null (p>0.05). See **Tables 3.18** to **3.23** for details.

Table 3.18. CSF sTREM2 Associations with Longitudinal Basal Ganglia ePVS Burden

	β	95% CI	*p-value*	*FDR p-value*
Basal Ganglia ePVS Burden				
ePVS Volume	$1.83x10^{-8}$	$3.99x10^{-9}$, $3.27x10^{-8}$	**0.01**	0.05
ePVS Count	$6.47x10^{-4}$	$2.56x10^{-4}$, 0.001	**0.001**	**0.03**
***APOE*-ε4 Status Interaction Basal Ganglia ePVS Burden**				
ePVS Volume	$-2.04x10^{-8}$	$-5.09x10^{-8}$, $1.01x10^{-8}$	0.19	0.35
ePVS Count	$-6.49x10^{-4}$	-0.001, $1.89x10^{-4}$	0.13	0.35
***APOE*-ε4 Carriers Basal Ganglia ePVS Burden**				
ePVS Volume	$-2.40x10^{-9}$	$-2.93x10^{-8}$, $2.45x10^{-8}$	0.86	0.90
ePVS Count	$5.61x10^{-5}$	$-6.52x10^{-4}$, $7.64x10^{-4}$	0.88	0.90
***APOE*-ε4 Non-carriers Basal Ganglia ePVS Burden**				
ePVS Volume	$2.54x10^{-8}$	$8.38x10^{-9}$, $4.24x10^{-8}$	**0.004**	**0.01**
ePVS Count	$8.76x10^{-4}$	$4.04x10^{-4}$, 0.001	**<0.001**	**0.007**
Diagnosis Interaction Basal Ganglia ePVS Burden				
ePVS Volume	$3.97x10^{-8}$	$7.60x10^{-9}$, $7.18x10^{-8}$	**0.02**	0.19
ePVS Count	$2.61x10^{-4}$	$-6.22x10^{-4}$, 0.001	0.56	0.78
Normal Cognition Basal Ganglia ePVS Burden				
ePVS Volume	$2.98x10^{-9}$	$-1.51x10^{-8}$, $2.10x10^{-8}$	0.75	0.89
ePVS Count	$5.17x10^{-4}$	$3.54x10^{-7}$, 0.001	**0.05**	0.35
MCI Basal Ganglia ePVS Burden				
ePVS Volume	$4.42x10^{-8}$	$1.52x10^{-8}$, $7.32x10^{-8}$	**0.003**	**0.03**
ePVS Count	$8.38x10^{-4}$	$6.29x10^{-5}$, 0.002	**0.03**	0.24
Sex Interaction Basal Ganglia ePVS Burden				
ePVS Volume	$-3.50x10^{-8}$	$-7.19x10^{-8}$, $1.84x10^{-9}$	0.06	0.58
ePVS Count	$-3.71x10^{-4}$	-0.001, $6.52x10^{-4}$	0.48	0.90
Male Basal Ganglia ePVS Burden				
ePVS Volume	$2.27x10^{-8}$	$6.31x10^{-9}$, $3.92x10^{-8}$	**0.007**	**0.05**
ePVS Count	$6.22x10^{-4}$	$1.72x10^{-4}$, 0.001	**0.007**	**0.05**

Female Basal Ganglia ePVS Burden				
ePVS Volume	-1.43×10^{-8}	-4.75×10^{-8}, 1.90×10^{-8}	0.40	0.83
ePVS Count	3.35×10^{-5}	-9.43×10^{-4}, 0.001	0.95	0.95

Note. ePVS volume represents a standardized measure of ePVS volume (values were divided by total basal ganglia tissue volume). Analyses performed on n=153 participants. Models were adjusted for age, sex, race/ethnicity, education, *APOE*-ε4 status, cognitive diagnosis, and Framingham Stroke Risk Profile (excluding points assigned for age). *APOE*-ε4, apolipoprotein E ε4. CI, confidence interval. ePVS, enlarged perivascular space. The parameter estimates (β) for the interaction models are for the *sTREM2 x time x APOE-ε4 carrier status* interaction term or the *sTREM2 x time x cognitive diagnosis* interaction term or the *sTREM2 x time x sex* interaction term and are interpreted as the difference in longitudinal change slopes between carriers and non-carriers or normal cognition and MCI or male and female. The parameter estimates (β) for the stratified models represent the changes in longitudinal slopes for ePVS burden associated with one unit change in sTREM2. Bold p-values meet the *a priori* significance threshold. FDR, false discovery rate.

Table 3.19. CSF MMP2 Associations with Longitudinal Basal Ganglia ePVS Burden

	β	95% CI	*p-value*	*FDR p-value*
Basal Ganglia ePVS Burden				
ePVS Volume	1.77×10^{-9}	1.27×10^{-10}, 3.41×10^{-9}	**0.03**	0.09
ePVS Count	6.13×10^{-5}	1.68×10^{-5}, 1.06×10^{-4}	**0.007**	**0.04**
***APOE*-ε4 Status Interaction Basal Ganglia ePVS Burden**				
ePVS Volume	-1.23×10^{-9}	-4.59×10^{-9}, 2.13×10^{-9}	0.47	0.56
ePVS Count	-9.43×10^{-5}	-1.84×10^{-4}, -4.63×10^{-6}	**0.04**	0.28
***APOE*-ε4 Carriers Basal Ganglia ePVS Burden**				
ePVS Volume	7.70×10^{-10}	-1.99×10^{-9}, 3.53×10^{-9}	0.58	0.76
ePVS Count	-4.66×10^{-6}	-7.63×10^{-5}, 6.70×10^{-5}	0.90	0.90
***APOE*-ε4 Non-carriers Basal Ganglia ePVS Burden**				
ePVS Volume	2.29×10^{-9}	1.86×10^{-10}, 4.40×10^{-9}	**0.03**	0.07
ePVS Count	9.81×10^{-5}	4.17×10^{-5}, 1.55×10^{-4}	**<0.001**	**0.008**
Diagnosis Interaction Basal Ganglia ePVS Burden				
ePVS Volume	2.47×10^{-9}	-1.36×10^{-9}, 6.30×10^{-9}	0.20	0.78
ePVS Count	2.31×10^{-5}	-7.78×10^{-5}, 1.24×10^{-4}	0.65	0.78
Normal Cognition Basal Ganglia ePVS Burden				
ePVS Volume	9.78×10^{-10}	-9.94×10^{-10}, 2.95×10^{-9}	0.33	0.80
ePVS Count	5.90×10^{-5}	3.98×10^{-6}, 1.14×10^{-4}	**0.04**	0.35
MCI Basal Ganglia ePVS Burden				
ePVS Volume	3.35×10^{-9}	-3.59×10^{-10}, 7.05×10^{-9}	0.08	0.36
ePVS Count	6.98×10^{-5}	-1.96×10^{-5}, 1.59×10^{-4}	0.12	0.44
Sex Interaction Basal Ganglia ePVS Burden				
ePVS Volume	6.35×10^{-10}	-2.99×10^{-9}, 4.26×10^{-9}	0.73	0.90
ePVS Count	3.73×10^{-5}	-6.11×10^{-5}, 1.36×10^{-4}	0.46	0.90
Male Basal Ganglia ePVS Burden				
ePVS Volume	1.46×10^{-9}	-5.79×10^{-10}, 3.51×10^{-9}	0.16	0.37
ePVS Count	4.10×10^{-5}	-1.33×10^{-5}, 9.52×10^{-5}	0.14	0.37
Female Basal Ganglia ePVS Burden				
ePVS Volume	1.69×10^{-9}	-1.25×10^{-9}, 4.64×10^{-9}	0.26	0.77
ePVS Count	7.27×10^{-5}	-1.34×10^{-5}, 1.59×10^{-4}	0.10	0.56

Note. ePVS volume represents a standardized measure of ePVS volume (values were divided by total basal ganglia tissue volume). Analyses performed on n=152 participants. Models were adjusted for

age, sex, race/ethnicity, education, *APOE*-ε4 status, cognitive diagnosis, and Framingham Stroke Risk Profile (excluding points assigned for age). *APOE*-ε4, apolipoprotein E ε4. CI, confidence interval. ePVS, enlarged perivascular space. The parameter estimates (β) for the interaction models are for the *MMP2 x time x APOE-ε4 carrier status* interaction term or the *MMP2 x time x cognitive diagnosis* interaction term or the *MMP2 x time x sex* interaction term and are interpreted as the difference in longitudinal change slopes between carriers and non-carriers or normal cognition and MCI or male and female. The parameter estimates (β) for the stratified models represent the changes in longitudinal slopes for ePVS burden associated with one unit change in MMP2. Bold p-values meet the *a priori* significance threshold. FDR, false discovery rate.

Table 3.20. CSF MMP3 Associations with Longitudinal Basal Ganglia ePVS Burden

	β	95% CI	*p-value*	*FDR p-value*
Basal Ganglia ePVS Burden				
ePVS Volume	$1.81x10^{-7}$	$2.02x10^{-8}$, $3.41x10^{-7}$	**0.03**	0.09
ePVS Count	0.006	0.002, 0.01	**0.004**	**0.04**
***APOE*-ε4 Status Interaction Basal Ganglia ePVS Burden**				
ePVS Volume	$1.80x10^{-7}$	$-1.98x10^{-7}$, $5.58x10^{-7}$	0.35	0.50
ePVS Count	0.002	-0.009, 0.01	0.73	0.73
***APOE*-ε4 Carriers Basal Ganglia ePVS Burden**				
ePVS Volume	$2.48x10^{-7}$	$-9.39x10^{-8}$, $5.89x10^{-7}$	0.15	0.59
ePVS Count	0.007	-0.002, 0.02	0.14	0.59
***APOE*-ε4 Non-carriers Basal Ganglia ePVS Burden**				
ePVS Volume	$1.40x10^{-7}$	$-4.86x10^{-8}$, $3.28x10^{-7}$	0.15	0.28
ePVS Count	0.006	$4.44x10^{-4}$, 0.01	**0.03**	0.08
Diagnosis Interaction Basal Ganglia ePVS Burden				
ePVS Volume	$-1.48x10^{-7}$	$-5.45x10^{-7}$, $2.49x10^{-7}$	0.46	0.78
ePVS Count	-0.01	-0.02, $-5.66x10^{-4}$	**0.04**	0.27
Normal Cognition Basal Ganglia ePVS Burden				
ePVS Volume	$1.76x10^{-7}$	$-2.30x10^{-8}$, $3.74x10^{-7}$	0.08	0.35
ePVS Count	0.008	0.003, 0.01	**0.002**	0.05
MCI Basal Ganglia ePVS Burden				
ePVS Volume	$6.33x10^{-9}$	$-3.98x10^{-7}$, $4.11x10^{-7}$	0.98	>0.99
ePVS Count	-0.003	-0.01, 0.007	0.52	0.95
Sex Interaction Basal Ganglia ePVS Burden				
ePVS Volume	$-2.72x10^{-7}$	$-6.24x10^{-7}$, $7.97x10^{-8}$	0.13	0.58
ePVS Count	-0.006	-0.02, 0.004	0.22	0.65
Male Basal Ganglia ePVS Burden				
ePVS Volume	$2.32x10^{-7}$	$3.03x10^{-8}$, $4.33x10^{-7}$	**0.02**	0.10
ePVS Count	0.007	0.002, 0.01	**0.009**	**0.05**
Female Basal Ganglia ePVS Burden				
ePVS Volume	$-1.33x10^{-8}$	$-3.07x10^{-7}$, $2.80x10^{-7}$	0.93	0.95
ePVS Count	0.001	-0.007, 0.01	0.78	0.95

Note. ePVS volume represents a standardized measure of ePVS volume (values were divided by total basal ganglia tissue volume). Analyses performed on n=151 participants. Models were adjusted for age, sex, race/ethnicity, education, *APOE*-ε4 status, cognitive diagnosis, and Framingham Stroke Risk Profile (excluding points assigned for age). *APOE*-ε4, apolipoprotein E ε4. CI, confidence interval. ePVS, enlarged perivascular space. The parameter estimates (β) for the interaction models are for the *MMP3 x time x APOE-ε4 carrier status* interaction term or the *MMP3 x time x cognitive diagnosis* interaction term or the *MMP3 x time x sex* interaction term and are interpreted as the difference in

longitudinal change slopes between carriers and non-carriers or normal cognition and MCI or male and female. The parameter estimates (β) for the stratified models represent the changes in longitudinal slopes for ePVS burden associated with one unit change in MMP3. Bold p-values meet the *a priori* significance threshold. FDR, false discovery rate.

Table 3.21. TNF-α Associations with Longitudinal Basal Ganglia ePVS Burden

	β	95% CI	*p-value*	*FDR p-value*
Basal Ganglia ePVS Burden				
ePVS Volume	$1.13x10^{-6}$	$-5.18x10^{-6}$, $7.45x10^{-6}$	0.72	0.85
ePVS Count	0.02	-0.14, 0.18	0.79	0.85
***APOE*-ε4 Status Interaction Basal Ganglia ePVS Burden**				
ePVS Volume	$-9.66x10^{-6}$	$-2.48x10^{-5}$, $5.48x10^{-6}$	0.21	0.35
ePVS Count	-0.14	-0.53, 0.25	0.48	0.56
***APOE*-ε4 Carriers Basal Ganglia ePVS Burden**				
ePVS Volume	$-6.12x10^{-6}$	$-1.99x10^{-5}$, $7.67x10^{-6}$	0.38	0.76
ePVS Count	-0.11	-0.44, 0.21	0.49	0.76
***APOE*-ε4 Non-carriers Basal Ganglia ePVS Burden**				
ePVS Volume	$2.94x10^{-6}$	$-4.13x10^{-6}$, $9.99x10^{-6}$	0.41	0.62
ePVS Count	0.05	-0.15, 0.24	0.64	0.74
Diagnosis Interaction Basal Ganglia ePVS Burden				
ePVS Volume	$3.00x10^{-6}$	$-1.15x10^{-5}$, $1.75x10^{-5}$	0.68	0.78
ePVS Count	0.31	-0.07, 0.70	0.11	0.57
Normal Cognition Basal Ganglia ePVS Burden				
ePVS Volume	$1.62x10^{-6}$	$-4.89x10^{-6}$, $8.12x10^{-6}$	0.62	0.87
ePVS Count	-0.03	-0.21, 0.15	0.76	0.89
MCI Basal Ganglia ePVS Burden				
ePVS Volume	$2.56x10^{-6}$	$-1.16x10^{-5}$, $1.67x10^{-5}$	0.72	0.99
ePVS Count	0.23	-0.12, 0.58	0.20	0.59
Sex Interaction Basal Ganglia ePVS Burden				
ePVS Volume	$-3.86x10^{-6}$	$-1.87x10^{-5}$, $1.10x10^{-5}$	0.61	0.90
ePVS Count	-0.11	-0.49, 0.27	0.58	0.90
Male Basal Ganglia ePVS Burden				
ePVS Volume	$2.43x10^{-6}$	$-5.28x10^{-6}$, $1.02x10^{-5}$	0.54	0.75
ePVS Count	0.06	-0.14, 0.25	0.57	0.75
Female Basal Ganglia ePVS Burden				
ePVS Volume	$-2.48x10^{-6}$	$-1.47x10^{-5}$, $9.76x10^{-6}$	0.69	0.95
ePVS Count	-0.06	-0.39, 0.27	0.73	0.95

Note. ePVS volume represents a standardized measure of ePVS volume (values were divided by total basal ganglia tissue volume). Analyses performed on n=327 participants. Models were adjusted for age, sex, race/ethnicity, education, *APOE*-ε4 status, cognitive diagnosis, and Framingham Stroke Risk Profile (excluding points assigned for age). *APOE*-ε4, apolipoprotein E ε4. CI, confidence interval. ePVS, enlarged perivascular space. The parameter estimates (β) for the interaction models are for the *TNF-α x time x APOE-ε4 carrier status* interaction term or the *TNF-α x time x cognitive diagnosis* interaction term or the *TNF-α x time x sex* interaction term and are interpreted as the difference in longitudinal change slopes between carriers and non-carriers or normal cognition and MCI or male and female. The parameter estimates (β) for the stratified models represent the changes in longitudinal slopes for ePVS burden associated with one unit change in TNF-α. Bold p-values meet the *a priori* significance threshold. FDR, false discovery rate.

Table 3.22. IL-6 Associations with Longitudinal Basal Ganglia ePVS Burden

	β	95% CI	*p-value*	*FDR p-value*
Basal Ganglia ePVS Burden				
ePVS Volume	8.58×10^{-7}	-3.28×10^{-6}, 4.99×10^{-6}	0.68	0.85
ePVS Count	-0.009	-0.11, 0.10	0.87	0.87
***APOE*-ε4 Status Interaction Basal Ganglia ePVS Burden**				
ePVS Volume	-1.52×10^{-5}	-3.65×10^{-5}, 6.01×10^{-6}	0.16	0.35
ePVS Count	-0.10	-0.65, 0.46	0.73	0.73
***APOE*-ε4 Carriers Basal Ganglia ePVS Burden**				
ePVS Volume	-1.42×10^{-5}	-3.55×10^{-5}, 7.17×10^{-6}	0.19	0.59
ePVS Count	-0.11	-0.61, 0.40	0.68	0.84
***APOE*-ε4 Non-carriers Basal Ganglia ePVS Burden**				
ePVS Volume	1.37×10^{-6}	-2.81×10^{-6}, 5.55×10^{-6}	0.52	0.71
ePVS Count	-0.007	-0.12, 0.11	0.91	0.91
Diagnosis Interaction Basal Ganglia ePVS Burden				
ePVS Volume	4.05×10^{-6}	-1.03×10^{-5}, 1.84×10^{-5}	0.58	0.78
ePVS Count	1.90×10^{-4}	-0.38, 0.38	>0.99	>0.99
Normal Cognition Basal Ganglia ePVS Burden				
ePVS Volume	4.84×10^{-7}	-3.31×10^{-6}, 4.28×10^{-6}	0.80	0.89
ePVS Count	-0.005	-0.11, 0.10	0.93	0.93
MCI Basal Ganglia ePVS Burden				
ePVS Volume	4.70×10^{-6}	-1.04×10^{-5}, 1.98×10^{-5}	0.54	0.95
ePVS Count	0.02	-0.37, 0.40	0.93	>0.99
Sex Interaction Basal Ganglia ePVS Burden				
ePVS Volume	9.57×10^{-7}	-1.37×10^{-5}, 1.57×10^{-5}	0.90	0.90
ePVS Count	-0.11	-0.49, 0.28	0.58	0.90
Male Basal Ganglia ePVS Burden				
ePVS Volume	3.41×10^{-7}	-4.37×10^{-6}, 5.05×10^{-6}	0.89	0.91
ePVS Count	-0.008	-0.13, 0.11	0.90	0.91
Female Basal Ganglia ePVS Burden				
ePVS Volume	4.43×10^{-6}	-9.02×10^{-6}, 1.79×10^{-5}	0.52	0.95
ePVS Count	-0.06	-0.42, 0.30	0.73	0.95

Note. ePVS volume represents a standardized measure of ePVS volume (values were divided by total basal ganglia tissue volume). Analyses performed on n=327 participants. Models were adjusted for age, sex, race/ethnicity, education, *APOE*-ε4 status, cognitive diagnosis, and Framingham Stroke Risk Profile (excluding points assigned for age). *APOE*-ε4, apolipoprotein E ε4. CI, confidence interval. ePVS, enlarged perivascular space. The parameter estimates (β) for the interaction models are for the *IL-6 x time x APOE-ε4 carrier status* interaction term or the *IL-6 x time x cognitive diagnosis* interaction term or the *IL-6 x time x sex* interaction term and are interpreted as the difference in longitudinal change slopes between carriers and non-carriers or normal cognition and MCI or male and female. The parameter estimates (β) for the stratified models represent the changes in longitudinal slopes for ePVS burden associated with one unit change in IL-6. Bold p-values meet the *a priori* significance threshold. FDR, false discovery rate.

Table 3.23. CSF MMP9 Associations with Longitudinal Basal Ganglia ePVS Burden

	β	95% CI	*p-value*	*FDR p-value*
Basal Ganglia ePVS Burden				
ePVS Volume	-8.16×10^{-8}	-4.03×10^{-7}, 2.39×10^{-7}	0.62	0.85
ePVS Count	-0.001	-0.010, 0.008	0.80	0.85
***APOE*-ε4 Status Interaction Basal Ganglia ePVS Burden**				
ePVS Volume	-3.95×10^{-7}	-1.03×10^{-7}, 2.36×10^{-7}	0.22	0.35
ePVS Count	-0.006	-0.02, 0.01	0.48	0.56
***APOE*-ε4 Carriers Basal Ganglia ePVS Burden**				
ePVS Volume	-3.56×10^{-7}	-8.41×10^{-7}, 1.29×10^{-7}	0.15	0.59
ePVS Count	-0.006	-0.02, 0.007	0.35	0.76
***APOE*-ε4 Non-carriers Basal Ganglia ePVS Burden**				
ePVS Volume	9.56×10^{-8}	-3.40×10^{-7}, 5.31×10^{-7}	0.67	0.74
ePVS Count	0.002	-0.01, 0.01	0.79	0.83
Diagnosis Interaction Basal Ganglia ePVS Burden				
ePVS Volume	1.91×10^{-7}	-4.70×10^{-7}, 8.53×10^{-7}	0.57	0.78
ePVS Count	0.009	-0.009, 0.03	0.34	0.78
Normal Cognition Basal Ganglia ePVS Burden				
ePVS Volume	-1.90×10^{-7}	-5.85×10^{-7}, 2.06×10^{-7}	0.34	0.80
ePVS Count	-0.005	-0.02, 0.006	0.39	0.81
MCI Basal Ganglia ePVS Burden				
ePVS Volume	-2.98×10^{-8}	-6.54×10^{-7}, 5.94×10^{-7}	0.92	>0.99
ePVS Count	0.003	-0.01, 0.02	0.72	0.99
Sex Interaction Basal Ganglia ePVS Burden				
ePVS Volume	-5.18×10^{-7}	-1.20×10^{-6}, 1.66×10^{-7}	0.14	0.58
ePVS Count	-0.008	-0.03, 0.01	0.40	0.90
Male Basal Ganglia ePVS Burden				
ePVS Volume	1.14×10^{-7}	-2.87×10^{-7}, 5.15×10^{-7}	0.58	0.75
ePVS Count	0.003	-0.008, 0.01	0.61	0.75
Female Basal Ganglia ePVS Burden				
ePVS Volume	-5.04×10^{-7}	-1.02×10^{-6}, 1.01×10^{-8}	0.05	0.56
ePVS Count	-0.008	-0.03, 0.009	0.33	0.83

Note. ePVS volume represents a standardized measure of ePVS volume (values were divided by total basal ganglia tissue volume). Analyses performed on n=142 participants. Models were adjusted for age, sex, race/ethnicity, education, *APOE*-ε4 status, cognitive diagnosis, and Framingham Stroke Risk Profile (excluding points assigned for age). *APOE*-ε4, apolipoprotein E ε4. CI, confidence interval. ePVS, enlarged perivascular space. The parameter estimates (β) for the interaction models are for the *MMP9 x time x APOE-ε4 carrier status* interaction term or the *MMP9 x time x cognitive diagnosis* interaction term or the *MMP9 x time x sex* interaction term and are interpreted as the difference in longitudinal change slopes between carriers and non-carriers or normal cognition and MCI or male and female. The parameter estimates (β) for the stratified models represent the changes in longitudinal slopes for ePVS burden associated with one unit change in MMP9. Bold p-values meet the *a priori* significance threshold. FDR, false discovery rate.

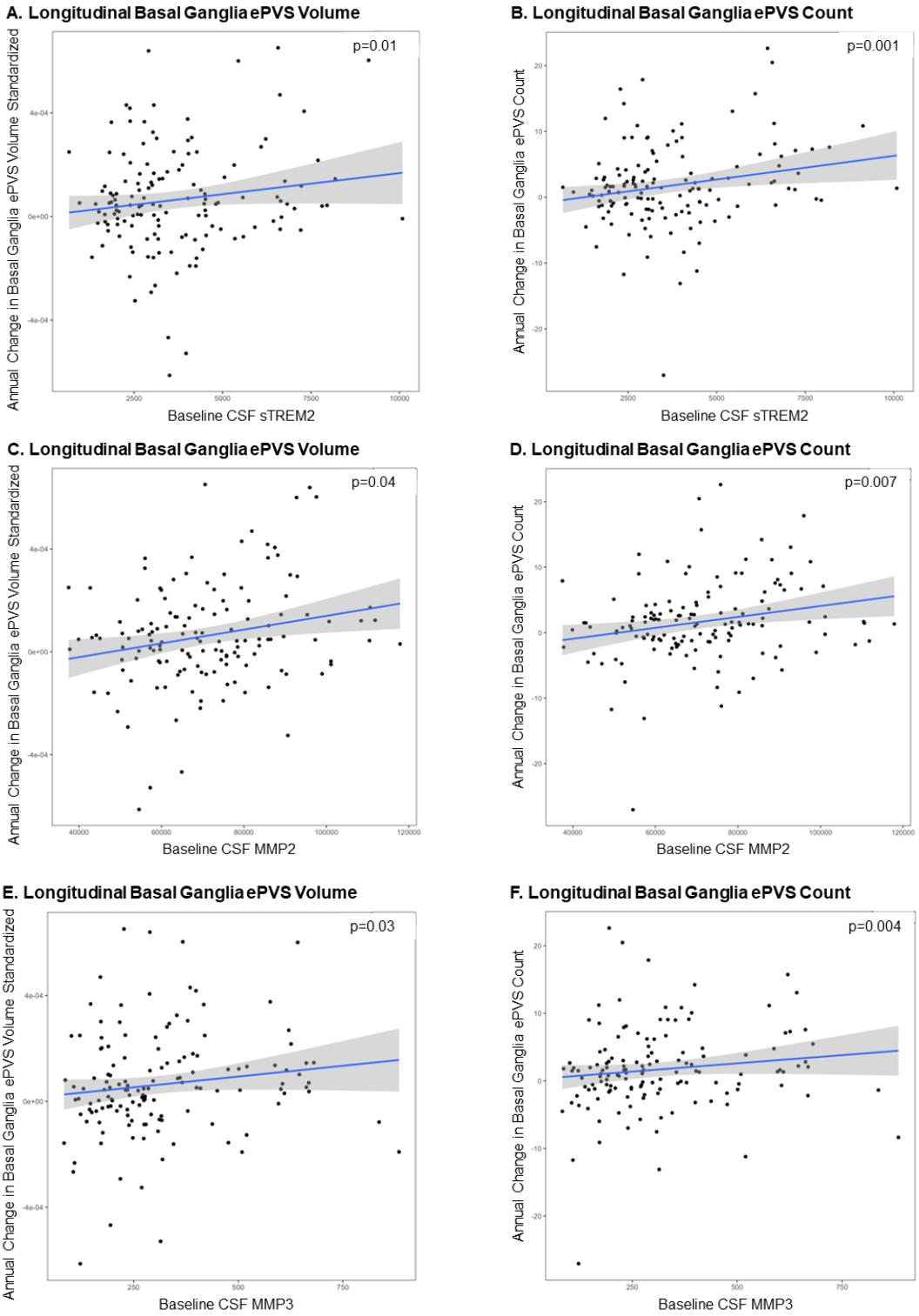

Figure 3.7. Baseline CSF inflammation marker associations with longitudinal basal ganglia ePVS burden. CSF sTREM2 associations with **(A)** longitudinal ePVS volume and **(B)** longitudinal ePVS count. CSF MMP2 associations with **(C)** longitudinal ePVS volume and **(D)** longitudinal ePVS count. CSF MMP3 associations with **(E)** longitudinal ePVS volume and **(F)** longitudinal ePVS count. The ePVS volume variable is standardized by dividing by basal ganglia tissue volume.

Pittsburgh Sleep Quality Index Score and Longitudinal ePVS Burden Outcomes

PSQI score was unrelated to longitudinal basal ganglia ePVS burden (p>0.17). See **Table 3.24** for details.

The *PSQI score x APOE-ε4 status* interaction term was associated with longitudinal basal ganglia standardized ePVS volume ($\beta=1.35x10^{-5}$, p=0.04) but not ePVS count (p=0.09). Results were the same when excluding outliers as well as when excluding participants with CVD and atrial fibrillation. In stratified models, PSQI score was unrelated to longitudinal basal ganglia ePVS burden (p>0.40) among *APOE-ε4* carriers. Among non-carriers, worse sleep quality was associated with a longitudinal decrease in basal ganglia ePVS count ($\beta=-0.22$, p=0.04) and standardized ePVS volume ($\beta=-8.83x10^{-6}$, p=0.02). Associations with standardized ePVS volume remained unchanged when excluding outliers as well as when excluding participants with CVD and atrial fibrillation. Associations with ePVS count were attenuated when excluding outliers (p=0.08) as well as when excluding participants with CVD and atrial fibrillation (p=0.06). See **Table 3.24** and **Figure 3.8** for details.

The *PSQI score x cognitive diagnosis* interaction term was unrelated to longitudinal basal ganglia ePVS burden (p>0.06). In stratified models, worse sleep quality was associated with longitudinal decrease in basal ganglia ePVS count ($\beta=-0.24$, p=0.03) and standardized ePVS volume ($\beta=-1.01x10^{-5}$, p=0.01) among normal cognition participants. Results were unchanged when excluding outliers as well as when excluding participants with CVD and atrial fibrillation. Among participants with MCI, results were null (p>0.71). See **Table 3.24** for details.

The *PSQI score x sex* interaction term was associated with longitudinal basal

ganglia standardized ePVS volume (β=-1.30x10^{-5}, p=0.04) but not ePVS count (p=0.14). In stratified models, PSQI score was unrelated to ePVS burden among male participants (p>0.82). Among female participants, worse sleep quality was associated with longitudinal decrease in basal ganglia ePVS count (β=-0.27, p=0.03) and standardized ePVS volume (β=-1.12x10^{-5}, p=0.01). Results were the same when excluding outliers as well as when excluding participants with CVD and atrial fibrillation. See **Table 3.24** for details.

Table 3.24. Sleep Quality Associations with Longitudinal Basal Ganglia ePVS Burden

	β	95% CI	*p-value*	*FDR p-value*
Basal Ganglia ePVS Burden				
ePVS Volume	-3.99x10^{-6}	-1.02x10^{-5}, 2.22x10^{-6}	0.21	0.81
ePVS Count	-0.11	-0.27, 0.05	0.17	0.81
***APOE*-ε4 Status Interaction Basal Ganglia ePVS Burden**				
ePVS Volume	1.35x10^{-5}	6.18x10^{-7}, 2.64x10^{-5}	**0.04**	0.24
ePVS Count	0.29	-0.05, 0.62	0.09	0.37
***APOE*-ε4 Carriers Basal Ganglia ePVS Burden**				
ePVS Volume	4.62x10^{-6}	-6.37x10^{-6}, 1.56x10^{-5}	0.41	0.53
ePVS Count	0.08	-0.17, 0.33	0.51	0.56
***APOE*-ε4 Non-carriers Basal Ganglia ePVS Burden**				
ePVS Volume	-8.83x10^{-6}	-1.64x10^{-5}, -1.25x10^{-6}	**0.02**	0.14
ePVS Count	-0.22	-0.43, -0.01	**0.04**	0.15
Diagnosis Interaction Basal Ganglia ePVS Burden				
ePVS Volume	1.17x10^{-5}	-7.63x10^{-7}, 2.41x10^{-5}	0.07	0.20
ePVS Count	0.19	-0.14, 0.52	0.26	0.36
Normal Cognition Basal Ganglia ePVS Burden				
ePVS Volume	-1.01x10^{-5}	-1.78x10^{-5}, -2.39x10^{-6}	**0.01**	0.09
ePVS Count	-0.24	-0.46, -0.03	**0.03**	0.09
MCI Basal Ganglia ePVS Burden				
ePVS Volume	1.90x10^{-6}	-8.53x10^{-6}, 1.23x10^{-5}	0.72	0.85
ePVS Count	-0.03	-0.29, 0.23	0.84	0.85
Sex Interaction Basal Ganglia ePVS Burden				
ePVS Volume	-1.30x10^{-5}	-2.55x10^{-5}, -5.25x10^{-7}	**0.04**	0.09
ePVS Count	-0.24	-0.56, 0.08	0.14	0.15
Male Basal Ganglia ePVS Burden				
ePVS Volume	9.55x10^{-7}	-7.42x10^{-6}, 9.33x10^{-6}	0.82	0.93
ePVS Count	-0.01	-0.23, 0.21	0.93	0.93
Female Basal Ganglia ePVS Burden				
ePVS Volume	-1.12x10^{-5}	-1.99x10^{-5}, -2.43x10^{-6}	**0.01**	0.08

ePVS Count	-0.27	-0.50, -0.03	**0.03**	0.12

Note. ePVS volume represents a standardized measure of ePVS volume (values were divided by total basal ganglia tissue volume). Analyses performed on n=311 participants. Models were adjusted for age, sex, race/ethnicity, education, *APOE*-ε4 status, cognitive diagnosis, and Framingham Stroke Risk Profile (excluding points assigned for age). *APOE*-ε4, apolipoprotein E ε4. CI, confidence interval. ePVS, enlarged perivascular space. The parameter estimates (β) for the interaction models are for the *sleep quality x time x APOE-ε4 carrier status* interaction term or the *sleep quality x time x cognitive diagnosis* interaction term or the *sleep quality x time x sex* interaction term and are interpreted as the difference in longitudinal change slopes between carriers and non-carriers or normal cognition and MCI or male and female. The parameter estimates (β) for the stratified models represent the changes in longitudinal slopes for ePVS burden associated with one unit change in sleep quality. Bold p-values meet the *a priori* significance threshold. FDR, false discovery rate.

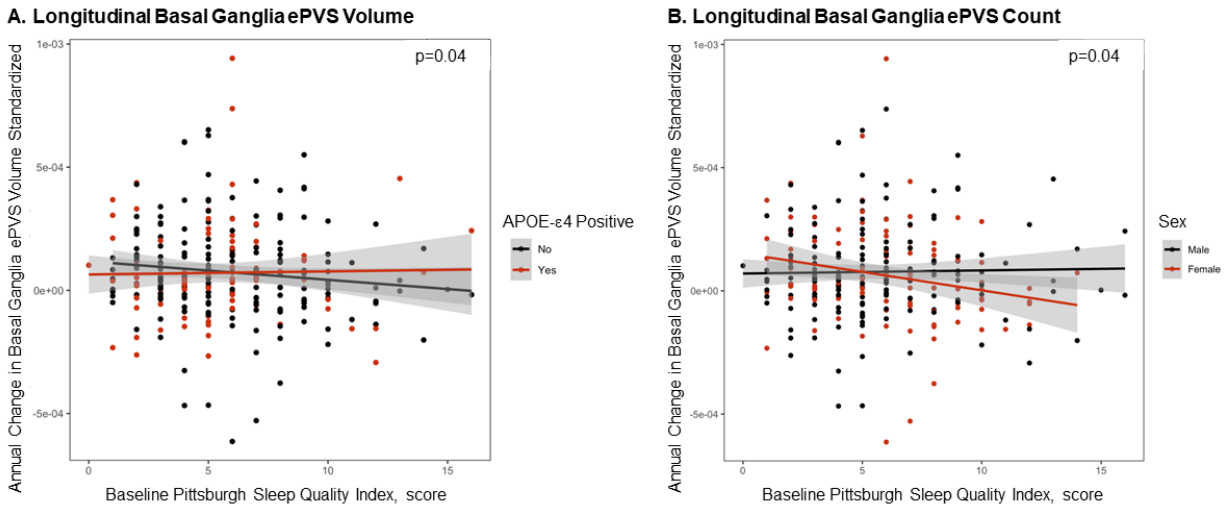

Figure 3.8. Baseline *PSQI score x APOE-ε4 status* and baseline *PSQI score x sex* interactions on longitudinal basal ganglia ePVS volume. **(A)** *Sleep quality x APOE-ε4 status* interaction term association with longitudinal ePVS volume and **(B)** *sleep quality x sex* interaction term association with longitudinal ePVS volume. The ePVS volume variable is standardized by dividing by basal ganglia tissue volume. In stratified models among *APOE*-ε4 non-carriers, sleep quality was associated with longitudinal ePVS volume (p=0.02). In stratified models among female participants, sleep quality was associated with longitudinal ePVS volume (p=0.01).

AD Biomarkers and Longitudinal ePVS Burden Outcomes

Associations between CSF $A\beta_{40}$, CSF $A\beta_{42}$, CSF t-tau, and CSF p-tau and ePVS burden were null (p>0.13). See **Tables 3.25** to **3.28** for details.

Associations between the *CSF $A\beta_{40}$ x APOE-ε4 status* and *CSF $A\beta_{42}$ x APOE-ε4 status* interaction terms and ePVS burden were null (p>0.18). See **Tables 3.25** and **3.26**

for details.

The *CSF t-tau x APOE-ε4 status* interaction term was associated with longitudinal basal ganglia ePVS count (β=-0.01, p=0.005) and standardized ePVS volume (β=-3.08x10^{-7}, p=0.03). In stratified models, CSF t-tau was unrelated to longitudinal basal ganglia ePVS burden among *APOE*-ε4 carriers (p>0.07). Among *APOE*-ε4 non-carriers, greater CSF t-tau levels were associated with longitudinal increase in basal ganglia ePVS count (β=0.007, p=0.007) and standardized ePVS volume (β=1.99x10^{-7}, p=0.03). Results were the same when excluding outliers as well as when excluding participants with CVD and atrial fibrillation. See **Table 3.27** and **Figure 3.9** for details.

The *CSF p-tau x APOE-ε4 status* interaction term was associated with longitudinal basal ganglia ePVS count (β=-0.08, p=0.01) but not standardized ePVS volume (p=0.07). In stratified models, CSF p-tau was unrelated to longitudinal basal ganglia ePVS burden among *APOE*-ε4 carriers (p>0.15). Among *APOE*-ε4 non-carriers, greater CSF p-tau levels were associated with longitudinal increase in basal ganglia ePVS count (β=0.06, p=0.005) and standardized ePVS volume (β=1.57x10^{-6}, p=0.03). Results were the same when excluding outliers as well as when excluding participants with CVD and atrial fibrillation. See **Table 3.28** for details.

Associations between the *CSF Aβ_{40} x cognitive diagnosis*, *CSF Aβ_{42} x cognitive diagnosis*, *CSF t-tau x cognitive diagnosis*, and *CSF p-tau x cognitive diagnosis* interaction terms and longitudinal basal ganglia ePVS burden were null (p>0.15). Stratified models were also null (p>0.20). See **Tables 3.25** to **3.28** for details.

Associations between the *CSF Aβ_{40} x sex*, *CSF Aβ_{42} x sex*, *CSF t-tau x sex*, and

CSF p-tau x sex interaction terms and longitudinal basal ganglia ePVS burden were null (p>0.06). In stratified models, greater CSF t-tau levels were associated with longitudinal increase in basal ganglia ePVS count (β=0.005, p=0.03) and standardized ePVS volume (β=1.84x10^{-7}, p=0.04) among male participants. The association with ePVS count among male participants was attenuated when excluding outliers (p=0.07) but associations remained when excluding participants with CVD and atrial fibrillation. Greater CSF p-tau levels were also associated with longitudinal increase in basal ganglia ePVS count (β=0.05, p=0.02) and standardized ePVS volume (β=1.71x10^{-6}, p=0.02) among male participants. Results were the same when excluding outliers as well as when excluding participants with CVD and atrial fibrillation. All other AD biomarker models stratified by sex were null (p>0.12). See **Tables 3.25** to **3.28** for details.

Table 3.25. CSF Aβ$_{42}$ Associations with Longitudinal Basal Ganglia ePVS Burden

	β	95% CI	*p-value*	*FDR p-value*
Basal Ganglia ePVS Burden				
ePVS Volume	3.68x10^{-8}	-6.68x10^{-8}, 1.40x10^{-7}	0.49	0.51
ePVS Count	0.001	-0.002, 0.004	0.45	0.51
***APOE*-ε4 Status Interaction Basal Ganglia ePVS Burden**				
ePVS Volume	1.96x10^{-7}	-9.41x10^{-8}, 4.87x10^{-7}	0.18	0.28
ePVS Count	0.001	-0.007, 0.009	0.78	0.85
***APOE*-ε4 Carriers Basal Ganglia ePVS Burden**				
ePVS Volume	1.92x10^{-7}	-6.82x10^{-8}, 4.53x10^{-7}	0.15	0.40
ePVS Count	0.003	-0.004, 0.01	0.44	0.59
***APOE*-ε4 Non-carriers Basal Ganglia ePVS Burden**				
ePVS Volume	-2.80x10^{-8}	-1.58x10^{-7}, 1.03x10^{-7}	0.67	0.73
ePVS Count	1.00x10^{-4}	-0.004, 0.004	0.96	0.96
Diagnosis Interaction Basal Ganglia ePVS Burden				
ePVS Volume	6.91x10^{-8}	-1.91x10^{-7}, 3.29x10^{-7}	0.60	0.81
ePVS Count	-0.005	-0.01, 0.002	0.16	0.80
Normal Cognition Basal Ganglia ePVS Burden				
ePVS Volume	-8.31x10^{-9}	-1.45x10^{-7}, 1.29x10^{-7}	0.90	0.96
ePVS Count	5.12x10^{-4}	-0.003, 0.004	0.80	0.96
MCI Basal Ganglia ePVS Burden				

ePVS Volume	$1.29x10^{-7}$	$-1.26x10^{-7}$, $3.84x10^{-7}$	0.32	0.62
ePVS Count	-0.002	-0.008, 0.004	0.50	0.62
Sex Interaction Basal Ganglia ePVS Burden				
ePVS Volume	$7.19x10^{-8}$	$-1.64x10^{-7}$, $3.08x10^{-7}$	0.55	0.66
ePVS Count	$-1.71x10^{-5}$	-0.007, 0.007	>0.99	>0.99
Male Basal Ganglia ePVS Burden				
ePVS Volume	$-1.19x10^{-8}$	$-1.37x10^{-7}$, $1.13x10^{-7}$	0.85	0.94
ePVS Count	$9.42x10^{-5}$	-0.003, 0.004	0.96	0.96
Female Basal Ganglia ePVS Burden				
ePVS Volume	$6.98x10^{-8}$	$-1.29x10^{-7}$, $2.68x10^{-7}$	0.49	0.91
ePVS Count	$1.02x10^{-4}$	-0.006, 0.006	0.97	0.97

Note. ePVS volume represents a standardized measure of ePVS volume (values were divided by total basal ganglia tissue volume). Analyses performed on n=153 participants. Models were adjusted for age, sex, race/ethnicity, education, *APOE*-ε4 status, cognitive diagnosis, and Framingham Stroke Risk Profile (excluding points assigned for age). *APOE*-ε4, apolipoprotein E ε4. CI, confidence interval. ePVS, enlarged perivascular space. The parameter estimates (β) for the interaction models are for the *$A\beta_{42}$ x time x APOE-ε4 carrier status* interaction term or the *$A\beta_{42}$ x time x cognitive diagnosis* interaction term or the *$A\beta_{42}$ x time x sex* interaction term and are interpreted as the difference in longitudinal change slopes between carriers and non-carriers or normal cognition and MCI or male and female. The parameter estimates (β) for the stratified models represent the changes in longitudinal slopes for ePVS burden associated with one unit change in $A\beta_{42}$. Bold p-values meet the *a priori* significance threshold. FDR, false discovery rate.

Table 3.26. CSF $A\beta_{40}$ Associations with Longitudinal Basal Ganglia ePVS Burden

	β	95% CI	*p-value*	*FDR p-value*
Basal Ganglia ePVS Burden				
ePVS Volume	$6.71x10^{-9}$	$-9.44x10^{-9}$, $2.29x10^{-8}$	0.41	0.51
ePVS Count	$3.09x10^{-4}$	$-1.36x10^{-4}$, $7.54x10^{-4}$	0.17	0.51
***APOE*-ε4 Status Interaction Basal Ganglia ePVS Burden**				
ePVS Volume	$2.14x10^{-9}$	$-3.46x10^{-8}$, $3.89x10^{-8}$	0.91	0.91
ePVS Count	$-3.44x10^{-4}$	-0.001, $6.83x10^{-4}$	0.51	0.68
***APOE*-ε4 Carriers Basal Ganglia ePVS Burden**				
ePVS Volume	$4.26x10^{-9}$	$-2.88x10^{-8}$, $3.73x10^{-8}$	0.80	0.87
ePVS Count	$-5.99x10^{-5}$	$-9.23x10^{-4}$, $8.03x10^{-4}$	0.89	0.89
***APOE*-ε4 Non-carriers Basal Ganglia ePVS Burden**				
ePVS Volume	$6.46x10^{-9}$	$-1.25x10^{-8}$, $2.55x10^{-8}$	0.50	0.67
ePVS Count	$3.72x10^{-4}$	$-1.78x10^{-4}$, $9.21x10^{-4}$	0.18	0.32
Diagnosis Interaction Basal Ganglia ePVS Burden				
ePVS Volume	$1.96x10^{-8}$	$-2.06x10^{-8}$, $5.97x10^{-8}$	0.34	0.80
ePVS Count	$-5.21x10^{-4}$	-0.002, $5.46x10^{-4}$	0.34	0.80
Normal Cognition Basal Ganglia ePVS Burden				
ePVS Volume	$-4.63x10^{-10}$	$-1.95x10^{-8}$, $1.85x10^{-8}$	0.96	0.96
ePVS Count	$2.13x10^{-4}$	$-3.39x10^{-4}$, $7.64x10^{-4}$	045	0.96
MCI Basal Ganglia ePVS Burden				
ePVS Volume	$2.57x10^{-8}$	$-1.46x10^{-8}$, $6.59x10^{-8}$	0.21	0.62
ePVS Count	$-1.10x10^{-4}$	-0.001, $8.71x10^{-4}$	0.83	0.83
Sex Interaction Basal Ganglia ePVS Burden				
ePVS Volume	$-1.76x10^{-8}$	$-5.14x10^{-8}$, $1.63x10^{-8}$	0.31	0.46
ePVS Count	$-5.02x10^{-4}$	-0.001, $4.28x10^{-4}$	0.29	0.46
Male Basal Ganglia ePVS Burden				

ePVS Volume	$1.09x10^{-8}$	$-9.03x10^{-9}$, $3.08x10^{-8}$	0.28	0.38
ePVS Count	$4.28x10^{-4}$	$-1.14x10^{-4}$, $9.70x10^{-4}$	0.12	0.21
Female Basal Ganglia ePVS Burden				
ePVS Volume	$-7.31x10^{-9}$	$-3.54x10^{-8}$, $2.08x10^{-8}$	0.61	0.91
ePVS Count	$-1.20x10^{-4}$	$-9.28x10^{-4}$, $6.88x10^{-4}$	0.77	0.91

Note. ePVS volume represents a standardized measure of ePVS volume (values were divided by total basal ganglia tissue volume). Analyses performed on n=153 participants. Models were adjusted for age, sex, race/ethnicity, education, *APOE*-ε4 status, cognitive diagnosis, and Framingham Stroke Risk Profile (excluding points assigned for age). *APOE*-ε4, apolipoprotein E ε4. CI, confidence interval. ePVS, enlarged perivascular space. The parameter estimates (β) for the interaction models are for the *$A\beta_{40}$ x time x APOE-ε4 carrier status* interaction term or the *$A\beta_{40}$ x time x cognitive diagnosis* interaction term or the *$A\beta_{40}$ x time x sex* interaction term and are interpreted as the difference in longitudinal change slopes between carriers and non-carriers or normal cognition and MCI or male and female. The parameter estimates (β) for the stratified models represent the changes in longitudinal slopes for ePVS burden associated with one unit change in $A\beta_{40}$. Bold p-values meet the *a priori* significance threshold. FDR, false discovery rate.

Table 3.27. CSF T-Tau Associations with Longitudinal Basal Ganglia ePVS Burden

	β	95% CI	*p-value*	*FDR p-value*
Basal Ganglia ePVS Burden				
ePVS Volume	$5.26x10^{-8}$	$-8.33x10^{-8}$, $1.88x10^{-7}$	0.45	0.51
ePVS Count	0.002	-0.002, 0.006	0.25	0.51
***APOE*-ε4 Status Interaction Basal Ganglia ePVS Burden**				
ePVS Volume	$-3.08x10^{-7}$	$-5.84x10^{-7}$, $-3.26x10^{-8}$	**0.03**	0.10
ePVS Count	-0.01	-0.02, -0.003	**0.005**	0.06
***APOE*-ε4 Carriers Basal Ganglia ePVS Burden**				
ePVS Volume	$-1.55x10^{-7}$	$-3.74x10^{-7}$, $6.47x10^{-8}$	0.17	0.40
ePVS Count	-0.005	-0.01, $5.64x10^{-4}$	0.08	0.40
***APOE*-ε4 Non-carriers Basal Ganglia ePVS Burden**				
ePVS Volume	$1.99x10^{-7}$	$2.52x10^{-8}$, $3.73x10^{-7}$	**0.03**	0.05
ePVS Count	0.007	0.002, 0.01	**0.007**	**0.04**
Diagnosis Interaction Basal Ganglia ePVS Burden				
ePVS Volume	$5.99x10^{-8}$	$-2.24x10^{-7}$, $3.43x10^{-7}$	0.68	0.81
ePVS Count	-0.002	-0.01, 0.005	0.57	0.81
Normal Cognition Basal Ganglia ePVS Burden				
ePVS Volume	$-7.13x10^{-9}$	$-1.97x10^{-7}$, $1.83x10^{-7}$	0.94	0.96
ePVS Count	0.002	-0.003, 0.008	0.44	0.96
MCI Basal Ganglia ePVS Burden				
ePVS Volume	$7.79x10^{-8}$	$-1.57x10^{-7}$, $3.13x10^{-7}$	0.51	0.62
ePVS Count	$8.99x10^{-4}$	-0.005, 0.007	0.76	0.83
Sex Interaction Basal Ganglia ePVS Burden				
ePVS Volume	$-2.54x10^{-7}$	$-5.30x10^{-7}$, $2.24x10^{-8}$	0.07	0.29
ePVS Count	-0.005	-0.01, 0.003	0.24	0.46
Male Basal Ganglia ePVS Burden				
ePVS Volume	$1.84x10^{-7}$	$9.26x10^{-9}$, $3.58x10^{-7}$	**0.04**	0.08
ePVS Count	0.005	$3.91x10^{-4}$, 0.01	**0.03**	0.08
Female Basal Ganglia ePVS Burden				
ePVS Volume	$-1.00x10^{-7}$	$-3.25x10^{-7}$, $1.24x10^{-7}$	0.38	0.91
ePVS Count	$6.83x10^{-4}$	-0.006, 0.007	0.83	0.91

Note. ePVS volume represents a standardized measure of ePVS volume (values were divided by total

basal ganglia tissue volume). Analyses performed on n=153 participants. Models were adjusted for age, sex, race/ethnicity, education, *APOE*-ε4 status, cognitive diagnosis, and Framingham Stroke Risk Profile (excluding points assigned for age). *APOE*-ε4, apolipoprotein E ε4. CI, confidence interval. ePVS, enlarged perivascular space. The parameter estimates (β) for the interaction models are for the *t-tau x time x APOE-ε4 carrier status* interaction term or the *t-tau x time x cognitive diagnosis* interaction term or the *t-tau x time x sex* interaction term and are interpreted as the difference in longitudinal change slopes between carriers and non-carriers or normal cognition and MCI or male and female. The parameter estimates (β) for the stratified models represent the changes in longitudinal slopes for ePVS burden associated with one unit change in t-tau. Bold p-values meet the *a priori* significance threshold. FDR, false discovery rate.

Table 3.28. CSF P-Tau Associations with Longitudinal Basal Ganglia ePVS burden

	β	95% CI	*p-value*	*FDR p-value*
Basal Ganglia ePVS Burden				
ePVS Volume	$5.87x10^{-7}$	$-5.16x10^{-7}$, $1.69x10^{-6}$	0.30	0.51
ePVS Count	0.02	-0.007, 0.05	0.14	0.51
***APOE*-ε4 Status Interaction Basal Ganglia ePVS Burden**				
ePVS Volume	$-2.07x10^{-6}$	$-4.33x10^{-6}$, $1.95x10^{-7}$	0.07	0.16
ePVS Count	-0.08	-0.14, -0.02	**0.01**	0.07
***APOE*-ε4 Carriers Basal Ganglia ePVS Burden**				
ePVS Volume	$-9.53x10^{-7}$	$-2.82x10^{-6}$, $9.18x10^{-7}$	0.32	0.54
ePVS Count	-0.04	-0.08, 0.01	0.15	0.40
***APOE*-ε4 Non-carriers Basal Ganglia ePVS Burden**				
ePVS Volume	$1.57x10^{-6}$	$1.79x10^{-7}$, $2.95x10^{-6}$	**0.03**	0.05
ePVS Count	0.06	0.02, 0.10	**0.005**	**0.04**
Diagnosis Interaction Basal Ganglia ePVS Burden				
ePVS Volume	$1.04x10^{-6}$	$-1.26x10^{-6}$, $3.34x10^{-6}$	0.37	0.80
ePVS Count	-0.007	-0.07, 0.05	0.83	0.83
Normal Cognition Basal Ganglia ePVS Burden				
ePVS Volume	$-1.70x10^{-7}$	$-1.65x10^{-6}$, $1.31x10^{-6}$	0.82	0.96
ePVS Count	0.01	-0.03, 0.06	0.53	0.96
MCI Basal Ganglia ePVS Burden				
ePVS Volume	$1.13x10^{-6}$	$-8.51x10^{-7}$, $3.12x10^{-6}$	0.26	0.62
ePVS Count	0.02	-0.03, 0.07	0.48	0.62
Sex Interaction Basal Ganglia ePVS Burden				
ePVS Volume	$-2.11x10^{-6}$	$-4.32x10^{-6}$, $1.03x10^{-7}$	0.06	0.29
ePVS Count	-0.04	-0.10, 0.02	0.20	0.46
Male Basal Ganglia ePVS Burden				
ePVS Volume	$1.71x10^{-6}$	$2.97x10^{-7}$, $3.13x10^{-6}$	**0.02**	0.07
ePVS Count	0.05	0.009, 0.09	**0.02**	0.07
Female Basal Ganglia ePVS Burden				
ePVS Volume	$-7.16x10^{-7}$	$-2.49x10^{-6}$, $1.06x10^{-6}$	0.43	0.91
ePVS Count	0.007	-0.04, 0.06	0.79	0.91

Note. ePVS volume represents a standardized measure of ePVS volume (values were divided by total basal ganglia tissue volume). Analyses performed on n=153 participants. Models were adjusted for age, sex, race/ethnicity, education, *APOE*-ε4 status, cognitive diagnosis, and Framingham Stroke Risk Profile (excluding points assigned for age). *APOE*-ε4, apolipoprotein E ε4. CI, confidence interval. ePVS, enlarged perivascular space. The parameter estimates (β) for the interaction models are for the *p-tau x time x APOE-ε4 carrier status* interaction term or the *p-tau x time x cognitive diagnosis* interaction term or the *p-tau x time x sex* interaction term and are interpreted as the difference in

longitudinal change slopes between carriers and non-carriers or normal cognition and MCI or male and female. The parameter estimates (β) for the stratified models represent the changes in longitudinal slopes for ePVS burden associated with one unit change in p-tau. Bold p-values meet the *a priori* significance threshold. FDR, false discovery rate.

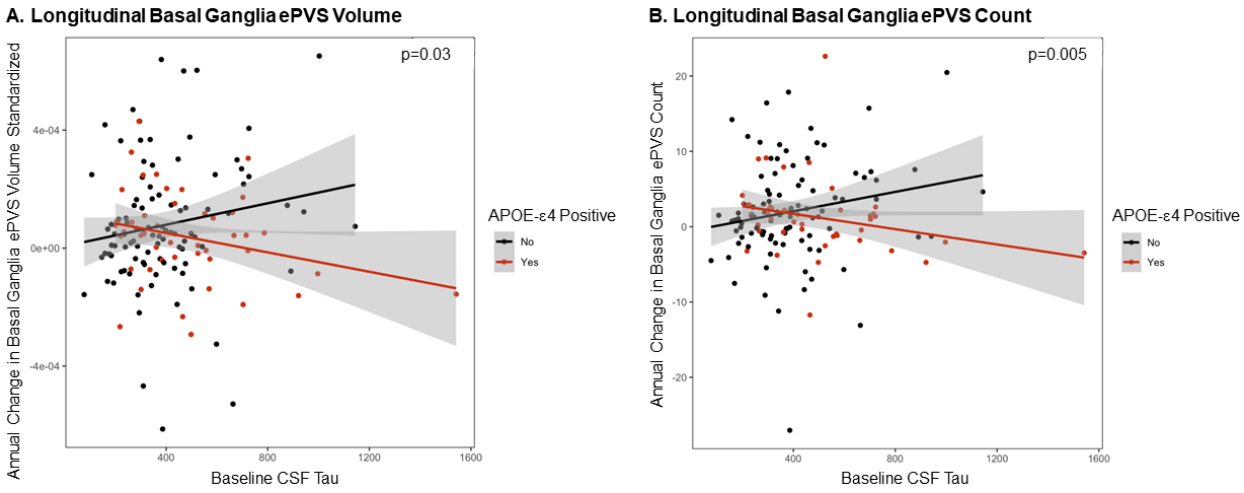

Figure 3.9. Baseline *CSF t-tau x APOE-ε4 status* interactions on longitudinal basal ganglia ePVS burden. **(A)** longitudinal ePVS volume and **(B)** longitudinal ePVS count. The ePVS volume variable is standardized by dividing by basal ganglia tissue volume. In stratified models among *APOE*-ε4 non-carriers, CSF t-tau levels were associated with longitudinal ePVS volume (p=0.03) and longitudinal ePVS count (p=0.007)

Discussion

ePVS, a purported marker of SVD, have not been widely studied,[97,150,152] and even fewer studies have employed a comprehensive ePVS quantification system. For this study, we applied a novel ePVS quantification method to assess potential drivers of ePVS formation. In older adults without clinical dementia or stroke at study entry, age was positively associated with basal ganglia ePVS count and volume at baseline. Other significant predictors of ePVS burden at baseline included vascular risk factors (aortic stiffening and hypertension), sTREM2 and MMP3 among *APOE*-ε4 non-carriers, and sleep quality among participants with MCI. There were interactions between CSF $A\beta_{42}$ and diagnosis, CSF t-tau and sex, and CSF p-tau and sex on ePVS burden at baseline.

Stratified results for significant AD biomarker interaction models yielded no significant associations, making interaction models difficult to interpret.

Age was not a significant predictor of longitudinal change in ePVS burden, however, increased age was associated with less ePVS burden accumulation among *APOE*-ε4 carriers and more increase in ePVS count among non-carriers. sTREM2, MMP2, and MMP3 were associated with longitudinal increase in ePVS burden, especially among *APOE*-ε4 non-carriers and male participants. Counter-intuitively, worse sleep quality was associated with less longitudinal increase in ePVS burden among *APOE*-ε4 non-carriers, normal cognition participants, and females. Increased t-tau and p-tau levels were associated with longitudinal increase in ePVS burden among *APOE*-ε4 non-carriers and male participants.

As expected, greater baseline age was strongly associated with greater baseline ePVS burden.[125,201] Increased age is one of the strongest risk factors for ePVS, especially in the basal ganglia.[125] Vascular health declines with age due to modifiable lifestyle factors as well as non-modifiable genetic factors that add prolonged stress to the system, resulting in changes to the mechanical and structural properties of the vessel wall, and ultimately increased vascular pathologies. ePVS appear to be another vascular pathology that increases with age.

Central arterial stiffening and hypertension medication usage both predict greater basal ganglia ePVS volume and count at baseline. Hypertension and aortic stiffening are closely related with some research suggesting arterial stiffness is an earlier marker of arterial aging that predicts subsequent blood pressure increase[137] and incident hypertension.[57,58] Aortic stiffening, and resulting increases in PWV, leads to damaging

pressure waves that travel into the brain and contribute to ePVS through multiple possible mechanisms.[183,202–206] These pathways include mechanical damage to blood vessel walls and surrounding tissue,[202] microvascular remodeling resulting in impaired perfusion,[75,207] blood brain barrier breakdown,[208,209] and inflammation[210,211] due to toxin infiltration into the PVS. The lenticulostriate arteries of the basal ganglia[212,213] appear early in the arterial tree. Therefore, these arteries are exposed to stronger pressure waves,[119] which could cause mechanical damage to tissue surrounding blood vessels,[202] particularly perforating arteries and arterioles that lack elastin and are not designed to dampen pulsatile energy.[202] Pulsatile energy in conjunction with microvascular remodeling can lead to hypoperfusion,[203,204] resulting in blood brain barrier breakdown.[205] With a leaky barrier, blood and other toxins could enter the PVS and create an inflammatory reaction that leads to PVS expansion.[183] All of these mechanisms may act synergistically to drive an enlargement of PVS over time.

APOE-ε4 carrier status did not modify associations between PWV and ePVS burden or hypertension medication usage and ePVS burden. Sex did not modify associations between PWV and ePVS burden or hypertension medication usage and ePVS burden, however, stratified results suggest that associations are driven by male participants. Among men, an increased number of risk factors may be contributing to arterial stiffening and these more prevalent risk factors may leave men vulnerable to ePVS development.

Circulating inflammatory markers, microglial activation markers, and basement membrane degradation markers were not predictive of baseline ePVS burden. TNF-α[216] and IL-6[217] play many roles throughout the body while the MMP[218] family and sTREM2

levels can fluctuate in the brain due to a multitude of reasons that may not directly affect the vessel wall.[219] These inflammatory markers are not specific to ePVS and therefore finding a signal between inflammation and ePVS using these markers could be difficult, especially with cross-sectional models that do not account for temporal ordering. However, greater sTREM2 levels were predictive of greater ePVS burden among *APOE*-ε4 non-carriers at baseline. While potentially spurious, *APOE*-ε4 carriers may be dealing with microglial activation due to reasons other than ePVS, like increased amyloid burden, which would add noise to any association between sTREM2 and ePVS among *APOE*-ε4 carriers. Interestingly, higher CSF sTREM2 levels may attenuate the risk for cognitive decline and neurodegeneration associated with the *APOE*-ε4 allele,[220] which indicates that *APOE* status may affect TREM2 expression levels.

Sleep quality was not predictive of baseline ePVS burden. While we do believe that poorer sleep quality could be directly related to ePVS burden,[127–129] the sleep measure used here only accounts for sleep quality over the previous month. Additionally, the sleep quality measure is self-reported which could be confounded by other variables such as cognitive impairment. The likelihood may be low of finding significant results with cross-sectional models aimed at relating a measure from the past month to ePVS, which have been developing throughout a person's entire life. However, worse sleep quality was associated with greater ePVS burden among participants with MCI. Participants with MCI likely have greater abnormal protein levels in their brains and healthy sleep habits are important for clearing abnormal proteins,[127] so when poor sleep accompanies higher abnormal protein levels, greater ePVS burden may be the result.

AD biomarkers were not predictive of baseline ePVS burden. In previous studies, AD biomarkers have been more strongly related to ePVS in the white matter compared to ePVS in the basal ganglia.[221] For this study, we focused solely on ePVS in the basal ganglia. The lack of cross-sectional AD biomarker findings in the current study may highlight how basal ganglia ePVS are not a primary clearance route for AD associated proteins.

Baseline age was not related to longitudinal change in ePVS burden. It is possible that the occurrence of ePVS increases with age but the rate of expansion of ePVS is constant, regardless of age. Initial appearance of ePVS may be directly related to advancing age but once ePVS are present (as is the case with most participants in the current study), the rate at which they grow is constant, and therefor there would be no age effect on longitudinal ePVS. Counterintuitively, there were interactions between age and *APOE*-ε4 status where greater age was associated with less ePVS burden increase among *APOE*-ε4 carriers. *APOE*-ε4 carriers may experience greater increases in ePVS burden earlier in life which could limit the potential for ePVS growth later in life.

Stiffening and hypertension were both related to baseline ePVS burden but not longitudinal ePVS burden. The lack of longitudinal findings could mean that stiffening and hypertension play a role in ePVS formation in midlife while late-life longitudinal associations depend on other factors, such as inflammation.

Greater baseline sTREM2 levels were predictive of longitudinal increase in basal ganglia ePVS burden. This result indicates microglial activation may be connected to ePVS formation. A connection between sTREM2 and ePVS aligns with previous literature that hypothesizes such connections may exist because activated microglia

release chemokines and cytokines that lead to BBB breakdown[222] and accumulation of fluid and toxic molecules in the PVS.[173] PVS also play a role in immune cell transport, so microglia activation may be indicative of an abundance of immune cells in the region, which could clog the PVS.[173,223] Associations between sTREM2 and longitudinal ePVS were driven by participants with MCI. Individuals with MCI likely have beta-amyloid pathology, which is associated with increased microglia activation and increased sTREM2.[220] The presence of beta-amyloid may result in prolonged microglia activation which could account for associations seen between sTREM2 and longitudinal ePVS burden among participants with MCI. So, the addition of microglial activation and downstream degradative processes could be a second hit that drives PVS towards enlargement in individuals with MCI. Greater baseline MMP2 and MMP3 levels were predictive of longitudinal increase in basal ganglia ePVS burden. Both MMP2 and MMP3 also drive BBB breakdown,[224,225] resulting in fluid and toxic protein infiltration into the PVS and ultimately PVS enlargement.[226] Associations with MMP2 levels appear to be driven by *APOE*-ε4 non-carriers while associations with MMP3 levels appear to be driven by normal cognition participants. The *APOE*-ε4 allele is known to activate a proinflammatory pathway that includes MMP9 and leads to BBB breakdown.[26] Meanwhile, *APOE*-ε3 and ε2 isoforms more effectively suppress MMP9 secretion.[227] So MMP associated BBB breakdown may occur primarily due to other MMPs, such as MMP2, for *APOE*-ε4 non-carriers.[228] MMP3 could be causing earlier insults, insults in normal cognition participants, to the PVS through BBB breakdown while later, in participants with MCI, sTREM2 exacerbates the situation and drives ePVS volume growth. Interestingly, associations between MMP3 and ePVS among normal cognition

participants were stronger for ePVS count while associations between sTREM2 and ePVS among participants with MCI were stronger for ePVS volume. MMP3 may be driving the initial PVS growth and then sTREM2 may be driving the existent ePVS to grow in volume even further.

Baseline sleep quality was not predictive of longitudinal change in basal ganglia ePVS burden. Again, while sleep quality likely has an effect on ePVS burden,[127–129] we may be limited here by the accuracy and subjectivity of our sleep measure. Variance exists in the measure and may limit our ability to detect a signal. Additionally, brain clearance associated with sleep may more preferentially occur through white matter PVS rather than basal ganglia PVS. However, among *APOE*-ε4 non-carriers, normal cognition participants, and female participants, worse sleep quality was associated with less longitudinal increase in ePVS burden. Prior research shows that *APOE*-ε4 carriers have worse objective sleep quality,[229] which may make them more susceptible to PVS enlargement compared to *APOE*-ε4 non-carriers. Normal cognition participants are healthier than participants with MCI and therefore may be less likely to develop ePVS in the context of poor subjective sleep quality. Lastly, female participants have less concomitant vascular pathology in general and therefore may be better able to cope with poor sleep quality without developing worse ePVS pathology.

Baseline AD biomarker levels were not related to longitudinal basal ganglia ePVS burden. While basal ganglia PVS may provide some clearance capacity for metabolic waste, they may not be a primary clearance route for AD related proteins. However, greater t-tau and p-tau levels were predictive of longitudinal increase in ePVS burden among *APOE*-ε4 non-carriers and male participants. Previous literature has shown an

association between basal ganglia ePVS and CSF t-tau levels.[132] The same work showed an association between lower CSF $A\beta_{42}$ levels and ePVS in the white matter, suggesting $A\beta_{42}$ may be more readily cleared through cortical PVS versus basal ganglia PVS. Effects of CSF t-tau levels on basal ganglia ePVS may vary by *APOE*-ε4 carrier status due to variance in how well different *APOE* alleles traffic protein to the PVS. The *APOE*-ε4 allele may impede the transport of t-tau and other toxic proteins to the PVS while the *APOE*-ε3 and ε2 alleles allow more efficient toxic protein transport,[230] which means PVS may be more susceptible to enlargement in the presence of ε3 and ε2 because these *APOE* species upregulate waste transport to the PVS. Associations between CSF t-tau levels and ePVS among men are surprising considering women generally have more tau pathology than men.[231,232] One possibility is that men clear tau from the parenchyma in a more efficient manner, which may result in increased tau burden in the PVS, increasing the chances of ePVS development. Future studies aimed at interrogating sex differences in associations between tau and ePVS, as well as the role *APOE* may play, would be highly interesting.

The current study has many strengths, the most notable of which is the utilization of a deep learning model to create a fully continuous, robust measure of ePVS burden for hundreds of baseline and longitudinal brain MRI scans. Studies utilizing continuous measures of ePVS are minimal and even fewer have used advanced computational techniques like deep learning. To our knowledge, the present study is among the first to apply a deep learning ePVS quantification technique to assess potential drivers of ePVS both cross-sectionally and longitudinally. Some limitations of the present study are worth mentioning though. Several different comparisons were run for multiple predictors

and while we do provide false discovery rate-corrected p-values in the results section, the likelihood of false positives is high and should be factored into interpretation of the results. The participants studied are on average college-educated, predominantly White/non-Hispanic, and older, which could limit the generalizability of the present findings. Also, throughout the longitudinal study, MRI scanner software and hardware has changed multiple times which can affect the appearance of ePVS in the image, and ultimately ePVS volume and count values.

We utilized deep learning to robustly quantify ePVS, an understudied SVD pathology. Age, aortic stiffening, and hypertension appear to be contributing factors to PVS enlargement in the basal ganglia at baseline while CSF sTREM2, CSF MMP2, and CSF MMP3 appear to be contributing factors to PVS enlargement in the basal ganglia longitudinally.

CHAPTER 4

CLINICAL CONSEQUENCES OF ENLARGED PERIVASCULAR SPACES

Introduction

Studies delineating the clinical manifestations of enlarged perivascular spaces (ePVS) have yielded mixed results, and there is still a relative paucity of high-quality clinical studies on this topic. Historically, ePVS were labelled benign and considered an epiphenomenon of neurodegeneration. However, emerging research suggests ePVS may indeed have clinical consequences. In population-based studies, ePVS burden was associated with incident, all-cause dementia[233] and vascular dementia.[134] Participants with more than 20 ePVS visible on a given axial magnetic resonance imaging (MRI) slice in the white matter or the basal ganglia were especially at risk for incident dementia and the risk was higher for white matter compared to basal ganglia ePVS.[233] Among patients with cognitive impairment, ePVS burden was associated with clinical Alzheimer's disease (AD)[234] and specifically, ePVS severity in the centrum semiovale was a positive predictor of AD-related cognitive impairment.[234] The odds ratio of an AD diagnosis nearly doubled from 3.57 in patients with a rating of 11-20 ePVS to 6.26 in patients with a rating of more than 20 ePVS in one axial MRI slice of the centrum semiovale on multivariable analyses.[234]

The failure of β-amyloid clearance, which could result from PVS damage, may drive increased β-amyloid accumulation in the parenchyma and has been linked to changes in oxidative stress,[235] neuroinflammation,[236] cell death and neurodegeneration. Therefore, ePVS could be highly associated with AD pathology. Indeed, increased PET-

detected β-amyloidosis was related to ePVS burden in the centrum semiovale in a study of 31 non-demented adults.[122] In a systematic review conducted by Smeijer et al. 2019, they examined ePVS and non-AD forms of dementia. Four of the reviewed studies assessed cross-sectional ePVS associations with the presence of vascular dementia using odds ratios (n=2) or ANOVA (n=2). All four studies reported significant associations between ePVS in the basal ganglia and the presence of vascular dementia.[174] Multiple studies now support the theory that ePVS are associated with dementia, but an important and persistent debate in the field is whether or not ePVS contribute to cognitive impairment or if they are simply a by-product of other disease processes.

In a study of healthy older men, ePVS in the basal ganglia and centrum semiovale correlated with white matter hyperintensities (WMHs) and were associated with worse non-verbal reasoning and visuospatial ability.[135] Participants with a range of 1-20 ePVS in the basal ganglia and centrum semiovale performed worse on visuospatial tasks than participants with no ePVS.[135] We recently found in the Vanderbilt Memory and Aging Project, a community-based cohort of older adults free of clinical dementia that ePVS related to worse information processing and executive function.[97] We then tested ePVS and other small vessel disease (SVD) markers (i.e., WMHs, lacunes, cerebral microbleeds) as competing predictors and found ePVS contributed independently to multiple cognitive outcomes. Compared to other SVD markers, ePVS accounted for the most variance in predicting executive function performance.[97] This recent work provides important evidence that ePVS may be a meaningful contributor to certain cognitive functions and act through a pathway independent from WMHs to

adversely affect cognition.[97] In one of the few studies assessing longitudinal consequences, large ePVS (>3 mm) burden predicted a steeper decline in information processing speed over time.[134] Overall, the presence of over 20 ePVS in the white matter on a single axial image of the brain is associated with an increased risk of developing AD and related dementias. ePVS in the basal ganglia seem to be associated with the cognitive domains of executive function and information processing speed.

Some published work has not found ePVS relate to cognition. In a meta-analysis of 5 studies, ePVS were found to have no significant association with cognition.[151] While this study included a robust sample of 2806 participants, methods across studies were not harmonized (e.g., 1.5T versus 3T MRI, different MRI sequences, and different cognitive tests were utilized). In a longitudinal study, baseline ePVS burden did not predict processing speed, executive function, or global cognitive decline over a 5-year follow-up period.[237] ePVS occasionally appear in the hippocampus, but a study of older adults without dementia found that ePVS in the hippocampus were not associated with memory function.[238] One of the challenges facing studies of ePVS is the variability in quantification methods utilized from study to study and this variability creates difficulty in making conclusive statements about the literature. Emerging methods for standardized quantification are discussed in Chapter 2.

As stated earlier, SVD exists in upwards of 87% of autopsy confirmed AD cases[96] and has clinical implications. However, ePVS, a purported marker of SVD, have not been as widely studied due to difficulties in accurate quantification and the common notion that ePVS are a by-product of neurodegeneration.[239]

ePVS have often been considered clinically benign, a conclusion that is supported by the literature.[151] However, a growing body of work, including our own research mentioned above,[97] suggests ePVS may be clinically relevant. To better quantify ePVS and understand their clinical relevance, standardized, fully quantitative methods are needed. Most other studies,[135,151] including our prior work,[97] rely on ordinal scores of ePVS burden based on a few (or less) image slices. To overcome past methodological limitations, the current study leverages machine learning to calculate ePVS volume and count for the entire basal ganglia. The ePVS quantification method implemented here is a novel deep learning algorithm that outputs continuous volume and count measures for the entire basal ganglia with minimal edits required.

We focus on the basal ganglia for two reasons. First, ePVS are more prominent in this region, and second, the basal ganglia plays a crucial role in mediating executive function and information processing, two of our cognitive outcomes of interest. We hypothesize that greater ePVS volume and count in the basal ganglia will be associated with worse cognition. Specifically, we expect the domains of information processing and executive function to be most affected as these functions rely on frontal subcortical circuits which run through the basal ganglia.[48,240] To our knowledge, this study is among the first to analyze associations between continuous measures of ePVS and longitudinal cognition. We additionally hypothesize that due to the damaging effects apolipoprotein E ε4 (*APOE*-ε4) can have on blood vessels, associations between ePVS burden and cognition will be stronger among *APOE*-ε4 carriers. Lastly, we hypothesize that associations will be stronger among participants with mild cognitive impairment (MCI). MCI participants are more susceptible than cognitively unimpaired individuals to

cognitive decline. The additional burden of SVD pathology, such as ePVS, may accelerate this decline leading to stronger cognitive associations among MCI participants.

Methods

For details about study cohort, brain MRI, ePVS quantification, neuropsychological assessment, and covariates, please refer to the Methods in Chapter 2 (pages 33-42).

Analytical Plan

Linear regression models related standardized ePVS volume and ePVS count to neuropsychological performance (one model per test). Models adjusted for age, sex, race/ethnicity, education, Framingham Stroke Risk Profile (excluding points for age), diagnosis, *APOE*-ε4 carrier status, and intracranial volume. Mixed-effects regression models related standardized ePVS volume and ePVS count at baseline to longitudinal neuropsychological performance (one model per test). Fixed effects included baseline age, sex, race/ethnicity, education, diagnosis, Framingham Stroke Risk Profile (minus age), *APOE*-ε4 carrier status, intracranial volume, ePVS burden (standardized volume or count), time (defined as years since first neuropsychological assessment), and an interaction term for *ePVS burden x time* which is the term of interest. Random effects included the intercept and time by each individual participant. To test hypotheses related to *APOE*-ε4, models were repeated with an *ePVS burden x APOE-ε4 carrier status* or *ePVS burden x time x APOE-ε4 carrier status* interaction term with follow-up

models stratified by carrier status (carrier and non-carrier). To test hypotheses related to cognitive diagnosis, models were repeated with an *ePVS burden x cognitive diagnosis* or *ePVS burden x time x cognitive diagnosis* interaction term with follow-up models stratified by cognitive diagnosis (normal cognition and MCI). Lower order interaction terms were included in all models when applicable. Sensitivity analyses were performed on all models (a) excluding participants with prevalent CVD and atrial fibrillation and (b) excluding outliers above 4 standard deviations. Significance was set *a* priori at $p<0.05$. All analyses were conducted using R 3.5.2 (www.r-project.org).

Results

Participant Characteristics

Participants included 327 adults (73±7 years, 59% male, 87% non-Hispanic white), including 169 cognitively unimpaired, 27 with early MCI, and 131 with MCI. Standardized basal ganglia ePVS volumes ranged 0.0005 to 0.01 while ePVS counts ranged 11 to 268. Standardized basal ganglia ePVS volume and ePVS count are highly correlated ($r=0.80$, $p<0.001$). The cohort was followed for 4.7±1.3 years. See **Table 2.1** in Chapter 2 for more details

ePVS Burden and Cross-sectional Neuropsychological Outcomes

Increased standardized ePVS volume was associated with worse Delis-Kaplan Executive Function System (DKEFS) Number Sequencing ($\beta=1554$, $p=0.002$), Wechsler Adult Intelligence Scale (WAIS)-IV Coding ($\beta=-974$, $p=0.003$), Executive Function Composite ($\beta=-81.9$, $p<0.001$), and Hooper Visual Organization Test ($\beta=-192$, $p=0.02$)

performances. When excluding outliers, ePVS volume associations with DKEFS Number Sequencing (p=0.26) and Hooper Visual Organization Test (p=0.84) performances were attenuated. When excluding participants with CVD and atrial fibrillation, the association between ePVS volume and Hooper Visual Organization Test was attenuated (p=0.12). See **Table 4.1** and **Figure 4.1** for details. Findings were comparable when ePVS count was used as the predictor.

Table 4.1. ePVS Volume Associations with Cross-sectional Cognition

	β	95% CI	*p-value*
ePVS Volume			
Boston Naming Test (30 Item)	-45.54	-208.4, 117.3	0.58
Animal Naming	-213.8	-479.6, 51.99	0.11
DKEFS Number Sequencing Test*	1554	553.1, 2556	**0.002**
WAIS-IV Coding	-973.5	-1610, -337.0	**0.003**
Executive Composite	-81.91	-120.3, -43.49	**<0.001**
Hooper Visual Organization Test	-191.9	-355.0, -28.73	**0.02**
Episodic Memory Composite	10.33	-30.21, 50.87	0.62
ePVS Count			
Boston Naming Test (30 Item)	-0.006	-0.02, 0.002	0.15
Animal Naming	-0.009	-0.02, 0.006	0.24
DKEFS Number Sequencing Test*	0.09	0.04, 0.15	**<0.001**
WAIS-IV Coding	-0.06	-0.09, -0.03	**<0.001**
Executive Composite	-0.005	-0.007, -0.003	**<0.001**
Hooper Visual Organization Test	-0.01	-0.02, -0.001	**0.03**
Episodic Memory Composite	-4.5×10^{-4}	-0.003, 0.002	0.68

Note. ePVS volume represents a standardized measure of ePVS volume (values were divided by total basal ganglia tissue volume). Analyses performed on n=326 participants. Models were adjusted for age, sex, race/ethnicity, education, *APOE*-ε4 status, cognitive diagnosis, and Framingham Stroke Risk Profile (excluding points assigned for age). CI, confidence interval. ePVS, enlarged perivascular space. *Higher values reflect worse performance.

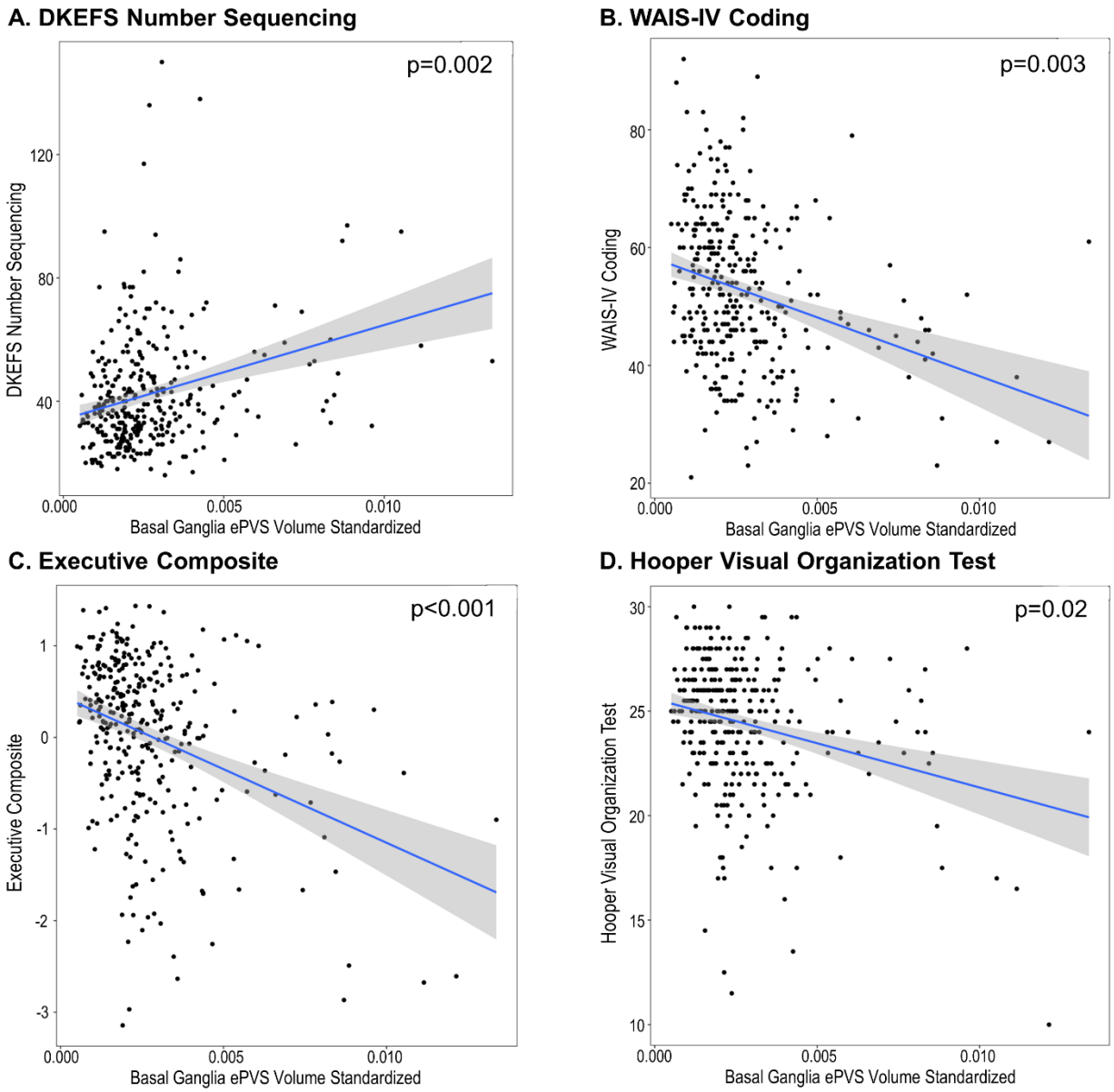

Figure 4.1. Cross-sectional basal ganglia ePVS volume associations with cognition. **(A)** DKEFS Number Sequencing, **(B)** WAIS-IV Coding, **(C)** Executive Composite, and **(D)** Hooper Visual Organization Test. Plots include outliers. For DKEFS Number Sequencing, higher values reflect worse performance. When excluding outliers, associations with DKEFS Number Sequencing and Hooper Visual Organization Test are attenuated (p-values>0.26) but associations with WAIS-IV Coding (p=0.002) and Executive Composite (p=0.001) remain. DKEFS, Delis-Keplan Executive Function System; WAIS, Wechsler Adult Intelligence Scale.

The *standardized ePVS volume x APOE-ε4 status* interaction term was associated with Boston Naming Test (β=-557, p<0.001) and Visuospatial (β=-326, p=0.05) performance. Models were attenuated when excluding outliers. When excluding for CVD and atrial fibrillation the model for Boston Naming Test persisted but the model for Visuospatial skills was attenuated. Among *APOE*-ε4 non-carriers, standardized ePVS volume was associated with worse Number Sequencing (β=1091, p=0.05) and Executive Function (β=-89.3, p<0.001) performance. Associations persisted when excluding participants with CVD and atrial fibrillation and when excluding outliers, the associations between standardized ePVS volume and Number Sequencing was attenuated. Among *APOE*-ε4 carriers, standardized ePVS volume was associated with worse Boston Naming Test (β=-362, p=0.03), Number Sequencing (β=2391, p=0.02), Coding (β=-1166, p=0.03), Executive Function (β=-70.3, p=0.05), and Visuospatial performance (β=-394, p=0.01). All associations among *APOE*-ε4 carriers were attenuated when excluding outliers (p-values>0.11) and when excluding for CVD and atrial fibrillation (p-values>0.10), only the association between standardized ePVS volume and Number Sequencing (β=2500, p=0.04) persisted. Findings were similar when ePVS count was used as the predictor. See **Table 4.2** and **Figure 4.2**.

Table 4.2. ePVS Burden x *APOE*-ε4 Interaction Models and Stratified by *APOE*-ε4 Status Associations with Cross-sectional Cognition

	β	95% CI	*p-value*
***APOE*-ε4 Carriers versus Non-carriers ePVS Volume**			
Boston Naming Test (30 Item)	-557	-875, -238	**<0.001**
Animal Naming	-175	-705, 354	0.51
DKEFS Number Sequencing Test*	1067	-926, 3059	0.29
WAIS-IV Coding	-537	-1804, 731	0.41

Executive Composite	17.3	-59.3, 93.8	0.66
Hooper Visual Organization Test	-326	-650, -3.15	**0.05**
Episodic Memory Composite	-42.2	-123, 38.5	0.30
***APOE*-ε4 Carriers versus Non-carriers ePVS Count**			
Boston Naming Test (30 Item)	-0.03	-0.04, -0.008	**0.004**
Animal Naming	0.001	-0.03, 0.03	0.93
DKEFS Number Sequencing Test*	0.06	-0.05, 0.17	0.26
WAIS-IV Coding	-0.02	-0.09, 0.05	0.35
Executive Composite	-0.001	-0.005, 0.003	0.58
Hooper Visual Organization Test	-0.02	-0.03, 0.001	0.07
Episodic Memory Composite	-0.002	-0.006, 0.003	0.46
***APOE*-ε4 Carriers ePVS Volume**			
Boston Naming Test (30 Item)	-362	-685, -39.8	**0.03**
Animal Naming	-243	-646, 159	0.23
DKEFS Number Sequencing Test*	2391	337, 4445	**0.02**
WAIS-IV Coding	-1166	-2234, -97.4	**0.03**
Executive Composite	-70.3	-139, -1.28	**0.05**
Hooper Visual Organization Test	-394	-704, -83.7	**0.01**
Episodic Memory Composite	-17.6	-87.2, 51.9	0.62
***APOE*-ε4 Carriers ePVS Count**			
Boston Naming Test (30 Item)	-0.03	-0.04, -0.007	**0.008**
Animal Naming	-0.01	-0.03, 0.01	0.42
DKEFS Number Sequencing Test*	0.17	0.05, 0.29	**0.006**
WAIS-IV Coding	-0.07	-0.13, -0.004	**0.04**
Executive Composite	-0.006	-0.01, -0.002	**0.002**
Hooper Visual Organization Test	-0.02	-0.04, -0.004	**0.02**
Episodic Memory Composite	-0.002	-0.006, 0.002	0.25
***APOE*-ε4 Non-carriers ePVS Volume**			
Boston Naming Test (30 Item)	124	-54.6, 302	0.17
Animal Naming	-239	-593, 115	0.18
DKEFS Number Sequencing Test*	1092	21.2, 2162	**0.05**
WAIS-IV Coding	-791	-1604, 22.2	0.06
Executive Composite	-89.3	-137, -41.9	**<0.001**
Hooper Visual Organization Test	-72.5	-263, 118	0.45
Episodic Memory Composite	26.1	-25.4, 77.5	0.32
***APOE*-ε4 Non-carriers ePVS Count**			
Boston Naming Test (30 Item)	0.0001	-0.009, 0.009	0.97
Animal Naming	-0.01	-0.03, 0.006	0.17
DKEFS Number Sequencing Test*	0.06	0.007, 0.11	**0.03**
WAIS-IV Coding	-0.05	-0.09, -0.01	**0.01**
Executive Composite	-0.004	-0.006, -0.002	**0.002**
Hooper Visual Organization Test	-0.004	-0.01, 0.006	0.40
Episodic Memory Composite	0.0003	-0.002, 0.003	0.85

Note. ePVS volume represents a standardized measure of ePVS volume (values were divided by total basal ganglia tissue volume). Analyses performed on n=326 participants (113 *APOE*-ε4 carriers and 213 *APOE*-ε4 non-carriers). Models were adjusted for age, sex, race/ethnicity, education, *APOE*-ε4 status, cognitive diagnosis, and Framingham Stroke Risk Profile (excluding points assigned for age). CI, confidence interval. ePVS, enlarged perivascular space. The parameter estimates (β) for the interaction models are for the *ePVS volume x APOE-ε4 carrier status* interaction term and is interpreted as the difference in slopes between carriers and non-carriers. The parameter estimates (β) for the stratified models represent the changes in neuropsychological outcomes associated with one

unit change in ePVS volume. *Higher values reflect worse performance. Bold p-values meet the *a priori* significance threshold.

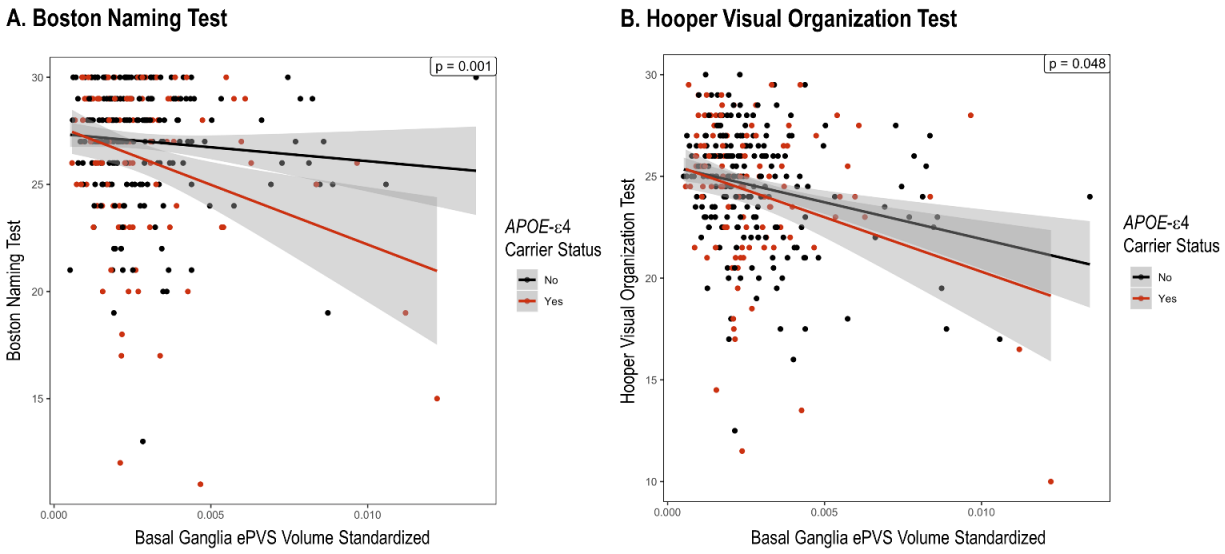

Figure 4.2. Cross-sectional *basal ganglia ePVS volume x APOE-ε4* status interactions on cognition. **(A)** Boston Naming Test (30-Item) and **(B)** Hooper Visual Organization Test. *APOE*-ε4, apolipoprotein E ε4.

The *standardized ePVS volume x cognitive diagnosis* interaction term was associated with Boston Naming Test (β=-347, p=0.04), Animal Naming (β=-578, p=0.04), DKEFS Number Sequencing (β=2456, p=0.02), and Hooper Visual Organization Test (β=-447, p=0.01) performances. All associations between *standardized ePVS volume x diagnosis* and cognition were attenuated when excluding outliers (p-values>0.13). When excluding for CVD and atrial fibrillation, all associations persisted except for the one with Boston Naming Test (p=0.19). Among cognitively unimpaired participants, all models between log-standardized ePVS volume and cognitive performance were null (p-values>0.19). Among participants with MCI, standardized ePVS volume was associated with worse Animal Naming (β=-389, p=0.03), DKEFS Number Sequencing (β=2432, p=0.006), WAIS-IV Coding (β=-1283,

p=0.003), Executive Function Composite (β=-110, p<0.001), and Hooper Visual Organization Test (β=-346, p=0.008) performances. When excluding outliers, standardized ePVS volume associations with WAIS-IV Coding (β=-1734, p=0.003) and Executive Function Composite (β=-118, p=0.008) performances persisted. When excluding for CVD and atrial fibrillation all associations persisted among participants with MCI except for the one with Hooper Visual Organization Test (p=0.07). Findings were similar when ePVS count was used as the predictor. See **Table 4.3** and **Figure 4.3**.

Table 4.3. ePVS Burden x Cognitive Diagnosis Interaction Models and Stratified by Cognitive Diagnosis Associations with Cross-sectional Cognition

	β	95% CI	*p-value*
Normal Cognition versus MCI ePVS Volume			
Boston Naming Test (30 Item)	-347	-683, -9.94	**0.04**
Animal Naming	-578	-1128, -28.6	**0.04**
DKEFS Number Sequencing Test*	2456	382, 4530	**0.02**
WAIS-IV Coding	-261	-1549, 1027	0.69
Executive Composite	-66.8	-147, 13.6	0.10
Hooper Visual Organization Test	-447	-785, -109	**0.01**
Episodic Memory Composite	0.95	-82.5, 84.4	0.98
Normal Cognition versus MCI ePVS Count			
Boston Naming Test (30 Item)	-0.02	-0.04, -0.002	**0.03**
Animal Naming	-0.03	-0.06, -0.004	**0.03**
DKEFS Number Sequencing Test*	0.14	0.03, 0.25	**0.01**
WAIS-IV Coding	-0.03	-0.10, 0.03	0.32
Executive Composite	-0.004	-0.008, 0.0005	0.08
Hooper Visual Organization Test	-0.03	-0.04, -0.009	**0.003**
Episodic Memory Composite	-0.0006	-0.005, 0.004	0.78
MCI ePVS Volume			
Boston Naming Test (30 Item)	-108	-382, 167	0.44
Animal Naming	-389	-740, -38.0	**0.03**
DKEFS Number Sequencing Test*	2432	696, 4168	**0.006**
WAIS-IV Coding	-1283	-2113, -453	**0.003**
Executive Composite	-110	-173, -47.7	**<0.001**
Hooper Visual Organization Test	-346	-600, -92.7	**0.008**
Episodic Memory Composite	-5.70	-61.2, 49.8	0.84
MCI ePVS Count			
Boston Naming Test (30 Item)	-0.01	-0.03, 0.004	0.12
Animal Naming	-0.02	-0.04, -0.002	**0.03**

DKEFS Number Sequencing Test*	0.16	0.06, 0.27	**0.002**
WAIS-IV Coding	-0.09	-0.14, -0.04	**<0.001**
Executive Composite	-0.007	-0.01, -0.003	**<0.001**
Hooper Visual Organization Test	-0.02	-0.04, -0.007	**0.004**
Episodic Memory Composite	-0.002	-0.006, 0.001	0.17
Normal Cognition ePVS Volume			
Boston Naming Test (30 Item)	104	-87.5, 295	0.29
Animal Naming	167	-287, 621	0.47
DKEFS Number Sequencing Test*	23.4	-1155, 1202	0.97
WAIS-IV Coding	-538	-1605, 528	0.32
Executive Composite	-35.8	-90.0, 18.4	0.19
Hooper Visual Organization Test	68.7	-172, 309	0.57
Episodic Memory Composite	11.7	-53.6, 77.0	0.72
Normal Cognition ePVS Count			
Boston Naming Test (30 Item)	0.002	-0.007, 0.01	0.69
Animal Naming	0.01	-0.01, 0.03	0.32
DKEFS Number Sequencing Test*	0.02	-0.04, 0.07	0.51
WAIS-IV Coding	-0.03	-0.08, 0.02	0.25
Executive Composite	-0.002	-0.005, 0.00007	0.06
Hooper Visual Organization Test	0.004	-0.007, 0.02	0.47
Episodic Memory Composite	0.0005	-0.003, 0.004	0.75

Note. ePVS volume represents a standardized measure of ePVS volume (values were divided by total basal ganglia tissue volume). Analyses performed on n=299 participants (130 MCI and 169 Normal Cognition). Models were adjusted for age, sex, race/ethnicity, education, *APOE*-ε4 status, cognitive diagnosis, and Framingham Stroke Risk Profile (excluding points assigned for age). CI, confidence interval. ePVS, enlarged perivascular space. The parameter estimates (β) for the interaction models are for the *ePVS volume x Cognitive Diagnosis* interaction term and is interpreted as the difference in slopes between MCI and Normal Cognition. The parameter estimates (β) for the stratified models represent the changes in neuropsychological outcomes associated with one unit change in ePVS volume. *Higher values reflect worse performance. Bold p-values meet the *a priori* significance threshold.

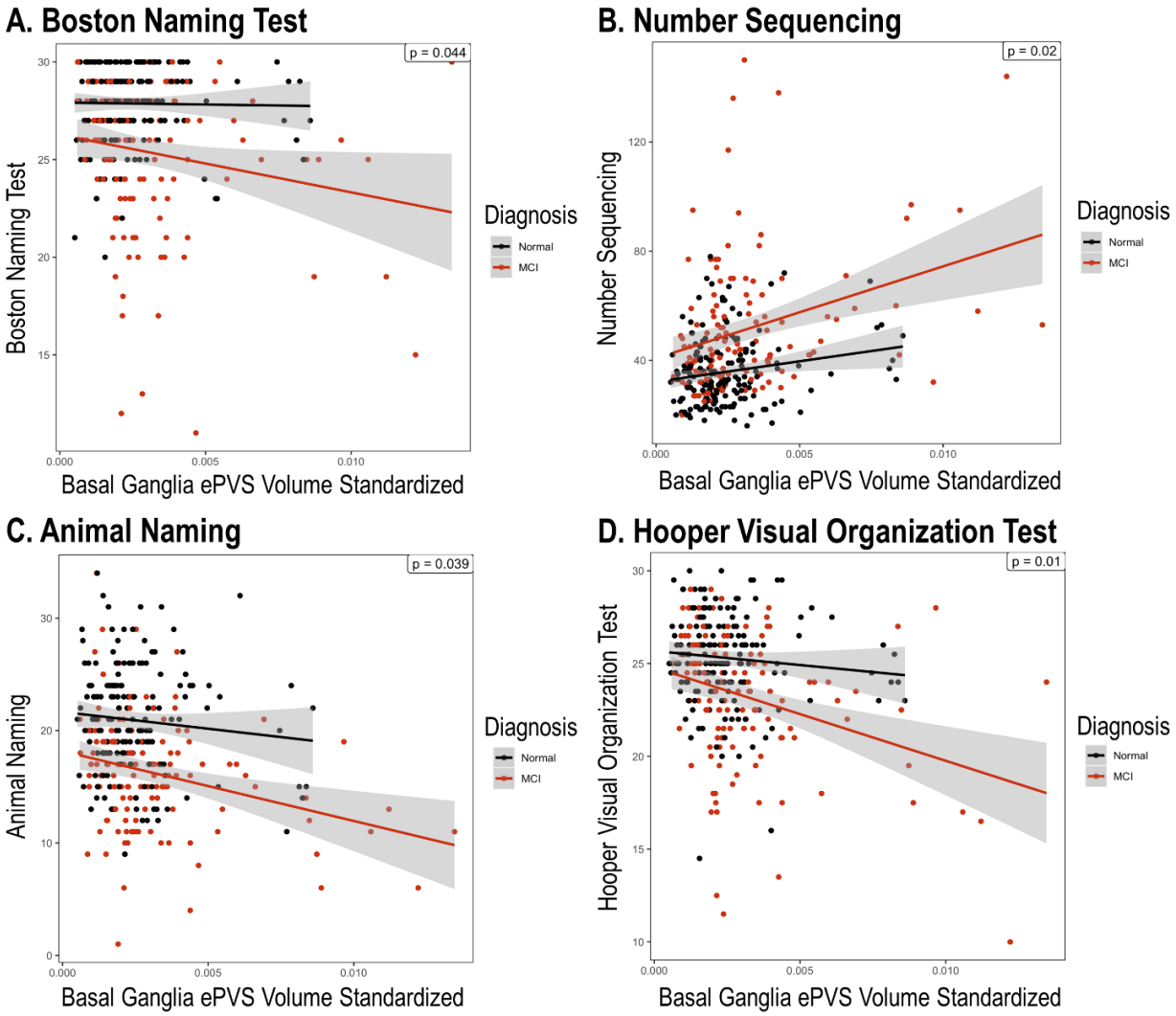

Figure 4.3. Cross-sectional *basal ganglia ePVS volume x cognitive diagnosis* interactions on cognition. **(A)** Boston Naming Test (30-Item), **(B)** Number Sequencing, **(C)** Animal Naming, and **(D)** Hooper Visual Organization Test. MCI, mild cognitive impairment.

ePVS Burden and Longitudinal Neuropsychological Outcomes

Increased standardized ePVS volume was associated with longitudinal decline in Boston Naming Test (β=-54.9, p=0.05), WAIS-IV Coding (β=-147, p=0.03), Executive Function Composite (β=-10.9, p=0.03), and Memory Composite (β=-10.6, p=0.02) performances. When excluding outliers, associations with WAIS-IV Coding and Executive Function Composite were attenuated (p-values>0.10). When excluding

participants with CVD and atrial fibrillation, all associations remained significant (p-values<0.03). ePVS count was associated with decline in Executive Function Composite performance (β=-6.9x10^{-4}, p=0.04) but all other cognitive outcomes were null (p-values>0.09). See **Table 4.4** and **Figure 4.4** for details.

Table 4.4. ePVS Burden Associations with Longitudinal Cognition

	β	95% CI	*p-value*
ePVS Volume			
Boston Naming Test (30 Item)	-54.85	-109.5, -0.20	**0.05**
Animal Naming	-14.50	-84.87, 55.86	0.69
DKEFS Number Sequencing Test*	33.13	-304.3, 370.5	0.85
WAIS-IV Coding	-146.5	-278.9, -14.10	**0.03**
Executive Composite	-10.88	-20.59, -1.17	**0.03**
Hooper Visual Organization Test	-20.33	-68.28, 27.63	0.41
Episodic Memory Composite	-10.63	-19.84, -1.42	**0.02**
ePVS Count			
Boston Naming Test (30 Item)	-7.7x10^{-4}	-0.004, 0.002	0.58
Animal Naming	-0.001	-0.005, 0.002	0.54
DKEFS Number Sequencing Test*	0.003	-0.01, 0.02	0.68
WAIS-IV Coding	-0.006	-0.01, 9.8x10^{-4}	0.09
Executive Composite	-6.9x10^{-4}	-0.001, -2.1x10^{-4}	**0.005**
Hooper Visual Organization Test	-1.7x10^{-4}	-0.003, 0.002	0.89
Episodic Memory Composite	-3.7x10^{-4}	-8.4x10^{-4}, 8.9x10^{-5}	0.11

Note. ePVS volume represents a standardized measure of ePVS volume (values were divided by total basal ganglia tissue volume). Analyses performed on n=326 participants. Models were adjusted for age, sex, race/ethnicity, education, *APOE*-ε4 status, cognitive diagnosis, and Framingham Stroke Risk Profile (excluding points assigned for age). CI, confidence interval. ePVS, enlarged perivascular space. The parameter estimates (β) are for the *ePVS volume x time* interaction term and is interpreted as the annual changes of neuropsychological outcomes associated with one unit change in ePVS volume. *Higher values reflect worse performance.

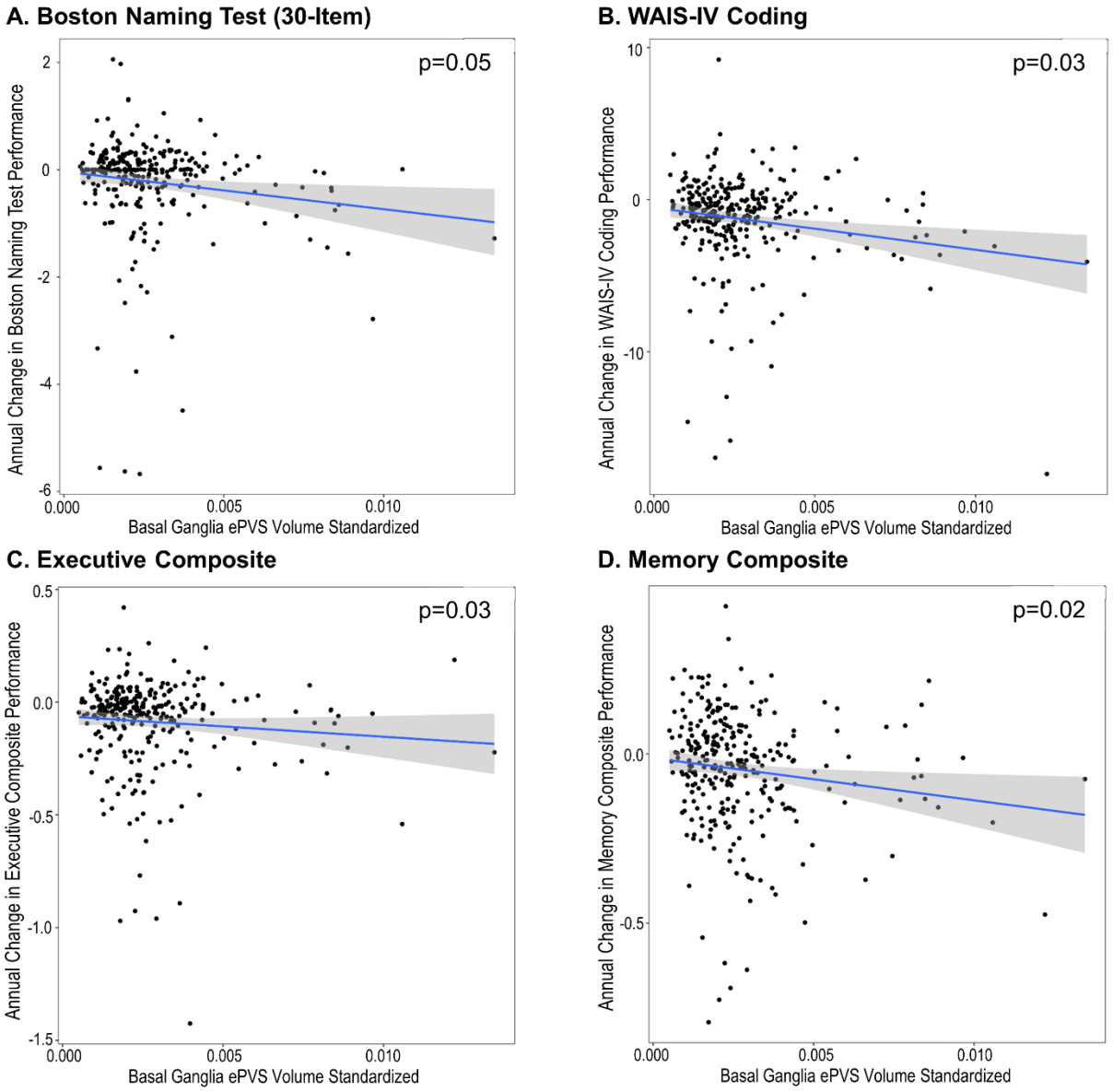

Figure 4.4. Baseline basal ganglia ePVS volume associations with longitudinal cognition. **(A)** Boston Naming Test (30-Item), **(B)** WAIS-IV Coding, **(C)** Executive Composite, and **(D)** Memory Composite. Plots include outliers. When excluding outliers, associations with WAIS-IV Coding and Executive Function were attenuated (p-values>0.10) but associations with Boston Naming Test (p=0.005) and Memory Composite (p=0.04) remain. WAIS, Wechsler Adult Intelligence Scale.

The *standardized ePVS volume x time x APOE-ε4 status* interaction term was unrelated to any longitudinal cognitive outcomes (p-values>0.11). Among *APOE*-ε4 non-carriers, standardized ePVS volume was associated with longitudinal decline in Boston

Naming Test (β=-77.7, p<0.001), Coding (β=-208, p<0.001), Executive Function (β=-14.5, p<0.001), and Episodic Memory (β=-11.5, p=0.01) performance. Associations persisted when excluding participants with CVD and atrial fibrillation and when excluding outliers. Among *APOE*-ε4 carriers, standardized ePVS volume was unrelated to longitudinal cognition. Findings were similar when ePVS count was used as the predictor. See **Table 4.5**.

Table 4.5. ePVS Burden x *APOE*-ε4 Interaction Models and Stratified by *APOE*-ε4 Status Associations with Longitudinal Cognition

	β	95% CI	*p-value*
***APOE*-ε4 Carriers versus Non-carriers ePVS Volume**			
Boston Naming Test (30 Item)	49.9	-75.6, 175	0.44
Animal Naming	84.6	-71.4, 241	0.29
DKEFS Number Sequencing Test*	-454	-1184, 277	0.22
WAIS-IV Coding	237	-55.0, 529	0.11
Executive Composite	12.6	-8.81, 34.1	0.25
Hooper Visual Organization Test	-25.3	-133, 82.7	0.65
Episodic Memory Composite	3.96	-16.9, 24.9	0.71
***APOE*-ε4 Carriers versus Non-carriers ePVS Count**			
Boston Naming Test (30 Item)	0.004	-0.002, 0.01	0.19
Animal Naming	0.006	-0.002, 0.01	0.14
DKEFS Number Sequencing Test*	0.0005	-0.04, 0.04	0.98
WAIS-IV Coding	0.006	-0.009, 0.02	0.43
Executive Composite	0.0001	-0.0009, 0.001	0.82
Hooper Visual Organization Test	0.0008	-0.005, 0.006	0.77
Episodic Memory Composite	-0.0002	-0.001, 0.0009	0.77
***APOE*-ε4 Carriers ePVS Volume**			
Boston Naming Test (30 Item)	-8.04	-165, 149	0.92
Animal Naming	49.8	-118, 218	0.56
DKEFS Number Sequencing Test*	-443	-1327, 440	0.32
WAIS-IV Coding	-32.3	-404, 340	0.86
Executive Composite	-2.16	-27.6, 23.3	0.87
Hooper Visual Organization Test	-62.9	-187, 61.5	0.32
Episodic Memory Composite	-9.68	-32.5, 13.2	0.41
***APOE*-ε4 Carriers ePVS Count**			
Boston Naming Test (30 Item)	0.003	-0.005, 0.01	0.48
Animal Naming	0.003	-0.006, 0.01	0.52
DKEFS Number Sequencing Test*	-0.0005	-0.05, 0.04	0.98
WAIS-IV Coding	-0.002	-0.02, 0.02	0.86
Executive Composite	-0.0006	-0.002, 0.0007	0.34

Hooper Visual Organization Test	-0.0002	-0.007, 0.006	0.96
Episodic Memory Composite	-0.0006	-0.002, 0.0006	0.30
***APOE*-ε4 Non-carriers ePVS Volume**			
Boston Naming Test (30 Item)	-77.7	-117, -38.3	**<0.001**
Animal Naming	-48.1	-118, 21.8	0.18
DKEFS Number Sequencing Test*	210	-115, 536	0.20
WAIS-IV Coding	-208	-317, -97.9	**<0.001**
Executive Composite	-14.5	-22.9, -6.10	**<0.001**
Hooper Visual Organization Test	-19.8	-59.1, 19.4	0.32
Episodic Memory Composite	-11.5	-20.3, -2.83	**0.01**
***APOE*-ε4 Non-carriers ePVS Count**			
Boston Naming Test (30 Item)	-0.002	-0.004, -0.0003	**0.02**
Animal Naming	-0.002	-0.004, -0.0003	0.09
DKEFS Number Sequencing Test*	0.007	-0.01, 0.02	0.42
WAIS-IV Coding	-0.007	-0.01, -0.002	**0.009**
Executive Composite	-0.0008	-0.001, -0.0004	**<0.001**
Hooper Visual Organization Test	-0.0007	-0.003, 0.001	0.47
Episodic Memory Composite	-0.0003	-0.0008, 0.0001	0.13

Note. ePVS volume represents a standardized measure of ePVS volume (values were divided by total basal ganglia tissue volume). Neuropsychological performance values represent the difference between last follow-up visit and baseline visit performances. The interaction term was ePVS burden x time x *APOE*-ε4 status. Analyses performed on n=326 participants (113 *APOE*-ε4 carriers and 213 *APOE*-ε4 non-carriers). Models were adjusted for age, sex, race/ethnicity, education, *APOE*-ε4 status, cognitive diagnosis, and Framingham Stroke Risk Profile (excluding points assigned for age). CI, confidence interval. ePVS, enlarged perivascular space. The parameter estimates (β) for the interaction models are for the *ePVS volume x time x APOE-ε4 carrier status* interaction term and is interpreted as the difference in annual changes of outcomes between carriers and non-carriers with one unit change in ePVS burden. The parameter estimates (β) for the stratified models are *ePVS burden x time* interaction term and represent annual changes in neuropsychological outcomes associated with one unit change in ePVS burden. *Higher values reflect worse performance. Bold p-values meet the *a priori* significance threshold.

The *standardized ePVS volume x time x cognitive diagnosis* interaction term was unrelated to any longitudinal cognitive outcomes (p-values>0.65). Among cognitively unimpaired participants, standardized ePVS volume was associated with decline in Boston Naming Test (β=-54.4, p=0.003) and WAIS-IV Coding (β=-165, p=0.04) performances while ePVS count was associated with decline in Boston Naming Test (β=-0.002, p=0.05), WAIS-IV Coding (β=-0.009, p=0.008), and Executive Function Composite ($\beta=-5.0\times10^{-4}$, p=0.02) performance. Associations persisted when excluding outliers (p-values<0.04) for all models except ePVS count and Executive Function

Composite (p=0.09), as well as when excluding participants with CVD and atrial fibrillation (p-values<0.02) for all models except ePVS count and Boston Naming Test (p=0.10). Among participants with MCI, all models were null (p-values>0.07). See **Table 4.6**.

Table 4.6. ePVS Burden x Cognitive Diagnosis Interaction Models and Stratified by Cognitive Diagnosis Associations with Longitudinal Cognition

	β	95% CI	*p-value*
Normal Cognition versus MCI ePVS Volume			
Boston Naming Test (30 Item)	25.6	-86.0, 137	0.65
Animal Naming	-1.60	-139, 135	0.98
DKEFS Number Sequencing Test*	127	-537, 790	0.71
WAIS-IV Coding	62.1	-203, 327	0.65
Executive Composite	-1.27	-20.8, 18.2	0.90
Hooper Visual Organization Test	-12.7	-113, 87.8	0.80
Episodic Memory Composite	-0.81	-19.2, 17.6	0.93
Normal Cognition versus MCI ePVS Count			
Boston Naming Test (30 Item)	0.003	-0.003, 0.008	0.35
Animal Naming	0.0008	-0.006, 0.008	0.81
DKEFS Number Sequencing Test*	0.01	-0.02, 0.04	0.51
WAIS-IV Coding	0.007	-0.006, 0.02	0.30
Executive Composite	-0.0006	-0.002, 0.0004	0.26
Hooper Visual Organization Test	0.002	-0.003, 0.007	0.43
Episodic Memory Composite	-0.0001	-0.001, 0.0008	0.78
MCI ePVS Volume			
Boston Naming Test (30 Item)	-27.1	-143, 88.4	0.64
Animal Naming	-0.29	-106, 106	>0.99
DKEFS Number Sequencing Test*	-140	-895, 614	0.71
WAIS-IV Coding	-107	-351, 137	0.39
Executive Composite	-8.08	-27.1, 11.0	0.40
Hooper Visual Organization Test	-18.2	-123, 86.9	0.73
Episodic Memory Composite	-10.6	-22.3, 1.11	0.08
MCI ePVS Count			
Boston Naming Test (30 Item)	0.001	-0.005, 0.008	0.67
Animal Naming	-0.0002	-0.006, 0.006	0.94
DKEFS Number Sequencing Test*	-0.002	-0.05, 0.04	0.92
WAIS-IV Coding	-0.0006	-0.02, 0.01	0.93
Executive Composite	-0.0009	-0.002, 0.0002	0.10
Hooper Visual Organization Test	0.002	-0.004, 0.008	0.57
Episodic Memory Composite	-0.0005	-0.001, 0.0002	0.16
Normal Cognition ePVS Volume			
Boston Naming Test (30 Item)	-54.4	-90.4, -18.3	**0.003**
Animal Naming	-31.5	-129, 65.5	0.52
DKEFS Number Sequencing Test*	165	-112, 443	0.24
WAIS-IV Coding	-165	-320, -10.1	**0.04**

Executive Composite	-9.42	-18.9, 0.09	0.05
Hooper Visual Organization Test	0.46	-36.8, 37.7	0.98
Episodic Memory Composite	-9.12	-23.2, 4.91	0.20
Normal Cognition ePVS Count			
Boston Naming Test (30 Item)	-0.002	-0.003, -0.00001	**0.05**
Animal Naming	-0.002	-0.007, 0.002	0.26
DKEFS Number Sequencing Test*	0.007	-0.005, 0.02	0.23
WAIS-IV Coding	-0.009	-0.02, -0.002	**0.008**
Executive Composite	-0.0005	-0.0009, -0.00009	**0.02**
Hooper Visual Organization Test	-0.0005	-0.002, 0.001	0.55
Episodic Memory Composite	-0.0003	-0.0009, 0.0003	0.28

Note. ePVS volume represents a standardized measure of ePVS volume (values were divided by total basal ganglia tissue volume). Neuropsychological performance values represent the difference between last follow-up visit and baseline visit performances. The interaction term was ePVS burden x time x cognitive diagnosis. Analyses performed on n=299 participants (169 normal cognition and 130 MCI). Models were adjusted for age, sex, race/ethnicity, education, *APOE*-ε4 status, cognitive diagnosis, and Framingham Stroke Risk Profile (excluding points assigned for age). CI, confidence interval. ePVS, enlarged perivascular space. The parameter estimates (β) for the interaction models are for the *ePVS volume x time x cognitive diagnosis* interaction term and is interpreted as the difference in annual changes of outcomes between normal cognition and MCI with one unit change in ePVS burden. The parameter estimates (β) for the stratified models are *ePVS burden x time* interaction term and represent annual changes in neuropsychological outcomes associated with one unit change in ePVS burden. *Higher values reflect worse performance. Bold p-values meet the *a priori* significance threshold.

Discussion

ePVS have not been widely studied,[97,150,152] especially regarding their associations with longitudinal cognition. We again applied a novel ePVS quantification method to assess cross-sectional and longitudinal clinical consequences of ePVS. Both markers of basal ganglia ePVS burden were associated with worse information processing, executive function, and visuospatial skills cross-sectionally. Additionally, basal ganglia ePVS burden was associated with longitudinal decline in language, information processing, executive function, and episodic memory. To our knowledge, the present study is among the first to apply a deep learning algorithm for ePVS quantification to assess clinical consequences of ePVS. This work is also among the first to analyze associations between ePVS and longitudinal cognition across multiple cognitive domains.

We found higher basal ganglia ePVS burden is cross-sectionally associated with worse cognition in domains of information processing, executive function, and visuospatial abilities at study entry. This observation is in agreement with prior studies including our own work,[97] using ordinal ePVS scores[135] and with other work reporting associations between ePVS ordinal scores and worse cross-sectional reasoning[135] and visuospatial ability.[135] The basal ganglia is an important part of the frontal-subcortical circuitry.[240] For example, the dorsolateral prefrontal circuit mediates executive functions and loops through the caudate nucleus and globus pallidus.[48] Therefore, damage to basal ganglia nuclei in the form of ePVS pathology, would presumably result in worse executive function. Multiple parallel circuits project from the cortex down to the basal ganglia and are integrated in the striatum,[241] contributing to information processing tasks.[242–244] So, when the caudate and putamen are damaged, worse performance on information processing tasks would be expected. Visuoperceptual functions are mediated in part by connections between the striatum and visual system,[241,245] which may account for associations between basal ganglia ePVS and visuospatial abilities.

When looking longitudinally, higher basal ganglia ePVS burden was associated with cognitive decline over the mean 4.7-year follow-up in nearly every domain assessed, including language, information processing, executive function, and episodic memory. With so many diverse domains implicated, basal ganglia ePVS may have a more global adverse effect on cognitive trajectory over time. Associations between ePVS burden and decline in executive function and information processing can likely be attributed to damage to the frontal-subcortical circuits traveling through the basal ganglia. In one of the very few studies relating ePVS to longitudinal cognition, large

ePVS assessed dichotomously as present or absent in the basal ganglia and white matter were similarly associated with decline in information processing speed only.[134] By contrast, we utilized a fully continuous ePVS measure, including all visible ePVS within the basal ganglia rather than just large ePVS, which might account for the more robust associations seen here. While we focused on basal ganglia ePVS in the present study, worse basal ganglia ePVS often correlate with worse SVD pathology in general[97] and may be a proxy for worse ePVS burden in other brain regions, such as the hippocampus.[246] The global longitudinal cognitive associations in the present study therefore may be the result of worse concomitant SVD pathology in regions outside the basal ganglia. Alternatively, executive function and information processing speed impairments could have downstream effects on the performance of other cognitive functions over time.

While measures of ePVS count and volume are highly correlated and yield comparable results, nuanced differences exist between the measures that may cause findings to vary slightly. A single ePVS can range in size from a few millimeters cubed to tens of millimeters cubed, so it is plausible that an individual may have a few extremely large basal ganglia ePVS, resulting in low count but large volumes. Alternatively, an individual may have hundreds of small basal ganglia ePVS, resulting in high count but smaller volumes. The first scenario may indicate severe damage to a few vessels in a specific region while the second scenario may reflect less severe but more widespread damage. Differences in these scenarios could account for the slightly varied results observed with longitudinal cognition. A larger cohort study may be needed to delineate the unique ways in which different ePVS patterns affect brain health. We primarily

focused on ePVS volume in this chapter because ePVS volume reflects total tissue affected, and prior SVD studies focused on WMHs have shown that volumetric assessments are more sensitive to detecting clinical symptoms when compared to count or even visual scores.[247,248]

APOE-ε4 carrier status modified the association between ePVS burden and cross-sectional cognition such that associations were driven by *APOE*-ε4 carriers, especially in domains of language and visuospatial skills. *APOE*-ε4 is a vascular risk modifier that drives increased blood-brain barrier breakdown[26] and is also associated with increased risk of poor cognitive outcomes.[249] These unfavorable characteristics of *APOE*-ε4 may be the main reason we see stronger associations between ePVS burden and cognition in ε4 carriers. When looking longitudinally, *APOE*-ε4 status did not modify any associations between ePVS burden and longitudinal cognition. When analyzing stratified models though, associations between ePVS burden and longitudinal cognition appear to be driven by *APOE*-ε4 non-carriers. Associations between ePVS burden and cognition appear to be driven by *APOE*-ε4 carriers for cross-sectional cognition and *APOE*-ε4 non-carriers when assessed longitudinally. Cross-sectional models may account for the detrimental effects of *APOE*-ε4 throughout an individual's entire life up until enrollment in the study (60+ years) whereas longitudinal models only account for late-life effects over a small sample of a person's life. Some research even suggests that risk for cognitive decline due to *APOE*-ε4 decreases after the age of 80.[25] So, it is possible that longitudinal associations between ePVS burden and cognition among *APOE*-ε4 carriers are being masked by decades of detrimental effects that have occurred leading up to the study.

Another key observation is that cognitive status modified the association between ePVS volume and cross-sectional cognition whereby associations with language, information processing, executive function, and visuospatial abilities were driven by participants with MCI. These participants likely already have extensive neurodegeneration. When additional pathological burden emerges in the form of SVD, participants may be more susceptible to worse cognitive outcomes. Longitudinally, however, cognitive diagnosis does not appear to modify associations between basal ganglia ePVS burden and cognitive trajectory. When looking at stratified results, associations exist between basal ganglia ePVS volume and longitudinal cognition for cognitively unimpaired participants but not for participants with MCI. The lack of an association among participants with MCI could be because by the time participants manifest clinical symptoms, they have extensive neurodegeneration. Any contributions of ePVS to longitudinal cognition may have already occurred earlier in the disease process, which would further demonstrate the utility of ePVS quantification in predicting adverse cognitive trajectory.

The current study has many strengths, the most notable of which is the utilization of a deep learning model to create a fully continuous, robust measure of ePVS burden for hundreds of brain MRI scans. Studies utilizing continuous measures of ePVS are minimal and even fewer have used advanced computational techniques like deep learning. To our knowledge, the present study is among the first to apply a deep learning ePVS quantification technique to assess cross-sectional and longitudinal cognitive associations with ePVS. An additional strength includes using an extensive neuropsychology protocol with up to seven years of follow-up data. Some limitations of

the present study are worth mentioning though. The participants studied are on average college-educated, predominantly White/non-Hispanic, and older, which could limit the generalizability of the present findings. Also, manual edits were performed on all machine learning model outputs of ePVS maps, which increases the likelihood of introducing human error into the measure. Additionally, sample attrition during follow-up biased our results toward the null hypothesis given participants who dropped out were more likely to have worse health than participants who were retained in the cohort.

We utilized deep learning to robustly quantify ePVS, an understudied SVD pathology. Additionally, basal ganglia ePVS are related to worse executive function, information processing, and visuospatial performances cross-sectionally as well as decline in language, information processing, executive function, and episodic memory performances longitudinally. ePVS appear to have the greatest impact on executive function and information processing, but when we follow older adults longitudinally, ePVS seem to also affect cognitive functions that localize to the temporal lobes. The present study highlights a pathway by which worse vascular health can contribute to cognitive decline.

CHAPTER 5

SUMMARY AND FUTURE DIRECTIONS

Vascular damage exists in upwards of 87% of AD cases[96] and can drive its own form of dementia,[250] which highlights how crucial healthy blood flow delivery is to maintaining a healthy brain. Proper blood flow delivery depends on the volume of blood, the speed of the blood, the pulsatility of the blood, and the ability of the blood-brain barrier (BBB) to efficiently transport nutrients from the blood to the parenchyma. Abnormalities in any of these functions can have a negative effect on brain health and that is what we have shown with this work.[6,31,74] Enlarged perivascular spaces (ePVS) have not been well studied but when visible on brain MRI they are thought to represent some form of damage to a component of the BBB.[251] When healthy, perivascular spaces (PVS) play a role in clearing metabolic waste from the brain,[104,106] so damage to the perivascular system could have a detrimental effect on brain health. Additionally, ePVS may disrupt proper nutrient delivery to the brain.

The overall aim of this project was to determine what factors may be driving ePVS development and the clinical impact that ePVS may have. We quickly decided that current methods for quantifying ePVS were insufficient. Prior methods rely on an ordinal rating of a single brain magnetic resonance imaging (MRI) slice[142,143] which can introduce ceiling effects, minimize variability, and eliminate the option of longitudinal assessment. Here we detailed an automated method for quantifying ePVS volumes and counts throughout entire brain regions using a deep learning U-net.[147,148] Using our new

measures of ePVS volume and count we tested what factors may play a role in the development of ePVS and whether or not *APOE*-ε4 was a contributor. We additionally set out to characterize the downstream clinical consequences of ePVS, focusing on a wide range of cognitive measures. Again, we tested whether *APOE*-ε4 moderated associations. Data for this project came from the Vanderbilt Memory and Aging Project, which is a longitudinal study of 335 older adults who were free of dementia and stroke at study entry.[252] T_1-weighted images were used for quantifying ePVS, cardiac MRI was used to quantify aortic stiffness, blood and cerebrospinal fluid samples were used to quantify inflammatory and AD biomarkers, a questionnaire was used to quantify sleep quality, and a comprehensive neuropsychological assessment was used to quantify cognition. We hypothesized that greater aortic stiffness at baseline would be associated with greater ePVS burden at baseline as well as longitudinal increase in ePVS burden over time and that such associations would be driven by *APOE*-ε4 carriers. We also hypothesized that greater ePVS burden at baseline would be associated with worse executive function and information processing, both cross-sectionally and longitudinally, and that associations would again be driven by *APOE*-ε4 carriers.

Deep learning U-nets have been used for brain MRI segmentation for at least 5 years, but our problem was unique because the pathology of interest is typically just a few voxels in size but occurs frequently throughout large portions of the brain. We found that a U-net worked remarkably well at segmenting ePVS when trained on 40 ground-truth images. Deep learning continues to prove to be a valuable tool in medical image segmentation. Future ePVS studies should utilize a deep learning model for ePVS segmentation to generate a robust and continuous measure of ePVS burden. The

automated method presented here is fast and often requires minimal edits. The method ensures consistent segmentation from image to image since model weights are unchanging compared to the human eye and human judgement, which are susceptible to inconsistencies. Finally, the ability to assess longitudinal change in a measure is extremely limited when using an ordinal measure; this method produces a continuous measure which is well-suited for longitudinal interpretation. The automated ePVS segmentation method presented with this work has already been used to segment ePVS in a subset of images from the Alzheimer's Disease Neuroimaging Initiative and was found to work well. The ePVS segmentation algorithm will be made available to other groups looking to capture a continuous volumetric measure of ePVS within their cohort.

Hypertension[136] and hypertensive arteriopathy[150] are associated with worse ePVS score in the basal ganglia. We found that pulse wave velocity (PWV), a measure of aortic stiffness, was associated with worse ePVS burden at baseline and that associations were driven by *APOE*-ε4 carriers. Aortic stiffness is closely related to hypertension but may be a more subtle marker that actually predicted future hypertension onset.[57,58] With greater aortic stiffness, damaging pressure waves enter the brain,[119] damage the vessel wall, lead to blood-brain barrier breakdown,[205] and drive PVS enlargement through inflammation.[183] *APOE*-ε4 acts as a vascular risk modifier and may be interacting with aortic stiffening to lead to greater ePVS burden.[253]

We also investigated other factors that may be associated with PVS enlargement, such as inflammation and poor sleep quality. We found that higher levels of CSF sTREM2, MMP2, and MMP3 were all associated with longitudinal increase in

ePVS burden, and many models remained significant even after applying a stringent false discovery rate correction. Associations were particularly strong among *APOE*-ε4 non-carriers and male participants, however, it should be noted that the study sample was 60% male. sTREM2 levels are indicative of microglial activation which can result in excess cytokines and chemokines that act to break down the BBB. MMP2 and MMP3 may both act to directly break down the BBB. With BBB break down comes fluid and protein infiltration into the PVS which is toxic and could drive enlargement.

To our knowledge, we are the first group to assess the longitudinal change of a continuous ePVS measure. The scanner, software, and head coil type can all influence the amount of ePVS we are able to detect on a given MR image. Strong harmonization techniques are crucial for generating reliable longitudinal data[195] and even then, technical variability still likely exists in the data.

Prior work from our group found that a higher ePVS score was associated with worse executive function and information processing at baseline.[97] Our findings using the automated volumetric and count measures of ePVS were in agreement with our prior work and found an additional association between ePVS and visuospatial performance. We also found that associations between ePVS and cross-sectional cognition were driven by *APOE*-ε4 carriers. One of the major novel aspects of our work was using a continuous ePVS measure to assess associations with longitudinal neuropsychological performance across multiple cognitive domains. We found that worse ePVS burden at baseline was associated with decline in executive function, information processing, language, and episodic memory. We were surprised to find temporal lobe functions of language and episodic memory implicated with basal ganglia

ePVS burden, but such associations may highlight the concomitant presence of pathology in the medial temporal lobe[254] (which we did not look for). Associations may also be due to downstream effects from damage to executive functions, or damage to basal ganglia circuits that play a role in working memory,[255] which is closely related to episodic memory.[256] Interestingly, associations between ePVS burden and cognitive decline appeared to be driven by *APOE*-ε4 non-carriers. Lack of an association among *APOE*-ε4 carriers could be because the detrimental effects of *APOE*-ε4 have accumulated over the 60 years leading up to study enrollment and masked any late-life longitudinal associations. A summary of our findings is shown in **Figure 5.1**.

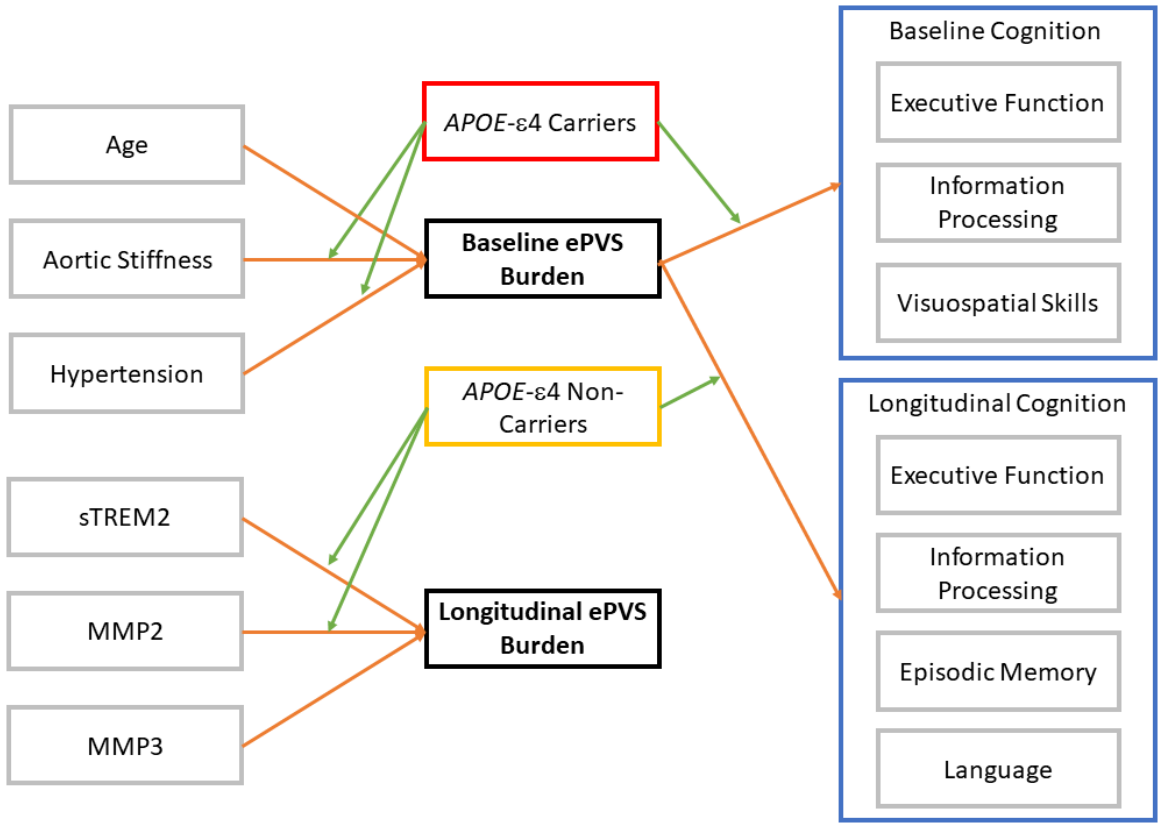

Figure 5.1. Summary of etiologies and cognitive consequences of ePVS burden. Pictured here is a summary of findings from this project. Orange arrows indicate associations that were found to be significant in participants of the Vanderbilt Memory and Aging Project. Green arrows represent interactions and the box from which the green arrows originate represent the participant population that is driving those associations. ePVS, enlarged perivascular space.

When interpreting the results of this project, there are some methodological factors to consider. First, the algorithm used to segment ePVS is not perfect which is highlighted by the statistics presented in Chapter 2 regarding the performance of the algorithm on the ground-truth test set. While the metrics do point towards the model working well, improvements are still possible. Extensive effort was put into generating ground-truth data that is as accurate as possible but human error will always occur, especially with a tedious problem in which many voxels are near the threshold intensity for what is and is not considered an ePVS. In future use cases, review of output images is recommended and in some cases edits may be necessary, because the model is not perfect. Additionally, differentiation between white matter damage, lacunes, and ePVS can be challenging on T_1-weighted imaging due to the similar intensity and morphology with which all three pathologies can occasionally appear. While errors still likely took place due to this issue, fluid attenuated inversion recovery images and white matter hyperintensity masks were consulted to maximize the accuracy of ground-truth segmentations.[98]

Another important consideration is that different scanner, software, and head coil types can affect the appearance of ePVS on brain MRI. While all baseline imaging data was captured with a uniform software and hardware configuration, follow-up data was not. These updates in software and hardware introduce methodological challenges that must be carefully considered. We utilized a harmonization technique that batches data based off the software and hardware configuration, and then uses Bayesian inference to bring the batches into better alignment with one another.[195] While we were pleased with our harmonized longitudinal data, technical variability likely still exists and biological

variability may have been slightly reduced. For these reasons, we are cautious when interpreting our analyses that utilize longitudinal ePVS data.

Future work should improve analyses of longitudinal ePVS change. Training data for deep learning model generation could be improved through incorporation of a T_2-weighted imaging sequence. T_2-weighted images offer better ePVS contrast than T_1-weighted images because ePVS appear bright and are surrounded by dark tissue on T_2. Still, the best technique for ePVS segmentation might include both T_1 and T_2-weighted images as a way to enhance the appearance of ePVS. Additionally, training data should include images from multiple scanner software and hardware configurations to improve the generalizability of the deep learning model and increase our ability to analyze ePVS longitudinal change. Future studies should also work to further evaluate drivers of longitudinal change in ePVS. Hypotheses and findings generated with this work must be repeated in other cohorts and tested with different biomarkers. Better understanding of the etiologies of ePVS will allow us to develop prevention and treatment strategies which will enable improved waste clearance from the parenchyma, resulting in a healthier and more resilient brain.

Taken together, we have shown what some potential etiologies of ePVS are and that ePVS do indeed have clinical consequences. The findings presented here show that ePVS warrant more study and that deep learning for ePVS quantification should be considered for future studies of brain MRI pathology. This body of research highlights another important avenue by which poor vascular health can affect brain health and result in cognitive decline. Future work should interrogate the mechanisms by which

ePVS disrupt healthy cognition by first creating a rodent model of ePVS and then sampling tissue surrounding the ePVS to assess molecular signals of damage.

REFERENCES

1. Williams LR, Leggett RW. Reference values for resting blood flow to organs of man. *Clin Phys Physiol Meas Off J Hosp Phys Assoc Dtsch Ges Med Phys Eur Fed Organ Med Phys*. 1989;10(3):187-217. doi:10.1088/0143-0815/10/3/001
2. Jefferson AL, Beiser AS, Himali JJ, et al. Low cardiac index is associated with incident dementia and Alzheimer disease: the Framingham Heart Study. *Circulation*. 2015;131(15):1333-1339. doi:10.1161/CIRCULATIONAHA.114.012438
3. Jefferson AL, Liu D, Gupta DK, et al. Lower cardiac index levels relate to lower cerebral blood flow in older adults. *Neurology*. 2017;89(23):2327-2334. doi:10.1212/WNL.0000000000004707
4. Sabayan B, van Buchem MA, Sigurdsson S, et al. Cardiac hemodynamics are linked with structural and functional features of brain aging: the age, gene/environment susceptibility (AGES)-Reykjavik Study. *J Am Heart Assoc*. 2015;4(1):e001294. doi:10.1161/JAHA.114.001294
5. Kresge HA, Khan OA, Wagener MA, et al. Subclinical Compromise in Cardiac Strain Relates to Lower Cognitive Performances in Older Adults. *J Am Heart Assoc*. 2018;7(4):e007562. doi:10.1161/JAHA.117.007562
6. Bown CW, Do R, Khan OA, et al. Lower Cardiac Output Relates to Longitudinal Cognitive Decline in Aging Adults. *Front Psychol*. 2020;11:569355. doi:10.3389/fpsyg.2020.569355
7. Shuang Wan EY, Shaik MA, Adhha A, et al. Pilot Evaluation of the Informant AD8 as a Case-Finding Instrument for Cognitive Impairment in General Practitioner Clinics of Singapore: A Brief Report. *J Am Med Dir Assoc*. 2016;17(12):1147-1150. doi:10.1016/j.jamda.2016.07.031
8. Cacciamani F, Tandetnik C, Gagliardi G, et al. Low Cognitive Awareness, but Not Complaint, is a Good Marker of Preclinical Alzheimer's Disease. *J Alzheimers Dis JAD*. 2017;59(2):753-762. doi:10.3233/JAD-170399
9. Melov S, Adlard PA, Morten K, et al. Mitochondrial oxidative stress causes hyperphosphorylation of tau. *PloS One*. 2007;2(6):e536. doi:10.1371/journal.pone.0000536
10. Lu T, Pan Y, Kao SY, et al. Gene regulation and DNA damage in the ageing human brain. *Nature*. 2004;429(6994):883-891. doi:10.1038/nature02661
11. Furuta T, Mukai A, Ohishi A, Nishida K, Nagasawa K. Oxidative stress-induced increase of intracellular zinc in astrocytes decreases their functional expression of P2X7 receptors and engulfing activity. *Met Integr Biometal Sci*. 2017;9(12):1839-1851. doi:10.1039/c7mt00257b
12. Krueger M, Härtig W, Frydrychowicz C, et al. Stroke-induced blood-brain barrier breakdown along the vascular tree - No preferential affection of arteries in different animal models and in humans. *J Cereb Blood Flow Metab Off J Int Soc Cereb Blood Flow Metab*. 2017;37(7):2539-2554. doi:10.1177/0271678X16670922
13. Miyanohara J, Kakae M, Nagayasu K, et al. TRPM2 Channel Aggravates CNS Inflammation and Cognitive Impairment via Activation of Microglia in Chronic Cerebral Hypoperfusion. *J Neurosci Off J Soc Neurosci*. 2018;38(14):3520-3533. doi:10.1523/JNEUROSCI.2451-17.2018
14. Spitsyna G, Warren JE, Scott SK, Turkheimer FE, Wise RJS. Converging language streams in the human temporal lobe. *J Neurosci Off J Soc Neurosci*. 2006;26(28):7328-7336. doi:10.1523/JNEUROSCI.0559-06.2006
15. Schwartz MF. Theoretical analysis of word production deficits in adult aphasia. *Philos Trans R Soc Lond B Biol Sci*. 2014;369(1634):20120390. doi:10.1098/rstb.2012.0390
16. Soble JR, Marceaux JC, Galindo J, et al. The effect of perceptual reasoning abilities on confrontation naming performance: An examination of three naming tests. *J Clin Exp Neuropsychol*. 2016;38(3):284-292. doi:10.1080/13803395.2015.1107030
17. Hawkins R, Hass WK, Ransohoff J. Measurement of regional brain glucose utilization in vivo using [2(-14)C] glucose. *Stroke*. 1979;10(6):690-703. doi:10.1161/01.str.10.6.690

18. Payabvash S, Souza LCS, Wang Y, et al. Regional ischemic vulnerability of the brain to hypoperfusion: the need for location specific computed tomography perfusion thresholds in acute stroke patients. *Stroke*. 2011;42(5):1255-1260. doi:10.1161/STROKEAHA.110.600940
19. Howard R, Trend P, Russell RW. Clinical features of ischemia in cerebral arterial border zones after periods of reduced cerebral blood flow. *Arch Neurol*. 1987;44(9):934-940. doi:10.1001/archneur.1987.00520210036016
20. Attwell D, Laughlin SB. An energy budget for signaling in the grey matter of the brain. *J Cereb Blood Flow Metab Off J Int Soc Cereb Blood Flow Metab*. 2001;21(10):1133-1145. doi:10.1097/00004647-200110000-00001
21. Brown DF, Risser RC, Bigio EH, et al. Neocortical synapse density and Braak stage in the Lewy body variant of Alzheimer disease: a comparison with classic Alzheimer disease and normal aging. *J Neuropathol Exp Neurol*. 1998;57(10):955-960. doi:10.1097/00005072-199810000-00007
22. Liebeskind DS. Collateral circulation. *Stroke*. 2003;34(9):2279-2284. doi:10.1161/01.STR.0000086465.41263.06
23. Cummings JL. Frontal-subcortical circuits and human behavior. *J Psychosom Res*. 1998;44(6):627-628. doi:10.1016/s0022-3999(98)00034-8
24. Pugh KG, Lipsitz LA. The microvascular frontal-subcortical syndrome of aging. *Neurobiol Aging*. 2002;23(3):421-431. doi:10.1016/s0197-4580(01)00319-0
25. Raber J, Huang Y, Ashford JW. ApoE genotype accounts for the vast majority of AD risk and AD pathology. *Neurobiol Aging*. 2004;25(5):641-650. doi:10.1016/j.neurobiolaging.2003.12.023
26. Bell RD, Winkler EA, Singh I, et al. Apolipoprotein E controls cerebrovascular integrity via cyclophilin A. *Nature*. 2012;485(7399):512-516. doi:10.1038/nature11087
27. Suri S, Mackay CE, Kelly ME, et al. Reduced cerebrovascular reactivity in young adults carrying the APOE ε4 allele. *Alzheimers Dement J Alzheimers Assoc*. 2015;11(6):648-657.e1. doi:10.1016/j.jalz.2014.05.1755
28. Alata W, Ye Y, St-Amour I, Vandal M, Calon F. Human apolipoprotein E ε4 expression impairs cerebral vascularization and blood-brain barrier function in mice. *J Cereb Blood Flow Metab Off J Int Soc Cereb Blood Flow Metab*. 2015;35(1):86-94. doi:10.1038/jcbfm.2014.172
29. Wierenga CE, Clark LR, Dev SI, et al. Interaction of age and APOE genotype on cerebral blood flow at rest. *J Alzheimers Dis JAD*. 2013;34(4):921-935. doi:10.3233/JAD-121897
30. Thambisetty M, Beason-Held L, An Y, Kraut MA, Resnick SM. APOE epsilon4 genotype and longitudinal changes in cerebral blood flow in normal aging. *Arch Neurol*. 2010;67(1):93-98. doi:10.1001/archneurol.2009.913
31. Bown CW, Liu D, Osborn KE, et al. Apolipoprotein E Genotype Modifies the Association Between Cardiac Output and Cognition in Older Adults. *J Am Heart Assoc*. 2019;8(15):e011146. doi:10.1161/JAHA.118.011146
32. Yip AG, McKee AC, Green RC, et al. APOE, vascular pathology, and the AD brain. *Neurology*. 2005;65(2):259-265. doi:10.1212/01.wnl.0000168863.49053.4d
33. Tiraboschi P, Hansen LA, Masliah E, Alford M, Thal LJ, Corey-Bloom J. Impact of APOE genotype on neuropathologic and neurochemical markers of Alzheimer disease. *Neurology*. 2004;62(11):1977-1983. doi:10.1212/01.wnl.0000128091.92139.0f
34. Faraci FM, Sobey CG. Role of potassium channels in regulation of cerebral vascular tone. *J Cereb Blood Flow Metab Off J Int Soc Cereb Blood Flow Metab*. 1998;18(10):1047-1063. doi:10.1097/00004647-199810000-00001
35. Kuschinsky W, Wahl M, Bosse O, Thurau K. Perivascular potassium and pH as determinants of local pial arterial diameter in cats. A microapplication study. *Circ Res*. 1972;31(2):240-247. doi:10.1161/01.res.31.2.240

36. Lynch JR, Tang W, Wang H, et al. APOE genotype and an ApoE-mimetic peptide modify the systemic and central nervous system inflammatory response. *J Biol Chem*. 2003;278(49):48529-48533. doi:10.1074/jbc.M306923200
37. Torre-Amione G, Kapadia S, Benedict C, Oral H, Young JB, Mann DL. Proinflammatory cytokine levels in patients with depressed left ventricular ejection fraction: a report from the Studies of Left Ventricular Dysfunction (SOLVD). *J Am Coll Cardiol*. 1996;27(5):1201-1206. doi:10.1016/0735-1097(95)00589-7
38. Azmi NH, Ismail M, Ismail N, Imam MU, Alitheen NBM, Abdullah MA. Germinated Brown Rice Alters Aβ(1-42) Aggregation and Modulates Alzheimer's Disease-Related Genes in Differentiated Human SH-SY5Y Cells. *Evid-Based Complement Altern Med ECAM*. 2015;2015:153684. doi:10.1155/2015/153684
39. Fleury C, Mignotte B, Vayssière JL. Mitochondrial reactive oxygen species in cell death signaling. *Biochimie*. 2002;84(2-3):131-141. doi:10.1016/s0300-9084(02)01369-x
40. Miyata M, Smith JD. Apolipoprotein E allele-specific antioxidant activity and effects on cytotoxicity by oxidative insults and beta-amyloid peptides. *Nat Genet*. 1996;14(1):55-61. doi:10.1038/ng0996-55
41. Jofre-Monseny L, Minihane AM, Rimbach G. Impact of apoE genotype on oxidative stress, inflammation and disease risk. *Mol Nutr Food Res*. 2008;52(1):131-145. doi:10.1002/mnfr.200700322
42. Girouard H, Iadecola C. Neurovascular coupling in the normal brain and in hypertension, stroke, and Alzheimer disease. *J Appl Physiol Bethesda Md 1985*. 2006;100(1):328-335. doi:10.1152/japplphysiol.00966.2005
43. Vaz Pérez A, Doehner W, von Haehling S, et al. The relationship between tumor necrosis factor-α, brain natriuretic peptide and atrial natriuretic peptide in patients with chronic heart failure. *Int J Cardiol*. 2010;141(1):39-43. doi:10.1016/j.ijcard.2008.11.146
44. Cushman M, Callas PW, McClure LA, et al. N-Terminal Pro-B-Type Natriuretic Peptide and Risk of Future Cognitive Impairment in the REGARDS Cohort. *J Alzheimers Dis JAD*. 2016;54(2):497-503. doi:10.3233/JAD-160328
45. Zlokovic BV. Neurovascular pathways to neurodegeneration in Alzheimer's disease and other disorders. *Nat Rev Neurosci*. 2011;12(12):723-738. doi:10.1038/nrn3114
46. Candelario-Jalil E, Thompson J, Taheri S, et al. Matrix metalloproteinases are associated with increased blood-brain barrier opening in vascular cognitive impairment. *Stroke*. 2011;42(5):1345-1350. doi:10.1161/STROKEAHA.110.600825
47. Metin Ö, Tufan AE, Cevher Binici N, Saraçlı Ö, Atalay A, Yolga Tahiroğlu A. [Executive Functions in Frontal Lob Syndrome: A Case Report]. *Turk Psikiyatri Derg Turk J Psychiatry*. 2017;28(2):135-138.
48. Bonelli RM, Cummings JL. Frontal-subcortical circuitry and behavior. *Dialogues Clin Neurosci*. 2007;9(2):141-151.
49. Alexander GE, DeLong MR, Strick PL. Parallel organization of functionally segregated circuits linking basal ganglia and cortex. *Annu Rev Neurosci*. 1986;9:357-381. doi:10.1146/annurev.ne.09.030186.002041
50. Aitken HP. Diagram of the Arterial Circulation of the Basal Ganglia. *N Engl J Med*. 1928;199(22):1084-1084. doi:10.1056/NEJM192811291992204
51. Desmond DW. The neuropsychology of vascular cognitive impairment: is there a specific cognitive deficit? *J Neurol Sci*. 2004;226(1-2):3-7. doi:10.1016/j.jns.2004.09.002
52. Prins ND, van Dijk EJ, den Heijer T, et al. Cerebral small-vessel disease and decline in information processing speed, executive function and memory. *Brain J Neurol*. 2005;128(Pt 9):2034-2041. doi:10.1093/brain/awh553

53. Gunning-Dixon FM, Raz N. Neuroanatomical correlates of selected executive functions in middle-aged and older adults: a prospective MRI study. *Neuropsychologia*. 2003;41(14):1929-1941. doi:10.1016/s0028-3932(03)00129-5
54. Montagne A, Barnes SR, Sweeney MD, et al. Blood-brain barrier breakdown in the aging human hippocampus. *Neuron*. 2015;85(2):296-302. doi:10.1016/j.neuron.2014.12.032
55. Schneider JA, Arvanitakis Z, Bang W, Bennett DA. Mixed brain pathologies account for most dementia cases in community-dwelling older persons. *Neurology*. 2007;69(24):2197-2204. doi:10.1212/01.wnl.0000271090.28148.24
56. Diaz-Otero JM, Garver H, Fink GD, Jackson WF, Dorrance AM. Aging is associated with changes to the biomechanical properties of the posterior cerebral artery and parenchymal arterioles. *Am J Physiol Heart Circ Physiol*. 2016;310(3):H365-375. doi:10.1152/ajpheart.00562.2015
57. Mitchell GF. Arterial stiffness and hypertension: chicken or egg? *Hypertens Dallas Tex 1979*. 2014;64(2):210-214. doi:10.1161/HYPERTENSIONAHA.114.03449
58. Kaess BM, Rong J, Larson MG, et al. Aortic stiffness, blood pressure progression, and incident hypertension. *JAMA*. 2012;308(9):875-881. doi:10.1001/2012.jama.10503
59. Murgo JP, Westerhof N, Giolma JP, Altobelli SA. Manipulation of ascending aortic pressure and flow wave reflections with the Valsalva maneuver: relationship to input impedance. *Circulation*. 1981;63(1):122-132. doi:10.1161/01.cir.63.1.122
60. Waldstein SR, Rice SC, Thayer JF, Najjar SS, Scuteri A, Zonderman AB. Pulse pressure and pulse wave velocity are related to cognitive decline in the Baltimore Longitudinal Study of Aging. *Hypertens Dallas Tex 1979*. 2008;51(1):99-104. doi:10.1161/HYPERTENSIONAHA.107.093674
61. Zeki Al Hazzouri A, Newman AB, Simonsick E, et al. Pulse wave velocity and cognitive decline in elders: the Health, Aging, and Body Composition study. *Stroke*. 2013;44(2):388-393. doi:10.1161/STROKEAHA.112.673533
62. Cui C, Sekikawa A, Kuller LH, et al. Aortic Stiffness is Associated with Increased Risk of Incident Dementia in Older Adults. *J Alzheimers Dis JAD*. 2018;66(1):297-306. doi:10.3233/JAD-180449
63. de Montgolfier O, Pinçon A, Pouliot P, et al. High Systolic Blood Pressure Induces Cerebral Microvascular Endothelial Dysfunction, Neurovascular Unit Damage, and Cognitive Decline in Mice. *Hypertens Dallas Tex 1979*. 2019;73(1):217-228. doi:10.1161/HYPERTENSIONAHA.118.12048
64. Bano D, Nicotera P. Ca2+ signals and neuronal death in brain ischemia. *Stroke*. 2007;38(2 Suppl):674-676. doi:10.1161/01.STR.0000256294.46009.29
65. Berliocchi L, Bano D, Nicotera P. Ca2+ signals and death programmes in neurons. *Philos Trans R Soc Lond B Biol Sci*. 2005;360(1464):2255-2258. doi:10.1098/rstb.2005.1765
66. Orrenius S, Zhivotovsky B, Nicotera P. Regulation of cell death: the calcium-apoptosis link. *Nat Rev Mol Cell Biol*. 2003;4(7):552-565. doi:10.1038/nrm1150
67. Iadecola C. The pathobiology of vascular dementia. *Neuron*. 2013;80(4):844-866. doi:10.1016/j.neuron.2013.10.008
68. Obermeier B, Daneman R, Ransohoff RM. Development, maintenance and disruption of the blood-brain barrier. *Nat Med*. 2013;19(12):1584-1596. doi:10.1038/nm.3407
69. Yang Y, Rosenberg GA. Blood-brain barrier breakdown in acute and chronic cerebrovascular disease. *Stroke*. 2011;42(11):3323-3328. doi:10.1161/STROKEAHA.110.608257
70. Lin J, Wang D, Lan L, Fan Y. Multiple Factors Involved in the Pathogenesis of White Matter Lesions. *BioMed Res Int*. 2017;2017:9372050. doi:10.1155/2017/9372050
71. Trauninger A, Leél-Ossy E, Kamson DO, et al. Risk factors of migraine-related brain white matter hyperintensities: an investigation of 186 patients. *J Headache Pain*. 2011;12(1):97-103. doi:10.1007/s10194-011-0299-3
72. Zhai FF, Ye YC, Chen SY, et al. Arterial Stiffness and Cerebral Small Vessel Disease. *Front Neurol*. 2018;9:723. doi:10.3389/fneur.2018.00723

73. Katulska K, Wykrętowicz M, Minczykowski A, et al. Gray matter volume in relation to cardio-vascular stiffness. *J Neurol Sci*. 2014;343(1-2):100-104. doi:10.1016/j.jns.2014.05.044
74. Bown CW, Khan OA, Moore EE, et al. Elevated Aortic Pulse Wave Velocity Relates to Longitudinal Gray and White Matter Changes. *Arterioscler Thromb Vasc Biol*. 2021;41(12):3015-3024. doi:10.1161/ATVBAHA.121.316477
75. Jefferson AL, Cambronero FE, Liu D, et al. Higher Aortic Stiffness Is Related to Lower Cerebral Blood Flow and Preserved Cerebrovascular Reactivity in Older Adults. *Circulation*. 2018;138(18):1951-1962. doi:10.1161/CIRCULATIONAHA.118.032410
76. Dirnagl U, Iadecola C, Moskowitz MA. Pathobiology of ischaemic stroke: an integrated view. *Trends Neurosci*. 1999;22(9):391-397. doi:10.1016/s0166-2236(99)01401-0
77. Szydlowska K, Tymianski M. Calcium, ischemia and excitotoxicity. *Cell Calcium*. 2010;47(2):122-129. doi:10.1016/j.ceca.2010.01.003
78. Jinno S, Kosaka T. Stereological estimation of numerical densities of glutamatergic principal neurons in the mouse hippocampus. *Hippocampus*. 2010;20(7):829-840. doi:10.1002/hipo.20685
79. Keller D, Erö C, Markram H. Cell Densities in the Mouse Brain: A Systematic Review. *Front Neuroanat*. 2018;12:83. doi:10.3389/fnana.2018.00083
80. Grajski KA, Bressler SL, Alzheimer's Disease Neuroimaging Initiative. Differential medial temporal lobe and default-mode network functional connectivity and morphometric changes in Alzheimer's disease. *NeuroImage Clin*. 2019;23:101860. doi:10.1016/j.nicl.2019.101860
81. Wakita H, Tomimoto H, Akiguchi I, Kimura J. Glial activation and white matter changes in the rat brain induced by chronic cerebral hypoperfusion: an immunohistochemical study. *Acta Neuropathol (Berl)*. 1994;87(5):484-492. doi:10.1007/BF00294175
82. Yao H, Sadoshima S, Ibayashi S, Kuwabara Y, Ichiya Y, Fujishima M. Leukoaraiosis and dementia in hypertensive patients. *Stroke*. 1992;23(11):1673-1677. doi:10.1161/01.str.23.11.1673
83. Garcia-Polite F, Martorell J, Del Rey-Puech P, et al. Pulsatility and high shear stress deteriorate barrier phenotype in brain microvascular endothelium. *J Cereb Blood Flow Metab Off J Int Soc Cereb Blood Flow Metab*. 2017;37(7):2614-2625. doi:10.1177/0271678X16672482
84. Ortiz GG, Pacheco-Moisés FP, Macías-Islas MÁ, et al. Role of the blood-brain barrier in multiple sclerosis. *Arch Med Res*. 2014;45(8):687-697. doi:10.1016/j.arcmed.2014.11.013
85. Becher B, Dodelet V, Fedorowicz V, Antel JP. Soluble tumor necrosis factor receptor inhibits interleukin 12 production by stimulated human adult microglial cells in vitro. *J Clin Invest*. 1996;98(7):1539-1543. doi:10.1172/JCI118946
86. Costantino CM, Baecher-Allan C, Hafler DA. Multiple sclerosis and regulatory T cells. *J Clin Immunol*. 2008;28(6):697-706. doi:10.1007/s10875-008-9236-x
87. Anderson AC, Anderson DE, Bregoli L, et al. Promotion of tissue inflammation by the immune receptor Tim-3 expressed on innate immune cells. *Science*. 2007;318(5853):1141-1143. doi:10.1126/science.1148536
88. Ljubisavljevic S, Stojanovic I. Neuroinflammation and demyelination from the point of nitrosative stress as a new target for neuroprotection. *Rev Neurosci*. 2015;26(1):49-73. doi:10.1515/revneuro-2014-0060
89. Ljubisavljevic S. Oxidative Stress and Neurobiology of Demyelination. *Mol Neurobiol*. 2016;53(1):744-758. doi:10.1007/s12035-014-9041-x
90. Braak H, Braak E. Staging of Alzheimer's disease-related neurofibrillary changes. *Neurobiol Aging*. 1995;16(3):271-278; discussion 278-284. doi:10.1016/0197-4580(95)00021-6
91. Chuang SY, Wang PN, Chen LK, et al. Associations of Blood Pressure and Carotid Flow Velocity with Brain Volume and Cerebral Small Vessel Disease in a Community-Based Population. *Transl Stroke Res*. 2021;12(2):248-258. doi:10.1007/s12975-020-00836-7

92. Tomoto T, Sugawara J, Tarumi T, et al. Carotid Arterial Stiffness and Cerebral Blood Flow in Amnestic Mild Cognitive Impairment. *Curr Alzheimer Res*. 2020;17(12):1115-1125. doi:10.2174/1567205018666210113155646
93. Shi Y, Thrippleton MJ, Makin SD, et al. Cerebral blood flow in small vessel disease: A systematic review and meta-analysis. *J Cereb Blood Flow Metab*. 2016;36(10):1653-1667. doi:10.1177/0271678X16662891
94. Liu Z, Ma H, Guo Z, et al. Impaired dynamic cerebral autoregulation is associated with the severity of neuroimaging features of cerebral small vessel disease. *CNS Neurosci Ther*. 2021;28(2):298-306. doi:10.1111/cns.13778
95. Li Q, Yang Y, Reis C, et al. Cerebral Small Vessel Disease. *Cell Transplant*. 2018;27(12):1711-1722. doi:10.1177/0963689718795148
96. Kapasi A, DeCarli C, Schneider JA. Impact of multiple pathologies on the threshold for clinically overt dementia. *Acta Neuropathol (Berl)*. 2017;134(2):171-186. doi:10.1007/s00401-017-1717-7
97. Passiak BS, Liu D, Kresge HA, et al. Perivascular spaces contribute to cognition beyond other small vessel disease markers. *Neurology*. 2019;92(12):e1309-e1321. doi:10.1212/WNL.0000000000007124
98. Wardlaw JM, Smith EE, Biessels GJ, et al. Neuroimaging standards for research into small vessel disease and its contribution to ageing and neurodegeneration. *Lancet Neurol*. 2013;12(8):822-838. doi:10.1016/S1474-4422(13)70124-8
99. Kida S, Steart PV, Zhang ET, Weller RO. Perivascular cells act as scavengers in the cerebral perivascular spaces and remain distinct from pericytes, microglia and macrophages. *Acta Neuropathol (Berl)*. 1993;85(6):646-652. doi:10.1007/BF00334675
100. Carare RO, Bernardes-Silva M, Newman TA, et al. Solutes, but not cells, drain from the brain parenchyma along basement membranes of capillaries and arteries: significance for cerebral amyloid angiopathy and neuroimmunology. *Neuropathol Appl Neurobiol*. 2008;34(2):131-144. doi:10.1111/j.1365-2990.2007.00926.x
101. Bown CW, Carare RO, Schrag MS, Jefferson AL. Physiology and Clinical Relevance of Enlarged Perivascular Spaces in the Aging Brain. *Neurology*. 2022;98(3):107-117. doi:10.1212/WNL.0000000000013077
102. Chen W, Song X, Zhang Y, Alzheimer's Disease Neuroimaging Initiative. Assessment of the Virchow-Robin Spaces in Alzheimer disease, mild cognitive impairment, and normal aging, using high-field MR imaging. *AJNR Am J Neuroradiol*. 2011;32(8):1490-1495. doi:10.3174/ajnr.A2541
103. Kwee RM, Kwee TC. Tumefactive Virchow-Robin spaces. *Eur J Radiol*. 2019;111:21-33. doi:10.1016/j.ejrad.2018.12.011
104. Albargothy NJ, Johnston DA, MacGregor-Sharp M, et al. Convective influx/glymphatic system: tracers injected into the CSF enter and leave the brain along separate periarterial basement membrane pathways. *Acta Neuropathol (Berl)*. 2018;136(1):139-152. doi:10.1007/s00401-018-1862-7
105. MacGregor Sharp M, Bulters D, Brandner S, et al. The fine anatomy of the perivascular compartment in the human brain: relevance to dilated perivascular spaces in cerebral amyloid angiopathy. *Neuropathol Appl Neurobiol*. 2019;45(3):305-308. doi:10.1111/nan.12480
106. Jessen NA, Munk ASF, Lundgaard I, Nedergaard M. The Glymphatic System: A Beginner's Guide. *Neurochem Res*. 2015;40(12):2583-2599. doi:10.1007/s11064-015-1581-6
107. Aldea R, Weller RO, Wilcock DM, Carare RO, Richardson G. Cerebrovascular Smooth Muscle Cells as the Drivers of Intramural Periarterial Drainage of the Brain. *Front Aging Neurosci*. 2019;11:1. doi:10.3389/fnagi.2019.00001

108. Pollock H, Hutchings M, Weller RO, Zhang ET. Perivascular spaces in the basal ganglia of the human brain: their relationship to lacunes. *J Anat*. 1997;191 (Pt 3):337-346. doi:10.1046/j.1469-7580.1997.19130337.x
109. Iliff JJ, Wang M, Liao Y, et al. A paravascular pathway facilitates CSF flow through the brain parenchyma and the clearance of interstitial solutes, including amyloid β. *Sci Transl Med*. 2012;4(147):147ra111. doi:10.1126/scitranslmed.3003748
110. Mestre H, Tithof J, Du T, et al. Flow of cerebrospinal fluid is driven by arterial pulsations and is reduced in hypertension. *Nat Commun*. 2018;9(1):4878. doi:10.1038/s41467-018-07318-3
111. Diem AK, MacGregor Sharp M, Gatherer M, Bressloff NW, Carare RO, Richardson G. Arterial Pulsations cannot Drive Intramural Periarterial Drainage: Significance for Aβ Drainage. *Front Neurosci*. 2017;11:475. doi:10.3389/fnins.2017.00475
112. van Veluw SJ, Hou SS, Calvo-Rodriguez M, et al. Vasomotion as a Driving Force for Paravascular Clearance in the Awake Mouse Brain. *Neuron*. 2020;105(3):549-561.e5. doi:10.1016/j.neuron.2019.10.033
113. Attems J, Jellinger K, Thal DR, Van Nostrand W. Review: sporadic cerebral amyloid angiopathy. *Neuropathol Appl Neurobiol*. 2011;37(1):75-93. doi:10.1111/j.1365-2990.2010.01137.x
114. Koo HW, Jo KI, Yeon JY, Kim JS, Hong SC. Clinical features of high-degree centrum semiovale-perivascular spaces in cerebral amyloid angiopathy. *J Neurol Sci*. 2016;367:89-94. doi:10.1016/j.jns.2016.05.040
115. Jochems ACC, Blair GW, Stringer MS, et al. Relationship Between Venules and Perivascular Spaces in Sporadic Small Vessel Diseases. *Stroke*. 2020;51(5):1503-1506. doi:10.1161/STROKEAHA.120.029163
116. Doubal FN, MacLullich AMJ, Ferguson KJ, Dennis MS, Wardlaw JM. Enlarged perivascular spaces on MRI are a feature of cerebral small vessel disease. *Stroke*. 2010;41(3):450-454. doi:10.1161/STROKEAHA.109.564914
117. Weller RO, Sharp MM, Christodoulides M, Carare RO, Møllgård K. The meninges as barriers and facilitators for the movement of fluid, cells and pathogens related to the rodent and human CNS. *Acta Neuropathol (Berl)*. 2018;135(3):363-385. doi:10.1007/s00401-018-1809-z
118. Riba-Llena I, Jiménez-Balado J, Castañé X, et al. Arterial Stiffness Is Associated With Basal Ganglia Enlarged Perivascular Spaces and Cerebral Small Vessel Disease Load. *Stroke*. 2018;49(5):1279-1281. doi:10.1161/STROKEAHA.118.020163
119. Rivera-Rivera LA, Schubert T, Turski P, et al. Changes in intracranial venous blood flow and pulsatility in Alzheimer's disease: A 4D flow MRI study. *J Cereb Blood Flow Metab Off J Int Soc Cereb Blood Flow Metab*. 2017;37(6):2149-2158. doi:10.1177/0271678X16661340
120. Mitchell GF. Effects of central arterial aging on the structure and function of the peripheral vasculature: implications for end-organ damage. *J Appl Physiol Bethesda Md 1985*. 2008;105(5):1652-1660. doi:10.1152/japplphysiol.90549.2008
121. Charidimou A, Jaunmuktane Z, Baron JC, et al. White matter perivascular spaces: an MRI marker in pathology-proven cerebral amyloid angiopathy? *Neurology*. 2014;82(1):57-62. doi:10.1212/01.wnl.0000438225.02729.04
122. Charidimou A, Hong YT, Jäger HR, et al. White matter perivascular spaces on magnetic resonance imaging: marker of cerebrovascular amyloid burden? *Stroke*. 2015;46(6):1707-1709. doi:10.1161/STROKEAHA.115.009090
123. Roher AE, Kuo YM, Esh C, et al. Cortical and leptomeningeal cerebrovascular amyloid and white matter pathology in Alzheimer's disease. *Mol Med Camb Mass*. 2003;9(3-4):112-122.
124. van Veluw SJ, Biessels GJ, Bouvy WH, et al. Cerebral amyloid angiopathy severity is linked to dilation of juxtacortical perivascular spaces. *J Cereb Blood Flow Metab Off J Int Soc Cereb Blood Flow Metab*. 2016;36(3):576-580. doi:10.1177/0271678X15620434

125. Charidimou A, Meegahage R, Fox Z, et al. Enlarged perivascular spaces as a marker of underlying arteriopathy in intracerebral haemorrhage: a multicentre MRI cohort study. *J Neurol Neurosurg Psychiatry*. 2013;84(6):624-629. doi:10.1136/jnnp-2012-304434
126. Zhang C, Chen Q, Wang Y, et al. Risk factors of dilated Virchow-Robin spaces are different in various brain regions. *PloS One*. 2014;9(8):e105505. doi:10.1371/journal.pone.0105505
127. Xie L, Kang H, Xu Q, et al. Sleep drives metabolite clearance from the adult brain. *Science*. 2013;342(6156):373-377. doi:10.1126/science.1241224
128. Del Brutto OH, Mera RM, Del Brutto VJ, Castillo PR. Enlarged basal ganglia perivascular spaces and sleep parameters. A population-based study. *Clin Neurol Neurosurg*. 2019;182:53-57. doi:10.1016/j.clineuro.2019.05.002
129. Opel RA, Christy A, Boespflug EL, et al. Effects of traumatic brain injury on sleep and enlarged perivascular spaces. *J Cereb Blood Flow Metab Off J Int Soc Cereb Blood Flow Metab*. 2019;39(11):2258-2267. doi:10.1177/0271678X18791632
130. Duperron MG, Tzourio C, Sargurupremraj M, et al. Burden of Dilated Perivascular Spaces, an Emerging Marker of Cerebral Small Vessel Disease, Is Highly Heritable. *Stroke*. 2018;49(2):282-287. doi:10.1161/STROKEAHA.117.019309
131. Luo X, Jiaerken Y, Yu X, et al. Associations between APOE genotype and cerebral small-vessel disease: a longitudinal study. *Oncotarget*. 2017;8(27):44477-44489. doi:10.18632/oncotarget.17724
132. Shams S, Martola J, Charidimou A, et al. Topography and Determinants of Magnetic Resonance Imaging (MRI)-Visible Perivascular Spaces in a Large Memory Clinic Cohort. *J Am Heart Assoc*. 2017;6(9):e006279. doi:10.1161/JAHA.117.006279
133. Yang S, Yuan J, Zhang X, et al. Higher ambulatory systolic blood pressure independently associated with enlarged perivascular spaces in basal ganglia. *Neurol Res*. 2017;39(9):787-794. doi:10.1080/01616412.2017.1324552
134. Ding J, Sigurðsson S, Jónsson PV, et al. Large Perivascular Spaces Visible on Magnetic Resonance Imaging, Cerebral Small Vessel Disease Progression, and Risk of Dementia: The Age, Gene/Environment Susceptibility-Reykjavik Study. *JAMA Neurol*. 2017;74(9):1105-1112. doi:10.1001/jamaneurol.2017.1397
135. Maclullich AMJ, Wardlaw JM, Ferguson KJ, Starr JM, Seckl JR, Deary IJ. Enlarged perivascular spaces are associated with cognitive function in healthy elderly men. *J Neurol Neurosurg Psychiatry*. 2004;75(11):1519-1523. doi:10.1136/jnnp.2003.030858
136. Liu DT, Liu YY, Kong YQ, Zhou LC, Hu WL. Clinical Correlation of Magnetic Resonance Imaging Features of Cerebral Small Vessel Disease. *World Neurosurg*. 2019;126:e586-e605. doi:10.1016/j.wneu.2019.02.099
137. Dernellis J, Panaretou M. Aortic stiffness is an independent predictor of progression to hypertension in nonhypertensive subjects. *Hypertens Dallas Tex 1979*. 2005;45(3):426-431. doi:10.1161/01.HYP.0000157818.58878.93
138. Calhoun DA, Jones D, Textor S, et al. Resistant hypertension: diagnosis, evaluation, and treatment: a scientific statement from the American Heart Association Professional Education Committee of the Council for High Blood Pressure Research. *Circulation*. 2008;117(25):e510-526. doi:10.1161/CIRCULATIONAHA.108.189141
139. Franklin SS, Jacobs MJ, Wong ND, L'Italien GJ, Lapuerta P. Predominance of isolated systolic hypertension among middle-aged and elderly US hypertensives: analysis based on National Health and Nutrition Examination Survey (NHANES) III. *Hypertens Dallas Tex 1979*. 2001;37(3):869-874. doi:10.1161/01.hyp.37.3.869

140. Henry-Feugeas MC, Roy C, Baron G, Schouman-Claeys E. Leukoaraiosis and pulse-wave encephalopathy: observations with phase-contrast MRI in mild cognitive impairment. *J Neuroradiol J Neuroradiol*. 2009;36(4):212-218. doi:10.1016/j.neurad.2009.01.003
141. Cambronero FE, Liu D, Neal JE, et al. APOE genotype modifies the association between central arterial stiffening and cognition in older adults. *Neurobiol Aging*. 2018;67:120-127. doi:10.1016/j.neurobiolaging.2018.02.009
142. Patankar TF, Mitra D, Varma A, Snowden J, Neary D, Jackson A. Dilatation of the Virchow-Robin space is a sensitive indicator of cerebral microvascular disease: study in elderly patients with dementia. *AJNR Am J Neuroradiol*. 2005;26(6):1512-1520.
143. Hansen TP, Cain J, Thomas O, Jackson A. Dilated perivascular spaces in the Basal Ganglia are a biomarker of small-vessel disease in a very elderly population with dementia. *AJNR Am J Neuroradiol*. 2015;36(5):893-898. doi:10.3174/ajnr.A4237
144. Boespflug EL, Schwartz DL, Lahna D, et al. MR Imaging–based Multimodal Autoidentification of Perivascular Spaces (mMAPS): Automated Morphologic Segmentation of Enlarged Perivascular Spaces at Clinical Field Strength. *Radiology*. 2018;286(2):632-642. doi:10.1148/radiol.2017170205
145. Ballerini L, Lovreglio R, Valdés Hernández M del C, et al. Perivascular Spaces Segmentation in Brain MRI Using Optimal 3D Filtering. *Sci Rep*. 2018;8:2132. doi:10.1038/s41598-018-19781-5
146. Boutinaud P, Tsuchida A, Laurent A, et al. 3D Segmentation of Perivascular Spaces on T1-Weighted 3 Tesla MR Images With a Convolutional Autoencoder and a U-Shaped Neural Network. *Front Neuroinformatics*. 2021;15:641600. doi:10.3389/fninf.2021.641600
147. Akkus Z, Galimzianova A, Hoogi A, Rubin DL, Erickson BJ. Deep Learning for Brain MRI Segmentation: State of the Art and Future Directions. *J Digit Imaging*. 2017;30(4):449-459. doi:10.1007/s10278-017-9983-4
148. Remedios SW, Roy S, Bermudez C, et al. Distributed Deep Learning Across Multi-site Datasets for Generalized CT Hemorrhage Segmentation. *Med Phys*. 2020;47(1):89-98. doi:10.1002/mp.13880
149. Wang X, Valdés Hernández M del C, Doubal F, et al. Development and initial evaluation of a semi-automatic approach to assess perivascular spaces on conventional magnetic resonance images. *J Neurosci Methods*. 2016;257:34-44. doi:10.1016/j.jneumeth.2015.09.010
150. Charidimou A, Boulouis G, Pasi M, et al. MRI-visible perivascular spaces in cerebral amyloid angiopathy and hypertensive arteriopathy. *Neurology*. 2017;88(12):1157-1164. doi:10.1212/WNL.0000000000003746
151. Hilal S, Tan CS, Adams HHH, et al. Enlarged perivascular spaces and cognition: A meta-analysis of 5 population-based studies. *Neurology*. 2018;91(9):e832-e842. doi:10.1212/WNL.0000000000006079
152. Paradise M, Crawford JD, Lam BCP, et al. Association of Dilated Perivascular Spaces With Cognitive Decline and Incident Dementia. *Neurology*. 2021;96(11):e1501-e1511. doi:10.1212/WNL.0000000000011537
153. Morris JC. The Clinical Dementia Rating (CDR): current version and scoring rules. *Neurology*. 1993;43(11):2412-2414. doi:10.1212/wnl.43.11.2412-a
154. Asman AJ, Landman BA. Formulating spatially varying performance in the statistical fusion framework. *IEEE Trans Med Imaging*. 2012;31(6):1326-1336. doi:10.1109/TMI.2012.2190992
155. Jenkinson M, Beckmann CF, Behrens TEJ, Woolrich MW, Smith SM. FSL. *NeuroImage*. 2012;62(2):782-790. doi:10.1016/j.neuroimage.2011.09.015
156. Nyúl LG, Udupa JK, Zhang X. New variants of a method of MRI scale standardization. *IEEE Trans Med Imaging*. 2000;19(2):143-150. doi:10.1109/42.836373
157. Kingma DP, Ba J. Adam: A Method for Stochastic Optimization. *ArXiv14126980 Cs*. Published online January 29, 2017. Accessed February 15, 2022. http://arxiv.org/abs/1412.6980

158. Kaplan E, Goodglass H, Weintraub S. *The Boston Naming Test*. Philadelpha, PA: Lea & Febiger; 1983.
159. Goodglass H, Kaplan E. *The Assessment of Aphasia and Related Disorders*. Philadelpha, PA: Lea & Febiger; 1983.
160. Wechsler D. Wechsler Adult Intelligence Scale- 4th Edition. Published online 2008.
161. Delis DC, Kaplan E, Kramer JH. Delis-Kaplan Executive Function System (D-KEFS): Examiner's Manual. Published online 2001.
162. Benton AL, Hamsher K, Sivan AB. *Multilingual Aphasia Examination*. Iowa City, IA: AJA Associates; 1994.
163. Hooper HE. *Hooper Visual Organization Test (HVOT)*. Los Angeles, CA: Western Psychological Services; 1983.
164. Glosser G, Cole L, Khatri U, DellaPietra L, Kaplan E. Assessing nonverbal memory with the Biber Figure Learning Test-Extended in temporal lobe epilepsy patients. *Arch Clin Neuropsychol Off J Natl Acad Neuropsychol*. 2002;17(1):25-35.
165. Delis DC, Kramer JH, Kaplan E, Ober B. *California Verbal Learning Test-II*. San Antonio, TX: The Psychological Corporation; 2000.
166. Sorensen T. A method of establishing groups of equal amplitude in plant sociology based on similarity of species content and its application to analyses of the vegetation on danish commons. *Det K Dan Vidensk Selsk Biol Skr*. 1948;V(4).
167. Dice LR. Measures of the Amount of Ecologic Association Between Species. *Ecology*. 1945;26(3):297-302. doi:10.2307/1932409
168. Pearson K. Notes on regression and inheritance in the base of two parents. *Proc R Soc Lond*. 1895;58:240-242.
169. Yeghiazaryan V, Voiculescu I. Family of boundary overlap metrics for the evaluation of medical image segmentation. *J Med Imaging Bellingham Wash*. 2018;5(1):015006. doi:10.1117/1.JMI.5.1.015006
170. Livne M, Hughes C, Deason L, Dudovitch G, hsudhof. *Surface Distance Metrics*. https://github.com/deepmind/surface-distance
171. Akaike H. A new look at the statistical model identification. Published online 1974. doi:10.1109/TAC.1974.1100705
172. Schwarz G. Estimating the dimension of a model. *Ann Stat*. 1978;6(2):461-464.
173. Zeng Q, Li K, Luo X, et al. The association of enlarged perivascular space with microglia-related inflammation and Alzheimer's pathology in cognitively normal elderly. *Neurobiol Dis*. 2022;170:105755. doi:10.1016/j.nbd.2022.105755
174. Smeijer D, Ikram MK, Hilal S. Enlarged Perivascular Spaces and Dementia: A Systematic Review. *J Alzheimers Dis JAD*. 2019;72(1):247-256. doi:10.3233/JAD-190527
175. Pantoni L. Cerebral small vessel disease: from pathogenesis and clinical characteristics to therapeutic challenges. *Lancet Neurol*. 2010;9(7):689-701. doi:10.1016/S1474-4422(10)70104-6
176. Damodarasamy M, Vernon RB, Pathan JL, et al. The microvascular extracellular matrix in brains with Alzheimer's disease neuropathologic change (ADNC) and cerebral amyloid angiopathy (CAA). *Fluids Barriers CNS*. 2020;17(1):60. doi:10.1186/s12987-020-00219-y
177. Zabel M, Schrag M, Crofton A, et al. A shift in microglial β-amyloid binding in Alzheimer's disease is associated with cerebral amyloid angiopathy. *Brain Pathol Zurich Switz*. 2013;23(4):390-401. doi:10.1111/bpa.12005
178. van Veluw SJ, Biessels GJ, Bouvy WH, et al. Cerebral amyloid angiopathy severity is linked to dilation of juxtacortical perivascular spaces. *J Cereb Blood Flow Metab Off J Int Soc Cereb Blood Flow Metab*. 2016;36(3):576-580. doi:10.1177/0271678X15620434

179. Kumar-Singh S. Cerebral amyloid angiopathy: pathogenetic mechanisms and link to dense amyloid plaques. *Genes Brain Behav*. 2008;7 Suppl 1:67-82. doi:10.1111/j.1601-183X.2007.00380.x
180. Nimmo J, Johnston DA, Dodart JC, et al. Peri-arterial pathways for clearance of α-Synuclein and tau from the brain: Implications for the pathogenesis of dementias and for immunotherapy. *Alzheimers Dement Amst Neth*. 2020;12(1):e12070. doi:10.1002/dad2.12070
181. Low A, Mak E, Rowe JB, Markus HS, O'Brien JT. Inflammation and cerebral small vessel disease: A systematic review. *Ageing Res Rev*. 2019;53:100916. doi:10.1016/j.arr.2019.100916
182. Webers A, Heneka MT, Gleeson PA. The role of innate immune responses and neuroinflammation in amyloid accumulation and progression of Alzheimer's disease. *Immunol Cell Biol*. 2020;98(1):28-41. doi:10.1111/imcb.12301
183. Aribisala BS, Wiseman S, Morris Z, et al. Circulating inflammatory markers are associated with magnetic resonance imaging-visible perivascular spaces but not directly with white matter hyperintensities. *Stroke*. 2014;45(2):605-607. doi:10.1161/STROKEAHA.113.004059
184. Hsieh CL, Koike M, Spusta SC, et al. A role for TREM2 ligands in the phagocytosis of apoptotic neuronal cells by microglia. *J Neurochem*. 2009;109(4):1144-1156. doi:10.1111/j.1471-4159.2009.06042.x
185. Klesney-Tait J, Turnbull IR, Colonna M. The TREM receptor family and signal integration. *Nat Immunol*. 2006;7(12):1266-1273. doi:10.1038/ni1411
186. Takahashi K, Rochford CDP, Neumann H. Clearance of apoptotic neurons without inflammation by microglial triggering receptor expressed on myeloid cells-2. *J Exp Med*. 2005;201(4):647-657. doi:10.1084/jem.20041611
187. Bechmann I, Galea I, Perry VH. What is the blood-brain barrier (not)? *Trends Immunol*. 2007;28(1):5-11. doi:10.1016/j.it.2006.11.007
188. Goetzl EJ, Banda MJ, Leppert D. Matrix metalloproteinases in immunity. *J Immunol Baltim Md 1950*. 1996;156(1):1-4.
189. Madri JA, Graesser D. Cell migration in the immune system: the evolving inter-related roles of adhesion molecules and proteinases. *Dev Immunol*. 2000;7(2-4):103-116. doi:10.1155/2000/79045
190. Leppert D, Waubant E, Galardy R, Bunnett NW, Hauser SL. T cell gelatinases mediate basement membrane transmigration in vitro. *J Immunol Baltim Md 1950*. 1995;154(9):4379-4389.
191. Xia M, Sreedharan SP, Dazin P, Damsky CH, Goetzl EJ. Integrin-dependent role of human T cell matrix metalloproteinase activity in chemotaxis through a model basement membrane. *J Cell Biochem*. 1996;61(3):452-458. doi:10.1002/(SICI)1097-4644(19960601)61:3%3C452::AID-JCB12%3E3.0.CO;2-L
192. Könnecke H, Bechmann I. The role of microglia and matrix metalloproteinases involvement in neuroinflammation and gliomas. *Clin Dev Immunol*. 2013;2013:914104. doi:10.1155/2013/914104
193. Agrawal S, Anderson P, Durbeej M, et al. Dystroglycan is selectively cleaved at the parenchymal basement membrane at sites of leukocyte extravasation in experimental autoimmune encephalomyelitis. *J Exp Med*. 2006;203(4):1007-1019. doi:10.1084/jem.20051342
194. Ramirez J, Berezuk C, McNeely AA, Scott CJM, Gao F, Black SE. Visible Virchow-Robin spaces on magnetic resonance imaging of Alzheimer's disease patients and normal elderly from the Sunnybrook Dementia Study. *J Alzheimers Dis JAD*. 2015;43(2):415-424. doi:10.3233/JAD-132528
195. Beer JC, Tustison NJ, Cook PA, et al. Longitudinal ComBat: A method for harmonizing longitudinal multi-scanner imaging data. *NeuroImage*. 2020;220:117129. doi:10.1016/j.neuroimage.2020.117129
196. Fortin JP, Cullen N, Sheline YI, et al. Harmonization of cortical thickness measurements across scanners and sites. *NeuroImage*. 2018;167:104-120. doi:10.1016/j.neuroimage.2017.11.024
197. Henjum K, Almdahl IS, Årskog V, et al. Cerebrospinal fluid soluble TREM2 in aging and Alzheimer's disease. *Alzheimers Res Ther*. 2016;8(1):17. doi:10.1186/s13195-016-0182-1

198. Minta K, Brinkmalm G, Al Nimer F, et al. Dynamics of cerebrospinal fluid levels of matrix metalloproteinases in human traumatic brain injury. *Sci Rep*. 2020;10:18075. doi:10.1038/s41598-020-75233-z
199. Palmqvist S, Zetterberg H, Blennow K, et al. Accuracy of brain amyloid detection in clinical practice using cerebrospinal fluid β-amyloid 42: a cross-validation study against amyloid positron emission tomography. *JAMA Neurol*. 2014;71(10):1282-1289. doi:10.1001/jamaneurol.2014.1358
200. Buysse DJ, Reynolds CF, Monk TH, Berman SR, Kupfer DJ. The Pittsburgh Sleep Quality Index: a new instrument for psychiatric practice and research. *Psychiatry Res*. 1989;28(2):193-213. doi:10.1016/0165-1781(89)90047-4
201. Choi Y, Nam Y, Choi Y, et al. MRI-visible dilated perivascular spaces in healthy young adults: A twin heritability study. *Hum Brain Mapp*. 2020;41(18):5313-5324. doi:10.1002/hbm.25194
202. Xu X, Wang B, Ren C, et al. Age-related Impairment of Vascular Structure and Functions. *Aging Dis*. 2017;8(5):590-610. doi:10.14336/AD.2017.0430
203. Jaruchart T, Suwanwela NC, Tanaka H, Suksom D. Arterial stiffness is associated with age-related differences in cerebrovascular conductance. *Exp Gerontol*. 2016;73:59-64. doi:10.1016/j.exger.2015.11.006
204. Tarumi T, Ayaz Khan M, Liu J, et al. Cerebral hemodynamics in normal aging: central artery stiffness, wave reflection, and pressure pulsatility. *J Cereb Blood Flow Metab Off J Int Soc Cereb Blood Flow Metab*. 2014;34(6):971-978. doi:10.1038/jcbfm.2014.44
205. Wu JS, Chen XC, Chen H, Shi YQ. A study on blood-brain barrier ultrastructural changes induced by cerebral hypoperfusion of different stages. *Neurol Res*. 2006;28(1):50-58. doi:10.1179/016164106X91870
206. Klarenbeek P, van Oostenbrugge RJ, Lodder J, Rouhl RPW, Knottnerus ILH, Staals J. Higher ambulatory blood pressure relates to enlarged Virchow-Robin spaces in first-ever lacunar stroke patients. *J Neurol*. 2013;260(1):115-121. doi:10.1007/s00415-012-6598-z
207. Osmond JM, Mintz JD, Dalton B, Stepp DW. OBESITY INCREASES BLOOD PRESSURE, CEREBRAL VASCULAR REMODELING, AND SEVERITY OF STROKE IN THE ZUCKER RAT. *Hypertension*. 2009;53(2):381-386. doi:10.1161/HYPERTENSIONAHA.108.124149
208. Taheri S, Gasparovic C, Huisa BN, et al. Blood-brain barrier permeability abnormalities in vascular cognitive impairment. *Stroke*. 2011;42(8):2158-2163. doi:10.1161/STROKEAHA.110.611731
209. Yang Y, Rosenberg GA. Blood-Brain Barrier Breakdown in Acute and Chronic Cerebrovascular Disease. *Stroke J Cereb Circ*. 2011;42(11):3323-3328. doi:10.1161/STROKEAHA.110.608257
210. Kim SY, Buckwalter M, Soreq H, Vezzani A, Kaufer D. Blood–brain barrier dysfunction–induced inflammatory signaling in brain pathology and epileptogenesis. *Epilepsia*. 2012;53(0 6):37-44. doi:10.1111/j.1528-1167.2012.03701.x
211. Qin L, Wu X, Block ML, et al. Systemic LPS causes chronic neuroinflammation and progressive neurodegeneration. *Glia*. 2007;55(5):453-462. doi:10.1002/glia.20467
212. Mitchell GF. Aortic stiffness and cerebral blood flow. *Am J Hypertens*. 2011;24(10):1056. doi:10.1038/ajh.2011.112
213. Mitchell GF, Parise H, Benjamin EJ, et al. Changes in arterial stiffness and wave reflection with advancing age in healthy men and women: the Framingham Heart Study. *Hypertens Dallas Tex 1979*. 2004;43(6):1239-1245. doi:10.1161/01.HYP.0000128420.01881.aa
214. Jiang L, Cai X, Yao D, et al. Association of inflammatory markers with cerebral small vessel disease in community-based population. *J Neuroinflammation*. 2022;19(1):106. doi:10.1186/s12974-022-02468-0
215. Weidner G. Why do men get more heart disease than women? An international perspective. *J Am Coll Health J ACH*. 2000;48(6):291-294. doi:10.1080/07448480009596270

216. Idriss HT, Naismith JH. TNF alpha and the TNF receptor superfamily: structure-function relationship(s). *Microsc Res Tech*. 2000;50(3):184-195. doi:10.1002/1097-0029(20000801)50:3<184::AID-JEMT2>3.0.CO;2-H
217. Rose-John S. Interleukin-6 Family Cytokines. *Cold Spring Harb Perspect Biol*. 2018;10(2):a028415. doi:10.1101/cshperspect.a028415
218. Cui N, Hu M, Khalil RA. Biochemical and Biological Attributes of Matrix Metalloproteinases. *Prog Mol Biol Transl Sci*. 2017;147:1-73. doi:10.1016/bs.pmbts.2017.02.005
219. Deczkowska A, Weiner A, Amit I. The Physiology, Pathology, and Potential Therapeutic Applications of the TREM2 Signaling Pathway. *Cell*. 2020;181(6):1207-1217. doi:10.1016/j.cell.2020.05.003
220. Franzmeier N, Suárez-Calvet M, Frontzkowski L, et al. Higher CSF sTREM2 attenuates ApoE4-related risk for cognitive decline and neurodegeneration. *Mol Neurodegener*. 2020;15(1):57. doi:10.1186/s13024-020-00407-2
221. Wang ML, Yu MM, Wei XE, Li WB, Li YH, Alzheimer's Disease Neuroimaging Initiative. Association of enlarged perivascular spaces with Aβ and tau deposition in cognitively normal older population. *Neurobiol Aging*. 2021;100:32-38. doi:10.1016/j.neurobiolaging.2020.12.014
222. da Fonseca ACC, Matias D, Garcia C, et al. The impact of microglial activation on blood-brain barrier in brain diseases. *Front Cell Neurosci*. 2014;8:362. doi:10.3389/fncel.2014.00362
223. Brown R, Benveniste H, Black SE, et al. Understanding the role of the perivascular space in cerebral small vessel disease. *Cardiovasc Res*. 2018;114(11):1462-1473. doi:10.1093/cvr/cvy113
224. Zhang Q, Zheng M, Betancourt CE, et al. Increase in Blood-Brain Barrier (BBB) Permeability Is Regulated by MMP3 via the ERK Signaling Pathway. *Oxid Med Cell Longev*. 2021;2021:6655122. doi:10.1155/2021/6655122
225. Nagel S, Su Y, Horstmann S, et al. Minocycline and hypothermia for reperfusion injury after focal cerebral ischemia in the rat: effects on BBB breakdown and MMP expression in the acute and subacute phase. *Brain Res*. 2008;1188:198-206. doi:10.1016/j.brainres.2007.10.052
226. Li Y, Li M, Yang L, et al. The relationship between blood-brain barrier permeability and enlarged perivascular spaces: a cross-sectional study. *Clin Interv Aging*. 2019;14:871-878. doi:10.2147/CIA.S204269
227. Ringland C, Schweig JE, Paris D, et al. Apolipoprotein E isoforms differentially regulate matrix metallopeptidase 9 function in Alzheimer's disease. *Neurobiol Aging*. 2020;95:56-68. doi:10.1016/j.neurobiolaging.2020.06.018
228. Wang H, Huang L, Wu L, et al. The MMP-2/TIMP-2 System in Alzheimer Disease. *CNS Neurol Disord Drug Targets*. 2020;19(6):402-416. doi:10.2174/1871527319666200812223007
229. Drogos LL, Gill SJ, Tyndall AV, et al. Evidence of association between sleep quality and APOE ε4 in healthy older adults. *Neurology*. 2016;87(17):1836-1842. doi:10.1212/WNL.0000000000003255
230. Liu CC, Zhao N, Fu Y, et al. ApoE4 Accelerates Early Seeding of Amyloid Pathology. *Neuron*. 2017;96(5):1024-1032.e3. doi:10.1016/j.neuron.2017.11.013
231. Palta P, Rippon B, Tahmi M, et al. Sex differences in in vivo tau neuropathology in a multiethnic sample of late middle-aged adults. *Neurobiol Aging*. 2021;103:109-116. doi:10.1016/j.neurobiolaging.2021.03.007
232. Hohman TJ, Dumitrescu L, Barnes LL, et al. Sex-Specific Association of Apolipoprotein E With Cerebrospinal Fluid Levels of Tau. *JAMA Neurol*. 2018;75(8):989-998. doi:10.1001/jamaneurol.2018.0821
233. Zhu YC, Dufouil C, Soumaré A, Mazoyer B, Chabriat H, Tzourio C. High degree of dilated Virchow-Robin spaces on MRI is associated with increased risk of dementia. *J Alzheimers Dis JAD*. 2010;22(2):663-672. doi:10.3233/JAD-2010-100378

234. Banerjee G, Kim HJ, Fox Z, et al. MRI-visible perivascular space location is associated with Alzheimer's disease independently of amyloid burden. *Brain J Neurol*. 2017;140(4):1107-1116. doi:10.1093/brain/awx003
235. Schrag M, Crofton A, Zabel M, et al. Effect of cerebral amyloid angiopathy on brain iron, copper, and zinc in Alzheimer's disease. *J Alzheimers Dis JAD*. 2011;24(1):137-149. doi:10.3233/JAD-2010-101503
236. Carrano A, Hoozemans JJM, van der Vies SM, van Horssen J, de Vries HE, Rozemuller AJM. Neuroinflammation and blood-brain barrier changes in capillary amyloid angiopathy. *Neurodegener Dis*. 2012;10(1-4):329-331. doi:10.1159/000334916
237. Benjamin P, Trippier S, Lawrence AJ, et al. Lacunar Infarcts, but Not Perivascular Spaces, Are Predictors of Cognitive Decline in Cerebral Small-Vessel Disease. *Stroke*. 2018;49(3):586-593. doi:10.1161/STROKEAHA.117.017526
238. Sim JE, Park MS, Shin HY, et al. Correlation Between Hippocampal Enlarged Perivascular Spaces and Cognition in Non-dementic Elderly Population. *Front Neurol*. 2020;11:542511. doi:10.3389/fneur.2020.542511
239. Barkhof F. Enlarged Virchow-Robin spaces: do they matter? *J Neurol Neurosurg Psychiatry*. 2004;75(11):1516-1517. doi:10.1136/jnnp.2004.044578
240. Cummings JL. Frontal-subcortical circuits and human behavior. *Arch Neurol*. 1993;50(8):873-880. doi:10.1001/archneur.1993.00540080076020
241. Brown LL, Schneider JS, Lidsky TI. Sensory and cognitive functions of the basal ganglia. *Curr Opin Neurobiol*. 1997;7(2):157-163. doi:10.1016/s0959-4388(97)80003-7
242. Riva D, Taddei M, Bulgheroni S. The neuropsychology of basal ganglia. *Eur J Paediatr Neurol EJPN Off J Eur Paediatr Neurol Soc*. 2018;22(2):321-326. doi:10.1016/j.ejpn.2018.01.009
243. McFarland NR, Haber SN. Thalamic relay nuclei of the basal ganglia form both reciprocal and nonreciprocal cortical connections, linking multiple frontal cortical areas. *J Neurosci Off J Soc Neurosci*. 2002;22(18):8117-8132.
244. Jaeger J. Digit Symbol Substitution Test. *J Clin Psychopharmacol*. 2018;38(5):513-519. doi:10.1097/JCP.0000000000000941
245. Saint-Cyr JA, Ungerleider LG, Desimone R. Organization of visual cortical inputs to the striatum and subsequent outputs to the pallido-nigral complex in the monkey. *J Comp Neurol*. 1990;298(2):129-156. doi:10.1002/cne.902980202
246. Jiménez-Balado J, Riba-Llena I, Garde E, et al. Prevalence of hippocampal enlarged perivascular spaces in a sample of patients with hypertension and their relation with vascular risk factors and cognitive function. *J Neurol Neurosurg Psychiatry*. 2018;89(6):651-656. doi:10.1136/jnnp-2017-316724
247. van Straaten ECW, Fazekas F, Rostrup E, et al. Impact of white matter hyperintensities scoring method on correlations with clinical data: the LADIS study. *Stroke*. 2006;37(3):836-840. doi:10.1161/01.STR.0000202585.26325.74
248. Davis Garrett K, Cohen RA, Paul RH, et al. Computer-mediated measurement and subjective ratings of white matter hyperintensities in vascular dementia: relationships to neuropsychological performance. *Clin Neuropsychol*. 2004;18(1):50-62. doi:10.1080/13854040490507154
249. Koizumi K, Hattori Y, Ahn SJ, et al. Apoε4 disrupts neurovascular regulation and undermines white matter integrity and cognitive function. *Nat Commun*. 2018;9(1):3816. doi:10.1038/s41467-018-06301-2
250. van der Flier WM, Skoog I, Schneider JA, et al. Vascular cognitive impairment. *Nat Rev Dis Primer*. 2018;4:18003. doi:10.1038/nrdp.2018.3
251. Wardlaw JM. Blood-brain barrier and cerebral small vessel disease. *J Neurol Sci*. 2010;299(1-2):66-71. doi:10.1016/j.jns.2010.08.042

252. Jefferson AL, Gifford KA, Acosta LMY, et al. The Vanderbilt Memory & Aging Project: Study Design and Baseline Cohort Overview. *J Alzheimers Dis JAD*. 2016;52(2):539-559. doi:10.3233/JAD-150914
253. Haan MN, Shemanski L, Jagust WJ, Manolio TA, Kuller L. The role of APOE epsilon4 in modulating effects of other risk factors for cognitive decline in elderly persons. *JAMA*. 1999;282(1):40-46. doi:10.1001/jama.282.1.40
254. Gertje EC, van Westen D, Panizo C, Mattsson-Carlgren N, Hansson O. Association of Enlarged Perivascular Spaces and Measures of Small Vessel and Alzheimer Disease. *Neurology*. 2021;96(2):e193-e202. doi:10.1212/WNL.0000000000011046
255. Barbas H, Wang J, Joyce MKP, García-Cabezas MÁ. Pathway mechanism for excitatory and inhibitory control in working memory. *J Neurophysiol*. 2018;120(5):2659-2678. doi:10.1152/jn.00936.2017
256. Müller NCJ, Konrad BN, Kohn N, et al. Hippocampal-caudate nucleus interactions support exceptional memory performance. *Brain Struct Funct*. 2018;223(3):1379-1389. doi:10.1007/s00429-017-1556-2